Pulmonary Arterial Wave Intensity Analysis in Health and Disease.

By

Nathan Dwyer

BMedSci (Hons), MBBS (Hons), FRACP

Submitted in fulfilment of the requirements for the degree of

Doctor of Philosophy

Faculty of Health Science
University of Tasmania
November 2010

Declaration

This thesis contains no material that has been accepted for a degree or diploma by the University or any other institution, except by way of background information and duly acknowledged in the thesis, and to the best of my knowledge and belief no material previously published or written by another person except where due acknowledgement is made in the text of the thesis, nor does the thesis contain any material that infringes copyright.

…………………………………………..
Nathan Dwyer
November 2010

Authority of Access

This thesis may be reproduced, archived, and communicated in any material form in whole or in part by the University of Tasmania or its agents, and may be made available for loan and copying in accordance with the *Copyright Act 1968*.

…………………………………………..
Nathan Dwyer
November 2010

Abstract

Wave intensity analysis (WIA) is a time-domain technique utilising high fidelity pressure and velocity measurements to determine the intensity, direction, type and timing of waves that may simultaneously exist. Travelling wavefronts represent elemental units of energy transmitted within and between the heart and blood vessels. Thus, WIA allows us to study ventricular-arterial interactions providing information on ventricular performance and the state of the circulation. In the pulmonary circulation WIA allows the study of upstream and downstream events that influence net pulmonary arterial blood flow.

WIA was performed in the pulmonary arteries of anaesthetised open-chest sheep, determining a normal mean wave speed of 2.1 ms^{-1}. Whilst wave reflection was minimal in healthy resting pulmonary arteries, two minor but clearly discernible backward travelling waves were identified that serve as important physiological markers. The first was an early systolic backward expansion wave representing open-end reflection from a site approximately 3 cm downstream, most likely from the main pulmonary bifurcation, and would serve to augment flow out of the right ventricle. The second was a late systolic backward compression wave representing closed-end reflection from a site approximately 20 cm downstream, most likely from the pulmonary microcirculation, and would serve to oppose flow out of the right ventricle. The open-end reflection was enhanced by increased pulmonary blood flow or circulating blood volume. With pulmonary vasoconstriction or obstruction, WIA was able to accurately determine the distance to the newly developed closed-end reflection site from which a backward compression arrives in mid-systole and opposes flow out of the right ventricle.

In human volunteers with normal or diseased pulmonary vasculature, wave speed was shown to increase linearly with pulmonary vascular resistance. The difficulties in reproducing instantaneous pulmonary blood velocity accurately in-vivo limited assessment of reflected waves.

Foreword

The current definition of pulmonary vascular disease in terms of the presence or absence of pulmonary hypertension, that is a mean pulmonary artery pressure ≥ 25 mmHg (Badesch *et al.*, 2009), is inadequate. As the pulmonary circulation is highly compliant with a substantial ability to recruit blood vessels, 50-60% of the pulmonary microcirculation is diseased before a pressure rise is manifest (Dalen *et al.*, 1967). Thus, pulmonary hypertension is a late manifestation of pulmonary vascular disease and therefore new techniques are required to define the condition at its earliest and perhaps more treatable stages.

The trend to explore genetic and subcellular processes means that important haemodynamic principles such as ventricular-vascular interactions have been neglected, particularly in the pulmonary vascular bed. A relatively new method called wave intensity analysis (WIA), relying on the simultaneous acquisition of blood velocity and pressure, has the potential to provide exciting insights into right ventricular-pulmonary arterial interactions. The basis of this approach is that a cardiac cycle is associated with the propagation of infinitesimal wavefronts defined by changes in pressure and velocity. WIA allows the identification of forward-travelling waves that arise from the heart and backward-travelling waves that are reflected from the distal vasculature, as well as the calculation of the instantaneous energy carried by these waves. These waves are further defined as compression waves that increase pressure or expansion waves that decrease pressure. With calculation of the wave speed, the wave intensity can be separated into the four potential wave types that may simultaneously exist; forward compression waves that increase pressure and velocity, forward expansion waves that decrease pressure and velocity, backward compression waves that increase pressure but decrease velocity, and backward expansion waves that decrease pressure but increase velocity. As WIA remains in the time domain, it has advantages over the prevailing frequency domain approach to wave reflection.

By potentially identifying reflected waves from the pulmonary vasculature WIA may have a role in the early detection and diagnosis of pulmonary vascular disease, allowing targeted therapy before right ventricular dysfunction becomes irreversible.

This thesis is divided into 10 chapters and may be thought of as a collection of experiments and observations that may be used as a foundation to extend our understanding of wave travel and reflection in the pulmonary circulation of sheep and humans using WIA. Chapter 1 is introductory in nature, describing the historical evolution of cardiopulmonary knowledge, outlining our current understanding of pulmonary circulatory physiology, and critically explores the literature related to investigation of wave reflection. Chapter 2 reports the methodology, experimental protocol and data analysis techniques in both the sheep and human studies. Chapter 3 qualitatively and quantitatively investigates wave intensity in the resting healthy pulmonary artery of sheep. Chapter 4 reports on the marked influences that pressure-velocity signal delays or wave speed calculation errors may have on wave intensity parameters. Chapter 5 explores the effects of high pulmonary blood flow on wave intensity parameters in sheep. Chapter 6 reports on the influence of reversible and irreversible acute changes in right ventricular afterload on wave intensity parameters in sheep. Chapter 7 explores whether progressive microsphere obliteration of the sheep's pulmonary microcirculation would lead to detectable changes in the wave speed or wave intensity parameters before a significant rise in mean pulmonary artery pressure manifests. Chapter 8 investigates the possible changes on wave intensity parameters after accounting for the pulmonary Windkessel (reservoir) pressure. Chapter 9 reports on the first study in humans to investigate pulmonary arterial wave intensity in healthy and diseased volunteers. Chapter 10 summarises the thesis, draws conclusions and plans new directions for pulmonary arterial WIA. A list of references is documented after Chapter 10.

Acknowledgements

I wish to sincerely thank my supervisor and mentor, **Professor David Kilpatrick**, for his constant support and guidance. Not only has he taught me to think critically and independently but also nurtured and mentored my clinical development, particularly in the field of cardiac physiology and pulmonary vascular disease.

I would like to extend my sincere appreciation to **Dr. Ah Chot Yong**, for his enthusiastic and tireless work in the animal laboratory, without which these data would not have been collected.

Many thanks to **Mr. Frank Sainsbury** for answering my endless and often untimely questions regarding information technology. His assistance has been invaluable.

Grateful thanks to **Dr. Jiun-Jr Wang** from the University of Calgary for providing the Matlab code that enabled the determination of the Windkessel parameters and edge-detection of the human pulmonary arterial blood velocity envelope.

Table of Contents

List of Figures

List of Tables

Abbreviation Glossary

A	area
A_R	area ratio
BCW	backward compression wave
BEW	backward expansion wave
C	capacitance/compliance
c	wave speed
CO	cardiac output
dI	net wave intensity
dP	pressure differential over the sampling interval
dU	velocity differential over the sampling interval
E	Young's modulus of elasticity
ECG	electrocardiogram
f	frequency
FCW	forward compression wave
FEW	forward expansion wave
Fr	French
h	vessel wall thickness
Hz	hertz
I	inertia
L	distance to reflection site
LA	left atrium (atrial)
LV	left ventricle (ventricular)
LVEDP	left ventricular end-diastolic pressure
LVSP	left ventricular systolic pressure
m	mass
No.	number
n	number
P	pressure (measured)
P_aO_2	systemic arterial partial pressure of oxygen
P_∞	asymptotic pressure
P_{ex}	excess (wave) pressure
P_{res}	reservoir (Windkessel) pressure
PA	pulmonary artery (arterial)
PAH	pulmonary arterial hypertension
PAP	pulmonary artery pressure
PASP	pulmonary artery systolic pressure
PCWP	pulmonary capillary wedge pressure
PEEP	positive end-expiratory pressure
PH	pulmonary hypertension
PV	pulmonary vein
PVR	pulmonary vascular resistance $[(P_{PA} - P_{LA})/Q_{PA}]$
Q	flow
R	resistance
R_c	reflection coefficient; index of wave reflection
r	internal vessel lumen radius
RHC	right heart catheterisation
RV	right ventricle

RVEDP	right ventricular end-diastolic pressure
RVSP	right ventricular systolic pressure
SD	standard deviation
TTE	transthoracic Doppler echocardiogram
t	time
U	velocity
V	volume
W	watts
WIA	wave intensity analysis
X_c	capacitative reactance
X_I	inertial reactance
Z	impedance
Z_c	characteristic impedance
Z_0	input impedance at zero hertz
+	forward
-	backward
ρ	density of blood
τ	diastolic exponential time constant

Project Aims

An open-chest sheep model was designed to investigate:

1. The normal resting pulmonary arterial wave intensity parameters.
2. The effects of increased pulmonary blood flow on wave intensity parameters.
3. The effects of increased right ventricular afterload on wave intensity parameters.
4. The influence of progressive microsphere obliteration of the pulmonary vascular bed on wave reflection and pulmonary arterial wave speed.
5. The influence of accounting for the Windkessel (reservoir) pressure on wave intensity analysis.

Human volunteers were investigated to:

1. Determine the normal resting pulmonary arterial wave intensity parameters.
2. Understand the pattern of wave reflection in different severities of pulmonary vascular disease.
3. Establish a normal range of human pulmonary arterial wave speeds.

Hypotheses

1. The right ventricle and pulmonary artery are so well matched in terms of impedance that wave reflection detected in the resting proximal pulmonary artery is minimal in both healthy humans and sheep.
2. During periods of increased pulmonary blood flow the proximal pulmonary artery will be characterised by open-end (negative) reflection to enhance right ventricular emptying.
3. During periods of increased right ventricular afterload the development of closed-end (positive) reflection will impair right ventricular emptying.
4. The incremental administration of pulmonary microspheres will lead to progressively increased pulmonary arterial wave speed and closed-end reflection prior to manifestation of increases in pulmonary artery pressure.
5. Taking the Windkessel effect of the pulmonary vascular bed into account will not greatly influence the interpretation of wave travel and reflection.
6. Humans with increasing severities of pulmonary vascular disease will develop progressive increases in closed-end reflection, leading to a backward compression wave arriving in mid-systole that opposes right ventricular emptying.
7. Human pulmonary arterial wave speed will increase proportionally with pulmonary artery pressure and pulmonary vascular resistance.

Chapter 1 Introduction

1.1 Historical Perspectives

1.1.1 The Role of the Pulmonary Circulation: A History of its Discovery

Galen of Pergamum (AD 127-200) was a prominent Roman physician and philosopher of Greek origin whose prolific research and observations in anatomy and physiology formulated strong theories that dominated and influenced medical science for over a millennium. Galen's theories were based on animal studies as human dissection was prohibited in ancient Rome.

The Galenic view was not of a blood circulation with the heart as a pump, but that the heart generated vital spirit (an admixture of refined blood and airy substance) that was a consumable fuel. As described in the sixth book of Galen's *De usu partium*, venous blood (dark red) was generated in the liver and arrived in the right side of the heart and traversed invisible pores in the interventricular septum to the left side of the heart, where it mixed with air (*pneuma*) arriving from the lungs to create spirit, and this arterial blood (brighter red) was then distributed to the body for nourishment. Galen considered that the sole purpose of the pulmonary artery was to provide nourishment to the lungs (Prioreschi, 1996). He believed the role of the pulmonary valve was to stop blood retreating to the heart when the lungs were compressed during expiration. This led to a regular supply of pulmonary nutrition and allowed the lungs to provide air for the left side of the heart. Galen felt the function of the tricuspid valve served to prevent the blood retreating back to the liver before it was consumed. With regards to the pulse, Galen believed that every part of an artery pulsated simultaneously and that the motion of the pulse was due to natural motions (active expansion and contraction) as opposed to forced motions (the heart causing arterial expansion and contraction).

Galen's description of the activities of the heart, arteries and veins endured until William Harvey established that blood circulates with the heart acting as a pump in the early seventeenth century. Prior to this monumental discovery, three men independently described the pulmonary circulation: Ibn al-Nafis, Michael Servetus, and Renaldus Columbus (Al-Ghazal, 2002; Prioreschi, 1996; Wilson, 1962).

Ibn al-Nafis (1213-1288), an eminent physician born in Damascus, first described our modern understanding of the pulmonary circulation in the thirteenth century, contradicting the prevailing Galenic theory of the heart. Much of Galen's work was translated into Arabic allowing Islamic physicians to study and comment on Galen's theories. Indeed, Ibn al-Nafis in his work from 1242 entitled *Sharh Tashrih al-Qanun Ibn Sina (Commentary on the Anatomy of Canon of Avicenna*) observed that the interventricular septum was no thinner than other parts of the heart wall which do not ooze blood and that there was no passage between the two cavities, therefore concluding that if blood was to pass from right to left, it must travel via the pulmonary pathway.

Michael Servetus (1511-1553), a Spanish physician, observed in his work *Christianismi Restitutio* (1553) that the notable size of the pulmonary artery and force of blood within it suggested it was not merely for nourishment of the lungs. He also observed the change in blood colour as it passed through the lungs. He concluded therefore that blood is urged forward from the right heart through the lungs and then elaborated by the lungs, pouring into the pulmonary vein where it is mixed with inspired air and through expiration is cleansed.

Renaldus Columbus (1516-1559), an Italian anatomist and surgeon, in his work *De re Anatomica* (1559) observed that the pulmonary veins were filled with blood in living animals, not air and vapours which would be subscribed under a Galenic framework. Columbus thus drew the conclusion that an admixture of air with the blood occurs in the lungs and that this blood circuits from the right ventricle through the pulmonary circulation to the left ventricle of the heart.

William Harvey (1578-1657), an English physician, made a significant conceptual leap derived from his own anatomical observations in 1616 that were later published in *Exercitatio Anatomica de Motu Cordis et Sanguinis in Animalibus* (1628). He described the continuous circulation of blood throughout the body between arteries and veins (not just occurring in the lungs), which was pumped by the heart. Harvey argued, from his own observations, that the large amount of blood passing through the heart each day could not be plausibly produced by the liver, as the amount was more than the body's intake of food by weight, therefore concluding that blood must be circulating. He also concluded through experimental observation that veins allowed blood to travel towards the heart and that valves maintained this unidirectional flow, allowing our current model of the circulation with the heart as a pump. Harvey had to postulate the existence of invisible vascular connections between arteries and veins, which were ultimately demonstrated by Marcello Malpighi (1628-1694) in frogs' lungs using a microscope in 1661.

Another English Physician, Richard Lower (1631-1691), studied the workings of the heart and lungs and published his major work *Tractatus de Corde* in 1669. He traced the circulation of blood as it passed through the lungs and learnt that it changed when exposed to air and concluded that the role of the circulation was to deliver blood to the lungs for admixture with air, which then transpired throughout the body. Though he did not discover oxygen, Lower did observe that where a fire burns well, humans could equally breathe well.

The discovery of oxygen over 100 years later is credited to Joseph Priestley (1733-1804), an English clergyman, in a 1775 paper titled *Experiments and Observations on Different Kinds of Air*. It seems the Swedish pharmacist Carl Scheele (1742-1786) first isolated oxygen in 1772, but his manuscript *Treatise on Air and Fire* was published after Priestley's in 1777. Antoine Lavoisier (1743-1794), a French chemist, extended this work, naming the isolated gas oxygen in 1779 and described its importance in respiration.

1.1.2 An Overview of the Major Advances in Haemodynamics

Sir Isaac Newton's (1642-1727) work *Philosophiæ Naturalis Principia Mathematica* contained the concept of fluid viscosity, which is central to the understanding of arterial blood flow, pressure-flow relationships and vascular resistance.

Stephen Hales (1677-1761), an English physiologist, studied the exchange between air and blood by measuring the amount of air absorbed by breathing and noted the large surface area of the alveolar capillaries was well suited to this absorption. He was the first, in 1727, to determine arterial blood pressure in an animal when he measured the rise of a column of blood in a glass tube bound into an artery. His essay, *Haemastaticks* (1733), contained experiments on the "force of blood", arterial flow rate, and the capacity of different blood vessels. Hales, through his experimental observation, saw the arterial system as a cushion where the arterioles resisted cardiac pulsations such that flow through the tissues was continuous. This was analogous to the air-filled domes of the contemporary fire engine that delivered continuous flow through the fire nozzle despite marked oscillations from the pump. In the German translation of *Haemastaticks*, the air-filled dome was referred to as a Windkessel, a term that has remained to describe the cushioning role of the arterial system.

A leader in the development of fluid dynamics was Leonhart Euler (1707-1783). He established the equations of fluid motion that are still used today, though he neglected viscosity. He developed theories regarding the velocity of pressure transmission. Daniel Bernoulli (1700-1782) developed an equation describing the pressure change with interconversion of potential to kinetic energy.

Jean Poiseuille (1799-1869) advanced the study of arterial haemodynamics by establishing the relationship between flow, pressure gradient and dimensions of a capillary tube. He showed experimentally in 1846 that flow was inversely related to the fourth power of the tube's internal diameter. Importantly his experiments confirmed Hales' belief that the greatest component of peripheral resistance was in the smallest blood vessels, by demonstrating high pressure in arteries down to 2 mm in diameter and low venous pressure in animals.

A major contribution to arterial haemodynamics was to describe the relationship between the elastic properties of arteries and the velocity of propagation of the arterial pulse attributed to Thomas Young (1773-1829) in 1808.

Whilst Joseph Fourier (1768-1830), a French mathematician and physicist, never contributed directly to arterial haemodynamics, his work on periodic functions and development of the Fourier series has been widely used in subsequent studies of pulsatile flow.

Claude-Louis Navier (1785-1836) first attempted to describe the equations for flow of viscous liquids in cylindrical tubes in 1827. George Stokes (1819-1903) reworked the problem in 1845 and developed the basic equations for the flow of viscous liquids, now known as the Navier-Stokes equations.

The field of arterial distensibility and wave velocity began to grow. The German brothers Wilhelm (1804-1891) and Ernst Weber (1795-1878) established many of the properties of propagated and reflected waves in their work *Wellenlehre* (1825). Moens in 1878 published his experimental work of wave propagation. Korteweg in 1878 later described the relationship between the arterial pulse wave velocity and Young’s elastic modulus of the arterial wall based upon the mathematical analysis of Moens’ data, thus referred to as the Moens-Korteweg equation.

Otto Frank (1865-1944), in addition to describing the influence of ventricular dimension on ventricular contraction (1895; later clarified by Starling in 1914) and the production of a manometer that could measure blood pressure fluctuations accurately (1903), developed a theoretical framework for arterial function with a ‘lumped’ distensible section (Windkessel) and ‘lumped’ peripheral resistance.

In 1922, Bramwell and Hill described cardiac function in relation to hydraulic load and showed how pulse wave velocity (a measure of arterial stiffness) increased with age and was an important component of the hydraulic load (Bramwell & Hill 1922).

The electromagnetic flowmeter was introduced independently by Kolin in 1936 and Wetterer in 1937, and allowed flow waves in various arteries to be described. Micromanometers were developed by Millar in 1972 allowing arterial pressure waves to be accurately determined. Electromagnetic velocity sensors were subsequently miniaturised and mounted on cardiac catheters to measure intra-arterial flow.

Throughout the nineteenth century invasive and non-invasive descriptions of the contours of the arterial pulse were made in the time domain, yet there is still no consensus statement on the description and terminology of the arterial pulse. With new methods to determine phasic pressure and flow in the twentieth century, more sophisticated methods for analysis of pressure and flow developed. John Womersley in 1955 demonstrated the arterial system could be viewed as being in a steady state of oscillation, so could be analysed in the frequency domain. The publication of McDonald's book Blood Flow in Arteries in 1960 introduced a wide audience to vascular flow theory and great period of activity resulted (Nichols *et al.*, 2005). More recently an alternative time-domain method for the study of wave travel in the circulation was developed by Parker and Jones (1990).

1.2 The Normal Pulmonary Circulation

The pulmonary circulation is complex in terms of anatomy and physiology and is vastly different to the systemic circulation. It is a low resistance, high capacitance vascular bed, interposed between the right and left sides of the heart, that can accommodate large increases in cardiac output with minimal elevations in pulmonary pressure, thus protecting the delicate alveolar capillaries. It has the unique role of oxygenating blood and the pulmonary microcirculation adapts rapidly to changes in the prevailing vascular and alveolar pressures to allow continuous pulmonary gas exchange.

A review of the diseased pulmonary vasculature is beyond the scope of this thesis, but suffice to say that many cardiac and pulmonary diseases are associated with recognisable structural changes to the conducting arteries that deliver blood to the alveolar walls. The subsequently increased pulmonary vascular resistance leads to abnormal elevations in pulmonary artery pressures, termed pulmonary hypertension, now simply defined as a resting mean pulmonary artery pressure ≥ 25 mmHg (Badesch *et al.*, 2009), that may lead to right ventricular failure and ultimately death. The important anatomical and physiological features of the normal pulmonary circulation are described below.

1.2.1 Anatomy

The pulmonary circulation extends from the pulmonary valve to the orifices of the pulmonary veins in the left atrium. Compared to the systemic circulation, the pulmonary circulation is shorter with a path length of around 34 cm, similar between the left and right lungs (Horsfield, 1978; Horsfield and Gordon, 1981; Singhal *et al.*, 1973). The major pulmonary arteries are elliptical in cross section rather than round (Attinger, 1963). In humans the pulmonary trunk is about 5 cm long and 3 cm in diameter (Caro, 1978; Harris and Heath, 1962) and exhibits tapering to its point of bifurcation (Attinger, 1963) into the right and left main pulmonary arteries.

In contrast to the systemic circulation there is immediate branching of the vessels within a few centimetres of the heart, which further branch rapidly and progressively (Gan and Yen, 1994; Glazier *et al.*, 1969). The medial layer of smooth muscle in the pulmonary arteries for any given calibre is comparably much thinner than in the systemic circulation (Patel *et al.*, 1960), reflecting the lower prevailing circulatory pressures with wall thicknesses of only 1 mm in the main pulmonary trunk (Harris and Heath, 1962).

The pulmonary arterial branches divide progressively and accompany bronchi and bronchioles before entering the gas exchange parenchyma. Pulmonary arteries of the same generation are much larger than their systemic counterparts. Thus the pulmonary vascular cross sectional area expands suddenly (Horsfield, 1978). The arterial distensibility is much higher than in the systemic circulation (Patel *et al.*, 1960) and pulmonary vessels do not seem to display increasing stiffness as they progress distally (Attinger, 1963; Patel *et al.*, 1960).

Arterial branches that accompany the bronchi remain in an axial position, that is, remain central to the wedge shaped acini that make up the lung. There are many more arteries than bronchi, due to the presence of supernumerary arteries that sharply branch from this central axis and divide to supply the alveolar capillary network. This means that an acinus is not perfused sequentially from the central axis to the pleura and periphery. Rather, the arterial blood supply is delivered at different points leading to complex directional patterns of flow that are not fully understood. Ultimately air and blood come into close proximity to allow pulmonary gas exchange across the air-blood barrier, composed of an endothelial and an epithelial cell sharing a fused basement membrane.

Fibrous connective tissue extends from the hilum to the pleura and incorporates a connective tissue sheath that surrounds extra-alveolar blood vessels and receives the radial insertions of alveolar septae, which is of great functional significance (Fishman and Fisher, 1985). This complex anatomical arrangement means that extra-alveolar vessels are surrounded by subatmospheric pressure that becomes more negative during inspiration (Lai-Fook, 1993). This means that the extra-alveolar vessels increase in diameter and length during inspiration due to the increased perivascular subatmospheric pressure generated by the radial pull of alveolar septae on the sheath of loose connective tissue surrounding the vessels.

Corner vessels do not have a muscular or adventitial layer and due to their anatomical location within the alveolar corners are able to resist collapse during inspiration, even if alveolar air pressure exceeds arterial pressures (Lamm *et al.*, 1991). Hence these vessels function as permanently open communications between arteries and veins, allowing continuous blood flow and gas exchange, regardless of the prevailing alveolar air pressure and status of the septal capillaries.

The alveolar walls have 90% of their volume occupied by a network of capillaries, the morphology of which has been described by Weibel (1963). This network of capillaries form a dense anastomosing hexagonal network, periodically fed and drained by arteries and veins, without obvious beginning or end. In contrast to the corner vessels the perfusion of the septal capillaries is sensitive to the mechanical influences of alveolar air pressure and become compressed and empty during inspiration. The alveolar capillary network alters number, size and shape depending on the prevailing forces mentioned.

The absence of high resistance arterioles in the pulmonary circulation leads to the transmission of much of the pulmonary arterial pressure to the alveolar capillaries and consequently highly pulsatile flow at the capillary level (Reuben, 1970) and even on the pulmonary venous side of the circulation (Bergel and Milnor, 1965; Maloney *et al.*, 1968). In the microcirculation, with vessel diameters below 120 µm, the pressure pulse dampens to 50% of the pulmonary pressure pulse with a higher degree of damping at higher pulse frequencies, but the flow pulse in minimally affected (Fishman and Fisher, 1985; Wiener *et al.*, 1966).

Pulmonary capillaries are more distensible than systemic capillaries and their calibre does increase with raised transmural pressure (Weibel and Gil, 1977), but this relationship is complex and the extent of distensibility is unclear (West *et al.*, 1975).

1.2.2 Physiology

1.2.2.1 Normal Resting Pulmonary Haemodynamics

The pulmonary resistance to the flow of blood is so small that the pulmonary artery pressure averages 14 mmHg (one-sixth of systemic levels) and the drop in pressure across the pulmonary bed is only about 5-10 mmHg, generating a blood flow of 6-7 $Lmin^{-1}$ (Kovacs *et al.*, 2009; Maggiorini *et al.*, 2001; Melot *et al.*, 1987; Naeije *et al.*, 1982). There are no gender differences in pulmonary haemodynamics when flow is corrected for body size. The normal pulmonary haemodynamic measures from healthy resting supine adult subjects are shown in Table 1-1.

As the pulmonary vasculature is highly compliant and recruitable, even mild elevations in resting pulmonary pressures indicate significant impairment of the pulmonary vasculature. Therefore, these patients may develop clinically significant rises in pulmonary pressure when vascular tone or pulmonary blood flow increase as occurs during acute hypoxia or exercise.

Consequent to the low pressures, the right ventricle is thin walled and is unable to adapt rapidly to loading conditions. Nevertheless, when operating under conditions of low pulmonary vascular impedance, the right ventricle is able to match the output of the larger left ventricle at a low energy cost. The normal right ventricle is able to tolerate acute rises in afterload to 50 mmHg. It can generate high pressures, even to systemic arterial levels, if the afterload develops gradually allowing the right ventricle to hypertrophy. However, once the afterload exceeds the right ventricle's capacity for adaptation, the right ventricle ultimately fails.

Pulmonary pressure and flow are routinely assessed with a triple lumen balloon-tipped thermodilution catheter inserted into a central vein and manipulated into the pulmonary artery under constant pressure wave monitoring (Swan *et al.*, 1970). This technique allows the sequential measurement of right atrial pressure (RAP), right ventricular pressure (RVP), pulmonary artery pressure (PAP) and pulmonary capillary wedge pressure (PCWP). A PCWP provides an accurate assessment of left atrial pressure (LAP) provided that the pulmonary vessels are fully recruited with a pulmonary capillary pressure higher than the prevailing alveolar air pressure, which is seen throughout the lung in normal recumbent euvolaemic patients. With the application of thermodilution or Fick principles, mean pulmonary blood flow (Q) can be calculated (Baim and Grossman, 2006). Pulmonary blood flow is equivalent to the cardiac output (CO) in the absence of shunting.

The pressure in the pulmonary artery varies throughout the respiratory cycle, being higher in expiration than inspiration and is synchronous with changes in pressure in the pleural space. The magnitude of change is in the order of 3-6 mmHg and to standardise measurements pulmonary pressures are normally recorded at end-tidal expiration.

Table 1-1. Normal Resting Pulmonary Arterial Haemodynamic Variables.

Variable	Mean	Range
CO ($Lmin^{-1}$)	6.4	4.4-8.4
CO ($Lmin^{-1}m^{-2}$)	3.5	2.5-4.5
Systolic PAP (mmHg)	19	13-26
Diastolic PAP (mmHg)	10	6-16
Mean PAP (mmHg)	13	7-19
PCWP (mmHg)	9	5-13
RAP (mmHg)	5	1-9
PVR ($dyn.s^{-1}.cm^{-5}$)	55	11-99
PVR ($mmHg.L^{-1}.min^{-1}$)	0.7	0.1-1.2

CO, cardiac output; PAP, pulmonary artery pressure; PCWP, pulmonary capillary wedge pressure; PVR, pulmonary vascular resistance; RAP, right atrial pressure. Range is from mean -2 SD to mean +2 SD. Adapted from Kovacs *et al.*, 2009; Maggiorini *et al.*, 2001; Melot *et al.*, 1987; Naeije *et al.*, 1982.

1.2.2.2 Pulmonary Vascular Resistance

The French physicist Poiseuille first established that resistance (R) to flow, defined as a pressure drop (ΔP) to flow (Q) ratio, is equal to the product of the length (l) of a tube by a viscosity constant (η) divided by the product of fourth power of the internal radius (r) by π:

$$R = \frac{\Delta P}{Q} = \frac{8l\eta}{\pi r^4}$$

This equation illustrates that resistance is exquisitely sensitive to small changes in vessel calibre radius. Clinically pulmonary vascular resistance (PVR) is calculated by determining the mean pressure drop across the circulation to the pulmonary blood flow ratio using an equation analogous to Ohm's law:

$$PVR = \frac{MeanPAP(mmHg) - PCWP(mmHg)}{CO(L\min^{-1})}$$

In general terms, the normal resting PVR is 1.0 $mmHg.L^{-1}.min^{-1}$ (Wood's Unit) in supine adults and can be expressed in $dynes.sec.cm^{-5}$ by multiplying by 79.9.

Some clinician-scientists use the mean pulmonary diastolic pressure to determine the transpulmonary gradient and calculate PVR (Professor David Kilpatrick, 2009, Personal Communication). This approach has the advantage of ignoring systolic pulmonary pressure, which is principally determined by the properties of the proximal pulmonary circulation and right ventricular systolic function. Therefore, use of the pulmonary diastolic pressure better describes the functional status of the distal pulmonary circulation than use of the mean pulmonary arterial pressure. However, this technique is not useful for the diagnosis of isolated proximal pulmonary arterial obstructions where the pulse pressure may be elevated but the diastolic pressure is normal, as may occur with the clinical entity chronic thromboembolic pulmonary hypertension.

Approximately 60% of the total PVR is attributed to precapillary resistance, where the major site of resistance is in the small muscular arteries 100-1000 µm and arterioles < 100 µm (Fishman and Fisher, 1985; Peacock and Rubin, 2004).

The inherent assumption in PVR calculations is that the pulmonary artery pressure-flow (PAP/Q) relationship is linear and crosses the pressure axis at a value of PCWP, allowing PVR to be constant whatever the level of pressure and flow. However, PVR does not assess a fixed attribute of the pulmonary circulation and the value depends on the prevailing level of pressure, volume and flow within the pulmonary circulation. As the pulmonary circulation is highly distensible with the ability to recruit closed vessels, the relationship between pressure and flow is curvilinear and only linear across a limited range of physiological flows. Thus PVR is a flow-dependent variable and cannot be used to evaluate changes in pulmonary vascular tone at variable mean flow.

Furthermore, PVR increases at either extreme of lung inflation. At low levels of inflation the alveolar capillaries are closed, narrowed or kinked as a result of lung collapse, leading to high PVR. As the lung is inflated, resistance falls, due to gradual opening of alveolar vessels. As inflation increases further, high alveolar pressures, causes collapse of alveolar vessels and increases PVR (Culver and Butler, 1980; Fishman and Fisher, 1985).

Many models have been developed that integrate changes in resistance and compliance to describe the curvilinear pressure-flow relationship. Permutt *et al.* (1962) proposed a vascular waterfall model made of parallel collapsible vessels with a distribution of closing pressures. At low pulmonary flow many vessels are derecruited (Glazier *et al.*, 1969), that is closed in response to intrinsic vascular tone and surrounding alveolar pressure, thus generating a PAP/Q curve that is concave to the flow axis and intercepts the pressure axis at the lowest closing pressure that has to be overcome to generate flow. As inflow pressure and flow increases previously closed vessels are recruited and previously narrow vessels distend. With complete recruitment, without changing compliance, a linear PAP/Q relationship exists, with a pressure intercept representing the mean of all closing pressures. These mechanisms explain a progressive decrease in the PAP/Q slope with increasing flow or pressure and an increase in PAP/Q slope with a fall in flow or pressure, as the effective cross sectional area of pulmonary resistance vessels changes. Therefore, the PAP/Q relationship will only cross the pressure axis at the PCWP in well-oxygenated lungs in supine resting subjects where there is complete vascular recruitment and no change in compliance. Permutt *et al.* (1962) suggested resistance calculations could be made provided the effective outflow pressure of the pulmonary circulation (mean closing pressure) replaces any apparent downstream pressures (left atrial pressure/PCWP). However, the effective mean closing pressure is extremely difficult to determine clinically.

These findings mean that a single PVR measurement cannot reliably describe the functional state of the entire normal pulmonary circulation at variable flow. Therefore, the commonly held assumption that PVR can be used to detect a change in the overall calibre of the pulmonary resistance vessels is erroneous. Thus a change in calculated resistance does not imply the presence of active constriction or dilatation. The resistive properties of the pulmonary circulation are better described by measuring pulmonary vascular pressure at several levels of flow. However, it is challenging to alter flow without affecting vascular tone, but may be achieved with low-dose dobutamine (Abdel Kafi *et al.*, 1998). Exercise may lead to increased PAP/Q slopes in patients with cardiac or pulmonary disease due to vasoconstriction induced by hypoxia or sympathetic nervous system activation (Abdel Kafi *et al.*, 1998; Janicki *et al.*, 1985).

Whilst PVR correlates with the severity of pulmonary vascular disease in humans it has shown to be a poor independent predictor of prognosis (Sniderman and Fitchett, 1988). This relates to the fact that PVR does not reflect the entire afterload of the right ventricle. The pulsatile nature of pulmonary flow plays an important role in determining right ventricle afterload. It has been shown that the pulsatile components of pressure and flow constitute from one-third to one-half of the total hydraulic power that is transferred from the right ventricle to the pulmonary vascular bed (Milnor *et al.*, 1966).

1.2.2.3 Pulmonary Haemodynamics During Exercise

The pulmonary circulation receives the entire output of the right ventricle and through vascular recruitment and distensibility can accommodate large increases in cardiac output with only a minimal rise in pulmonary arterial pressure (PAP). Excellent haemodynamic studies demonstrate that with mild to moderate levels of exercise PAP and PCWP rise only minimally in healthy normal adults (Gurtner *et al.*, 1975; Holmgren *et al.*, 1960). With the onset of exercise, mean PAP rises by 3-5 mmHg with the systolic increase greater than the diastolic increase (Fishman and Fisher, 1985). As exercise increases cardiac output proportionally more than the transpulmonary gradient, PVR falls during exercise to remain below 1 Wood's Unit (Ekelund and Holmgren, 1967; Groves *et al.*, 1987; Gurtner *et al.*, 1975; Holmgren *et al.*, 1960; Wagner *et al.*, 1986).

Well-trained athletes have resting PAP within the same range as healthy normal adults, but high levels of exercise in these subjects raises PAP substantially more than normal adults. Athletes, who are able to raise their cardiac output to 25 $Lmin^{-1}$, may increase their PAP to 50 mmHg (Bevegard *et al.*, 1963). The rise in pulmonary pressures in highly trained athletes has been confirmed in non-invasive transthoracic echocardiographic studies (Bossone *et al.*, 1999b). However, as PCWP also rises to levels approaching 25 mmHg, the pressure gradient across the pulmonary vascular bed remains unchanged and the PVR falls to remain below 1 Wood's Unit during high levels of exercise (Bevegard *et al.*, 1963). It appears exercise induced pulmonary hypertension in well-trained athletes is explained by transmission of increased left-atrial pressure. Because the individual pulmonary pressure response to exercise is variable, the diagnosis of pulmonary hypertension based on a mean pulmonary artery pressure of > 30 mmHg during exercise has been removed from the current definition (Badesch *et al.*, 2009).

1.2.2.4 The Influence of Age on Resting and Exercise Pulmonary Haemodynamics

Mean pulmonary artery pressure rises minimally with age (Kovacs *et al.*, 2009) and cardiac output falls slightly (Peacock and Rubin, 2004), resulting in a PVR that increases slightly with age, but importantly remaining below 100 dyn.s.cm^{-5} or 1.2 Wood's Units in healthy elderly adults (Bevegard *et al.*, 1963; Granath *et al.*, 1964; Granath and Strandell, 1964; Holmgren *et al.*, 1960).

Despite mean pulmonary pressure rising more than their younger counterparts during exercise (Kovacs *et al.*, 2009; Mahjoub *et al.*, 2009), the PVR falls with exercise and remains below 1 Wood's Unit in healthy elderly subjects aged 61-83 years (Ekelund and Holmgren, 1967; Granath *et al.*, 1964).

Table 1-2. Resting Supine Pulmonary Haemodynamic Variables Stratified by Age.

Variables (mean + SE)	16-28 (Yrs)	61-83 (Yrs)
CO (Lmin^{-1})	7.6 ± 0.3	5.6 ± 0.3
Mean PAP (mmHg)	13 ± 1	16 ± 1
PCWP (mmHg)	8 ± 1	9 ± 1
PVR (Wood's Units)	0.68 ± 0.08	1.20 ± 0.09
PVR (dyn.s^{-1}cm^{-5})	54 ± 6	96 ± 7

CO, cardiac output; PAP, pulmonary artery pressure; PCWP, pulmonary capillary wedge pressure; PVR, pulmonary vascular resistance. Adapted from Ekelund and Holmgren, 1967; Granath *et al.*, 1964.

1.2.2.5 Passive Regulation of the Pulmonary Circulation

1.2.2.5.1 Left Atrial Pressure and Cardiac Output

An increase in cardiac output at a given left atrial pressure (LAP) increases PAP but decreases PVR because of variable combination of vascular recruitment and distension. An increase in LAP at a given flow is passively transmitted to an increase PAP in a less than one-for-one proportion, depending on the state of arterial distension and the presence or absence of a closing pressure higher than LAP (Melot *et al.*, 1995).

1.2.2.5.2 Lung Volume

When lung volumes increase above functional residual capacity the alveolar vessels exposed to alveolar pressures compress and resistance increases. In contrast the extra-alveolar vessels, which are exposed to interstitial pressure, demonstrate decreased resistance. The opposite effects are observed with a decrease in lung volume below functional residual capacity (Hughes *et al.*, 1968). A combination of alveolar and extra-alveolar resistances determines overall PVR.

With inspiration the main pulmonary arterial pressure falls by a few millimetres of mercury as a result of changes in systemic venous return, intrathoracic pressure and mechanical deformation of the vasculature bed. The rate and depth of breathing modifies the time lag between blood flow into and out of the lungs. For example, the left ventricular pressure falls with deep inspiration and increases after 2-3 seconds following commencement of expiration (Fishman and Fisher, 1985).

1.2.2.5.3 Gravity

Pulmonary blood flow increases from non-dependent to dependent regions at the lung base under the influence of gravity. The ultimate configuration of the alveolar wall and its contained vessels depends upon three prevailing pressures: arterial inflow pressure, venous return pressure and intra-alveolar air pressure. In the upright lung a distribution of arterial and venous pressures due to the effects of gravity have led to the description of three zones from apex to base related to the following pressure combinations (West *et al.*, 1964):

Zone 1 – alveolar pressure > arterial pressure > venous pressure
Zone 2 – arterial pressure > alveolar pressure > venous pressure
Zone 3 – arterial pressure > venous pressure > alveolar pressure

These are functional rather than true anatomical regions and shift according to the relative relationships between the alveolar, arterial and venous pressures.

In zone 1 blood perfusion is confined to the corner vessels (Rosenzweig *et al.*, 1970), while most septal vessels are closed. Blood flow is not sustained to the apices, where pulsatile arterial flow allows the pulmonary capillaries to be perfused only during systole (Fishman and Fisher, 1985). Zone 1 is extended in clinical situations of low flow or increased alveolar pressure such as during ventilation with positive end-expiratory pressure (Anthonisen and Milic-Emili, 1966; Bryan *et al.*, 1964).

In zone 2 the alveolar pressure is the effective closing pressure, and the PAP-alveolar pressure gradient drives flow. In zone 2 the apparent outflow pressure (pulmonary venous pressure) is irrelevant to flow. Therefore in this region, calculation of PVR is meaningless.

In zone 3 the venous pressure exceeds the flattening capabilities of the alveolar air pressure, and so capillary volume and compliance increases. Thus corner vessels are no longer recognizable as distinct vessels and the whole alveolar surface is perfused and available for gas exchange. In zone 3 the driving pressure for flow is the PAP-pulmonary venous pressure gradients. Lungs of recumbent healthy humans are normally completely in zone 3 conditions.

An additional zone 4 has been described by Hughes *et al.* (1968) in the most dependent region of the upright lung. Despite the increased intravascular pressure here, flow decreases and is thought to be due to increased compression of the extra-alveolar vessels because this region expands with reduced lung volume or with pulmonary oedema (Naeije, 2004).

1.2.2.6 Active Regulation of the Pulmonary Circulation

1.2.2.6.1 Hypoxia

The observation that pulmonary vascular tone and pressure increases with hypoxia was first reported by Von Euler and Liljestrand (1946). This mechanism is thought to improve arterial oxygenation by matching perfusion to alveolar ventilation. The response is universal in mammals and birds, but with considerable interspecies and inter-individual variation. In humans the response is modest but rapid, developing within seconds and is fully developed after 1-3 minutes, reversing in less than one minute (Fishman and Fisher, 1985).

The hypoxic-pulmonary pressor response is mainly caused by constriction of the small arterioles (Dawson *et al.*, 1979). Small pulmonary veins also constrict in response to hypoxia but do not usually contribute more than 20-30% of the increase in pulmonary vascular resistance (Hillier *et al.*, 1997). The vasoconstrictive action may develop in response to intra-alveolar or arterial hypoxaemia (Marshall and Marshall, 1983). The mechanism of hypoxic pulmonary vasoconstriction is incompletely understood, but hypoxia is thought to inhibit smooth muscle cell voltage-dependent potassium channels (this process is not endothelial dependant), resulting in membrane depolarisation, influx of calcium and cell shortening (Jabr *et al.*, 1997; Weir and Archer, 1995).

1.2.2.6.2 Mediators

Pulmonary vascular tone has been shown to be modulated by a number of endothelium-derived and circulating mediators in the normal and pathological circulation (Barnes and Liu, 1995). Endothelium-derived vasodilators include nitric oxide (mediated by cyclic-guanosine monophosphate), prostacyclin (mediated by cyclic-adenosine monophosphate) and endothelium-derived hyperpolarising factor. The major endothelium-derived vasoconstrictor is endothelin (Horgan *et al.*, 1991).

1.2.2.6.3 Autonomic Nervous System

Despite the pulmonary circulation being richly innervated by adrenergic, cholinergic and non-adrenergic non-cholinergic pathways, the autonomic nervous system appears to play only a minimal role in the control of pulmonary vascular tone. Most autonomic innervation is to the proximal pulmonary arterial tree suggesting a more important role in the modulation of proximal compliance (Barnes and Liu, 1995; Downing and Lee, 1980).

The pulmonary circulation appears to alter compliance of the large elastic arteries and the resistance of precapillary vessels such that capillary blood flow remains unchanged. Agents that decrease small artery calibres (and increase resistance) simultaneously stiffen the larger pulmonary arteries (capacitance vessels), leading to unaltered transmission of flow to the capillaries (Reuben, 1970; Reuben, 1971).

1.2.3 Impedance

The concept of pulmonary vascular resistance (PVR) remains a useful concept in the study of the pulmonary circulation but assumes a steady-flow haemodynamic system with laminar flow through thin, non-distensible circular tubes with a constant viscosity of blood. Clearly this is a gross approximation to the real situation in a complex circulatory system. PVR neglects the pulsatile nature of pulmonary flow, the vascular distensibility, the anomalous viscosity of blood, the inertia of fluid and vascular walls, the pulse-wave velocity, and reflected waves. For example, two different pathologies such as chronic thromboembolic pulmonary hypertension and idiopathic pulmonary hypertension may lead to elevated pulmonary pressures with the same mean pulmonary artery and pulmonary capillary wedge pressure, yet vastly different pulse pressures. These two conditions may have a similar PVR but entirely different pulsatile load on the right ventricle. Thus, PVR gives an incomplete description of the forces that oppose pulmonary arterial flow, which may be better described by pulmonary vascular impedance, a concept that is further developed below.

1.2.3.1 Distensibility

A key feature of the pulmonary circulation is that it is highly distensible or compliant (Reuben *et al.*, 1970a). The viscoelastic properties of the proximal pulmonary arteries allow for the conduction and storage of blood. The electrical analogy of compliance is capacitance and represents the volume distensibility that is the volume change per unit increase in pressure. A whole range of compliance values have been reported in living, post-mortem, low-pressure, high-pressure situations as well amongst different ages in humans. This range from 0.7 $ml.mmHg^{-1}$ to 5.7 $ml.mmHg^{-1}$ (Harris and Heath, 1962) makes it difficult to provide an exact meaningful number for all situations. At normal levels of pulmonary pressure, the pressure-volume curve is approximately linear (like pressure-flow curves) but is non-linear at low driving pressures. Additionally this pressure-volume relationship is sensitive to the pressure history, that is displays hysteresis (Beck and Hildebrandt, 1983).

As pulmonary pressures are low, the application of Laplace's Law (tension = distending pressure × radius) indicates a low average pulmonary arterial wall tension of 30 000 $dynes.cm^{-1}$ (30 Nm^{-1}) compared to an aortic wall tension of 200 000 $dynes.cm^{-1}$ (200 Nm^{-1}) according to Harris and Heath (1962). The forces opposing wall tension include: passive resistance to stretch resulting from elastic fibres, collagen and muscular tissue, active smooth muscle constriction, and surface tension between endothelium and blood, which is probably more important in capillaries than in larger blood vessels. To resist unnecessary elongation of arteries during systole, these vessels are more extensible in the short axis than in the long axis. Due to the combinations of elastic and collagen fibres in the vessel wall, the length-tension relationship is not linear and the vessel walls become less extensible the more they are stretched. Blood vessels also experience viscous resistance to stretch. When a blood vessel is distended the various fibres exert a frictional force upon each other and this resistance is dependent on time, such that the faster the expansion the greater the friction. Whilst this has been demonstrated to occur in the aorta, in animal pulmonary arteries the magnitude of this force is minimal (Harris and Heath, 1962).

It is difficult to partition the total pulmonary vascular compliance, with some believing most compliance is in the larger pulmonary arteries (Shoukas, 1975) and others believing that most compliance is in the microcirculation (Gan and Yen, 1994; Vreim and Staub, 1973).

The effect of distensibility is to dissociate the phases of pressure and flow curves so that flow precedes pressure (Harris and Heath, 1962). When arterial walls are stiff they are less distensible and the greater the amplitude of a pressure wave will be for a given flow wave. The capacitative reactance (X_c) is the opposition to the motion of blood that distensibility provides. Hence the capacitative reactance varies inversely with the capacitance (C). Additionally, a high frequency wave of flow produces a smaller change in pressure than a slow sinusoidal wave of flow, so capacitative reactance varies inversely with the pulse frequency (f). Hence:

$$X_c = \frac{1}{2\pi fC}$$

Capacitative reactance (X_c) and resistance (R) are both measures of forces that oppose the motion of blood, but they have a different timing and dimension as a result of the phase angle introduced by distensibility. As these forces are 90° out of phase, it is not possible to add them together and they have to be represented as vectors at right angles to each other. The resultant vector has a phase angle and a magnitude that is the hypotenuse (Z). This is known as the impedance, which from Pythagoras's theorem is:

$$Z = \sqrt{R^2 + X_c^2}$$

$$Z = \sqrt{R^2 + \left(\frac{1}{2\pi fC}\right)^2}$$

When resistance is zero, the phase angle of a pure capacitance is -90°. With increasing resistance the phase angle diminishes.

1.2.3.2 Inertia

Blood provides a viscous resistance to flow and shifting this mass of blood introduces forces of inertia (I), which oppose movement, called inertial reactance (X_I). This force is proportional to the change in velocity and mass of the blood. In a system of pure inertial reactance, at the instantaneous onset of flow and greatest acceleration of blood, inertia and hence pressure is at a maximum. The consequence in such a system is that pressure leads flow.

X_I varies proportionally with the mass of blood (m) and the frequency of the pulsation (f), such that high frequency changes in flow increase inertia much more than low frequency changes.

$$X_I = 2\pi fm$$

X_I is represented at right angles to R, but is in the opposite direction to the capacitative reactance, as the two forms of reactance are 180° out of phase. The hypotenuse (Z) represents impedance with a magnitude of:

$$Z = \sqrt{R^2 + X_I^2}$$

$$Z = \sqrt{R^2 + (2\pi fm)^2}$$

Z has a phase angle and when resistance is zero the phase angle is +90°.

1.2.3.3 Distensibility and Inertia

In a system comprising distensibility and inertia the reactances due to distensibility and inertia act in opposite directions such that the resultant reactance is:

$$X = X_I - X_C = 2\pi fm - \frac{1}{2\pi f C}$$

The combined impedance is:

$$Z = \sqrt{R^2 + \left(2\pi fm - \frac{1}{2\pi fC}\right)^2}$$

The relative magnitude of capacitative and inertial reactance determines if the flow wave precedes or follows the pressure wave.

The combination of the forces of distensibility, inertia and resistance are unlikely to occur in the same vascular region and are likely to spread throughout the pulmonary circulation in a complex fashion. The pressure and flow waves take time to travel to the distal circulation and may well be reflected back to alter the pressure and flow relationship.

1.2.3.4 Calculating Pulmonary Vascular Impedance

Pulmonary vascular impedance describes the ratio of oscillatory pressure to oscillatory flow and helps study the opposition to pulsatile as well as steady flow, thus giving insight into the characteristics of the pulmonary vasculature. Under pulsatile conditions the instantaneous relation between pressure and flow undergoes phasic variations as a result of distensibility and inertia in the system. All complex periodic waveforms can be explained in terms of simple sine and cosine waves by means of Fourier's Theorem (Attinger *et al.*, 1966; Fishman and Fisher, 1985; Nichols *et al.*, 2005; Patel *et al.*, 1965):

$$y = a_0 + a_1\sin x + a_2\sin 2x + a_3\sin 3x + \ldots. + b_1\cos x + b_2\cos 2x + b_3\cos 3x + \ldots.$$

Here, a_0 represents the mean height of the wave. The term $a_1\sin x + b_1\cos x$ contains those components of the lowest frequency and is called the first harmonic. This is the basic frequency of the total wave (the heart rate). The term $a_2\sin 2x + b_2\cos 2x$ is called the second harmonic and so on. For all practical purposes the pressure and flow waves are adequately described by Fourier analysis to the sixth harmonic, which is 6 Hz for a heart rate of 60 min^{-1} or 15 Hz for a heart rate of 150 min^{-1}. Therefore, vascular impedance is a function of frequency and is expressed as a spectrum with the magnitude and phase of the impedance specified for various frequencies (Figure 1-1).

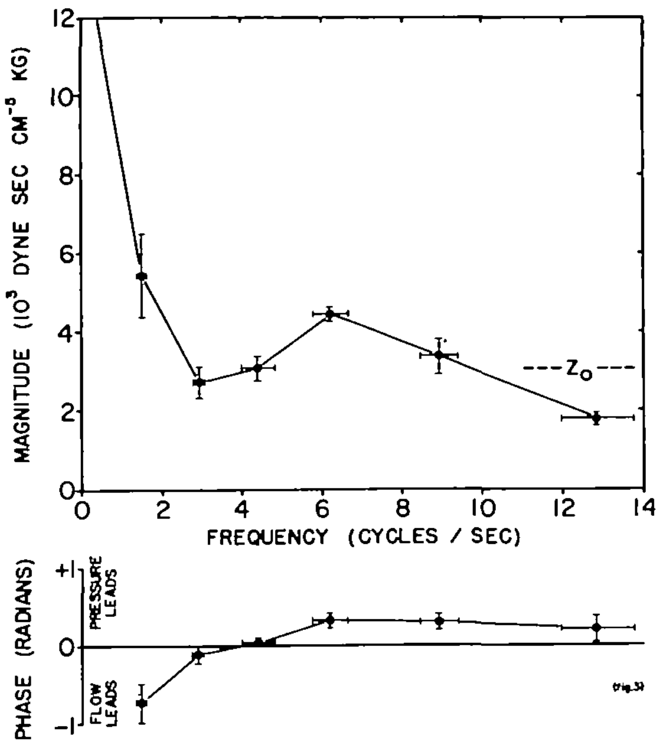

Figure 1-1. Example of pulmonary vascular impedance output from 13 dogs with information only in the frequency domain. From Bergel and Milnor (1965).

The usefulness of this application relies on the assumption the pulmonary circulation acts as a linear system, that is, a purely sinusoidal flow oscillation produces a purely sinusoidal pressure oscillation of the same frequency. In a linear system the impedance is independent of the shape and magnitude of the applied pressure pulse as long as the dimensions of the vascular bed, the physical properties of the blood vessels and the viscosity of blood remains constant. Bergel and Milnor (1965) demonstrated in dogs that the pulmonary circulation was linear within the limits of accuracy of the methods used.

Several types of vascular impedance can be calculated. Input impedance determines the pressure-flow relationship of the vascular bed beyond the point measured. Pulmonary vascular impedance at zero hertz (Z_0) is the ratio of mean pressure to mean velocity and corresponds to PVR. Characteristic impedance (Z_c) is the input impedance in the absence of wave reflection and determines the dimensions and elastic properties of the vascular walls. Z_c is calculated as the average pressure/flow ratio at the highest frequencies or as the linearized slope of the early systolic pulmonary artery pressure/flow relationship. Z_c is dependent on the ratio of inertia and compliance of the pulmonary circulation and can be approximated by the equation:

$$Z_c = \frac{(\rho / \pi r^4)}{\Delta \pi r^2 / \Delta P}$$

where ρ is the density of blood, r the mean internal radius, $\rho/\pi r^4$ the inertance, and $\Delta\pi r^2/\Delta P$ the compliance of the pulmonary arterial tree.

The characteristic impedance may also be determined from the average value of the input impedance at high frequencies (Bergel and Milnor, 1965). The assumption being at higher frequencies there is increasing dissipation making it likely that reflected waves will be unimportant at higher harmonics. An average of higher harmonics is calculated as noise increases with increasing frequency.

The concept of impedance uses the relationship between pulsatile pressure and pulsatile flow to make inferences regarding the resistance and compliance of the pulmonary vascular bed as well as wave reflections. Whilst impedance better describes the forces that oppose right ventricular ejection than pulmonary vascular resistance it is still not a perfect model.

1.3 Waves and Wave Reflections

The wave nature of flow in arteries has long been recognised (Young, 1809). A wave is a propagated disturbance through a medium with an exchange between kinetic and potential energy without the need for net transport of material. An arterial wave involves simultaneous changes in pressure and flow and travels faster than the bulk flow velocity of blood. In arterial systems the waves are predominantly longitudinal waves where the displacement of the medium is parallel to the direction of wave propagation. Arterial waves travel much slower than in rigid tubes as a result of the distensibility of the arterial wall.

Physiologists have long been interested in the shape of the measured pressure and flow waveforms, which result from a complex, dynamic interaction between the mechanical properties of the ventricle and arteries. In healthy humans the pulmonary artery pressure and flow waves are well matched and superimposable yet, in patients with severe pulmonary hypertension, the morphology and synchrony change such that the pressure wave is characterized by a late systolic peak whilst the flow wave has a mid- to late-systolic deceleration (Nichols *et al.*, 2005).

It was Wetterer (1956) who first suggested that reflected waves from arterial bifurcations as well as the periphery accounted for differences in pressure and flow waves. He also suggested that reflected waves return sooner and are of higher amplitude when the peripheral resistance of the arterial tree is increased or compliance is reduced.

The theory of linear transmission lines used to describe wave travel in arteries (Jager *et al.*, 1965; Karakash, 1950) indicates that pressure and flow waves are reflected at all impedance changes such as bifurcations or tapering sections. Pressure and flow waves are only identical in a system without reflections, that is a system of infinite length or one terminating in matched impedance. The propagation of pressure and flow waves in the pulmonary vasculature depend on its architecture, viscoelastic properties of its walls, its distensibility and the motion and properties of blood (Fishman and Fisher, 1985). Indeed, experiments have demonstrated that right ventricular output decreases because of an increased afterload if, at any given resistance, pulmonary arterial compliance decreases and/or wave reflection increases (Elzinga *et al.*, 1980; Furuno *et al.*, 1991).

Investigations of wave travel and reflection may therefore serve as useful physiological markers of the status of the pulmonary circulation and for the detection of downstream vascular disease.

1.3.1 Wave Analysis Using Impedance Methods

Impedance calculations (Nichols *et al.*, 2005; Westerhof *et al.*, 1972) have enabled the separation of measured pressure and flow waves into forward-travelling (the initial or primary waves generated by the heart heading toward the periphery) and backward-travelling waves (those reflected from the periphery that return toward the heart). The mean flow and pressure terms are disregarded in this type of reflection analysis.

In a reflectionless tube the pressure-flow relation is given by the characteristic impedance (Z_c) of that tube. It holds for each harmonic that:

$$P/U = P_+/U_+ = P_i/U_i = Z_c \tag{1a}$$

Where P is measured pressure and U is measured flow; the subscript + pertains to forward and i to initial. The measured pressure and flow waves, when reflections are present, are the sum of forward (+) and backward (-) waves:

$$P = P_+ + P_- \tag{2}$$

$$U = U_+ + U_- \tag{3}$$

It holds for each harmonic that:

$$P_+/U_+ = Z_c \tag{1b}$$

and

$$P_-/U_- = -Z_c \tag{1c}$$

When reflections are present the ratio of harmonics of the measured pressure and flow waves gives the input impedance (Z_{in}) of the arterial tree:

$$P/U = (P_+ + P_-)/(U_+ + U_-) = Z_{in} \tag{4}$$

In the reflectionless situation ($P_- + U_- = 0$) the input impedance (Z_{in}) equals the characteristic impedance (Z_c).

The relation between forward and backward waves is given by the reflection coefficient (Γ) such that:

$$P_- = \Gamma P_+ \qquad (5)$$

$$U_- = \Gamma U_+ \qquad (6)$$

The reflection coefficient may be rewritten as an impedance relation (Karakash, 1950):

$$\Gamma = (Z_{in} - Z_c)/(Z_{in} + Z_c) \qquad (7)$$

Substitution and rearrangement of eq. (5) into eq. (2) and eq. (6) into eq. (3) gives:

$$P_+ = P/(1+ \Gamma) \qquad (8)$$

$$U_+ = U/(1- \Gamma) \qquad (9)$$

The Fourier components may now be separated into their forward components from eqs. (8) and (9) together with eq. (7) where the reflection coefficient for each harmonic is computed; as well as their backward components from eqs. (5) and (6).

The forward and backward waves may alternatively be expressed by (Hollander, 1998; Murgo *et al.*, 1981):

$$P_+ = (P + Z_c)/2$$

$$P_- = (P - Z_c)/2$$

$$U_+ = (U + P/Z_c)/2$$

$$U_- = (U - P/Z_c)/2$$

The input impedance as a function of frequency is determined by means of Fourier analysis of the measured pressure and flow waves (Patel *et al.*, 1965).

Addition of the individual harmonics leads to the generation of forward- and backward-travelling waves as a function of time. All waves are treated in the same manner and illustrated using forward pressure (Attinger *et al.*, 1966):

$$P_+(t) = \sum_{n=1}^{k} P_{+,n} \cos(n\omega t + \varphi_n)$$

where n is the harmonic number; $P_{+,n}$ indicates the modulus of the n^{th} harmonic for forward pressure and φ_n its phase-angle; $\omega = 2\pi f$ where f is the frequency of the first harmonic (heart rate); and k indicates the upper limit of summation.

Impedance analysis has proven to be a useful tool in the study of reflected waves. However, it does assume that the system is in a steady-state oscillation and that there is a linear relation between pressure and flow at each frequency. In addition, impedance analysis is carried out in the frequency domain (Figure 1-1), making it very difficult to relate features of the Fourier transform to specific times in the cardiac cycle. Hence, such techniques are not widely used by clinicians who can intuitively understand events in the time domain.

1.3.2 Wave Analysis Using the Method of Characteristics

An alternative time-domain analysis of wave propagation based on the method of characteristics solution of the one-dimensional conservation equations for flow in the arteries has been relatively recently developed (Parker and Jones, 1990; Parker *et al.*, 1988). This technique has its origins in the study of gas systems (Liepmann and Roshko, 1957) and allows the delineation of forward- and backward-travelling waves. Whilst the method of characteristics is a complex mathematical construct based on Riemann's invariant theory the result is surprisingly simple to use.

Any finite waveform can be described as the sum of successive incremental waves called "wavefronts", defined as infinitesimal changes in pressure and velocity (Liepmann and Roshko, 1957). The method of characteristics follows the propagation of infinitesimal waves in space and time without assumption of linearity or periodicity. The one-dimensional equations of flow in elastic tubes where viscous losses are negligible may be written (Lighthill, 1978; Skalak, 1972):

$$A_t + (UA)_z = 0$$

$$U_t + UU_z = -P_z/\rho$$

where A is the cross-sectional area, U and P are the spatially averaged velocity and pressure respectively, ρ is the density of the fluid, z is the distance along the tube, t is time, and subscripts denote partial differentiation. This assumes that viscous losses and flow out of the artery locally are negligible and that the velocity profile is uniform (Parker and Jones, 1990).

If the area of the tube depends only upon the instantaneous local pressure, A = A (P) then:

$$P_t + UP_z + \rho c^2 U_z = 0$$

$$U_t + 1/\rho P_z + UU_z = 0$$

where $c(P) = \sqrt{A/\rho(dA/dP)}$ is the wave speed, which in general is a function of the elastic properties of the arteries, such that a less compliant vessel will have a higher wave speed.

These equations are hyperbolic and, along the characteristic directions, $dz/dt = U \pm c$, reduce to the ordinary differential equations:

$$dU/dt \pm 1/\rho c dP/dt = 0$$

This can be solved in terms of Riemann functions as outlined by Parker and Jones (1990). Along characteristic directions the flow is steady and the relationship between $dP_\pm$ and $dU_\pm$ follows from the conservation of mass and momentum:

$$dP_{\pm} = \pm \rho c dU_{\pm} \quad \text{(A)}$$

(water hammer equation; Ghidaoui *et al.*, 2005; Joukowski, 1898), where + refers to the forward- and – to the backward-travelling wavefronts. These equations give the general relation between the velocity and pressure across a wavefront and in a simple travelling wave (Parker *et al.*, 1988).

Now assuming a linear system where the changes in pressure and velocity associated with the waves are additive when they intersect:

$$dP = dP_{+} + dP_{-} \quad \text{(B)}$$

$$dU = dU_{+} + dU_{-} \quad \text{(C)}$$

It is possible to separate the measured P and U into forward- and backward-travelling components if the wave speed is constant using the water hammer equation:

$$dP_{\pm} = (dP \pm \rho c dU)/2 \quad \text{(D)}$$

$$dU_{\pm} = \pm (dP \pm \rho c dU)/2\rho c \quad \text{(E)}$$

Now the forward and backward waveforms (Figure 1-2) can be obtained by integrating the corresponding pressure and velocity differences according to:

$$P_{+} = P_{0} + \sum_{0}^{t} dP_{+}$$

$$P_{-} = \sum_{0}^{t} dP_{-}$$

$$U_{\pm} = \sum_{0}^{t} dU_{\pm}$$

where P_0 is the integration factor which is the initial undisturbed (diastolic) pressure, and t is the time of one cardiac cycle. The integration constant for velocity is often presumed to be zero as there is minimal flow during late diastole.

As required by the water hammer equations, the forward pressure and velocity are exactly alike with the scale factor ρc (Figure 1-2). Similarly the backward pressure and velocity are identical with the scale factor –ρc (Figure 1-2). For both pressure and velocity the forward and backward waves sum to give the measured waveform. This technique of separating the waves into forward and backward components gives results identical to those achieved by impedance methods, $Z_c = P/U = \rho c$ (Hollander, 1998; Van Den Wijngaard *et al.*, 2008; Westerhof *et al.*, 1972).

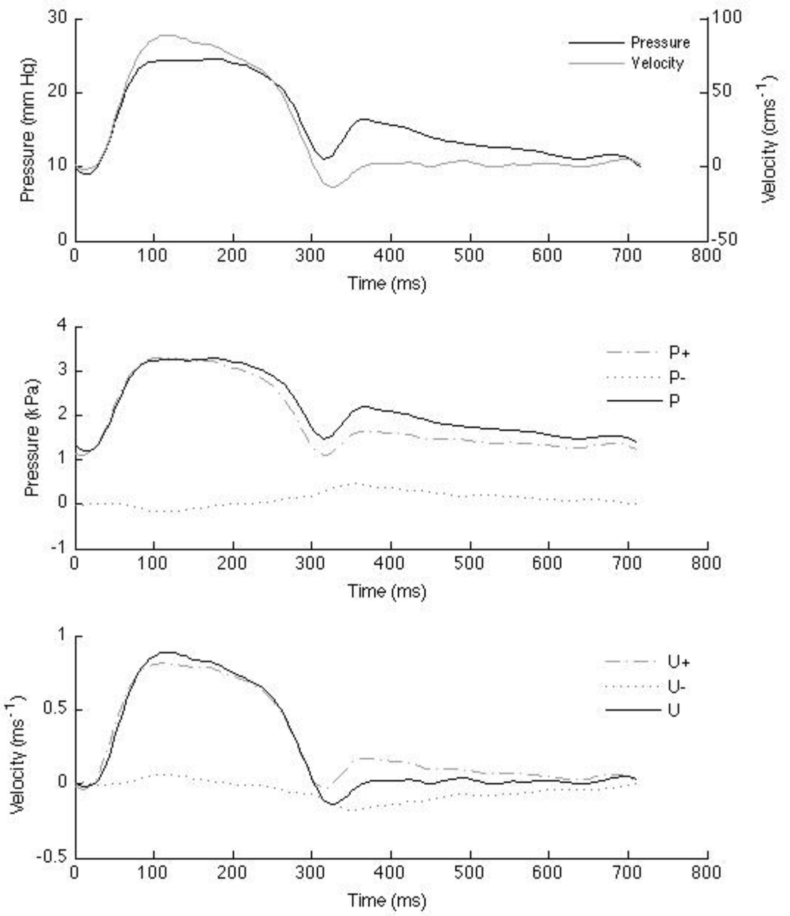

Figure 1-2. Measured pulmonary pressure (P) and velocity (U) separated into forward (+) and backward (-) components.

From the method of characteristics, a pertubation introduced into an artery will create changes in P and U which propagate as a wave with a speed U + c in the forward direction and speed U – c in the backward direction. U is the velocity of blood and c is the wave speed (the speed the wave would travel if blood velocity is zero). U is often less than c in arteries, allowing waves to travel in the backwards direction.

Wavefronts may travel forward toward the periphery, or backward toward the heart after reflection. Wavefronts with positive pressure changes ($dP > 0$) are called compression wavefronts and those with a negative pressure change ($dP < 0$) are called expansion wavefronts. Wavefronts associated with decreasing pressure are called expansion waves because the terminology has its origins in gas dynamics. This may be confusing terminology when applied to arterial dynamics, as an expansion wave implies an increase in arterial diameter (dilatation) when, in fact, an expansion wave decreases arterial diameter. Therefore it has been proposed that expansion waves should be called decompression waves (Hughes *et al.*, 2008; Sugawara *et al.*, 2009). Throughout this thesis the term expansion has been retained.

An increase in pressure (compression wavefront) can result in either acceleration or deceleration of blood, depending on the direction of travel (Table 1-3). A forward-travelling compression wavefront will accelerate blood velocity (Figure 1-3) whilst a backward-travelling compression wavefront will decelerate blood velocity. The opposite pattern is seen with decreasing pressure (expansion wavefront), such that a forward-travelling expansion wavefront decelerates flow and a backward-travelling expansion wavefront will accelerate flow (Figure 1-4).

Table 1-3. Origin and Nature of Waves.

Pressure	Velocity	Wavefront	Wave Origin	Wave Nature
↑	↑	Compression	Proximal (Forwards)	Accelerating
↑	↓	Compression	Distal (Backwards)	Decelerating
↓	↑	Expansion	Distal (Backwards)	Accelerating
↓	↓	Expansion	Proximal (Forwards)	Decelerating

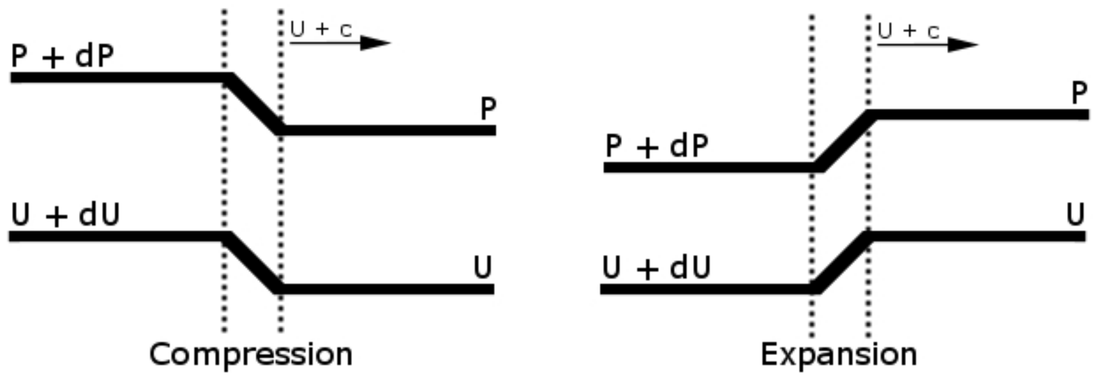

Figure 1-3. Pressure (P) and velocity (U) changes associated with forward compression and expansion wavefronts. Adapted from Jones *et al.*, 1992.

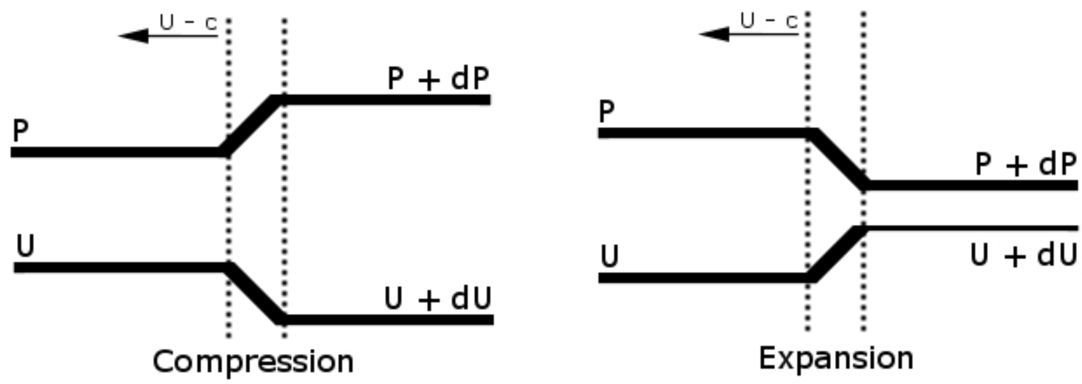

Figure 1-4. Pressure (P) and velocity (U) changes associated with backward compression and expansion wavefronts. Adapted from Jones *et al.*, 1992.

1.3.3 Wave Intensity Analysis

Net wave intensity (dI) is simply defined as (Parker and Jones, 1990):

$$dI = dPdU$$

where dP is the change of pressure across a wavefront and dU is the change in velocity across the wavefront. The net wave intensity can be determined without the knowledge of wave speed and wave separation. Wave intensity can be determined at any site in the circulatory system. The product dPdU represents the rate of energy flux per unit area (W/m^2) associated with the wavefront.

From Equation A above it follows that:

$dP_+ = \rho c dU_+$

and $dP_- = \rho c dU_-$

Hence substituting into Equations B & C above gives:

$dPdU = (dP_+ + dP_-)(dP_+/\rho c + dP_-/\rho c)$

which may be rewritten:

$dPdU = (dP_+^2 - dP_-^2)/\rho c$

Here, forward-travelling wavefronts, both compression and expansion, make a positive contribution to this product while backward-travelling wavefronts make a negative contribution. Thus wave intensity indicates the net magnitude and direction of the wavefronts at any given time (Figure 1-5). Wave intensity may be zero if there are either no wavefronts present or equal magnitude forward and backward wavefronts.

Importantly, with knowledge of the wave speed, the forward (I_+) and backward (I_-) wave intensity for the separated waves can be determined (Figure 1-5):

$dI_+ = + (dP + \rho c dU)^2/4\rho c$

$dI_- = - (dP - \rho c dU)^2/4\rho c$

The following notation now expresses these relationships:

$dI_\pm = \pm (dP \pm \rho c dU)^2/4\rho c$

The separated wave intensity has units of W/m^2 and for each wave can be integrated over time to give the wave energy $I_\pm$, which has units of J/m^2:

$$I_\pm = \int_0^T dI_\pm dt$$

where T is the duration of one cycle.

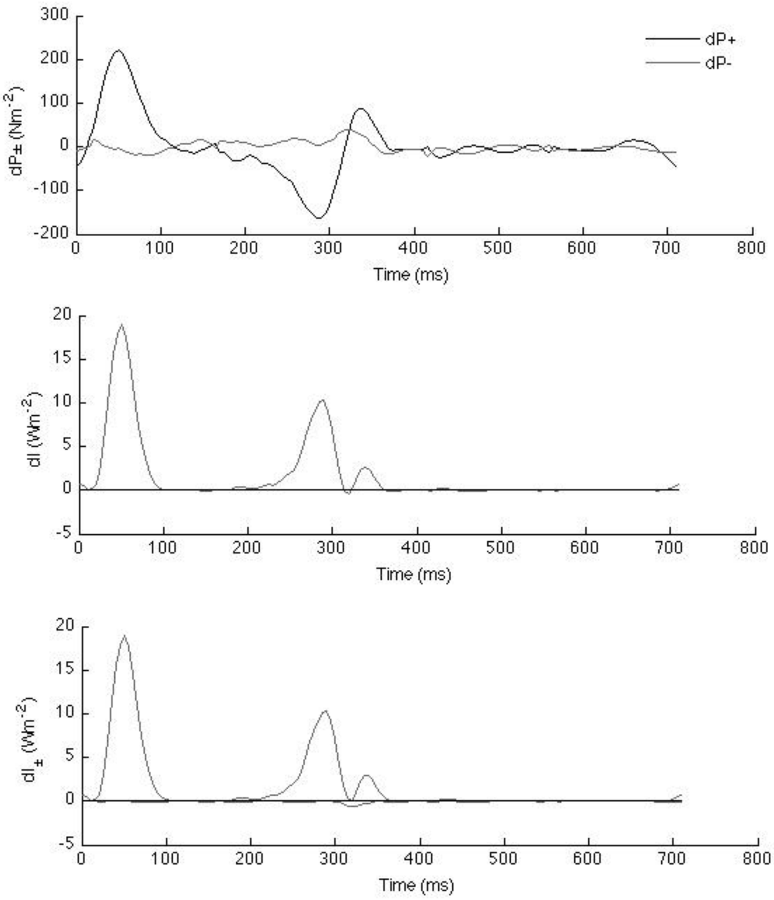

Figure 1-5. The top panel shows the change in forward pressure (dP+) and backward pressure (dP-) for the same pressure and velocity data shown in Figure 1-2. dP± > defines a compression wave and dP± < 0 defines an expansion wave. The middle panel shows the net wave intensity (dI) and the lower panel wave intensity separated into forward (dI_+) and backward (dI_-) components. Information remains in the time domain.

The above definition of wave intensity has the disadvantage that its magnitude depends upon the sampling interval over which dP and dU are measured, such that lower sampling frequencies result in greater intensity. However, qualitative changes in wave intensity are unaffected by the sampling interval. An alternative definition using time derivatives rather than differences overcomes this problem and allows data acquired at different sampling intervals to be compared directly (Ramsey and Sugawara, 1997):

dI'=(dP/dt)(dU/dt)

However, this results in complex units ($Wm^{-2}s^{-2}$) that are not direct measures of wave power and complicate the calculation of wave energy.

The calculation of dPdU does not include work done against the mean pressure and flow and so is not a measure of the total work done by the heart. Indeed, aortic peak wave intensity is approximately 30% of the calculated total hydraulic power per unit area (Khir *et al.*, 2001a). It does, however, provide an indication of the instantaneous working state of the heart under the influence of afterload by describing the rate at which work is done.

1.3.4 Wave Reflection

Waves are expected to be reflected wherever the properties of an artery change (mismatch in impedance), which may be a tapering or dilated vessel, a bifurcation, or distal differences in distensibility. If the impedances of daughter and parent vessels are well matched at a bifurcation then there is no wave reflection (Womersley, 1958). Impedances are well matched at bifurcations if the distensibility or cross sectional areas of daughter and parent vessels are equal (Womersley, 1958). Less distensible daughter vessels must have a greater combined cross sectional area than parent vessels for perfect matching.

If the cross sectional area of daughter vessels is significantly smaller than the parent vessel without a significant change in distensibility, then positive or closed-end reflection occurs. Here the phase of the reflected wave is unchanged from the incident wave such that an incident forward compression wave is reflected as a backward compression wave.

When the combined area of daughter vessels is very large or the daughter vessels are significantly more distensible than the parent vessel then negative or open-end reflection occurs. Here the phase of the reflected wave is reversed such that an incident forward compression wave is reflected as a backward expansion wave.

Assuming constant distensibility, the ideal area ratio of daughter-to-parent areas (A_R) such that no reflection occurs is between 1.1-1.2 (Nichols *et al.*, 2005; Wang, 1997). When A_R falls below 1.1 the magnitude of positive closed-end reflection increases. When A_R increases above 1.2 the magnitude of negative open-end reflection increases.

An index of wave reflection, R_c may be determined using impedance methods from the extent of the difference between input impedance at zero hertz, Z_0, and characteristic impedance, Z_c, (Naeije, 2004):

$$R_c = \frac{(1 - Z_c / Z_0)}{(1 + Z_c / Z_0)}$$

The problem with determining a reflection coefficient using impedance techniques is that it is a global coefficient determined at the point of measurement and does not allow us to distinguish the contribution that many individual backward waves from different reflection points may be making (Westerhof *et al.*, 1972).

A wave reflection coefficient may be easily determined in the time-domain from the separated backward and forward wave intensity as the ratio of the cumulative energy of a reflected (backward-travelling) wave to the cumulative energy of the incident (forward-travelling) wave (Hollander *et al.*, 2001). This differs from other definitions of reflection coefficient that use the ratio of pressures of the reflected and incident waves (Nichols *et al.*, 2005), but is a sensible and easy calculation with physiological meaning.

1.3.4.1 Estimating the Distance to a Reflection Site

1.3.4.1.1 Impedance Methods

It is possible to use impedance methods to determine the distance to reflection sites in arterial systems (Westerhof *et al.*, 1973). Here the first minimum in impedance modulus (first zero crossing of phase) represents the frequency at which the distance to the effective reflecting site corresponds to one-quarter of a wavelength.

Thus, distance = wavelength/4, where wavelength = wave speed/frequency. Another method uses the time delay between the separated forward and backward components of the pressure waveform (Van Den Bos *et al.*, 1976). The time from the initial pressure upstroke to the pressure inflection point may be assumed to be the time that a wave takes to run forward, be reflected and arrive back, and hence with knowledge of the wave speed the distance can be determined (Murgo *et al.*, 1980).

These methods can only predict the distance to a reflection site and not the amplitude or ratio of wave reflections. In addition they can only estimate a global or average reflection site and have no ability to distinguish multiple reflection sites. To overcome these issues, Pythoud et al. (1996b) developed a method involving the deconvolution of the backward pressure wave in the time domain allowing the most important reflection site locations and their amplitudes to be determined from the "reflection profile" (Pythoud *et al.*, 1996b). The accuracy of this model was limited by the poor resolution of the peaks, even in a situation of total occlusion, limiting its application to very proximal reflection sites.

1.3.4.1.2 Wave Intensity Methods

The separated backward wave intensity can be used to easily estimate the distance to multiple reflection sites. The onset of the separated backward wave intensity indicates the length of time (Δt) that it takes the forward wave to travel to the reflection site and arrive back to the measurement site. If the wave speed (c) is known, then the distance to the reflection site (L) can be calculated:

$L = c\Delta t/2$.

This has proven to be an accurate technique in elastic tubes with the calculated distance on average within 1.7 ± 4.6% of the true measured distance (Khir and Parker, 2002).

1.3.4.2 Determining Wave Speed (Pulse Wave Velocity)

There are many methods employed to calculate wave speed (c) and all have limitations as outlined below. As the separation of forward and backward waves using the wave intensity method is sensitive to the value of c used (Khir *et al.*, 2001b), accurate determination is critical.

1.3.4.2.1 Distensibility

Wave speed, c, can be expressed in terms of the elastic properties of the arteries:

$$c = \sqrt{\frac{Eh}{\rho 2R}}$$

In this Moens-Korteweg equation E is the elastic modulus, R the vessel radius, h wall thickness and ρ fluid density. Wave speed may alternatively be expressed in terms of the Bramwell-Hill equation:

$$c = \sqrt{A/\rho D}$$

where ρ is the density of blood, A is area, and D = (1/A)(dA/dP) is the distensibility of the arterial wall. As density is relatively constant it can be seen that stiff arteries with lower distensibility have higher wave speeds. Wave speed is also pressure dependent, varying nonlinearly with pressure as distension varies the cross-sectional area and wall thickness (Hisland and Anliker, 1973).

1.3.4.2.2 Foot-to-Foot

As it is difficult to determine the viscoelastic properties of the arteries, wave speed has traditionally been determined by the foot-to-foot methods (Mcdonald, 1968), where the time (Δt) it takes for a pulse wave to travel between two measurement sites of known separation (L) is measured, such that c = L/Δt. Pressure or velocity waves may be used and acquired simultaneously using pressure transducers, Doppler ultrasound, or applanation tonometry at peripheral sites. Alternatively, but perhaps less accurately, one transducer can be moved between two positions with subsequent gating to the R wave of the electrocardiogram. Although there are challenges in determining the foot of a wave, the foot alters less than the systolic peak or dicrotic notch as the wave propagates making it a more reliable measure. This technique is limited by the ability to accurately determine the foot of the wave and distances between acquisition sites, particularly within tortuous vessels.

1.3.4.2.3 Pressure-Velocity (PU) Loop Method

It is the local wave speed at the site of simultaneous pressure (P) and velocity (U) measurement, not the average speed over a distance, which is important for wave intensity analysis. Local wave speed can be determined from the water hammer equation, $dP_{\pm} = \pm \rho c dU_{\pm}$, using values in early systole where it is assumed there are only forward-travelling wavefronts and a linear relationship between the change in pressure (dP) and the change in velocity (dU). This is a reasonable assumption as there is minimal or no wave motion during late diastole (Dujardin *et al.*, 1982; Nichols *et al.*, 2005). By plotting P against U, the slope of the linear portion in early systole divided by blood density, ρ, will give c (slope = $dP/dU = \rho c$). This is the PU-loop method (Khir *et al.*, 2001b). Indeed, this method compares favourably to the traditional foot-to-foot method being on average 2.9 ± 0.8% slower in vitro (Khir and Parker, 2002). This technique has also been validated in vivo (Khir *et al.*, 2004). The PU-loop method is sensitive to the region of the curve used to determine the slope.

1.3.4.2.4 Sum of the Squares Technique

Wave speed may also be determined by a single-point technique (sum of the squares technique), developed principally to assess wave speed in coronary arteries and correlates well with foot-to-foot methods (Davies *et al.*, 2006b). In these arteries the PU-loop technique cannot be employed due to wave reflection in early systole. The single-point technique exploits the observation that an incorrect wave speed will result in self-cancelling forward and backward artefacts. Thus wave speed is determined by minimizing the total forward and backward wave intensity over at least one complete cardiac cycle, simplified to:

$$c = \frac{1}{\rho}\sqrt{\frac{\sum dP^2}{\sum dU^2}}$$

Here the sums are taken over an integer number of cardiac cycles. This technique is appropriate for long arteries but has been recently criticised and deemed inappropriate for estimating wave speed in the coronary circulation (Kolyva *et al.*, 2008). These authors showed that the single-point technique yielded erroneous changes in coronary wave speed induced by a proximal stenosis or distal vasodilatation and that their findings were better explained by a lumped reservoir model. The single-point technique can lead to erroneous results when measurements are performed very close to a large reflection site such that there is significant concurrence between forward and backward waves (Aguado-Sierra *et al.*, 2006). This appears to be a theoretical rather than practical limitation.

1.3.4.2.5 Characteristic Impedance

Characteristic impedance employs the average of the impedance moduli over a specified range of high frequencies for which it is assumed that wave reflections are negligible. Many frequency ranges have been used and there is no consensus range. In fact the value of characteristic impedance varies substantially with the selection of the frequency range (Aguado-Sierra *et al.*, 2006; Dujardin and Stone, 1981). The characteristic impedance = ρc when the input impedance is defined as P/U.

1.3.4.2.6 β Stiffness Parameter

The β stiffness parameter was developed to measure wave speed non-invasively using ultrasound techniques (Harada *et al.*, 2002). It relates the logarithm of the ratio of systolic (P) and diastolic pressure (P_0) to the relative changes in vessel diameter (D), $\ln(P/P_0) = \beta(D-D_0)/D_0$, where D_0 is the diastolic diameter. Wave speed can be calculated from the β stiffness parameter, $c = (\beta P/2\rho)^{1/2}$. However, wall tracking techniques are required, which are not widely available, and there is no consensus as to which layer should be tracked.

1.3.5 Advantages of Wave Intensity Analysis

Wave intensity analysis (WIA) has a number of advantages over impedance methods. Information remains in the time-domain, which makes it easier to relate events directly to time, unlike impedance methods where the sinusoidal waveforms only have a phase and frequency (Figure 1-1). As wavefronts are located in space and time, individual waves may be simultaneously identified allowing upstream or downstream events and their impact on the right ventricle to be determined and to be related directly to time, which is more intuitive to clinician-scientists than frequency domain analyses. WIA allows excellent resolution of forward- and backward-travelling waves enabling accurate determination of multiple reflection sites. This is in contrast to impedance methods that can only estimate a single global or average reflection site. Unlike impedance methods there is no assumption of linearity when calculating net wave intensity and no assumption of periodicity so WIA can be used on individual beats in real time, even during irregular arrhythmias. With impedance analysis an event that affects only systole will affect the Fourier components of all frequencies, this is not a problem for WIA. Furthermore, WIA can accommodate viscoelastic, convective and frictional effects (Khir and Parker, 2002) and allows the wave power, wave energy and the timing of waves to be easily quantified.

Whilst WIA requires a linear assumption for the separation of waves into their forward- and backward-travelling components, this does not introduce significant errors as shown by Pythoud (1996a). These authors proposed a nonlinear technique for wave separation, also based on the method of characteristics, but they found the difference between the linear and nonlinear techniques was in the order of 5-10% (Pythoud *et al.*, 1996a). Also, the accuracy with which we can measure flow is ±5% in vivo, which is the same order of magnitude of the friction and nonlinear corrections (Pythoud *et al.*, 1996a). Thus, the nonlinear method is unlikely to warrant the extra mathematical work required.

WIA also has benefits over another time-domain method, called the augmentation index, to quantify the magnitude of reflected waves. The augmentation index depends upon detecting a change in the shape of the pressure waveform, which is presumed to represent arrival of a reflected wave (Murgo *et al.*, 1980; Nichols, 2005). The accuracy of this technique relies on the ability to detect an inflection point or shoulder on the pressure waveform, which is not always obvious (Khir *et al.*, 2007; Westerhof *et al.*, 2006). Analysis of wave reflection should always ideally involve techniques based on simultaneous measurement of pressure and flow, rather than on pressure waveform analysis alone (Segers *et al.*, 2007), which suits WIA.

1.3.6 Studies Utilising Wave Intensity Analysis

A wave-intensity analysis (WIA) of forward and backward wave travel has proven to be an effective research tool, quantifying the amplitude and direction of energy transfer in the aorta (Jones *et al.*, 1992; Jones and Sugawara, 1993; Jones *et al.*, 2002; Khir and Parker, 2005; Koh *et al.*, 1998; Penny *et al.*, 2008), coronaries (Davies *et al.*, 2006a; Sun *et al.*, 2000; Sun *et al.*, 2004), other systemic arteries (Niki *et al.*, 2002; Niki *et al.*, 1999; Ohte *et al.*, 2003; Zambanini *et al.*, 2005) as well as the dog pulmonary circulation (Hollander *et al.*, 2004; Hollander *et al.*, 2001), foetal lamb pulmonary circulation (Smolich *et al.*, 2008), the venous circulation (Wang *et al.*, 2006), the chambers of the heart (Flewitt *et al.*, 2007; Hobson *et al.*, 2007; Lanoye *et al.*, 2005; Sun *et al.*, 2006; Wang *et al.*, 2005), and with intra-aortic counterpulsation balloons (Khir *et al.*, 2003). A detailed discussion of all of the wave intensity parameters in individual vascular beds is beyond the scope of this thesis. Most of this research has been conducted in one of three associated centres: Imperial College, London; University of Calgary, Canada; or The Heart Institute of Japan, Tokyo.

To perform WIA pressure and flow velocity data from the same measurement site are required. Ideally pressure and velocity should be simultaneously acquired, though it is possible to successfully use sequentially acquired data (Hughes *et al.*, 2008). In addition, it is possible to non-invasively determine wave intensity in some vessels such as the carotid artery using echocardiographic techniques (Niki *et al.*, 2002). Here, an echocardiographic tracking system measures carotid arterial diameter changes which correlate with the pressure waveform (Sugawara *et al.*,

2000) and are subsequently calibrated to a sphygmomanometer determined blood pressure. The blood velocity is determined using Doppler techniques. It would be extremely difficult to conduct WIA entirely non-invasively in the pulmonary artery as it can be difficult to image transthoracically and there are errors in determining pulmonary pressures by echocardiographic methods resulting in poor reproducibility.

1.3.7 The Reservoir-Wave Hypothesis

By dilating during systole, the pulmonary arteries act as a reservoir for blood, which is subsequently expelled during diastole. Hales in 1733 first described the cushioning effect of the arterial system to maintain nearly constant blood flow to the tissue. This reservoir function is important because if the arteries were rigid pressure changes would occur at the same time throughout the system, and the blood flow into the microcirculation would instantaneously match the blood flow out of the ventricle, such that there would be no blood flow during diastole. The reservoir function termed the arterial Windkessel was popularised by Otto Frank in 1899. He formalised a two-element Windkessel model consisting of a resistance and compliance element (Sagawa *et al.*, 1990), which is useful for diastole but fails to model systole accurately. The two-element Windkessel has been modified over years with the addition of characteristic impedance (three-element; Figure 1-6) and total arterial inertance (four-element), either in series or parallel, to the model to better predict systolic pressure. The fitting results improve with increasing model complexity, but the meaning of the parameters become less certain physiologically (Segers *et al.*, 2008; Westerhof *et al.*, 2009).

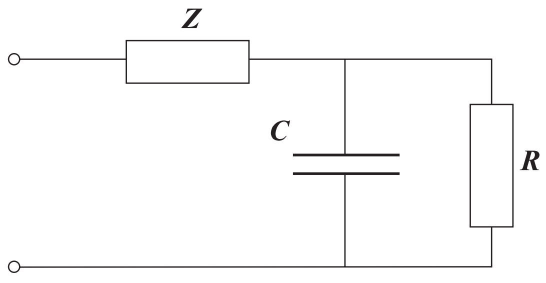

Figure 1-6. The three-element Windkessel model represented as an electrical circuit. R, resistance; C, pulmonary arterial compliance; Z, characteristic impedance.

Furthermore, forward and backward waves fail to explain the pressure and flow waveforms of diastole. This shortcoming of wave intensity analysis and the impedance approach to wave travel is illustrated in the $P_{\pm}$ and $U_{\pm}$ curves (Figure 1-2), such that during diastole unrealistically large, ever-expanding, self-cancelling values of U_{+} and U_{-} occur. During diastole $P_{\pm}$ declines regularly in the absence of measurable velocity, suggesting this is due to a Windkessel effect and not wave motion.

It is clear that not all changes in pressure are due to wave travel and that pressure may also change in response to alterations in volume in a compliant vessel. Consequently, a unifying reservoir-wave hypothesis was developed to better explain the pressure and flow waveforms (Wang *et al.*, 2003). Here the measured pressure is separated into a Windkessel (reservoir) pressure (P_{res}), which varies in time but is uniform throughout the arterial system, and an excess pressure (P_{ex}), which is a distance (x)- and time (t)-varying pressure, thought of as the pressure that drives waves:

$$P(x,t) = P_{res}(t) + P_{ex}(x,t)$$

The arterial reservoir pressure is proportional to the instantaneous blood volume. The reservoir charges when inflow exceeds outflow during systole and empties during diastole. The variation of reservoir pressure is determined by the difference between inflow and outflow and the change in volume:

$$\frac{dP_{res}(t)}{dt} = \frac{dP_{res}}{dV_{res}}\frac{dV_{res}(t)}{dt} = \frac{Q_{in}(t) - Q_{out}(t)}{C} \tag{1}$$

where $C = dV_{res}/dP_{res}$ and is the compliance of the whole arterial tree and assumed to be constant. The outflow may be described by a simple resistive relationship:

$$Q_{out}(t) = (P_{res}(t)-P_{\infty})/R.$$

Here the outflow is driven by the difference between P_{res} and the asymptotic pressure of the exponential decay (P_∞), at which point flow through the microcirculation is zero. R is the effective resistance of the peripheral circulation.

Substituting Q_{out} in terms of P_{res} and P_∞, into Equation 1 may be rewritten:

$$\frac{dP_{res}(t)}{dt} + \frac{P_{res}(t) - P_\infty}{RC} = \frac{Q_{in}(t)}{C} \tag{2}$$

And the general solution is:

$$P_{res}(t) - P_\infty = (P_0 - P_\infty)e^{\frac{-1}{RC}} + e^{\frac{-1}{RC}} \int_{t_0}^{t} \frac{Q_{in}(t')}{C} e^{\frac{t'}{RC}} dt' \tag{3}$$

in which t_0 and P_0 are the time and pressure at the onset of ejection. During diastole, when $Q_{in} = 0$, the solution is an exponential function, falling with the time constant, $\tau = RC$. To solve the equation R, C, and P_∞ are determined using experimental data. It is believed that waves are minimal during the last two-thirds of diastole; therefore measured pressure must approximate P_{res} during this time. P_∞ and τ can then be determined by fitting the late-diastolic pressure data to Equation 3. An alternative energy balance method for determining the Windkessel parameters that does not rely on initial values and iterations exists and is based on the conservation of mass and energy (Cappello *et al.*, 1995).

Once P_{res} is calculated, the excess pressure can be determined. When wave separation is performed on the excess pressure, the problem of physiologically meaningless self-cancelling waves during diastole has disappeared. The reservoir pressure accounts for the majority of the measured pressure during diastole and so the wave pressure is effectively zero during diastole. Any superimposed waves account for the high frequency changes to the pressure waveform.

The Windkessel is a lumped model of the arterial system and on its own cannot be used to study wave travel and reflection. The model is criticised for its implication that wave speed is infinite (Segers *et al.*, 2008) with pressure changes taking place simultaneously throughout the arterial tree. However, this criticism is only relevant if attempting to explain diastolic pressure decay in terms of wave theory (Wang *et al.*, 2003). Indeed, Wang (2003) elegantly showed that during late diastole (when wave motion is negligible) there are no measurable differences in pressure throughout the length of the aorta, indicating that pressure is a function of time only, not of distance. The reservoir-wave hypothesis is intriguing; allowing waves to travel on a time-varying Windkessel with more accurate wave separation during diastole. It has been used to successfully model aortic flow (Wang *et al.*, 2003) and the systemic venous circulation (Wang *et al.*, 2006). Wang (2003) showed that, in the absence of reflections, the aortic wave pressure (excess pressure) was proportional to the measured aortic flow; and the ratio of wave pressure to flow was numerically equivalent to characteristic impedance, thus demonstrating resistive behaviour.

The implications of the reservoir-wave hypothesis are still being investigated. There are no published data systematically studying the changes in wave intensity parameters that may occur when WIA is performed on the excess (wave) pressure. Therefore, there is no information on the incremental benefit achieved by this more complex reservoir-wave approach. Left ventricular filling has been investigated using WIA performed on the excess pressure, which excludes the influence of left ventricular compliance (Flewitt *et al.*, 2007). These authors demonstrated that once the Windkessel effects were removed from WIA, the energy of diastolic suction was 2.6 times greater. This implies that there may be value in considering reservoir effects prior to analysing wave motion.

1.4 Pulmonary Arterial Blood Flow

1.4.1 Pulmonary Pressure and Velocity Waveforms

Unlike the systemic pressure-velocity relationship, the pulmonary artery pressure and velocity curves are well matched (Fishman and Fisher, 1985; Figure 1-2). The pulmonary arterial pressure waveform normally displays a rapid rise to a rounded

peak during systole followed by a brief small incisura and a gradual decrease during diastole (Braunwald *et al.*, 1956). The flow waveform differs from the pressure waveform in that the incisura is lower than the foot of the wave. The pressure and flow waveforms match even as they propagate distally, suggesting that significant wave reflections do not occur in the proximal pulmonary circulation (Caro, 1978; Fishman and Fisher, 1985; Nichols *et al.*, 2005).
The mean blood velocity in the pulmonary trunk is similar to the aortic mean velocity, however, the peak pulmonary velocity of $0.7 ms^{-1}$ is lower than the aortic peak of $1.2 ms^{-1}$ (Caro, 1978) due to the larger diameter of the pulmonary trunk.

Characteristic changes to the pulmonary arterial flow pattern are observed when assessed non-invasively with pulsed Doppler techniques in patients with pulmonary hypertension. In these patients the peak ejection velocity is lower (related to pulmonary artery dilatation), a decrease in time to peak flow occurs, plus a concavity to the right or a notch in late systole is seen (Bossone *et al.*, 1999a; Dabestani *et al.*, 1987; Kitabatake *et al.*, 1983). As the velocity notching corresponds to augmentation of simultaneously acquired pulmonary pressure it may represent early wave reflection causing deceleration of flow (Kitabatake *et al.*, 1983). It is important to note however, that pulmonary flow notching has not been frequently observed in patients with pulmonary hypertension investigated with electromagnetic catheter techniques (Nichols *et al.*, 2005). Furthermore, the time to peak flow is heavily influenced by heart rate and cardiac output limiting its diagnostic ability for pulmonary hypertension.

Other studies have looked at the pressure waveform in patients with pulmonary hypertension and showed that those with chronic thromboembolic pulmonary hypertension had increased pressure augmentation and shortened time to the first inflection point than patients with idiopathic pulmonary hypertension as a result of earlier wave reflection from proximal obstructions (Castelain *et al.*, 2001; Nakayama *et al.*, 2001; Nakayama *et al.*, 1997).

1.4.2 Pulmonary Wave Speed

The human pulmonary arterial wave speed has been determined to be 1.8 ms^{-1} (Caro and Harrison, 1962; Gozna *et al.*, 1974; Milnor *et al.*, 1969) and in dogs around 2.5 ms^{-1} (Hollander *et al.*, 2001; O' Rourke and Milnor, 1971). These values are approximately half of that noted in the ascending aorta (Hollander, 1998; Khir *et al.*, 2001a; Koh *et al.*, 1998). Unlike the systemic circulation the pulmonary arterial wave speed does not seem to increase towards the periphery (Attinger, 1963). In humans the wave speed does not increase as dramatically with age as occurs in the systemic circulation (Gozna *et al.*, 1974). The wave speed increases markedly with distending pressure (Bargainer, 1967; Patel *et al.*, 1963). In fact in patients with pulmonary hypertension wave speed has been shown to increase to values of 4.8 ms^{-1} (Caro, 1978; Chen *et al.*, 1990; Kussmaul *et al.*, 1992; Milnor *et al.*, 1969; Reuben, 1970).

1.4.3 Normal Pulmonary Vascular Impedance

1.4.3.1 Dogs

The impedance modulus falls rapidly from its maximum at zero hertz (corresponding to pulmonary vascular resistance) to its first minimum at 2-3 Hz and increases again to a maximum at 5-6 Hz (Bergel and Milnor, 1965; Patel *et al.*, 1963). At low frequencies, the phase angle is negative, indicating that flow leads pressure (Figure 1-1). In the pulmonary circulation the characteristic impedance is half that of the aorta and acts as though there is a single site of reflection about 17 cm from the main pulmonary artery (Bargainer, 1967; Bergel and Milnor, 1965). This is considered to be an average value of multiple reflecting sites from the lung periphery. The global reflection coefficient was approximately 0.3, which is one-third that of the systemic circulation (Bergel and Milnor, 1965; Reuben *et al.*, 1971).

An increase in the magnitude of the pressure-flow ratio at all frequencies indicates a decreased pulmonary arterial distensibility (Elkins and Milnor, 1971; Nichols *et al.*, 2005). A shift of the first minimum and maximum to higher frequencies indicates an increased wave velocity or a change in the dominant reflection site (Bargainer, 1967; Bergel and Milnor, 1965; Reuben *et al.*, 1971; Van Den Bos *et al.*, 1982).

The spectrum of pulmonary vascular impedance is minimally affected by normal breathing (Murgo and Westerhof, 1984) or by disease processes that affect only the smallest pulmonary vessels (Furuno *et al.*, 1991; Pagnamenta *et al.*, 2000), thereby implying that impedance calculations are relatively insensitive to changes in the distal vasculature. In contrast the impedance spectra is significantly influenced by proximal pulmonary arterial obstruction (Elzinga *et al.*, 1980; Fitzpatrick and Grant, 1990).

Impedance calculations have been helpful in determining how energy expended by the right ventricle is partitioned. The oscillatory components comprise about one-third of total energy expended by the right ventricle and are dissipated principally in the large arteries. The steady-flow components are dissipated in the microcirculation, where resistance to blood flow is high (Milnor *et al.*, 1966). Most of the RV energy is spent overcoming the frictional resistance to blood flow and a small amount is used to distend arteries during systole. It has been shown that the right ventricle and its load are well matched such that pump efficiency is maximal (Piene and Sund, 1982).

1.4.3.2 Humans

Impedance patterns in healthy humans are similar to those in dogs (Chen *et al.*, 1990; Milnor *et al.*, 1969; Murgo and Westerhof, 1984). In patients with pulmonary hypertension secondary to left heart disease the modulus increased at all frequencies and the curve was shifted to the right, indicating increased characteristic impedance and wave speed (Chen *et al.*, 1990; Kussmaul *et al.*, 1992; Milnor *et al.*, 1969; Yin *et al.*, 1983). These findings are similar to results in animal experiments with serotonin infusion or pulmonary embolization (Bergel and Milnor, 1965; Van Den Bos *et al.*, 1982).

Kussmaul *et al.* (1988) showed that mean pulmonary pressure and characteristic impedance increased with exercise only in patients with ischaemic heart disease, suggesting exercise induced ischaemia increased the pulsatile load to the right ventricle and impaired the hydraulic efficiency of right ventricular-pulmonary artery coupling.

1.4.4 Pulmonary Arterial Wave Intensity

Wave travel and reflection has been well characterised utilising wave intensity analysis (WIA) in the human and dog proximal aorta. It shows a consistent pattern of wave intensity peaks with an early forward compression wave, closely followed by a smaller backward-travelling compression wave (reflected from the distal circulation), and then a forward-travelling expansion wave (Jones *et al.*, 2002; Khir *et al.*, 2001a; Khir *et al.*, 2004; Koh *et al.*, 1998; Macrae *et al.*, 1997). In comparison pulmonary arterial wave intensity has only been studied to a limited degree and there have been no human studies. Wave intensity analysis has been undertaken in the pulmonary arteries of dogs (Hollander, 1998; Hollander *et al.*, 2004; Hollander *et al.*, 2001) and the foetal pulmonary circulation of lambs (Smolich *et al.*, 2008). Smolich *et al.*'s work is not relevant to adult pulmonary studies but does highlight the excellent ability of wave intensity analysis to resolve backward running waves and provide important insights into right ventricular-pulmonary artery interactions. These authors showed that the mid-systolic fall in foetal pulmonary trunk blood flow was due to cyclical pulmonary vasoconstriction leading to a large backward compression wave.

Hollander's (1998) results showed that the forward wave travel in the pulmonary artery behaved like the aorta, though with much lower intensity, and differed principally in the pattern of wave reflection. She suggested that the proximal pulmonary artery behaves as a fixed open-end (negative) reflector such that the incident forward compression wave is reflected as a backwards expansion wave and the incident forward expansion wave is reflected as a backwards compression wave from a site approximately 3 cm downstream. The notion that the pulmonary artery behaves as an open-end reflector is supported by studies in lungs that demonstrate daughter-to-parent vessel ratios of 1.2-1.3 (Caro and Saffman, 1965; Collins and Maccario, 1979). There did not appear to be reflection from the distal circulation in Hollander's pivotal animal work. However, the consistent presence of an additional early systolic backward-travelling wave was left without explanation. Furthermore, there was no account of pressure-velocity signal delays and possible errors in the calculation of wave speed, thus raising the possibility that some of the reflected waves were enhanced or even artefacts. Therefore, wave reflection in the pulmonary vascular bed requires reinvestigation and perhaps reinterpretation.

There have been no studies investigating wave intensity parameters in the human pulmonary circulation, but may be a useful research tool to understand the integrated relationship between the right ventricle and pulmonary vascular bed in health and disease. The primary pathological change in idiopathic pulmonary arterial hypertension is remodelling and obliteration of the pulmonary arterioles less than 100 μm in diameter. WIA may demonstrate new or increased reflection from these sites, manifest as a backwards compression wave. The progressive increase in right ventricular afterload may lead to stiffening of the proximal pulmonary arteries resulting in increased wave speed and therefore earlier and enhanced wave reflection. Systolic right ventricular loading by early and accentuated reflected waves increases right ventricular work and may lead to right ventricular hypertrophy and ultimately right ventricular failure. Thus, prominent or early arrival of wave reflection may be an early marker of clinically important pulmonary hypertension. If so, the modification of wave reflection with medical therapy may become a rational therapeutic target. It is not known of course whether increased pulmonary arterial wave reflection is only present in severe pulmonary vascular disease and therefore is actually a late marker.

Chapter 2 Materials and Methods

2.1 Animal Methods

2.1.1 Experimental Animals

The experimental protocol was approved by the Animal Ethics Committee of the University of Tasmania (Project Number A0009700) and met the standards of the National Health and Medical Research Council of Australia (NHMRC) animal usage guidelines of replacement, refinement and reduction. All sheep were obtained from the University of Tasmania's animal farm at Cambridge, Tasmania.

Twenty-one healthy Polworth-Comeback cross sheep of either gender (10 male), weighing between 30 and 55 kg (average weight 41.1 ± 5.8 kg) were used for this study.

2.1.2 Animal Preparation and Instrumentation

A single animal was brought to our animal laboratory directly from the farm on the day of the procedure. They were fasted twelve hours prior to the procedure after placing in a fenced area. All sheep had the left jugular region cleared of wool and were anaesthetized with sodium pentobarbitone (Virbac Pty. Ltd., Peakhurst, Australia) 30 mg/kg-body weight injected intravenously via the cannulated jugular vein. Anaesthesia was maintained throughout the experiment with an intravenous infusion of sodium pentobarbitone at a maintenance dose of 3-8 mg/kg/hour. Blood pressure and heart rate levels monitored efficacy of anaesthesia. Each sheep had a tracheostomy performed and was subsequently ventilated using a mechanical ventilator (Engstrom Erica, Engstrom Medical, Sweden) with oxygen-enriched air at a tidal volume of 15 ml/kg and rate of 16-20 breaths/minute. On the basis of frequent arterial blood gas analysis (ABL800, Radiometer Medical, Copenhagen, Denmark) the ventilatory parameters and oxygen supplement were adjusted to maintain arterial O_2 tension at 100-120 mmHg and arterial CO_2 tension at 35-40 mmHg. Base deficits were corrected with sodium bicarbonate as required. Heating the surgical table with an electrical heater and draping blankets maintained body temperature. Normal saline 0.9% (Baxter Healthcare, Toongabbie, Australia) was infused through the jugular vein at a rate of 60 ml/hour for maintenance and boluses as required.

The animal was placed in the right lateral position and a left thoracotomy in the fourth intercostal space with removal of the 5th rib was performed. The pericardium was opened and the proximal portion of the main pulmonary artery was prepared for the probe of the ultrasound flow meter. Fat pads and adventitial tissue were dissected off and the vessel was separated from the aortic root by blunt dissection. The diameter of the main pulmonary artery in this region ranged from 18-29 mm; measured by encircling it with thread. Pulmonary arterial flow was measured using a suitably sized cuff-like transit-time ultrasound flow probe (Triton Technology Inc., San Diego, CA, USA) that was mounted around the proximal main pulmonary artery as near to the pulmonary valve as possible, usually 2-3 cm distal to it. This signal was filtered on-line at 100 Hz and converted to velocity using pulmonary arterial cross-sectional area (the external radius was estimated from the size of the flow probe used). A high-fidelity 7F micromanometer tipped catheter (Model SPC 771S, Millar Instruments Inc., Houston, TX, USA) was inserted antegrade through the wall of the pulmonary artery via a puncture wound just above the pulmonary valve, which was closed around the catheter with a purse-string suture if necessary. The pressure transducer was positioned as close as possible to the flow probe without interfering with either signal (usually 10 mm proximal from the flow probe, towards the pulmonary valve).

Left ventricular pressures were measured via a 6F fluid-filled pigtail catheter (Medtronic Inc., Minneapolis, MN, USA) passed retrograde across the aortic valve via the left carotid artery. Right ventricular pressures were measured via a 7F fluid-filled pigtail catheter (Medtronic Inc., Minneapolis, MN, USA) inserted antegrade across the tricuspid valve via the left jugular vein. Each ventricular pressure was measured via a pressure transducer (Statham P23ID, Statham Lab.

Inc., Puerto Rico) on a multichannel recorder (7D Polygraph, Grass Instrument Co., Quinsy, MA, USA). The systems were flushed with heparinised saline (10 I.U./mL) at appropriate intervals to maintain patency. The animal was also anti-coagulated with 5 000-10 000 I.U. of heparin (Hospira, Mulgrave, Australia) every four hours.

Electrocardiographic (ECG) leads were connected to both forelegs and the left hind leg, allowing a single ECG channel for timing of signals that was passed through a bio-amplifier (ML132, ADInstruments, Bella Vista, Australia).

At the end of the experiment, the animal was euthanized with an overdose of sodium pentobarbitone.

2.1.3 Data Acquisition

2.1.3.1 Signal Calibration

For the micromanometer in the pulmonary artery a calibration signal was sent from the pressure control unit (PCU-2000, Millar Instruments Inc., Houston, TX, USA) to the acquisition computer and was subsequently zeroed to atmospheric pressure at the level of the right atrium. The ultrasound flow probes were calibrated against the preset calibration signals of the flow meter, which were also sent to the acquisition computer. The fluid-filled catheters were calibrated to a mercury manometer and zeroed to atmospheric pressure at the level of the right atrium. Zero drift was checked at intervals.

2.1.3.2 Measurements

Haemodynamics were allowed to stabilise for approximately 30 minutes after completion of surgery or an intervention. Control and interventional haemodynamic recordings of 10-15 seconds duration were made with the ventilator off at end-expiration to control for the effects of respiration. All analogue signals were passed through anti-aliasing, low-pass filters with a cut-off frequency of 100 Hz and were then sampled at a frequency of 1 kHz using a MacLab 8S analogue-to-digital data acquisition system (ADInstruments, Bella Vista, Australia) interfaced with the programmable acquisition software LabChart Software v5.0 (AdInstruments, Bella Vista, Australia). A sampling frequency of 1 kHz was determined to allow suitable data collection at high heart rates anticipated with some medical interventions. The data were saved to a personal computer (Acer Veriton 5500G, Australia) as text files and subsequently analysed using customised and automated scripts prepared in Matlab R2008b (The Mathworks Inc., Natick, MA, USA).

2.1.3.3 Post Acquisition Signal Processing

As wave intensity analysis relies on the first derivative, which tends to magnify signal noise especially at high sampling frequencies, digital filtering was necessary. The pressure and velocity signals were filtered using a second-order 31-point Savitzky-Golay filter, which reduces signal noise with minimal influence on peak magnitudes and widths (Savitzky and Golay, 1964).

Ensemble averaging was not performed so that beat-to-beat variations could be understood. The high quality signals allowed individual beats to be analysed. Ensemble averaging has the advantages of removing random noise but requires determination of a fiducial point, which if not selected accurately and consistently leads to artificially smoothed pressure and velocity traces. Therefore, for each data set, the analysis was performed on four individual randomly selected beats, and the reversible interventions were repeated three times on each animal, such that the average result for each sheep intervention was over twelve beats.

2.1.4 Experimental Protocols

The sequence of interventions was varied from animal to animal, with the exception of autologous blood clot pulmonary embolization, which was always the final protocol given the irreversible nature of the intervention.

2.1.4.1 Determining Resting Pulmonary Artery and Aortic Wave Intensity Analysis

Pressure and velocity measurements in the resting animal were analysed in detail in 12 animals. In a single animal the flow probe was placed on the proximal descending aorta with simultaneous high-fidelity pressure measurements using the Millar catheter to allow comparison of aortic and pulmonary arterial wave intensity analysis.

2.1.4.2 Investigating the Influence of High Pulmonary Arterial Flow

2.1.4.2.1 Adenosine

In 6 animals increased pulmonary arterial flow was achieved with the vasodilator adenosine (Sigma-Aldrich, Castle Hill, Australia), administered intravenously at 200 $\mu kg^{-1} min^{-1}$ to determine the influence of increased flow on wave intensity analysis. Adenosine causes pulmonary vasodilatation via nitric-oxide dependant pathways (Konduri and Mital, 2000) and is rapidly reversible with an extremely short half-life of less than 10 seconds (Klabunde, 1983).

2.1.4.2.2 Volume Loading

Intravascular volume was expanded in 5 sheep by the administration of 1.5-2.0 L of intravenous normal saline 0.9% (Baxter Healthcare, Toongabbie, Australia) and the loading conditions were determined using left ventricular end-diastolic pressure (LVEDP). The increased volume load led to a substantial increase in pulmonary blood flow. The volume loading was reversed by diuresing with 40-80 mg of intravenous frusemide (Sandoz, Pyrmont, Australia).

2.1.4.3 Investigating the Influence of Increased Pulmonary Arterial Afterload

2.1.4.3.1 Hypoxia

Hypoxaemia was achieved in 8 animals by removing the supplemental oxygen source and increasing the inspired fraction of nitrogen (N_2) to 80%. A systemic partial pressure of oxygen (P_aO_2) < 40 mmHg was generally required to achieve an increase in mean pulmonary arterial pressure of 10 mmHg. The effects of hypoxia were rapidly reversible.

2.1.4.3.2 Pulmonary Emboli

Nine animals had their pulmonary arteries embolized with macro-emboli utilising autologous blood clot produced by a modification of the technique of Dalen *et al.* (1966). Prior to being anti-coagulated, 20 mL of blood was drawn from the jugular venous sheath and allowed to coagulate. The serum was then removed and the clotted blood was passed through a drawing-up needle via a syringe to generate small clots of 1-2 mm diameter and 2-5 mm length. These emboli would be expected to lodge in similar sized pulmonary arteries. Six millilitres of these autologous blood clots were injected via the jugular vein sheath to simulate pulmonary emboli. Sometimes the mean pulmonary pressure fell back towards baseline levels soon after embolization and further 3-6 mL aliquots were delivered until an approximate 10 mmHg stable increase in mean pulmonary artery pressure was achieved. Measurements were made after the pressures and heart rate were stable for at least 5 minutes.

2.1.4.3.3 Positive End-Expiratory Pressure (PEEP)

In 9 animals 20 cm H_2O PEEP was achieved by altering the ventilator controls.

2.1.4.3.4 Left Main Pulmonary Artery Clamping

In 8 animals the left main pulmonary artery was completely clamped by large forceps with rubberised tips to minimise trauma.

2.1.4.3.5 Left Main Pulmonary Artery Clamping Following Pulmonary Emboli

In 2 animals the left main pulmonary artery was clamped following the administration of autologous blood clot pulmonary emboli and the development of elevated pulmonary artery pressures.

2.1.4.3.6 Pulmonary Vein Clamping

In 5 animals clamping two of the four pulmonary veins with large atraumatic forceps was attempted.

2.1.4.4 Investigating the Influence of Progressive Microsphere Administration

In 4 animals 70-110 µm glass microspheres (Microspheres-Nanospheres, Cold Spring, NY, USA) were progressively delivered to the pulmonary circulation to explore the effects on wave intensity parameters. The mass of microspheres to be delivered were divided into two equal doses and suspended in normal saline, which was subsequently slowly injected (over 1-2 minutes) via two fixed 16 gauge cannulae into the left and right main pulmonary arteries, thus preventing delivery to only the dependant lung. The dosing schedule is shown in Table 2-1. Measurements were made after pressures and heart rate had maintained a stable value for three minutes, which generally occurred five minutes after the delivery of microspheres. Although there appeared to be little haemodynamic variation after 5 minutes a resting period of 30 minutes occurred between microsphere dosing to allow sufficient equilibration.

Table 2-1. Microsphere Dosing Schedule

70-110 µm Microsphere Dose	Mass (gm)	No. Beads ($\times 10^4$)	Cumulative No. Beads ($\times 10^4$)
M1	0.10	0.2	0.2
M2	0.25	0.5	0.7
M3	0.50	1.0	1.7
M4	0.75	1.5	3.2
M5	1.00	2.0	5.2
M6	1.00	2.0	7.2
M7	1.00	2.0	9.2
M8	1.00	2.0	11.2
M9	1.00	2.0	13.2
M10	1.00	2.0	15.2

No., number.

2.2 Human Methods

2.2.1 Human Subjects

The experimental protocol was approved by the Tasmanian Health and Medical Human Research Ethics Committee (Project Number H0010100) and met the standards outlined in the *National Statement on the Ethical Conduct of Human Research* (National Health and Medical Research Council of Australia, 2007).

Twenty-five volunteers (mean age 58 ± 14 years; 3 male) who were undergoing routine right heart catheterisation (RHC) for the investigation of unexplained dyspnoea agreed to participate in this research. The research protocol was discussed with the patient at the pre-assessment clinic and an information sheet was provided. All volunteers provided written consent. There were no adverse events to report.

2.2.2 Preparation and Instrumentation

All right heart catheterisation studies were undertaken in the Cardiac Catheterisation Laboratory of the Royal Hobart Hospital, Tasmania, Australia.

Patients were pre-medicated with 10 mg of oral diazepam or 1 mg of intravenous midazolam. 10 mL of 2% lignocaine was instilled around the right femoral vein and a 7-Fr sheath was inserted via the Seldinger technique into the right femoral vein. A 4-lumen 110 cm 7-Fr Swan-Ganz catheter (Edwards Lifesciences, Irvine, CA, USA) was floated to the right heart and resting measurements of right atrial, right ventricular, pulmonary arterial and pulmonary capillary wedge pressures (PCWP) were made at end-expiration utilising a pressure transducer (21BB ITL Healthcare, Chelsea Heights, Australia). This was zeroed to atmospheric pressure at the level of the right atrium. Zero drift was checked at intervals.

Cardiac output was determined by the thermodilution technique and the average of four consecutive values that varied less than 10% was used for calculations. The Swan-Ganz lumens were flushed with heparinised saline at appropriate intervals to maintain patency. Electrocardiographic (ECG) leads were connected to both arms and the left leg, allowing three ECG channels for timing of signals. All haemodynamic monitoring was recorded using a Horizon SE Haemodynamic System (Mennen Medical Ltd., Yavne, Israel) and subsequently analysed off-line.

Patients were categorised into four groups according to their mean pulmonary artery pressure (mPAP). Those with normal resting pulmonary haemodynamics (mPAP < 25 mmHg) were considered to have normal pulmonary vasculature (normal group). Those with mPAP ≥ 25-34 mmHg had mild pulmonary arterial hypertension (PAH). Those with mPAP ≥ 35-44 mmHg had moderate PAH and if mPAP ≥ 45 mmHg they were considered to have severe PAH. Patients with left heart disease (PCWP > 18 mmHg) were excluded from analysis.

2.2.3 Data Acquisition

2.2.3.1 Measurements

When the routine right heart study had been completed and left heart disease excluded, the Swan-Ganz catheter was positioned in the proximal main pulmonary artery and verified fluoroscopically. Proximal pulmonary artery blood velocity was measured using pulsed-wave Doppler gated to the location of the catheter tip via transthoracic echocardiography (Vivid-i, General Electric Ultrasound, Tirat Carmel, Israel). The optimal velocity profile was obtained through careful manipulation of the position of the probe (3SRS 2.5-5 MHz) and adjusting the velocity scale and intensity. When this was achieved ECG noise was generated by rapidly tapping the leads to use as a fiducial marker. The patient was then instructed to stop breathing at end-tidal volume to control for the effects of respiration and a 20 second recording of simultaneous pulmonary artery pressure and velocity was obtained.

2.2.3.2 Post Acquisition Signal Processing

The pulmonary artery pressure and ECG recordings were printed and scanned at a resolution of 600 d.p.i. These were subsequently digitised (DigitizeIt 1.5.8, Bormisoft, Germany) and the text files saved to a personal computer. The echocardiographic screenshots containing the Doppler velocity profile and ECG recording were exported as bitmaps and imported into Matlab R2008b (The Mathworks Inc., Natick, MA, USA) where all further analysis was performed using customised programs. A script was written to detect the edge of the Doppler velocity profile. Both the pressure and velocity waveforms were subsequently resampled at 200 Hz. As wave intensity analysis relies on the first derivative, which tends to magnify signal noise, the pressure and velocity signals were filtered using a first-order eleven-point Savitzky-Golay filter, which reduces signal noise with minimal influence on peak magnitudes and widths (Savitzky and Golay, 1964). The pressure waveforms were always of high quality. The velocity profiles were challenging to obtain and consistent edge detection was difficult, with significant random noise. For these reasons ensemble averaging of 20-25 velocity and pressure waveforms was performed using the ECG R wave as a fiducial marker.

2.3 Data Analysis

2.3.1 Wave Intensity Analysis

By convention the direction of wave travel was referenced to the direction of blood flow, such that waves arising from the right ventricle were defined as forward travelling and those arising from the pulmonary vasculature as backward travelling. Forward (dI_+) and backward (dI_-) wave intensity, normalised to the sampling interval, dt, (0.001s in animals; 0.005 in humans) was computed by:

$$dI_\pm = \pm (dP/dt \pm \rho c(dU/dt))^2/4\rho c$$

where dP and dU are respectively the pressure and velocity differences over one sampling interval, ρ is the density of blood assumed to be 1060 kgm^{-3} and c is wave speed (see 2.3.3).

In all figures dI_+ (forward-travelling wave) peaks are positive deflections and dI_- (backward-travelling or reflected wave) peaks are negative deflections. The pressure gradients across the forward- and backward-travelling waves were used to determine a wave's type, such that $dP > 0$ signifies a compression wave and $dP < 0$ signifies an expansion wave:

$$dP_+ = (dP + \rho c dU)/2$$
$$dP_- = (dP - \rho c dU)/2$$

In all figures the waves are shaded such that waves that increase forward flow (forward compression and backward expansion wave) are shaded black and those waves that reduce forward flow (forward expansion and backward compression wave) are shaded white.

For backward-travelling waves, the distance to the site of wave reflection was calculated as the product of wave speed and one-half of the time interval between the peak of the backward-travelling wave and the peak of the preceding incident forward-travelling wave. The magnitude of wave reflection was obtained from the reflection coefficient, defined as the ratio of the backward-travelling wave to the incident forward-travelling wave, with the reflection coefficient being negative (open-end) if the reflected wave changed type and positive (closed-end) if the type of wave remained the same.

2.3.2 Quantification of Waves

Peak wave intensities ($Wm^{-2}s^{-2}$) were determined by automated Matlab algorithms across individual cardiac cycles. The cumulative wave intensity was considered to be the wave energy and was calculated by integrating the wave intensity over the time period the wave occupied to give units of $Wm^{-2}s^{-1}$. The proportion of cumulative wave intensity was calculated by expressing the cumulative wave intensity of an individual wave as a percentage of total cumulative wave intensity in the cardiac cycle.

2.3.3 Wave Speed

Wave speed was determined using the single-point technique across complete cardiac cycles (Davies *et al.*, 2006b).

$$c = \frac{1}{\rho}\sqrt{\frac{\sum dP^2}{\sum dU^2}}$$

2.3.4 Pressure-Velocity Delays

Time lags between pressure and velocity data points may occur from hardware processing delays or differences in probe positioning (see Chapter 4). These were corrected prior to carrying out wave intensity analysis by generating pressure-velocity loops (PU-loops) and adjusting the timing of the signals, such that there was a straight line relationship in early systole, whose slope/ρ matched that of wave speed determined via the single-point technique.

2.3.5 Reservoir-Wave Analysis

Wave intensity analysis was reanalysed on some animal data using the excess pressure (P_{ex}), determined after the Windkessel or reservoir pressure (P_{res}) had been subtracted from the measured pressure (P); $P = P_{res} + P_{ex}$. This approach is discussed in detail in Section 1.3.7. The general solution used was:

$$P_{res}(t) - P_\infty = (P_0 - P_\infty)e^{\frac{-1}{RC}} + e^{\frac{-t}{RC}} \int_{t_0}^{t} \frac{Q_{in}(t')}{C} e^{\frac{t'}{RC}} dt'$$

where t_0 and P_0 are the time and pressure at the onset of ejection. During diastole when the flow in (Q_{in}) is zero, the solution is an exponential, falling with the time constant (τ) = RC, where R is the effective resistance of the pulmonary circulation and C is the compliance of the whole pulmonary tree.

The approach of Wang (2003) was adopted to fit the Windkessel to measured pulmonary arterial pressure by calculating the parameters of R, C and P_∞ iteratively using a nonlinear search algorithm to minimise the mean-squared error between the calculated P_{res} and the measured P over the last two-thirds of diastole. The minimisation is performed using the Matlab routine "fminsearch", which uses the Nelder-Mead simplex (direct search) method. As initial estimates, C = 1.0 mL.mmHg^{-1}, P_∞ = 15 mmHg, and R = 5 mm.HgL^{-1}.min^{-1} were used. The wave speed used to separate excess (wave) pressure into the forward and backward components was calculated on the measured pressure and velocity using the formula in Section 2.3.3.

2.4 Statistical Analysis

Statistical analyses were performed in Matlab R2008b (The Mathworks Inc., Natick, MA, USA). Continuous data are reported as mean ± one standard deviation. Effect sizes are given as a mean and a 95% confidence interval (CI) of the mean. Comparisons were made using Student's paired two-tailed t-tests. Comparisons between multiple groups were made using one-way analysis of variance (ANOVA). Values of $p < 0.05$ were considered significant.

Chapter 3 Resting Ovine Pulmonary Arterial Wave Intensity Analysis

3.1 Anticipated Wave Intensity in the Resting Pulmonary Artery

As the left and right ventricle serve similar purposes of blood ejection it is anticipated that the forward-travelling waves in the pulmonary artery behave in a similar fashion to the aorta with an early forward-travelling compression wave followed by a forward-travelling expansion wave. However, as the pulmonary artery is a low-pressure circuit with more rounded pressure and velocity waveforms (smaller pressure and velocity differentials) significantly lower wave intensities are expected. It is likely that the right ventricle and pulmonary artery are so well matched in terms of impedance that there will be minimal or no wave reflection in resting healthy animals when pressure-velocity signal delays have been properly accounted for.

3.2 Results

In the resting pulmonary arteries of twelve healthy sheep investigated, five predominant waves were identified over the cardiac cycle, with all of the forward- and backward-travelling waves having dissipated during diastole (Figure 3-1). The resting haemodynamic parameters are shown in Table 3-1. The normal pulmonary arterial wave speed was 2.1 ± 0.3 ms^{-1}. Whilst the peak intensity, timing, and cumulative wave intensity values of the individual waves varied between animals, when expressed as a proportion of total cumulative wave intensity less variation was manifest (Table 3-2).

Table 3-1. Resting Haemodynamic Parameters.

	Baseline (n = 12)
Heart Rate (min^{-1})	92 ± 7
Cardiac Output ($Lmin^{-1}$)	3.6 ± 0.9
Mean PA Pressure (mmHg)	15.6 ± 3.0
RVSP (mmHg)	25.7 ± 16.8
RVEDP (mmHg)	1.6 ± 4.3
LVSP (mmHg)	120.0 ± 14.0
LVEDP (mmHg)	5.6 ± 2.5
PVR (Wood's Units)	2.8 ± 1.6
PaO_2 (mmHg)	100 ± 2

Values are means ± standard deviation; LVEDP, left ventricular end diastolic pressure; LVSP, left ventricular systolic pressure; n, number of sheep; PA, pulmonary artery; PaO_2, systemic arterial partial pressure of oxygen; RVSP, right ventricle systolic pressure; RVEDP, right ventricular end diastolic pressure.

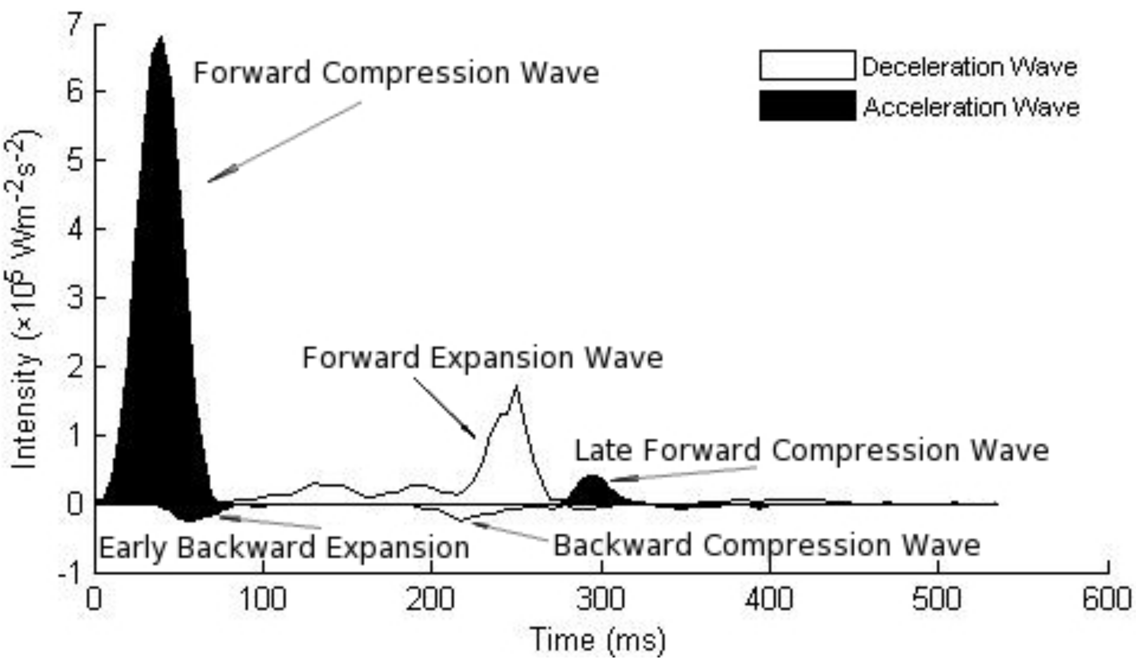

Figure 3-1. The typical pattern of wave intensity in the resting proximal pulmonary artery over a single cardiac cycle.
All wave intensity figures are shaded such that waves that accelerate forward flow (forward compression and backward expansion waves) are shaded black and those waves that decelerate forward flow (forward expansion and backward compression waves) are shaded white.

As wave intensity has been performed in the proximal pulmonary artery (PA), all waves originating from the right ventricle travel in the forward direction (positive wave intensity) and four distinct phases of right ventricular ejection were distinguished (Figure 3-1):

1. An early systolic compression wave accounting for acceleration of blood in the PA.
2. An intervening period of near zero intensity during mid-ejection, where there is no change in blood acceleration.
3. A late systolic expansion wave, that may develop slowly (resulting in a broad wave) and decelerates the blood volume ejected into the PA, occurred 208 ± 23 ms after the early compression wave.
4. A late systolic compression wave appeared 287 ± 31 ms after the early compression wave and 76 ± 23 ms after the late expansion wave.

Two backward-travelling waves (negative wave intensity) originating from the periphery were identified (Figure 3-1):

1. An early systolic expansion wave appeared 28 ± 8 ms after the forward-travelling compression wave, indicating open-end (negative) reflection from a site 2.9 ± 0.8cm downstream at a mean wave speed of 2.1 ms^{-1}. This wave enhances forward blood velocity.
2. A late systolic compression wave appeared 207 ± 43 ms after the forward-travelling compression wave, indicating closed-end (positive) reflection from a site 21.2 ± 4.4 cm downstream. This wave slows forward blood velocity.

Very little energy was carried by these backward-travelling waves illustrated by the low cumulative wave intensity (Table 3-2).

As the forward compression wave (dP+) was reflected back as an expansion wave (dP-), the wave reflection from this proximal reflector site (2.9 ± 0.8cm downstream) was negative; that is from an open-end source. The ratios of the cumulative wave intensities indicate that the reflection coefficient, R_c = -0.02 ± 0.02 (Table 3-2).

The forward compression wave (dP+) was also reflected back as a compression wave (dP+) from a closed-end source located 21.2 ± 4.4 cm downstream. The ratios of the cumulative wave intensities indicate that $R_c = 0.03 \pm 0.02$ (Table 3-2).

Aortic wave intensity was performed in the proximal descending aorta of one animal to allow comparison to the pulmonary arterial wave intensity (Table 3-2). The pulmonary arterial pressure and velocity waveforms are characteristically rounded compared to the more triangular systolic peaks of the aorta (Figure 3-2). The peak velocities are similar at approximately 85 cms^{-1}, but the mean aortic pressure is approximately 5 times greater and the aortic pulse pressure approximately 2 times greater. The forward wave intensity in the aorta was greater than in the pulmonary artery (Table 3-2) and the aortic wave speed was also much faster than pulmonary wave speed at 4.2 ms^{-1}. In comparison to the pulmonary artery, a single site of reflection arising 13 cm downstream was evident as a backward compression wave that arrived in the proximal aorta during mid-systole. This was a closed-end type of reflection with $R_c = 0.03$.

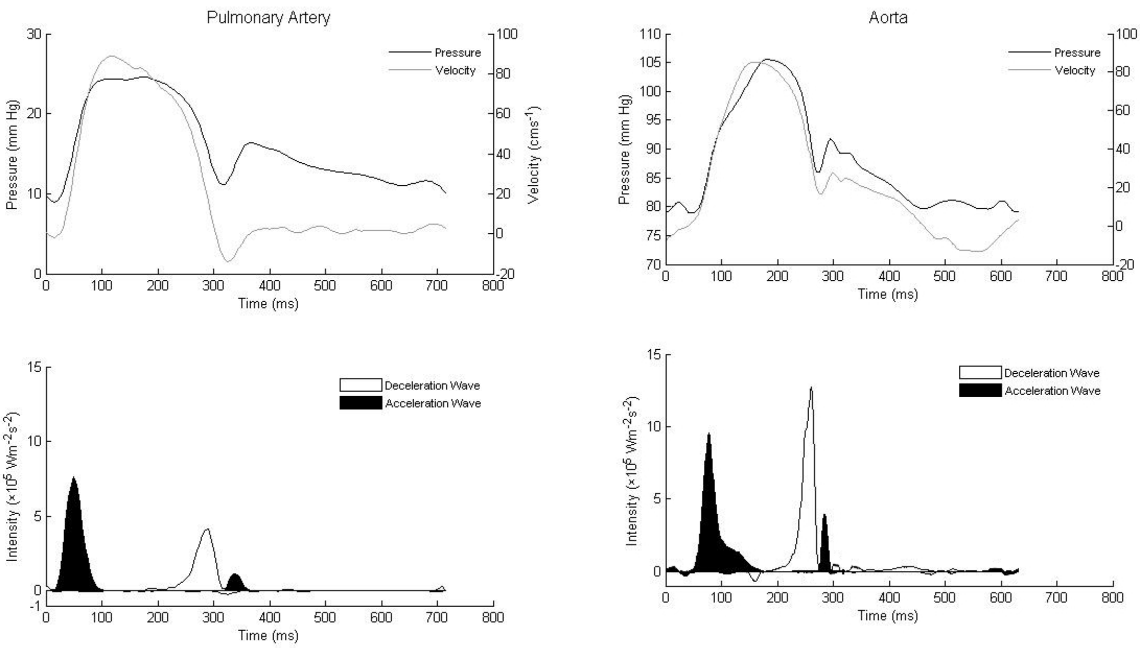

Figure 3-2. Wave intensity in the resting pulmonary artery and aorta with corresponding pressure and velocity traces.

Table 3-2. Resting Pulmonary Arterial and Aortic Wave Intensity Parameters

	Pulmonary Artery (n = 12)	**Aorta (n = 1)**
Peak Wave Intensity ($\times 10^4$ $Wm^{-2}s^{-2}$)		
Early Forward Compression	78.70 ± 43.25	95.85
Late Forward Expansion	23.14 ± 12.53	127.43
Late Forward Compression	3.25 ± 2.87	39.23
Early Backward Expansion	1.27 ± 1.49	-
Backward Compression	1.44 ± 1.11	-9.17
Cumulative Wave Intensity ($\times 10^2$ $Wm^{-2}s^{-1}$)		
Early Forward Compression	238.03 ± 108.03	311.78
Late Forward Expansion	117.17 ± 56.08	313.34
Late Forward Compression	9.20 ± 6.51	45.86
Early Backward Expansion	2.72 ± 3.38	-
Backward Compression	4.55 ± 3.43	13.56
Proportion of Cumulative Wave Intensity (%)		
Early Forward Compression	62.7 ± 10.0	45.6
Late Forward Expansion	31.6 ± 9.4	45.9
Late Forward Compression	3.2 ± 2.7	6.6
Early Backward Expansion	1.0 ± 1.2	-
Backward Compression	1.5 ± 1.3	1.9
Wave Speed (ms^{-1})	2.1 ± 0.3	4.2
Peak Blood Velocity (ms^{-1})	0.88 ± 0.01	0.84
Distance to Reflection Site (cm)		
Early Backward Expansion	2.9 ± 0.8	-
Late Backward Compression	21.2 ± 4.4	13.2
Reflection Coefficient		
BEW/FCW	-0.02 ± 0.02	-
BCW/FCW	0.03 ± 0.02	0.03

Values are means ± SD; BCW, backward compression wave; BEW, backward expansion wave; FCW, forward compression wave; LV, left ventricle; LVEDP, left ventricular end diastolic pressure; n, number of sheep; PA, pulmonary artery.

3.3 Discussion

The similar pattern of forward wave travel in both the pulmonary artery and aorta suggest that the left and right ventricles behave identically from a hydraulic point of view. In early systole the right ventricle generates a forward compression wave that accelerates the stroke volume to peak velocity and increases pulmonary pressure. During mid-systole there is a variable period of minimal wave travel, corresponding to the time that blood is moving under its own momentum (velocity remains constant) whilst the rate of ventricular myofibril shortening is unchanged. During late systole the rate of myofibril shortening slows and there is a reduction in pressure and velocity generation manifest as a forward-travelling expansion wave. The deceleration may develop slowly and then more rapidly, such that the forward-travelling wave has a broad or slowly increasing intensity that peaks in late systole. The forward expansion wave serves to decelerate the ejected volume of blood, which momentarily reverses and is reflected from the closed semilunar valves in the forward direction as a late systolic forward compression wave. During diastole all of the waves have dissipated.

The energy carried by these forward travelling waves in the aorta and pulmonary artery is clearly different. The low-pressure and highly compliant pulmonary circulation leads to rounded pressure and velocity waveforms and therefore smaller pressure and velocity differentials (dP and dU), resulting in lower wave intensity ($dI = dP \times dU$). Previously reported aortic wave intensity values vary greatly depending on the species and sampling interval used and range from 6-19 $\times 10^5$ $Wm^{-2}s^{-2}$ for the early forward compression wave and from 2.3-10.4 $\times 10^5$ $Wm^{-2}s^{-2}$ for the late systolic forward expansion wave (Hollander, 1998; Khir *et al.*, 2001a; Koh *et al.*, 1998; Parker *et al.*, 1988) when normalised to the sampling interval. It is possible to normalise the intensity to the sampling interval (convert Wm^{-2} to $Wm^{-2}s^{-2}$) by multiplying the intensity value by the sampling frequency in hertz squared. Previously reported peak intensity of the forward compression wave was 6.0×10^5 $Wm^{-2}s^{-2}$ and 4.4×10^5 $Wm^{-2}s^{-2}$ for the forward expansion wave in the pulmonary artery of dogs (Hollander, 1998), which compares favourably to the present results.

The greater intensities of the aortic waves reflect the greater hydraulic work conducted by the left ventricle to shift blood in the higher pressure and less compliant systemic circulation. The fact that the aorta is less compliant than the pulmonary artery is evident by the two-fold increase in aortic wave speed at 4.2 ms^{-1}. Characteristically the aortic forward expansion wave is of significantly lower amplitude than the forward compression wave, reflecting the greater hydraulic work required to accelerate the blood than to decelerate it. In the present series the single aortic measurement demonstrates a relatively larger forward expansion wave, which may result from taking the measurements at the end of a long experimental protocol when long duration of anaesthesia had occurred resulted in lower systemic blood pressures, perhaps from volume depletion and myocardial impairment.

The other major difference between the systemic and pulmonary circulations is in their pattern of wave reflection. The aorta demonstrates a single site of closed-end reflection where the forward compression wave is reflected in a positive manner as a backward-travelling compression wave that arrives during mid-systole, this serves to impair left ventricular emptying. This finding has been previously demonstrated (Hollander, 1998; Khir *et al.*, 2001a; Koh *et al.*, 1998; Parker *et al.*, 1988). The closed-end reflector arises 13 cm downstream from the measurement site, corresponding to a region below the diaphragm where aortic tapering has been previously reported (Nichols *et al.*, 2005).

The healthy pulmonary vasculature is characterised by minimal wave reflection indicating a well-matched right ventricular-pulmonary arterial system. Others have shown that the right ventricle is well-matched to its afterload (Piene and Sund, 1982). Indeed backward-travelling waves were not always present in the sheep. When present the backward waves do not carry substantial energy yet they may still be important physiological markers providing information about two different reflection sites and perhaps the status of the pulmonary circulation.

The first backward-travelling wave arises from a site 2.9 ± 0.8 cm downstream where it appears that the proximal pulmonary bifurcation behaves as an open-end reflector. Here the incident forward compression wave is reflected in a negative manner as a backward expansion wave, arriving in the proximal pulmonary artery in early systole. This wave would have a physiological benefit by aiding the ejection of blood from the right ventricle at a lower energy cost, a clear advantage during high pulmonary flow situations such as exercise. The presence of an early backward expansion wave implies that the cross sectional area of the left and right pulmonary arteries is greater than the main pulmonary trunk. This is contrary to the observations of Fry *et al.* (1962) where their combined area was 10% smaller. However, their calculations were made on pulmonary arterial casts in eight dogs and may not represent the in vivo geometry. The notion that the pulmonary artery behaves as an open-end reflector is supported, however, by studies in isolated perfused lungs that demonstrate a daughter-to-parent vessel area ratio of 1.2-1.3 (Caro and Saffman, 1965; Collins and Maccario, 1979), a ratio that leads to open-end reflection (Wang, 1997).

The second backward-travelling wave arises 21.2 ± 4.4 cm downstream, corresponding to a closed-end reflection site and arrives in the proximal pulmonary artery during late systole. Here the incident systolic forward compression wave is reflected in a positive manner as a late backward compression wave. The site of reflection is most likely from the peripheral microvasculature and is supported by measurements that demonstrate a total arterial length of 200 mm in the pulmonary circulation (Horsfield, 1978; Singhal *et al.*, 1973).

The reflective coefficients of both backward travelling waves are small. Only 2-3% of the incident wave energy is reflected backwards towards the right ventricle, again attesting to the notion that the right ventricle and pulmonary circulation are well matched in terms of impedance changes. Whilst these backward travelling or reflected waves carry little energy they may still bear physiological significance and perhaps could be used as markers of early pulmonary vascular disease. These ideas will be explored in later chapters.

The present results are partially in keeping with Hollander (2001) who also provided compelling evidence that the proximal pulmonary vasculature behaves as a fixed open-end reflector with the forward compression wave (FCW) reflected as a backward expansion wave (BEW) and the forward expansion wave (FEW) reflected as a backward compression wave (BCW). However, once the velocity time lag has been corrected for, a different interpretation of the findings is required based upon the following points:

1. The BCW did not invariably follow the FEW, suggesting that the open-end reflection is not fixed in time as Hollander (2001) implied and therefore the presence of a more distal reflection site likely exists.
2. The estimated distance to the reflection site was different for the two incident waves. If the FCW is reflected as a BEW the estimated distance to the reflection site is 2.6 ± 0.6 cm. If the FEW is reflected as a BCW the distance to the reflection site is 6.5 ± 3.9 cm. The estimated distances should be very similar if reflected from the same site.
3. The reflection coefficients were different for the two incident waves. It was 0.043 ± 0.025 for the BEW/FCW compared to 0.025 ± 0.034 for the BCW/FEW. The reflection coefficients should be more similar if reflected from the same site.
4. The late BCW was frequently broad suggesting a more widespread and spatially diverse reflection site, which is in keeping with reflection from the peripheral vasculature.
5. The late FCW is not followed by a late BEW.
6. During hypoxia (see Chapter 5) the BEW was maintained but a BCW did not follow the incident FEW.

These observations provide strong evidence that the open-end reflection is not fixed throughout the entire cardiac cycle. They also support the notion that the late BCW arises from closed-end reflection at the level of the terminal arterioles approximately 21 cm downstream. Open-end reflection may only be present during early systole because as blood is emptied into the reservoir-like pulmonary arteries the area ratio of daughter-to-parent vessels may fall to the theoretical value of 1.1-1.2 where no wave reflection occurs. In early systole, however, the area ratio may be greater than 1.2 allowing for open-end reflection. Indeed it is easy to understand that conformational changes of the pulmonary vasculature occur throughout the cardiac cycle when the dynamic activities of the heart and blood vessels are observed in the open-chest sheep.

The large standard deviations relative to the mean values for the reflection coefficient highlight the large range in the reflected wave intensity. Reflected waves are only a small proportion of the total wave energy at rest. This may suggest that there are significant energy losses as a result of damping during wave travel, but it is more likely that impedance is so well matched throughout the system that wave reflection is minimised. These data suggests only 2% of the incident forward compression energy is reflected as an early backward expansion wave and a further 3% as a late backward compression wave. These are significantly less than 20% reported by Hollander (1998, 2001). Interspecies variation may be an explanation as it has been recognised that wave reflections in dogs are less than in humans (Nichols *et al.*, 2005), therefore it is possible that there is greater spatial dispersion and less reflection in sheep. It is more likely, however, that Hollander not accounting for time delays in the pressure-velocity signals explains the differences. Indeed if WIA is performed without accounting for signal delays a BEW/FCW reflection coefficient of 0.24 is obtained which is in keeping with Hollander's measurements (see Chapter 4).

3.3.1 Limitations

Wave reflection may be different in anaesthetised animals. However, patterns of impedance in conscious, unanaesthetised dogs was similar to those in the anaesthetised open-chest preparation (Milnor *et al.*, 1966) suggesting our qualitative interpretation of wave reflection in sheep would not be altered. However, the use of anaesthetic agents that have negative inotropic effects and induce systemic vasodilatation may lead to quantitative changes. It is possible that wave speed and wave intensity are lower than in ambulatory animals.

Using a cuff-type flow probe may lead to errors in velocity determination if the velocity profile is not uniform across the vessel cross sectional area. However, it seems from experimental data in humans and dogs that the pulmonary arterial velocity profile is symmetrical (Caro, 1978; Reuben *et al.*, 1970b). The cuff-type flow probe may have constricted or minimised normal pulsatile distension, thus overestimating true pulmonary blood velocity, arterial pressure and wave speed, and therefore overestimating cumulative wave energies. The assumption was made that the pulmonary artery was circular and that the cross-sectional area of the vessel was constant throughout the cardiac cycle, which leads to minor but constant errors in blood velocity calculations. In addition it is not certain that wave speed is constant throughout the cardiac cycle.

The energy of wave travel is only a small part of the external work of the heart, which in turn is a fraction of the total energy expended by the heart. Therefore, whilst wave intensity analysis gives an idea of the working state of the heart as well as downstream vascular reflective conditions, conclusions cannot be drawn about the optimal working state of the heart, only optimal patterns of wave travel that minimise opposition to right ventricular ejection.

3.4 Conclusion

The normal pulmonary arterial wave speed in sheep is 2.1 ± 0.3 ms^{-1}. Wave reflection in the resting pulmonary arteries of sheep is minimal with only 2-3% of the incident wave energy reflected backwards, suggesting that impedance is tightly matched throughout the pulmonary vasculature. When present, two sites of wave reflection were identified. The main pulmonary bifurcation seems to behave as an open-end reflector during early systole, leading to the generation of a backward travelling expansion wave that would serve to enhance right ventricular emptying. The open-end reflector does not appear fixed throughout the entire cardiac cycle. The distal pulmonary microcirculation seems to behave as a closed-end reflector, leading to the generation of a late systolic compression wave. Although the intensities of these backward travelling waves are small they may serve as important physiological markers of early pulmonary vascular disease.

Chapter 4 Influences on Wave Intensity Analysis

During analysis of data collected for Chapter 3 it became apparent that manipulating the relationship between pressure and velocity could enhance or diminish the backward-travelling wave intensity and even create the presence of otherwise unexplained artificial waves. This chapter explores these sources of error in detail and emphasises the importance of accounting for these errors before wave intensity analysis (WIA) is undertaken.

4.1 Pressure-Velocity Signal Delays

When WIA is performed without adjustments to the pulmonary arterial pressure and velocity signal timing the same qualitative findings that Hollander (2001) reported in dogs are made (Figure 4-1). In the unadjusted analysis an early systolic backward compression wave precedes the systolic forward compression wave. This could not be adequately explained by wave reflection as all waves have dissipated in diastole (Khir *et al.*, 2001b; Nichols *et al.*, 2005). It is possible that retrograde transmission of pressure fluctuations from left atrial contraction could lead to this wave. This is plausible as it is recognised that pressure and flow pulses may be transmitted between the pulmonary artery and the left atrium (Collins and Maccario, 1979; Pinkerson, 1967; Wiener *et al.*, 1966). In our data the early backward compression wave arises 160 ms after the P wave and with a wave speed of 1.9ms^{-1} has travelled 32 cm, in another animal it was estimated to be 36 cm. This is in keeping with the estimated 34 cm length of the pulmonary vascular bed from cast studies (Horsfield, 1978; Horsfield and Gordon, 1981; Singhal *et al.*, 1973). Also, the transit time between the pulmonary artery and pulmonary veins is in the order of 80-160 ms (Hollander *et al.*, 2004; Pinkerson, 1967). However, clamping two of the four pulmonary veins did not dampen this wave and rapid right ventricular pacing did not alter the timing or appearance of this wave, suggesting that the very early systolic backward compression wave does not arise from left atrial activity. Perhaps the very early backward compression wave was an artefact of a constricting effect of the cuff-like flow probe on the pulmonary artery. However, this backward compression wave was detectable even when pressure was measured distal to the flow probe itself, raising the possibility that the early backward compression wave was indeed an artefact related to delays between the pressure-velocity signals.

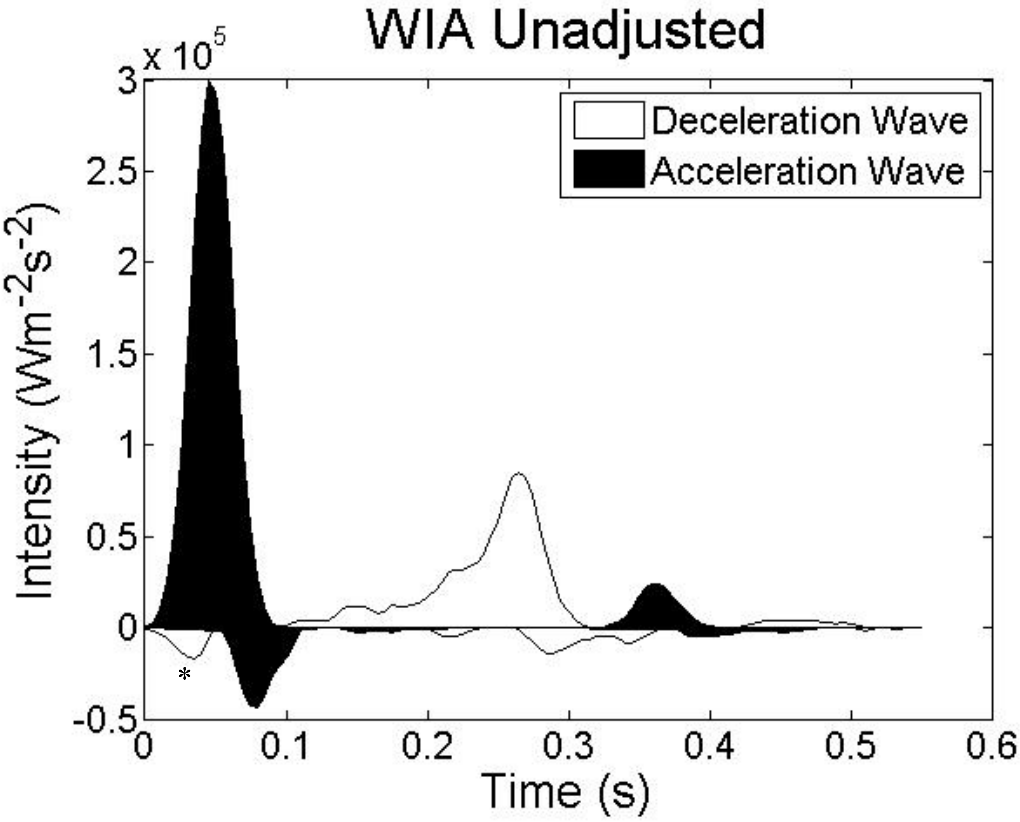

Figure 4-1. Pulmonary arterial wave intensity analysis (WIA) over a single cardiac cycle performed without adjustment of the velocity signal timing, demonstrating an unexplained early systolic backward compression wave (marked with asterisk).

It is unlikely that there are significant pressure signal delays as the high fidelity solid-state pressure transducers used in these experiments have a very high frequency response exceeding 5 kHz with a phase delay of less than 1 ms (Millar Instruments 2009). In contrast the transit time flow meters from which the velocity signal is derived have a time delay of up to 26 ms depending on the model and filter frequency used (Transonic Systems Inc. 2009). More powerful filters use higher orders of the low-pass Butterworth output filter, which require longer time to process the data. Further delays are compounded by non-simultaneous location of the pressure and flow sensors. There was a frequent need to position the pressure sensor proximal to the flow sensor to minimise signal interference. In the pulmonary circulation, where wave speeds are a relatively slow 2.0 ms^{-1}, differences in transducer positioning may also be critical. For example, if the pressure transducer is positioned 1cm proximal to the flow transducer an additional 5 ms delay in the velocity signal would be introduced. Consequently, the flow signal frequently lags the pressure signal, which exaggerates backward wave intensity and may even introduce artificial waves (Figure 4-1, Figure 4-2, Figure 4-3). Furthermore, signal delays affect the linearity of the pressure-velocity relationship in early systole resulting in inaccurate determination of wave speed that further compounds errors in wave separation (see Section 4-2).

The errors generated by signal delay are not trivial. It has been shown that significant impedance phase errors of 40 degrees occur even with a 4 mm difference in relative location of probes or a 7 ms signal processing delay (Westerhof *et al.*, 1973; Westerhof and Noordergraaf, 1970). During the era of impedance analysis, signal delays were not often accounted for, thus suggesting that some conclusions from these studies should be interpreted cautiously.

Hollander (1998) believed the difference in time delays between the pressure and velocity transducers were less than 5 ms (below the sampling interval of 200 Hz), so no time adjustments were made. Additionally, Hollander calculated wave speed from the pressure-velocity slope in early systole without signal timing adjustments, thus leading to errors in the calculation of wave speed and further compounding errors in backward-travelling wave separation. If Hollander had knowledge of the pressure-velocity loops suggested by Khir (2001), the fact that the velocity signal significantly lags the pressure signal would have been more apparent.

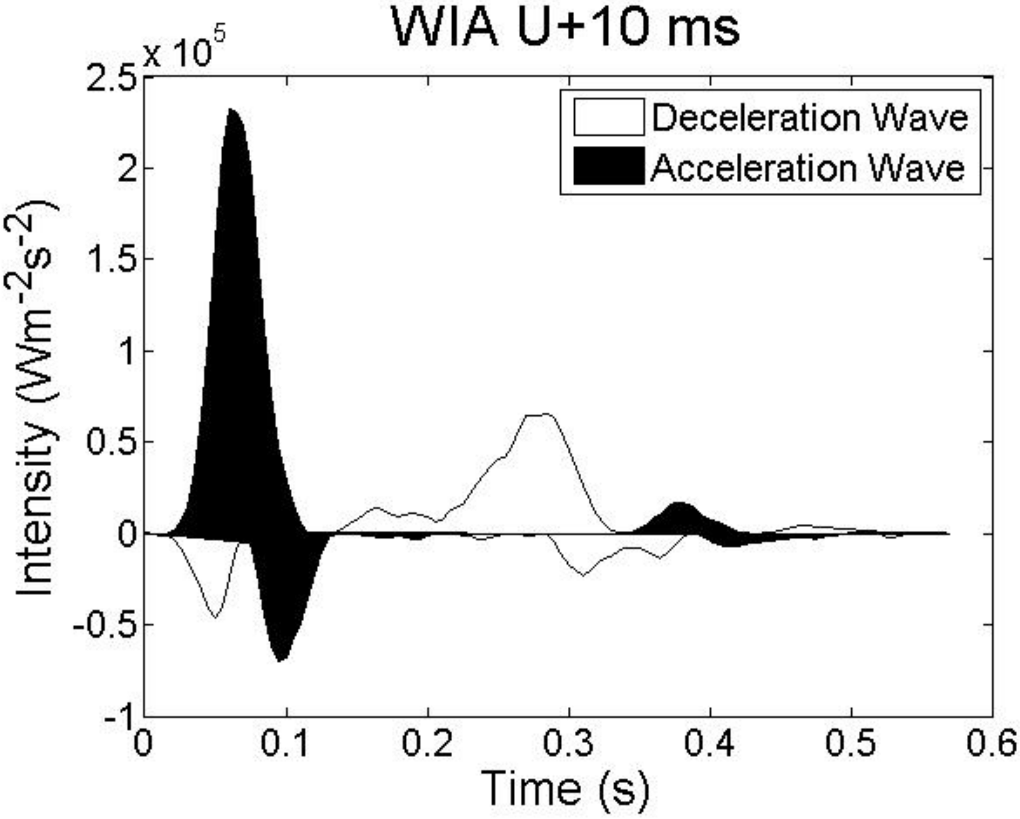

Figure 4-2. Pulmonary arterial wave intensity analysis (WIA) performed after the velocity signal has been delayed a further 10 ms behind the pressure signal, demonstrating exaggeration of the backward travelling waves.

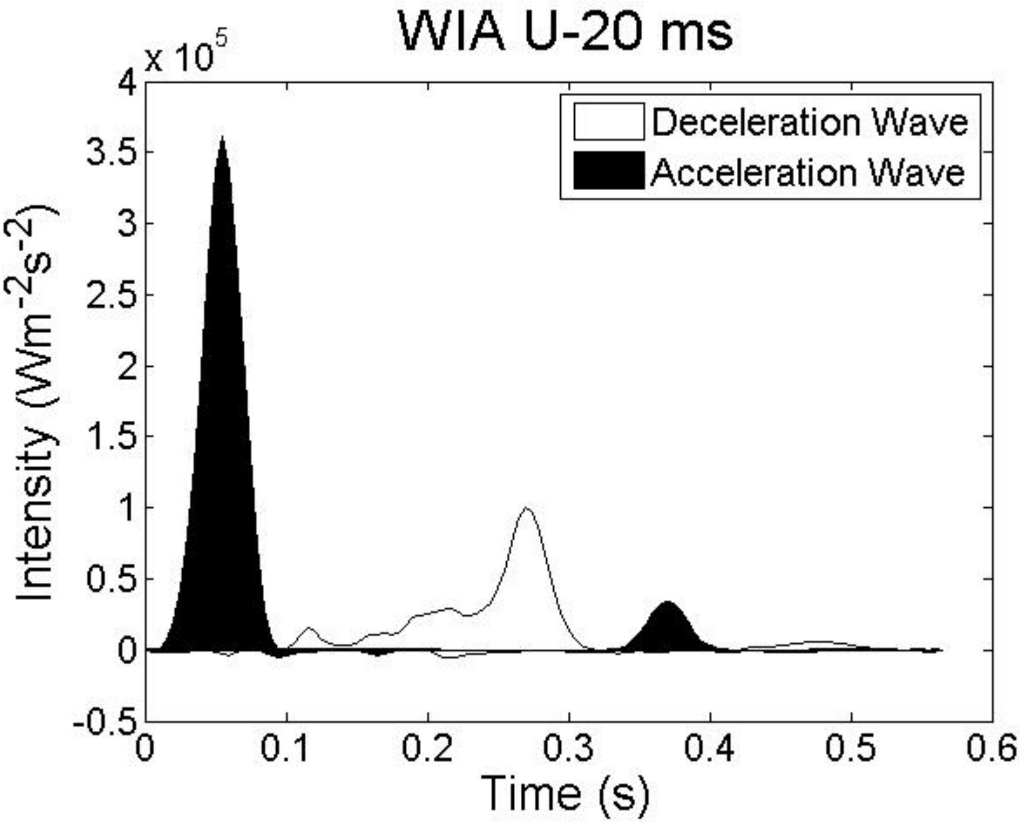

Figure 4-3. Pulmonary arterial wave intensity analysis (WIA) performed after the velocity signal has been advanced 20 ms (to correct the lag behind the pressure signal), demonstrating suppression of the backward travelling wave.

Thought was given to measuring the time delay in the transit-time flow system used, but this proved to be technically challenging, and the resultant accuracy would be of the same order of magnitude as the accuracy in co-locating the pressure and flow transducers. Therefore the pressure-velocity loop (PU-loop) method was used to quantify the signal delays in all of the analyses (Swalen and Khir, 2009). This method relies on the validity of the water hammer equation, $dP_{\pm} = \rho c dU_{\pm}$ (Joukowski, 1898), which states that changes in pressure and velocity are linearly related in the absence of wave reflections, a situation that occurs in early systole. Thus the pressure and velocity signals can be varied relative to each other until a linear relationship is generated in early systole, which may be performed visually or with automated algorithms. The time adjustment required to achieve the linear relationship becomes the correction factor (Figure 4-4, Figure 4-5). This method of correction has a very firm theoretical foundation based upon the conservation of mass and momentum from which the water hammer equation is derived (Ghidaoui *et al.*, 2005).

When the mean velocity lag behind pressure of 18 ± 3 ms was corrected for in the analyses the very early systolic backward compression wave disappeared. Contributions to this signal delay include the minimum 5-10 ms signal processing time (Personal Communication, Triton Technologies) and the non-simultaneous location of the sensor technology. It is clear that velocity signal delays substantially exaggerate wave intensity as well as introduce artificial waves (Khir and Parker, 2002) and therefore these time delays needed to be accurately accounted for.

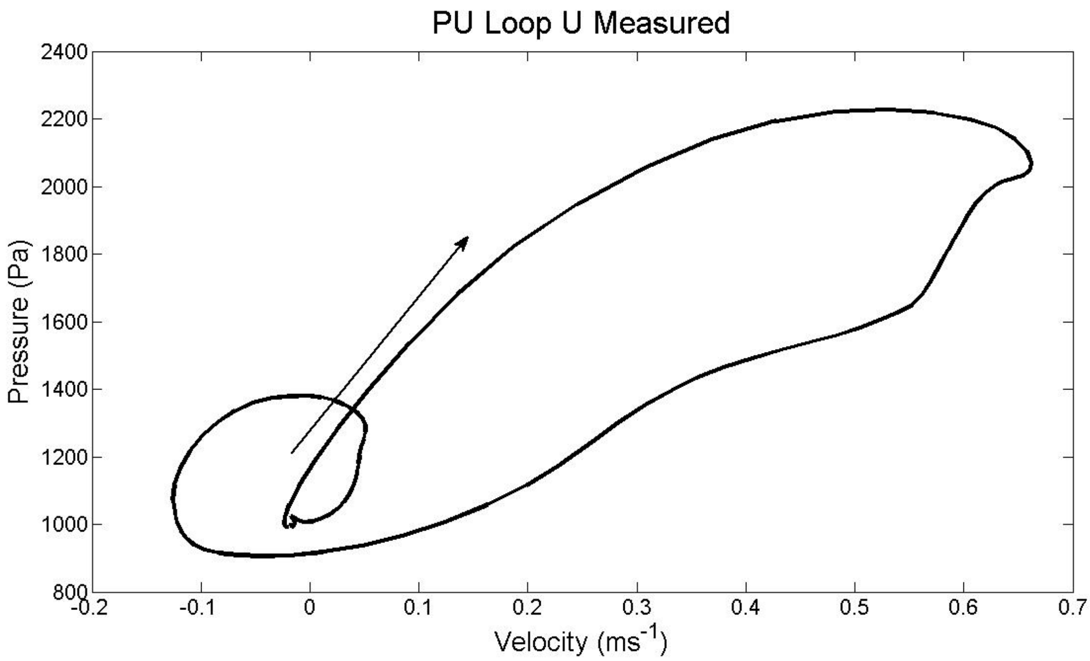

Figure 4-4. A Pressure-Velocity (PU) Loop for a single resting cardiac cycle without adjustments of the velocity signal delay.
Here velocity is lagging pressure by approximately 20 ms, and in early systole (marked by arrow), the loop is concave to the pressure axis. It is possible to see that wave speed calculated from dP/dU × 1/ρ in early systole would lead to an artificially high value and subsequently further errors in wave separation.

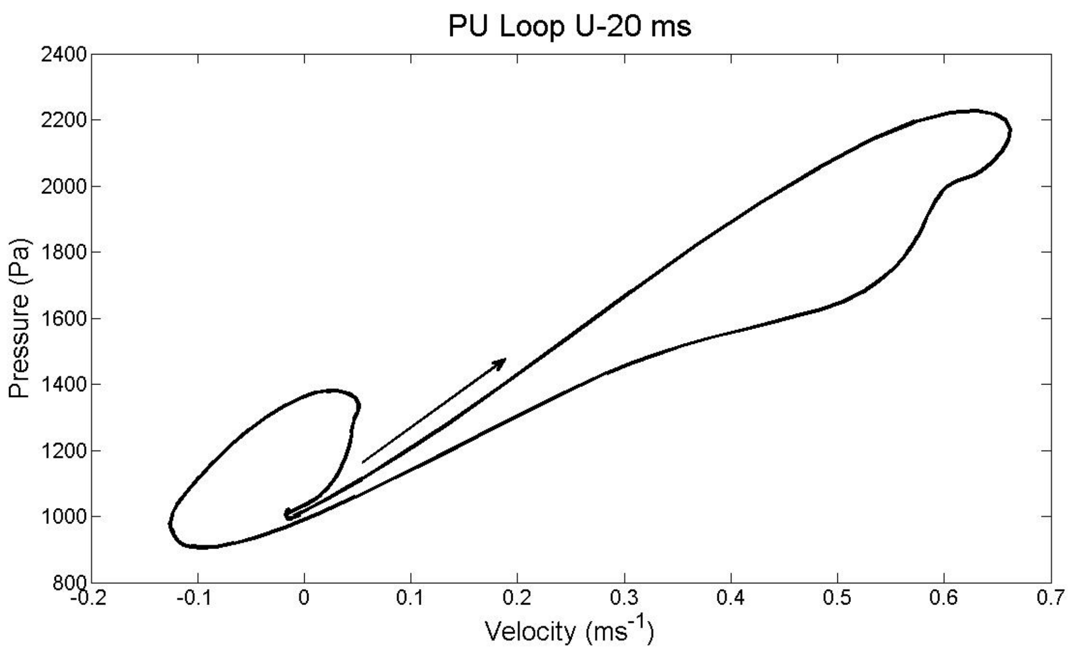

Figure 4-5. A Pressure-Velocity (PU) Loop for a single resting cardiac cycle with the velocity signal delay reduced by 20 ms.
In early systole (marked by arrow), there is now a linear relationship between P and U as predicted by the water hammer equation, and wave speed can now be accurately determined and compares favourably to the single-point technique.

Tables 4-1 to 4-3 demonstrate the great variation in peak and cumulative wave intensity as well as the proportion of total cumulative wave energy of the backward-travelling wave when delays between the velocity and pressure signals are manipulated for a single cardiac cycle. Here the correct wave speed has been calculated using the independent single-point technique. If signal delays were not accounted for, similar results and interpretation as that of Hollander would have been achieved. Once the lag of the flow waveform behind the pressure waveform has been corrected, the energy of the backward-travelling wave falls. If no time adjustments are made the backward expansion wave carries substantially more energy and has a reflection coefficient of 0.24 very similar to Hollander (2001). However, if the correct time adjustments are made the size of the backward expansion wave falls with the reflection coefficient reducing to 0.02 (Table 4-4). Furthermore, signal timing adjustments lead to different times to peak wave intensity thus altering the calculated distance to reflection site, though not as substantially as alterations in wave intensity (Table 4-4).

Table 4-1. Peak wave intensity values for time adjusted velocity signals.

Peak Wave Intensity ($\times 10^5$ $Wm^{-2}s^{-2}$)	U+10 ms	U+5 ms	U	U-5 ms	U-10 ms	U-15 ms	U-20 ms
Early FCW	4.57	5.93	7.56	9.05	10.44	11.03	10.94
Late FEW	1.43	1.40	1.40	1.45	1.46	1.49	1.55
Late FCW	0.39	0.44	0.44	0.44	0.43	0.41	0.40
Early BEW	3.46	3.31	2.81	2.04	1.27	0.74	0.39
Late BCW	0.46	0.40	0.32	0.23	0.18	0.15	0.12
Early BCW	2.61	1.92	1.28	0.75	0.35	0.09	0.00

BCW, backward compression wave; BEW, backward expansion wave; FCW, forward compression wave; FEW, forward expansion wave; ms, milliseconds; U, measured velocity; +, increased velocity delay behind pressure; -, reduced velocity delay behind pressure.

Table 4-2. Cumulative wave intensity values for time adjusted velocity signals.

Cumulative Wave Intensity ($\times 10^3$ $Wm^{-2}s^{-1}$)	U+10 ms	U+5 ms	U	U-5 ms	U-10 ms	U-15 ms	U-20 ms
Early FCW	16.70	19.04	21.74	24.31	26.66	28.37	29.31
Late FEW	9.78	10.11	10.39	10.65	10.88	11.15	11.29
Late FCW	1.14	1.27	1.38	1.48	1.59	1.63	1.63
Early BEW	11.60	6.26	5.24	4.23	2.33	1.22	0.56
Late BCW	1.97	1.59	1.30	0.98	0.73	0.46	0.26
Early BCW	6.11	4.85	3.33	1.91	0.89	0.20	0.00

BCW, backward compression wave; BEW, backward expansion wave; FCW, forward compression wave; FEW, forward expansion wave; ms, milliseconds; U, measured velocity; +, increased velocity delay behind pressure; -, reduced velocity delay behind pressure.

Table 4-3. Proportion of total cumulative wave intensity for time adjusted velocity signals.

Proportion of Cumulative Wave Intensity (%)	U+10 ms	U+5 ms	U	U-5 ms	U-10 ms	U-15 ms	U-20 ms
Early FCW	35.3	44.2	50.1	55.8	61.9	65.9	68.1
Late FEW	20.7	23.4	24.0	24.4	25.3	25.9	26.2
Late FCW	2.4	3.0	3.2	3.4	3.7	3.8	3.8
Early BEW	24.5	14.5	12.1	9.7	5.4	2.8	1.3
Late BCW	4.2	3.7	3.0	2.3	1.7	1.1	0.6
Early BCW	12.9	11.3	7.7	4.4	2.1	0.5	0.0

BCW, backward compression wave; BEW, backward expansion wave; FCW, forward compression wave; FEW, forward expansion wave; ms, milliseconds; U, measured velocity; +, increased velocity delay behind pressure; -, reduced velocity delay behind pressure.

Table 4-4. Reflection coefficient values and estimated distance to reflection site for time adjusted velocity signals.

	U+10 ms	U+5 ms	U	U-5 ms	U-10 ms	U-15 ms	U-20 ms
Ratio Wave Energy BEW/FCW	0.69	0.33	0.24	0.17	0.09	0.04	0.02
Ratio Wave Energy BCW/FCW	0.12	0.08	0.06	0.04	0.03	0.02	0.01
Distance to Reflection Site BEW (cm)	2.4	1.9	1.9	2.4	2.4	2.4	2.9
Distance to Reflection Site BCW (cm)	30.2	30.2	29.7	30.2	30.8	30.8	31.3

BCW, backward compression wave; BEW, backward expansion wave; FCW, forward compression wave; ms, milliseconds; U, measured velocity; +, increased velocity delay behind pressure; -, reduced velocity delay behind pressure.

4.2 Wave Speed Calculation Errors

The correct determination of wave speed, c, is essential to the accurate separation as well as the magnitude and timing of forward and backward travelling waves. If wave speed is only determined by the average of dP/dU in early systole when it is assumed that no backward waves are present, then this value of c cannot be confidently used to demonstrate that early systolic backward waves are indeed not present. Fortunately, an independent method for the calculation of wave speed has been developed (Davies *et al.*, 2006b). This single-point technique uses the simultaneously acquired pressure and velocity signals to minimize wave energy over complete cardiac cycles:

$$c = \frac{1}{\rho}\sqrt{\frac{\sum dP^2}{\sum dU^2}}$$

This technique does not rely on a period during which there are no backward travelling waves and can be easily used to calculate wave speed in automated algorithms.

If delays in the velocity signal are not accounted for, the calculation of wave speed from dP/dU in early systole will be artificially high, in the order of 3.0 ms^{-1} (Figure 4-4). Also, as will be demonstrated later, a similar 70-80% increase in wave speed leads to overestimation of backward-travelling wave energies. This is also likely to be a source of error in Hollander's work. When the velocity signal delays have been accounted for a linear relationship between dP and dU in early systole is clearly demonstrated (Figure 4-5) allowing wave speed to be calculated far more accurately, either by automated algorithms or line of best fit by eye. This still does not overcome the assumptions of absence of backward waves in early systole. However, when wave speed is calculated to be 1.73 ± 0.36 ms^{-1} by the independent single-point technique using baseline haemodynamic data in 12 sheep it compares favourably to the wave speed of 1.92 ± 0.40 ms^{-1} determined from the slope fitted by eye when time delays have been accounted for. Whilst the hand fitting of the slope by eye leads to a statistically significant ($p < 0.001$) approximate 10% increase in wave speed (difference 0.19 ms^{-1}; 95% CI 0.11 to 0.27 ms^{-1}) as will be shown later this does not lead to an important increase in backward-travelling wave energy. As the wave speeds determined by the two independent techniques compare favourably, the PU-loop can confidently be utilized to determine the time adjustments required to make a linear relationship in early systole and is a valid method.

When utilizing the single-point technique to calculate wave speed automatically in signals without great beat-to-beat variation it does not matter if a single beat or 20 seconds worth of cardiac cycles undergo analysis, with wave speeds of 1.78 ± 0.21 and 1.79 ± 0.21 ($p = 0.49$) respectively. The sampling frequency does not influence the calculation of wave speed by the single-point technique.

It is clear that not accounting for velocity signal delays can lead to errors in the calculation of wave speed (unless the single-point technique is used). The effect that altered wave speed determination has on wave separation is explored below.

The variations in wave intensity parameters that occur when wave speed is altered from its true value (determined independently by the single-point technique) for a single resting cardiac cycle where the velocity signal delay has been accounted for are shown in Tables 4-5 to 4-8. Generally as the wave speed moves from underestimation to overestimation the energy carried by the early backward expansion wave rises, becomes a much greater proportion of total wave energy and results in a greater reflection coefficient. Nevertheless, estimations of wave speed to within 10% of the true value should not alter the qualitative results substantially. The influences of extreme errors in wave speed estimation on wave intensity are graphically represented in Figures 4-6 to 4-8. When wave speed is overestimated by 80% the early systolic backward-travelling expansion wave peaks before the incident forward-travelling compression wave, which leads to a non-sensical negatively located reflection site (Figure 4-8 & Table 4-8).

4.3 Conclusion

The accurate interpretation of wave intensity parameters and wave reflection requires pressure and velocity signal timing delays to be carefully considered and accounted for prior to wave intensity analysis being undertaken. Otherwise, backward-travelling wave energy may be exaggerated or in extreme cases artificial backward-travelling waves generated. The easiest method to account for signal delays that may arise from signal processing times or co-location differences of the transducers is to utilise graphically the pressure-velocity loop to generate a linear relationship between pressure and velocity in early systole.

Table 4-5. Peak wave intensity (×10^4 $Wm^{-2}s^{-2}$) with varying wave speed

Wave Speed Change (%)	Wave Speed (ms^{-1})	Early FCW	Late FEW	Late FCW	Early BEW	Late BCW	Early BCW
-80	0.38	210.03	30.41	8.47	5.82	5.08	101.52
-60	0.76	139.46	20.09	5.29	4.17	1.95	30.95
-40	1.15	119.19	17.10	4.35	3.85	1.24	10.67
-20	1.53	111.78	15.95	4.08	3.82	1.22	2.98
-10	1.72	110.15	15.68	4.02	3.86	1.22	1.22
-5	1.81	109.67	15.59	4.00	3.88	1.23	0.68
0	1.91	109.36	15.53	3.99	3.91	1.24	0
+5	2.01	109.19	15.49	3.99	3.94	1.25	0
+10	2.10	109.16	15.47	3.98	3.97	1.26	0
+20	2.29	109.41	15.47	3.99	4.05	1.28	0
+40	2.67	110.88	15.63	4.05	4.41	1.33	0
+60	3.06	113.24	15.91	4.13	5.11	1.46	0
+80	3.44	116.19	16.29	4.24	7.90	1.96	0

BCW, backward compression wave; BEW, backward expansion wave; FCW, forward compression wave; FEW, forward expansion wave.

Table 4-6. Cumulative wave intensity (×10^2 $Wm^{-2}s^{-1}$) with varying wave speed

Wave Speed Change (%)	Wave Speed (ms^{-1})	Early FCW	Late FEW	Late FCW	Early BEW	Late BCW	Early BCW
-80	0.38	529.52	191.88	35.71	7.15	20.09	238.14
-60	0.76	360.96	131.96	23.00	4.90	9.66	68.55
-40	1.15	313.39	111.92	19.23	4.45	3.05	20.45
-20	1.53	296.81	111.96	17.30	4.94	2.64	4.71
-10	1.72	293.92	111.58	16.56	4.99	2.78	1.29
-5	1.81	293.29	111.35	16.67	5.26	2.71	0.65
0	1.91	293.10	111.74	16.53	5.67	2.74	0
+5	2.01	293.27	112.28	16.41	5.97	3.41	0
+10	2.10	293.77	112.18	16.32	6.29	3.86	0
+20	2.29	295.56	113.27	16.35	7.09	4.23	0
+40	2.67	301.66	116.31	16.16	14.34	5.56	0
+60	3.06	309.75	120.12	16.27	22.26	11.13	0
+80	3.44	319.63	124.66	16.49	32.36	14.93	0

BCW, backward compression wave; BEW, backward expansion wave; FCW, forward compression wave; FEW, forward expansion wave.

Table 4-7. Proportion of total cumulative wave intensity (%) with varying wave speed

Wave Speed Change (%)	Wave Speed (ms^{-1})	Early FCW	Late FEW	Late FCW	Early BEW	Late BCW	Early BCW
-80	0.38	51.79	18.77	3.49	0.70	1.97	23.29
-60	0.76	60.26	22.03	3.84	0.82	1.61	11.44
-40	1.15	65.63	24.49	4.03	0.93	0.64	4.28
-20	1.53	67.71	25.54	3.95	1.13	0.60	1.07
-10	1.72	68.18	25.88	3.84	1.16	0.65	0.30
-5	1.81	68.22	25.90	3.88	1.22	0.63	0.15
0	1.91	68.20	26.00	3.85	1.32	0.64	0
+5	2.01	67.99	26.03	3.81	1.38	0.79	0
+10	2.10	67.94	25.94	3.78	1.46	0.89	0
+20	2.29	67.71	25.95	3.75	1.62	0.97	0
+40	2.67	66.44	25.62	3.56	3.16	1.23	0
+60	3.06	64.60	25.05	3.39	4.64	2.32	0
+80	3.44	62.91	24.54	3.25	6.37	2.94	0

BCW, backward compression wave; BEW, backward expansion wave; FCW, forward compression wave; FEW, forward expansion wave.

Table 4-8. Reflection coefficient and estimated distance to reflection site with varying wave speed

Wave Speed Change (%)	Wave Speed (ms^{-1})	Ratio Wave Energy BEW/FCW ($\times 10^{-2}$)	Ratio Wave Energy BCW/FCW ($\times 10^{-2}$)	Distance to Reflection Site BEW (cm)	Distance to Reflection Site BCW (cm)
-80	0.38	1.35	3.79	0.57	7.45
-60	0.76	1.36	2.68	0.95	14.90
-40	1.15	1.42	0.97	1.43	18.62
-20	1.53	1.66	0.89	2.29	25.21
-10	1.72	1.70	0.95	2.58	28.36
-5	1.81	1.79	0.92	2.72	29.94
0	1.91	1.93	0.93	2.86	31.51
+5	2.01	2.04	1.16	3.01	33.09
+10	2.10	2.14	1.31	3.15	34.67
+20	2.29	2.40	1.43	3.44	37.82
+40	2.67	4.75	1.84	3.34	44.12
+60	3.06	7.19	3.59	3.82	37.43
+80	3.44	10.13	4.67	-0.86	42.11

BCW, backward compression wave; BEW, backward expansion wave; FCW, forward compression wave.

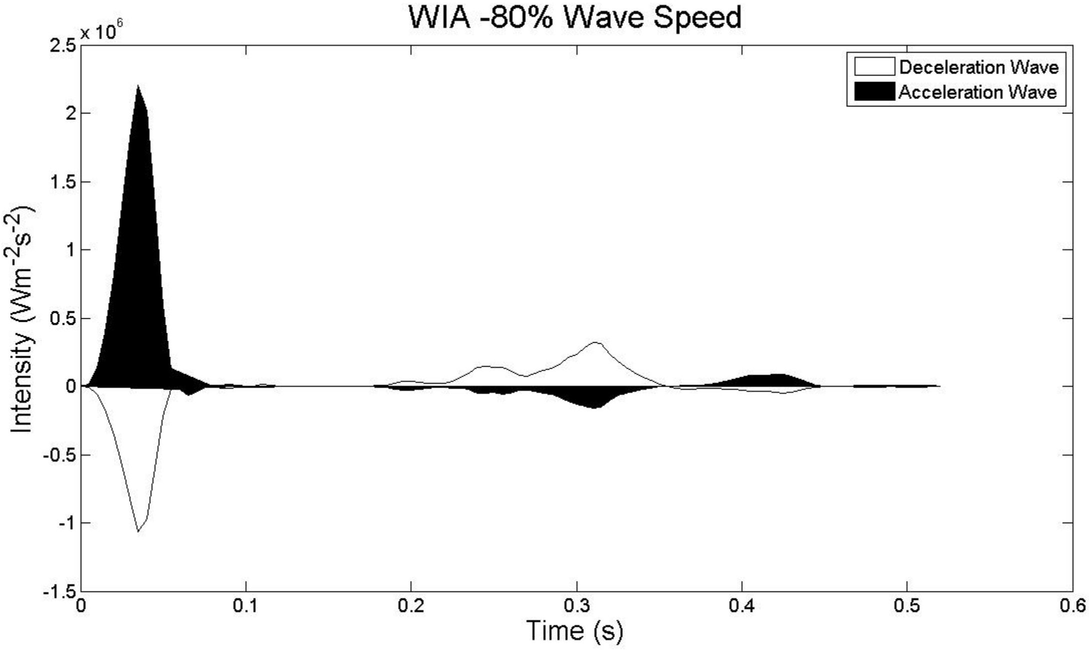

Figure 4-6. Wave intensity performed on resting pressure and velocity using an 80% reduction in calculated wave speed with velocity delays accounted for.

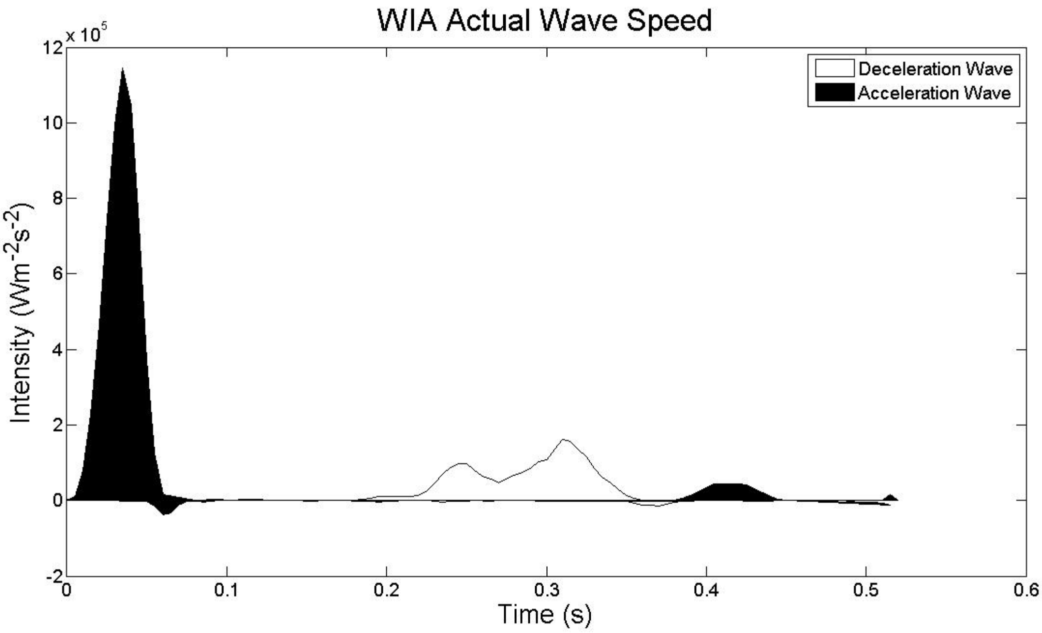

Figure 4-7. Wave intensity performed on resting pressure and velocity using the actual wave speed calculated by the single-point technique with velocity delays accounted for.

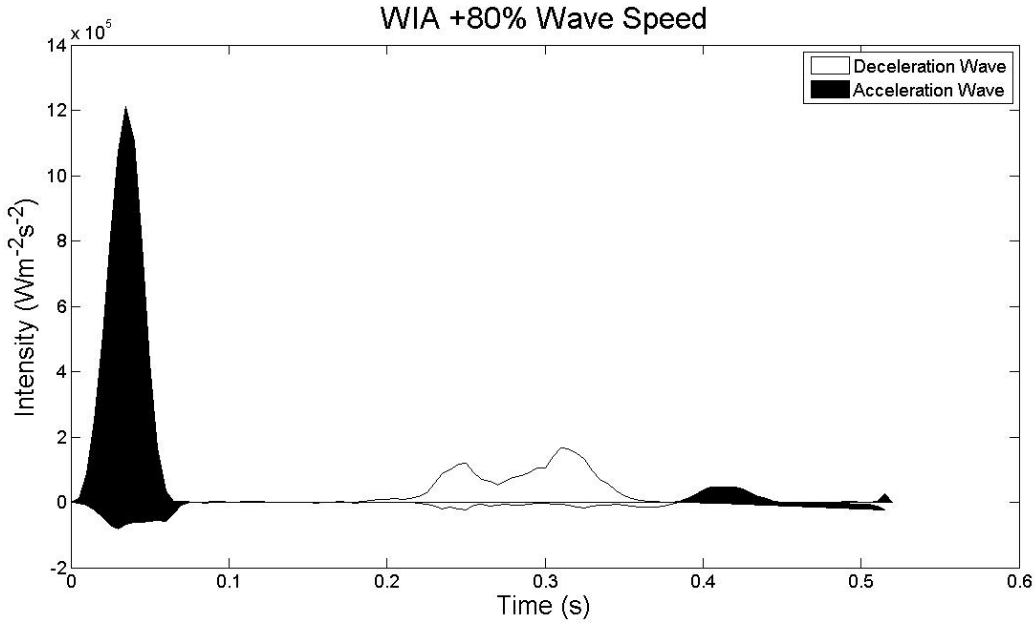

Figure 4-8. Wave intensity performed on resting pressure and velocity using an 80% increase in calculated wave speed with velocity delays accounted for.

Chapter 5 Pulmonary Arterial Wave Intensity Analysis during High Pulmonary Flow

5.1 Anticipated Wave Intensity

It was shown in Chapter 3 that the proximal pulmonary artery is characterised by open-end reflection in early systole, such that the forward compression wave of right ventricular ejection is reflected from a site approximately 3 cm downstream as a backward expansion wave. Such open-end proximal reflection may serve a physiological advantage by aiding right ventricular ejection without raising pulmonary pressures greatly, which would have particular advantages during high flow situations such as exercise. The pulmonary vasculature is known to be highly compliant with the ability to recruit blood vessels, thus minimising pressure rises during high flow situations and serving to protect the delicate alveolar capillaries. It is anticipated that during situations of high pulmonary blood flow open-end reflection will be enhanced.

With the administration of the vasodilator adenosine leading to increased pulmonary blood flow it is anticipated that the area ratio of daughter-to-parent vessels in the proximal circulation will increase, which would lead to an enhanced negative reflection coefficient and a larger backward expansion wave. Additionally, with a dilated microcirculation the energy of the late backward compression wave would be significantly reduced.

Similarly under a situation of high vascular volume, as evidenced by elevated left ventricular end-diastolic filling pressures (LVEDP), the increased pulmonary artery distension is anticipated to result in geometrical changes to the arteries to increase the reflection coefficient and enhance the backward-travelling expansion wave energy. Additionally, with a passively distended microcirculation the energy of the late backward compression wave would be reduced. As a result of the elevated preload with increased vascular volume, the force of myocardial contraction is expected to increase (Starling's mechanism), leading to increased forward-travelling wave energy.

5.2 Adenosine

5.2.1 Results

The administration of 200 $\mu kg^{-1}min^{-1}$ of adenosine intravenously resulted in a marked increase in pulmonary blood flow from 2.4 ± 0.5 $Lmin^{-1}$ to 3.3 ± 0.5 $Lmin^{-1}$ ($p < 0.001$). The increased pulmonary blood flow was associated with a small but statistically significant rise in mean pulmonary artery pressure from 14.5 ± 1.3 mmHg to 17.7 ± 1.5 mmHg ($p < 0.001$). Adenosine had a systemic vasodilatory effect with peak systolic blood pressure falling from 144 ± 7mmHg to 109 ± 10 mmHg ($p < 0.001$) without a significant change in left ventricular end-diastolic pressure (LVEDP); 6.1 ± 3.9 mmHg to 6.3 ± 4.5 mmHg ($p = 0.97$). The pulmonary vascular resistance (PVR) did not alter significantly with adenosine (3.4 ± 1.2 vs 3.6 ± 2.1; $p = 0.40$). The proximal pulmonary arterial wave speed was not altered by adenosine: 2.2 ± 0.4 ms^{-1} to 2.3 ± 0.3 ms^{-1} ($p = 0.10$). Forward-travelling wave energies increased minimally but statistically significantly with adenosine administration (Table 5-1). Importantly, the backward expansion wave was enhanced by adenosine (Table 5-1) with the cumulative wave intensity increasing from 3.9 ± 2.8 × 10^2 $Wm^{-2}s^{-1}$ to 10.8 ± 9.3 × 10^2 $Wm^{-2}s^{-1}$ ($p = 0.01$). The reflection coefficient increased from -0.02 ± 0.01 to -0.05 ± 0.04 ($p = 0.02$). The distance to the proximal reflection site remained unaltered; 2.8 ± 1.0 cm to 2.5 ± 0.6 cm ($p = 0.97$). In contrast, however, the distance to the distal reflection site moved more peripherally from 22.6 ± 9.0 cm to 26.1 ± 6.2 cm ($p = 0.01$). There was no associated increase in the reflection coefficient (0.03 ± 0.03 vs 0.03 ± 0.02; $p = 0.63$) or energy carried by the late backward-travelling compression wave (6.5 ± 4.6 vs 7.0 ± 4.0 × 10^2 $Wm^{-2}s^{-1}$; $p = 0.63$).

Table 5-1. Wave Intensity and Haemodynamic Parameters at Rest and During Adenosine Infusion

	Control (n = 6)	Adenosine (n = 6)	P Value
Peak Wave Intensity ($\times 10^4$ $Wm^{-2}s^{-2}$)			
Early Forward Compression	60.22 ± 10.50	76.59 ± 13.99	0.004
Late Forward Expansion	23.39 ± 13.11	39.19 ± 20.01	< 0.001
Late Forward Compression	6.69 ± 3.24	8.57 ± 4.04	0.009
Early Backward Expansion	1.69 ± 1.21	4.68 ± 4.03	0.008
Backward Compression	1.61 ± 1.17	1.68 ± 0.73	0.80
Cumulative Wave Intensity ($\times 10^2$ $Wm^{-2}s^{-1}$)			
Early Forward Compression	206.78 ± 26.48	249.36 ± 35.15	0.001
Late Forward Expansion	97.22 ± 40.99	159.36 ± 57.21	<0.001
Late Forward Compression	14.99 ± 6.29	19.41 ± 7.79	0.001
Early Backward Expansion	3.94 ± 2.76	10.75 ± 9.28	0.01
Backward Compression	6.54 ± 4.63	7.03 ± 3.97	0.63
Proportion of Cumulative Wave Intensity (%)			
Early Forward Compression	63.6 ± 8.0	56.6 ± 7.1	<0.001
Late Forward Expansion	28.7 ± 8.1	34.9 ± 8.4	0.001
Late Forward Compression	4.4 ± 1.3	4.2 ± 1.1	0.36
Early Backward Expansion	1.2 ± 0.9	2.6 ± 2.6	0.04
Backward Compression	2.1 ± 1.7	1.7 ± 1.3	0.30
Reflection Coefficient			
BEW/FCW	-0.02 ± 0.01	-0.05 ± 0.04	0.02
BCW/FCW	0.03 ± 0.03	0.03 ± 0.02	0.63
Wave Speed (ms^{-1})	2.2 ± 0.4	2.3 ± 0.3	0.10
Distance to Reflection Site (cm)			
Early Backward Expansion	2.8 ± 1.0	2.5 ± 0.6	0.97
Late Backward Compression	22.6 ± 9.0	26.1 ± 6.2	0.01
Heart Rate (min^{-1})	92 ± 7	99 ± 13	0.02
Peak Blood Velocity (ms^{-1})	0.79 ± 0.01	0.87 ± 0.01	< 0.01
Cardiac Output ($Lmin^{-1}$)	2.4 ± 0.4	3.3 ± 0.3	<0.001
LVEDP (mmHg)	6.1 ± 3.9	6.3 ± 4.5	0.97
LVSP (mmHg)	144.0 ± 7.4	109.7 ± 10.0	< 0.001
Mean PA Pressure (mmHg)	14.5 ± 1.3	17.7 ± 1.5	<0.001
PVR (Wood's Units)	3.4 ± 1.2	3.6 ± 2.1	0.40

Values are means ± SD; BEW, backward expansion wave; BCW, backward compression wave; FCW, forward compression wave; LVEDP, left ventricular end-diastolic pressure; LVSP, left ventricular systolic pressure; n, number of sheep; PA, pulmonary artery; PVR, pulmonary vascular resistance.

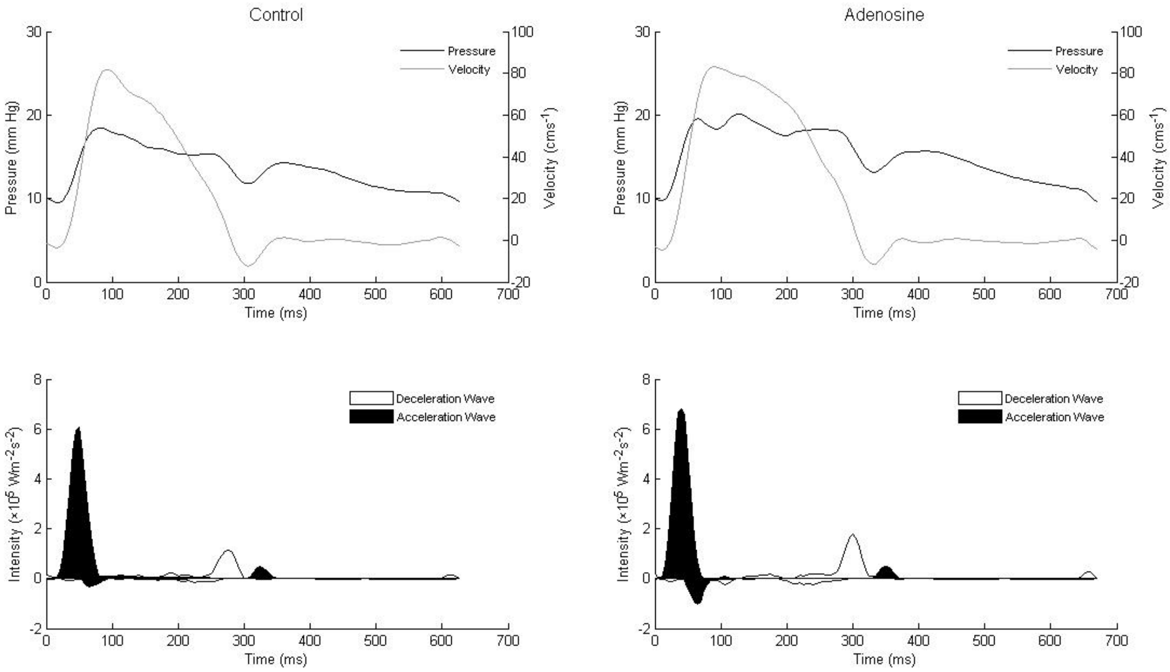

Figure 5-1. Wave intensity at rest and during adenosine infusion with corresponding pressure and velocity traces.

5.2.2 Discussion

The high doses of adenosine (200 μkg^{-1}min^{-1}) used in these experiments leads to marked systemic and possibly pulmonary vasodilatation. At lower doses (≤ 60 μkg^{-1}min^{-1}) a selective effect on the pulmonary circulation may have been achieved (Reid *et al.*, 1990), but the increase in pulmonary blood flow would not have been as dramatic. The pulmonary vascular resistance did not fall with adenosine as expected. This could mean that adenosine is not a pulmonary vasodilator in sheep and that the 38% increase in cardiac output is purely due to inotropic effects, supported by an increase in stroke volume from 26 mL/beat to 33 mL/beat. In addition adenosine had a mild chronotropic effect with the heart rate increasing by 8%, which may be mediated by a reduction in cardiac vagal tone (Conradson *et al.*, 1987). It is likely that pulmonary vasodilation has occurred because there has been a 38% increase in cardiac output without a large rise in pulmonary arterial pressure. This can only be achieved through pulmonary vasodilation or vascular recruitment and as the lungs of the animals are likely to be entirely in a zone 3 condition, which is a fully vascular recruited situation, the increased flow most likely occurs in response to pulmonary vasodilatation. The unchanged pulmonary vascular resistance could be attributed to lack of reduction in left ventricular end-diastolic pressure (LVEDP), despite a 23% reduction in systemic blood pressure, which therefore leads to an increased transpulmonary gradient. Indeed, other authors have observed a 55% increase in LVEDP and a 60% increase in mean pulmonary arterial pressure with adenosine infusion in man (Reid *et al.*, 1990). Theoretically adenosine may have negative inotropic effects through its known ability to antagonise myocardial catecholamines (Hedqvist and Fredholm, 1979), yet this is unlikely as the stroke volume increased in the animals. Adenosine may alternatively cause reduced ventricular compliance via coronary distension, which has been observed in experimental animals (Vogel *et al.*, 1982). Interestingly, when results for individual animals are examined, the LVEDP increased in three animals and fell in three animals, suggesting that there is marked interindividual variation in the left ventricular compliance response to adenosine.

It is certainly recognised that there is significant interspecies and interindividual variation in response to drugs. A number of vasodilators and vasoconstrictors were trialled in the preliminary stages of this research. Adenosine appeared to behave as a potent vasodilator. Serotonin has previously been widely used to induce pulmonary vasoconstriction in dogs (Bergel and Milnor, 1965; Van Den Bos *et al.*, 1982). However, of six sheep infused with intravenous serotonin at low doses (5 $\mu gkg^{-1}min^{-1}$), in addition to marked elevations in mean pulmonary pressure, three animals developed severe bronchoconstriction, which has not been previously reported. These sheep required high-pressure ventilatory support and P_aO_2 fell from 98 ± 6 mmHg to 62 ± 7 mmHg (p = 0.002).

With adenosine infusion the wave energies increased minimally but statistically significantly highlighting the small increase in hydraulic work that was required to shift blood in response to the slightly higher pulmonary pressures that were generated with the huge increase in flow. Similar results were observed in one animal infused with isoprenaline (2 $\mu gkg^{-1}min^{-1}$) which had marked inotropic and chronotropic effects leading to flow increasing by 1 $Lmin^{-1}$ and mean pulmonary pressure rising. There was no change in the pattern of wave intensity but all of the intensities increased, a finding previously seen with dobutamine infusion in sheep (Penny *et al.*, 2008).

Adenosine increased the reflection coefficient of the proximal open-end reflector site leading to increased wave energy of the backward expansion wave. This suggests that the area ratio of the daughter-to-parent vessels increased as a result of increased pulmonary blood flow and subsequent distension of the downstream vasculature. Adenosine did not seem to alter the compliance or cause significant distension of the proximal pulmonary artery as evidenced by lack of change in pulmonary arterial wave speed. Furthermore, the increase in peak blood velocity with the increase in cardiac output suggests the proximal pulmonary artery did not dilate significantly. Therefore, it is likely that the cross sectional area of the daughter vessels increased more than the proximal pulmonary artery leading to enhanced open-end reflection.

It was anticipated with pulmonary arterial vasodilation that reflection from the distal microcirculation would be minimised. However, there was no difference in the reflection coefficient for this reflector site and the cumulative wave energy of the backwards compression did not alter significantly. Instead, it appears that the reflection site moved more distally by 3.5 cm in keeping with vasodilatation of the microcirculation. Furthermore, the backward compression wave broadened in keeping with a more spatially diverse reflection site as may occur with variable vasodilatation of the distal circulation.

It is important to consider that the distance to reflection site calculations are estimations based upon the proximal pulmonary artery wave speed, which is assumed to be constant as it travels distally. It is likely that with microvascular distension the wave speed increases distally, thus enhancing the propagation of incident wave energy and minimising damping. This allows more wave energy to be reflected back and thus artificially raises the reflection coefficient despite a likely fall in the distal reflection properties. The potential phenomenon of wave speed increasing as it propagates distally would also lead to an underestimation of the true distance to the reflection site.

5.3 Increased Blood Volume

5.3.1 Results

Infusing 1.5-2 litres of normal saline increased the circulating blood volume and raised the left ventricular end-diastolic pressure (LVEDP) from 5.8 ± 6.1 mmHg to 14.7 ± 8.8 mmHg ($p < 0.001$). Via Starling's mechanism this led to a significant increase in cardiac output from 3.8 ± 1.0 $Lmin^{-1}$ to 4.7 ± 0.7 $Lmin^{-1}$ ($p < 0.001$). The combination of increased cardiac output and elevated LVEDP caused mean pulmonary arterial pressures to rise significantly from 19.9 ± 2.7 mmHg to 25.9 ± 3.2 mmHg ($p < 0.001$). The increased pulmonary vascular distension led to a significant rise in proximal pulmonary arterial wave speed from 1.8 ± 0.4 ms^{-1} to 2.3 ± 0.4 ms^{-1} ($p < 0.001$). Evidence of the passive distension of the pulmonary circulation with fluid loading is provided by the fall in pulmonary vascular resistance from 3.7 ± 1.4 to 2.4 ± 1.4 Wood's Units ($p = 0.01$).

Fluid loading led to a substantial increase in the peak and cumulative intensities of all of the waves (Table 5-2). Importantly, the cumulative wave intensity of the early backward expansion wave increased significantly with fluid loading from $1.64 \pm 1.53 \times 10^2\ Wm^{-2}s^{-1}$ to $13.95 \pm 7.53 \times 10^2\ Wm^{-2}s^{-1}$. The reflection coefficient of the proximal reflector site increased from -0.01 ± 0.01 to -0.04 ± 0.02 ($p < 0.001$). With fluid loading the distance to the proximal open-end reflection site remained unchanged from 2.6 ± 0.5 cm to 2.6 ± 0.7 cm ($p = 0.30$).

The cumulative intensity of the backward compression wave increased from 0.47 ± 0.93 to $2.95 \pm 4.05 \times 10^2\ Wm^{-2}s^{-1}$ ($p = 0.02$) with an increase in the reflection coefficient from 0.2% to 1.0% ($p = 0.04$). The distance to the distal reflection site increased from 23.4 ± 1.4 cm to 34.3 ± 3.4 cm ($p = 0.01$).

Table 5-2. Wave Intensity and Haemodynamic Parameters at Rest and During High Volume Loading

	Control (n = 5)	High LVEDP (n = 5)	P Value
Peak Wave Intensity ($\times 10^4$ $Wm^{-2}s^{-2}$)			
Early Forward Compression	73.31 ± 20.24	141.38 ± 63.73	<0.001
Late Forward Expansion	17.15 ± 5.15	21.56 ± 6.57	0.06
Late Forward Compression	0.34 ± 0.60	3.85 ± 1.85	<0.001
Early Backward Expansion	1.23 ± 1.00	8.56 ± 4.14	<0.001
Backward Compression	0.41 ± 0.81	0.96 ± 1.21	0.12
Cumulative Wave Intensity ($\times 10^2$ $Wm^{-2}s^{-1}$)			
Early Forward Compression	201.02 ± 44.69	343.07 ± 140.46	<0.001
Late Forward Expansion	80.33 ± 25.18	111.49 ± 11.81	<0.001
Late Forward Compression	0.96 ± 1.80	10.01 ± 5.89	<0.001
Early Backward Expansion	1.64 ± 1.53	13.95 ± 7.53	<0.001
Backward Compression	0.47 ± 0.93	2.95 ± 4.05	0.02
Proportion of Cumulative Wave Intensity (%)			
Early Forward Compression	70.8 ± 5.3	68.2 ± 12.5	0.28
Late Forward Expansion	28.2 ± 5.2	26.1 ± 11.7	0.37
Late Forward Compression	0.3 ± 0.5	2.3 ± 1.4	<0.001
Early Backward Expansion	0.5 ± 0.4	2.9 ± 1.5	<0.001
Backward Compression	0.1 ± 0.3	0.6 ± 0.9	0.04
Reflection Coefficient			
BEW/FCW	-0.01 ± 0.01	-0.04 ± 0.02	<0.001
BCW/FCW	0.002 ± 0.004	0.010 ± 0.014	0.04
Wave Speed (ms^{-1})	1.8 ± 0.4	2.3 ± 0.4	<0.001
Distance to Reflection Site (cm)			
Early Backward Expansion	2.6 ± 0.5	2.6 ± 0.7	0.30
Late Backward Compression	23.4 ± 1.4	34.3 ± 3.4	0.01
Heart Rate (min^{-1})	124 ± 6	110 ± 3	<0.001
Peak Blood Velocity (ms^{-1})	0.84 ± 0.01	0.88 ± 0.01	0.08
Cardiac Output ($Lmin^{-1}$)	3.8 ± 1.0	4.7 ± 0.7	<0.001
LVEDP (mmHg)	5.8 ± 6.1	14.7 ± 8.8	<0.001
LVSP (mmHg)	128.0 ± 5.6	131.2 ± 5.2	<0.001
Mean PA Pressure (mmHg)	19.9 ± 2.7	25.9 ± 3.2	<0.001
PVR (Wood's Units)	3.7 ± 1.4	2.4 ± 1.4	0.01

Values are means ± SD; BEW, backward expansion wave; BCW, backward compression wave; FCW, forward compression wave; LVEDP, left ventricular end-diastolic pressure; LVSP, left ventricular systolic pressure; n, number of sheep; PA, pulmonary artery; PVR, pulmonary vascular resistance.

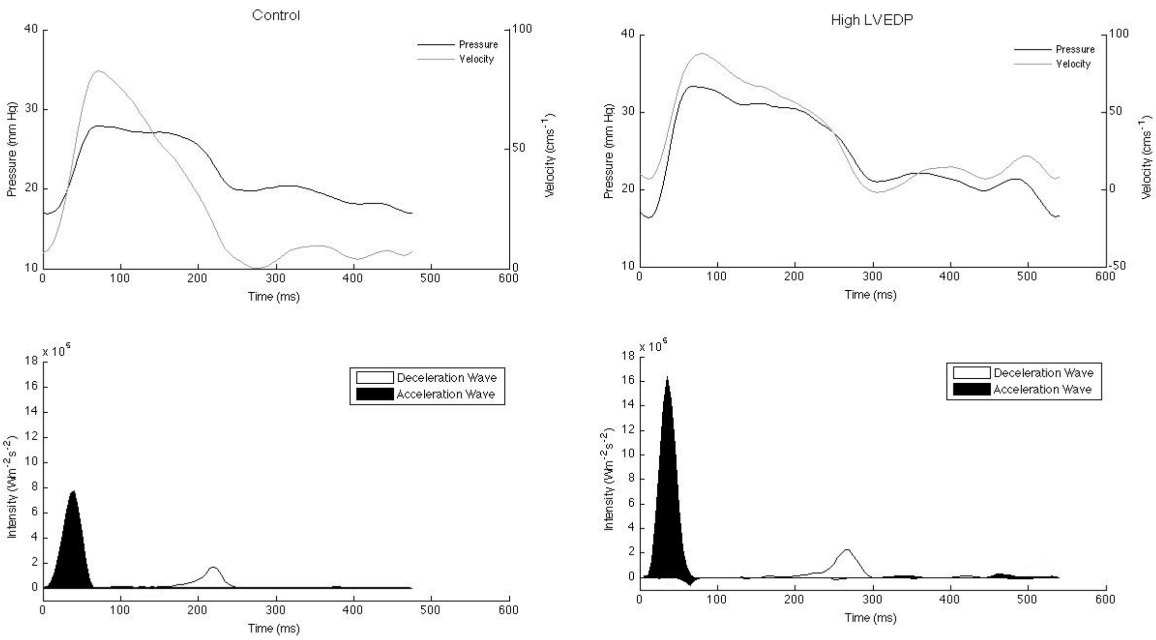

Figure 5-2. Wave Intensity at Rest and During High Volume Loading.

5.3.2 Discussion

The increased volume load without an increase in heart rate suggests that the increased cardiac output is generated by Starling's mechanism. The increase in cumulative wave energy of the forward-travelling waves highlights the increased hydraulic work of the right ventricle required to shift blood in this volume-loaded state. The increased pulmonary arterial wave speed suggests compliance of the proximal vascular bed fell with fluid loading. However, pulmonary vascular compliance does not seem to alter with volume loading in other animal models (Dujardin *et al.*, 1982; Grant and Canty Jr, 1989; Piene, 1976).

The increased backward-travelling wave energy is not only a function of the increased forward-travelling energy but an increased reflection coefficient of both the proximal and distal reflector sites. With fluid loading, 4% of the forward compression wave is reflected in an open-end manner as a backward expansion wave compared to just 1% at baseline. Similarly with fluid loading 1% of the forward compression wave is reflected in a closed-end manner as a backward compression wave compared to just 0.2% at baseline.

The distance to the proximal open-end reflector site was unchanged at 2.7 cm, most likely arising from the main pulmonary bifurcation. The enhanced reflection coefficient of -0.04 indicates that volume loading increased the cross sectional area of the daughter vessels significantly more than the parent vessels. Indeed, there is some evidence that the compliance of the pulmonary artery increases with reducing vessel size (Gan and Yen, 1994; Maloney *et al.*, 1970), suggesting that for the same increase in distending pressure the daughter vessels may increase their cross-sectional area proportionally more than the parent vessels.

The energy of the backward-travelling compression wave increased significantly approximately 6-fold. It is unlikely that the volume loading and subsequent distension of the distal pulmonary circulation would enhance closed-end reflection. Volume loading would be expected to minimise wave reflection from the distal circulation. In keeping with distension of the distal microcirculation, the distance from which the late backward compression wave arises moves more distally from 23.4 ± 1.4 cm to 34.3 ± 3.4 cm ($p = 0.01$). This places the reflection site on the pulmonary venous side of the circulation. Given the pulmonary circulation is approximately 34 cm long this makes the left atrium a plausible site of wave reflection here. However, as the backward compression wave was frequently broad, indicating a spatially diverse reflection site, and was of low magnitude, significant errors could be made in determining the peak of the wave. This would lead to errors in calculating the true distances involved.

Distension of the pulmonary microcirculation is unlikely to increase the reflection coefficient of a closed-end system. Instead, the increased reflection coefficient for this part of the vascular bed is likely to be simply a function of the increased energy of the forward compression wave in association with an increased wave speed leading to less damping of the wave as it travels distally. This, in turn, leads to more wave energy being available to reflect, thus artificially increasing the reflection coefficient.

These results provide indirect evidence that wave speed does not continue to increase as it propagates distally. If the calculation of proximal pulmonary arterial wave speed significantly underestimated the mean wave speed then the distance to the reflection site would be underestimated, therefore placing the reflection site further within the left side of the heart, beyond the left atrium, which seems unlikely.

5.4 Limitations

Although it was assumed that increased pulmonary blood flow and fluid loading led to passive distension of the pulmonary circulation this could not be confirmed, as attempts to measure pulmonary vascular volume were not made. In order to assess whether an intervention leads to passive or active change in pulmonary vasomotor status, pulmonary vascular volume and pressures need to be simultaneously assessed (Yu, 1969). For example, increases in both pulmonary pressure and pulmonary blood volume indicate passive vascular distension. Whereas changes in pressure and volume parameters in the opposite direction indicate active pulmonary vasomotor activity such that increased pulmonary pressure and reduced pulmonary blood volume imply active vasoconstriction.

5.5 Conclusions

With high flow states distension and recruitment of the pulmonary circulation in response to adenosine or fluid loading minimises the rise in mean pulmonary artery pressure. In both high flow situations it seems the daughter-to-parent area ratio distal to the main pulmonary artery bifurcation increases, such that open-end reflection is enhanced, resulting in increased energy carried by the backwards expansion wave. This would serve to enhance ejection of blood from the right ventricle during early systole. Both high flow situations result in the closed-end reflection site moving more distally, probably as a result of distension of the pulmonary microcirculation.

Chapter 6 Pulmonary Arterial Wave Intensity Analysis with Acute Increases in Afterload

6.1 Introduction

In Chapters 3 and 5 it was demonstrated that the proximal pulmonary artery is characterised by open-end reflection, which is enhanced during high-flow and volume loaded conditions, probably as a result of geometrical changes leading to an increased area ratio of the daughter-to-parent vessels after the main pulmonary artery bifurcation. The late backward-travelling compression wave, most likely arising from the distal microcirculation, carries little energy indicating that the pulmonary circulation has well matched impedance throughout. A series of experiments was undertaken to increase right ventricular afterload and investigate the effects on wave intensity parameters. In particular, it was necessary to explore whether changes in the timing and energy of the backward-travelling compression wave was sensitive enough to detect a plausible site of obstruction.

6.2 Hypoxia

6.2.1 Anticipated Wave Intensity

Hypoxia is known to cause acute pulmonary vasoconstriction leading to elevations in pulmonary artery pressure. It is anticipated that the increased rate of work of the right ventricle during hypoxia will be manifest as increased forward-travelling wave energy and that the subsequent increase in proximal pulmonary arterial tone would lead to an increase in wave speed. Additionally, the vasoconstriction would enhance closed-end reflection leading to increased reflection of the forward-travelling compression wave as a backward-travelling compression wave, which would arrive earlier in systole as a result of the increased wave speed. Furthermore, as a result of vascular distension the open-end reflection site is expected to remain.

6.2.2 Results

Mean P_aO_2 fell during the inspiration of 80% N_2 from 101 ± 2 mmHg to 32 ± 3 mmHg ($p < 0.001$). This degree of hypoxia reversibly increased mean pulmonary artery pressure from 16.0 ± 3.0 mmHg to 26.8 ± 3.6 mmHg ($p < 0.001$) and the wave speed from 2.1 ± 0.3 ms^{-1} to 2.9 ± 0.4 ms^{-1} ($p < 0.001$). The hypoxia induced pulmonary vasoconstriction is manifest as an increase in the pulmonary vascular resistance from 3.3 ± 1.4 to 5.0 ± 2.3 Wood's Units ($p = 0.02$).

During hypoxia the peak and cumulative wave intensities increased (Table 6-1), but the early systolic forward compression wave became a smaller proportion of cumulative wave energy at 50.3 ± 10.3 % down from 64.8 ± 12.9 %.

The early systolic backward expansion wave remained during the presence of hypoxia, increasing from 4.12 ± 3.44 to 16.35 ± 14.23 × 10^2 $Wm^{-2}s^{-1}$ ($p < 0.001$). The reflection coefficient increased from -0.02 ± 0.01 to -0.05 ± 0.05 ($p < 0.01$). Importantly, the distance to this proximal reflection site did not change significantly (normoxia, 2.6 ± 0.6 cm and hypoxia, 2.3 ± 0.9 cm; $p = 0.58$).

A new broad backwards compression wave (Figure 6-1) arrived in the proximal pulmonary artery in mid-systole, 94 ± 27 ms after the forward-travelling compression wave. The reflection site was 13.5 ± 4.5 cm downstream. The reflection coefficient for the backward-travelling compression wave increased from +0.02 ± 0.01 to + 0.11 ± 0.07 (Table 6-1).

Table 6-1. Wave Intensity and Haemodynamic Parameters at Rest and During Hypoxia

	Control (n = 8)	Hypoxia (n = 8)	P Value
Peak Wave Intensity ($\times 10^4$ $Wm^{-2}s^{-2}$)			
Early Forward Compression	79.24 ± 30.16	129.74 ± 76.16	0.002
Late Forward Expansion	25.88 ± 15.77	72.89 ± 31.14	< 0.001
Late Forward Compression	4.89 ± 4.11	9.94 ± 11.80	0.08
Early Backward Expansion	1.85 ± 1.53	6.43 ± 5.24	< 0.001
Backward Compression	1.54 ± 1.31	7.17 ± 3.30	< 0.001
Cumulative Wave Intensity ($\times 10^2$ $Wm^{-2}s^{-1}$)			
Early Forward Compression	251.29 ± 77.17	381.72 ± 182.32	<0.001
Late Forward Expansion	119.77 ± 70.19	295.21 ± 115.38	< 0.001
Late Forward Compression	12.75 ± 10.34	24.15 ± 33.72	0.15
Early Backward Expansion	4.12 ± 3.44	16.35 ± 14.23	< 0.001
Backward Compression	4.64 ± 3.68	35.02 ± 19.35	< 0.001
Proportion of Cumulative Wave Intensity (%)			
Early Forward Compression	64.8 ± 12.9	50.3 ± 10.3	<0.001
Late Forward Expansion	29.8 ± 11.7	39.2 ± 6.9	<0.001
Late Forward Compression	3.2 ± 2.0	3.2 ± 4.7	0.984
Early Backward Expansion	1.1 ± 0.9	2.3 ± 2.2	0.007
Backward Compression	1.2 ± 0.8	5.0 ± 2.9	<0.001
Reflection Coefficient			
BEW/FCW	-0.02 ± 0.01	-0.05 ± 0.05	0.001
BCW/FCW	0.02 ± 0.01	0.11 ± 0.07	<0.001
Wave Speed (ms^{-1})	2.1 ± 0.3	2.9 ± 0.4	<0.001
Distance to Reflection Site (cm)			
Early Backward Expansion	2.6 ± 0.6	2.3 ± 0.9	0.350
Late Backward Compression	24.1 ± 7.7	13.5 ± 4.5	<0.001
PaO_2 (mmHg)	101 ± 2	32 ± 3	<0.001
Heart Rate (min^{-1})	105 ± 17	117 ± 18	0.018
Peak Blood Velocity (ms^{-1})	0.87 ± 0.01	0.98 ± 0.04	< 0.001
Cardiac Output ($Lmin^{-1}$)	3.4 ± 1.0	4.0 ± 1.3	0.007
LVEDP (mmHg)	5.5 ± 2.6	8.4 ± 4.1	< 0.001
Mean PA Pressure (mmHg)	16.0 ± 3.0	26.8 ± 3.6	<0.001
PVR (Wood's Units)	3.3 ± 1.4	5.0 ± 2.3	0.02

Values are means ± standard deviation; BCW, backward compression wave; BEW, backward expansion wave; FCW, forward compression wave; LV, left ventricle; LVEDP, left ventricular end diastolic pressure; n, number of sheep; PA, pulmonary artery; PaO_2, systemic arterial partial pressure of oxygen; PVR, pulmonary vascular resistance.

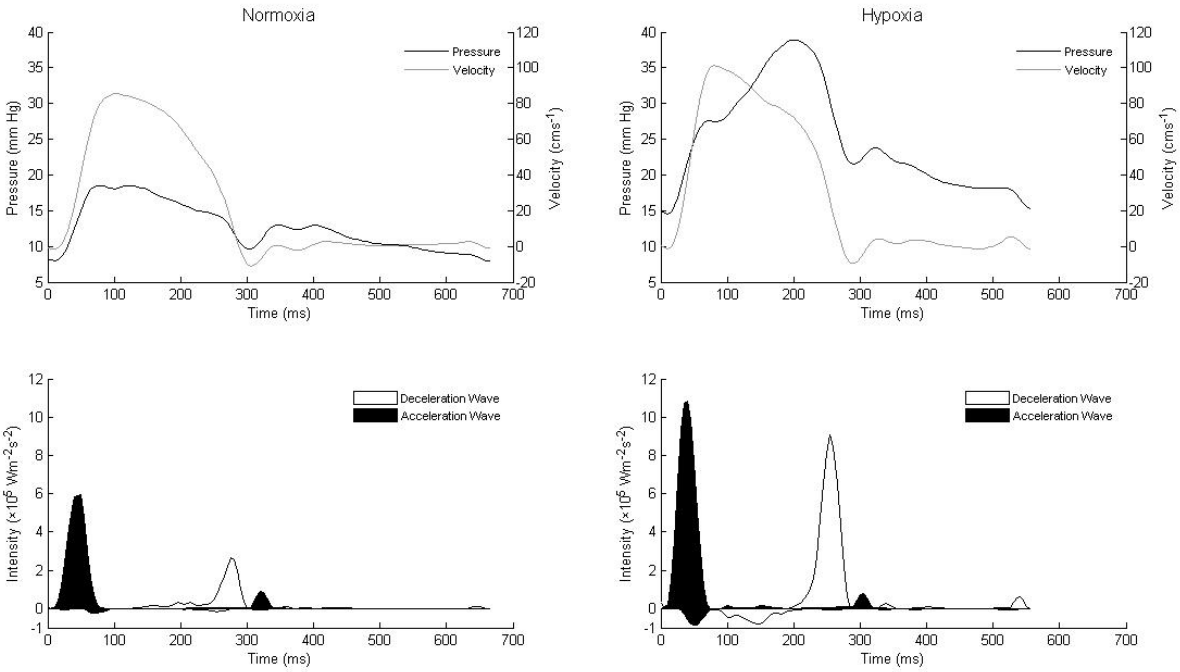

Figure 6-1. Wave Intensity at Rest and During Hypoxia.

6.2.3 Discussion

Hypoxia is known to increase sympathetic activity (Mazzeo *et al.*, 1991), which may increase right ventricular contractility, evidenced by an 11% increase in heart rate and small increase in stroke volume from 32.3 mL/beat to 34.2 mL/beat. Increased right ventricular contractility is also supported by the observed increase in the rate of pressure and velocity rise (increased dP and dU) leading to an increase in peak and cumulative intensity of the forward compression wave (Table 6-1). The increased energy of the forward-travelling wave reflects the increased rate of hydraulic work done by the right ventricle. The increased cardiac output suggests that preload has not been significantly reduced by hypoxic pulmonary vasoconstriction and the increased energy of the forward-travelling compression wave supports this notion. Interestingly, the forward-travelling expansion wave becomes a greater proportion of the total wave energy during hypoxia, rising from 30% to 39%. This suggests that during increased right ventricular afterload, the rate of myofibril deceleration during late systole is significantly faster, leading to enhancement of the forward expansion wave energy.

During hypoxia backward-travelling waves become a much greater proportion of total cumulative wave energy. This not only relates to increased forward-travelling wave energy being available for reflection but also, more importantly, from enhanced reflection coefficients of both dominant reflection sites. At the proximal open-end reflector during hypoxia, 5% of the incident forward compression wave was negatively reflected as a backward expansion wave compared to 2% during normoxia ($p < 0.01$). This does not appear to be a substantial increase in the reflection coefficient but does generate a 12.23×10^2 $Wm^{-2}s^{-1}$ increase in the cumulative wave intensity of the backward-travelling expansion. This increase may enhance right ventricular emptying during the period of increased right ventricular afterload. These findings imply that the daughter-to-parent area ratio increases as a geometrical response to increased pressure and distension. The alternative explanation that enhanced negative reflection results from increased daughter vessel distensibility does not seem plausible during periods of hypoxia, as vessel stiffness is likely to increase with sympathetic activation.

During hypoxia the mid-systolic backward compression wave becomes an impressive $5.0 \pm 2.9\%$ of the total cumulative wave energy. With hypoxia, 11% of the incident forward compression wave is reflected in a positive manner as a backward compression wave compared to 2% with normoxia, highlighting the enhanced closed-end reflection from pulmonary vasoconstriction. More importantly, WIA was able to demonstrate that the closed-end reflection site moved more proximally appearing 13.5 ± 4.5 cm downstream and entirely replaced the more distal closed-end reflection site seen at 24.1 ± 7.7 cm during normoxia. It is possible that wave speed increases distally under periods of hypoxia, thus the calculated reflection site would be underestimated. Nevertheless, the new closed-end reflection site corresponds to the location of the small arterioles that are influenced by the hypoxic vasoconstrictor response (Dawson *et al.*, 1979; Marshall and Marshall, 1983).

Proximal pulmonary arterial wave speed increased by 0.8 ms^{-1} (38%) during hypoxia, suggesting that downstream vascular changes lead to alterations of proximal pulmonary arterial compliance. The reduced proximal compliance may result from passive distension secondary to the increased pulmonary pressure, direct proximal vasoconstrictive effects of hypoxia, or more likely from active proximal vasoconstriction driven by sympathetic stimulation in response to hypoxia. The heart rate, however, increased by only 15 beats/minute suggesting the sympathetic system is not overwhelmingly active. The increased peak blood velocity during hypoxia provides some evidence that passive proximal pulmonary dilatation did not occur. It is recognised that sympathetic stimulation causes constriction of the large proximal pulmonary arteries (Barnes and Liu, 1995; Downing and Lee, 1980). The sympathetic reduction in compliance may have been even more pronounced if the adventitia was not removed to allow placement of the flow transducer. It has been shown that proximal pulmonary artery compliance falls with increasing mean pulmonary artery pressure or increasing heart rate during which proximal pulmonary artery constriction occurs (Kornet *et al.*, 1998).

The present findings are consistent with other studies that demonstrated a 30% increase in wave speed and reduced proximal pulmonary compliance with hypoxia (Zuckerman *et al.*, 1992). Such a phenomenon has physiological advantages, as the enhanced wave speed will allow the transmission of pressure and velocity waveforms distally to maintain pulmonary capillary perfusion in the face of vasoconstriction. Of course this advantage comes at the expense of right ventricular efficiency, as the increased wave speed leads to the earlier return of the amplified backward compression wave during mid-systole, further increasing the right ventricular afterload. Milnor *et al.* (1969) in studies of power dissipation in the pulmonary bed showed that decreased arterial distensibility is of similar importance to increased resistance in the elevation of right ventricular load with pulmonary hypertension.

6.3 Pulmonary Emboli

6.3.1 Anticipated Wave Intensity

Autologous blood clot pulmonary embolization was undertaken to simulate obstruction of medium to small pulmonary arteries without necessarily altering the vasoactive state of the pulmonary vasculature. It was anticipated that embolization would enhance closed-end reflection from the medium pulmonary arteries, which in conjunction with an increased wave speed would lead to amplification of the energy and earlier arrival of the backward-travelling compression wave.

6.3.2 Results

The administration of 6-12 mL of autologous blood-clot pulmonary emboli led to irreversible haemodynamic impairment. The mean pulmonary artery pressure increased substantially from 17.4 ± 2.7 to 29.3 ± 5.0 mmHg ($p < 0.001$), with a concurrent elevation in pulmonary vascular resistance from 4.6 ± 1.8 to 8.0 ± 3.5 Wood's Units ($p < 0.001$). Cardiac output was maintained following embolization, changing from 3.2 ± 0.8 to 3.3 ± 0.8 $Lmin^{-1}$ ($p = 0.47$). Pulmonary arterial wave speed increased dramatically from 2.2 ± 0.3 ms^{-1} to 3.1 ± 0.7 ms^{-1} ($p < 0.001$).

During embolization the peak intensity of the early forward compression wave fell from 71.57 ± 26.57 to 64.47 ± 24.26 × 10^2 $Wm^{-2}s^{-2}$ ($p = 0.01$), whilst the peak and cumulative intensities for the remaining waves increased (Table 6-2). The two dominant backward travelling waves become a much greater proportion of cumulative wave intensity (Table 6-2). The early backward expansion wave energy increased from 4.84 ± 3.26 to 12.63 ± 10.40 × 10^2 $Wm^{-2}s^{-1}$ ($p < 0.001$) with an increase in the reflection coefficient from -0.02 ± 0.01 to -0.05 ± 0.04 ($p < 0.001$). The backward compression wave increased from 4.43 ± 3.08 to 38.84 ± 27.94 × 10^2 $Wm^{-2}s^{-1}$ ($p < 0.001$) with an increase in the reflection coefficient from 0.02 ± 0.01 to 0.18 ± 0.13 ($p < 0.001$).

The distance to the proximal open-end reflector changed from 2.7 ± 0.8 to 1.5 ± 1.3 cm ($p < 0.001$), whilst the distal closed-end reflector moved more proximally from 22.8 ± 8.7 to 15.9 ± 3.6 cm ($p < 0.001$) downstream from the measurement location.

Table 6-2. Wave Intensity and Haemodynamic Parameters at Rest and During Pulmonary Embolization

	Control (n = 9)	PE (n = 9)	P Value
Peak Wave Intensity ($\times 10^4$ $Wm^{-2}s^{-2}$)			
Early Forward Compression	71.57 ± 26.57	64.47 ± 24.26	0.01
Late Forward Expansion	32.66 ± 24.00	61.87 ± 25.26	< 0.001
Late Forward Compression	7.30 ± 6.56	9.28 ± 10.74	0.33
Early Backward Expansion	1.89 ± 1.26	4.04 ± 3.06	<0.001
Backward Compression	1.43 ± 0.89	7.75 ± 6.34	<0.001
Cumulative Wave Intensity ($\times 10^2$ $Wm^{-2}s^{-1}$)			
Early Forward Compression	229.82 ± 66.33	221.10 ± 63.84	0.265
Late Forward Expansion	132.15 ± 61.84	211.03 ± 74.03	<0.001
Late Forward Compression	17.88 ± 14.01	19.11 ± 21.90	0.768
Early Backward Expansion	4.84 ± 3.26	12.63 ± 10.40	<0.001
Backward Compression	4.43 ± 3.08	38.84 ± 27.94	<0.001
Proportion of Cumulative Wave Intensity (%)			
Early Forward Compression	59.7 ± 13.0	45.0 ± 10.4	<0.001
Late Forward Expansion	33.4 ± 10.7	41.5 ± 7.5	<0.001
Late Forward Compression	4.6 ± 3.1	3.8 ± 4.2	0.365
Early Backward Expansion	1.2 ± 0.8	2.3 ± 1.7	<0.001
Backward Compression	1.2 ± 0.8	7.4 ± 4.2	<0.001
Reflection Coefficient			
BEW/FCW	-0.02 ± 0.01	-0.05 ± 0.04	<0.001
BCW/FCW	0.02 ± 0.01	0.18 ± 0.13	<0.001
Wave Speed (ms^{-1})	2.2 ± 0.3	3.1 ± 0.7	<0.001
Distance to Reflection Site (cm)			
Early Backward Expansion	2.7 ± 0.8	1.5 ± 1.3	<0.001
Late Backward Compression	22.8 ± 8.7	15.9 ± 3.6	<0.001
PaO_2 (mmHg)	97 ± 9	73 ± 9	0.010
Heart Rate (min^{-1})	109 ± 10	115 ± 12	<0.001
Peak Blood Velocity (ms^{-1})	0.85 ± 0.01	0.82 ± 0.02	0.03
Cardiac Output ($Lmin^{-1}$)	3.2 ± 0.8	3.3 ± 0.8	0.472
LVEDP (mmHg)	5.2 ± 3.5	6.3 ± 3.9	0.01
Mean PA Pressure (mmHg)	17.4 ± 2.7	29.3 ± 5.0	<0.001
PVR (Wood's Units)	4.6 ± 1.8	8.0 ± 3.5	<0.001

Values are means ± SD; BCW, backward compression wave; BEW, backward expansion wave; FCW, forward compression wave; LV, left ventricle; LVEDP, left ventricular end diastolic pressure; n, number of sheep; PA, pulmonary artery; PaO_2, systemic arterial partial pressure of oxygen; PE, pulmonary embolus; PVR, pulmonary vascular resistance.

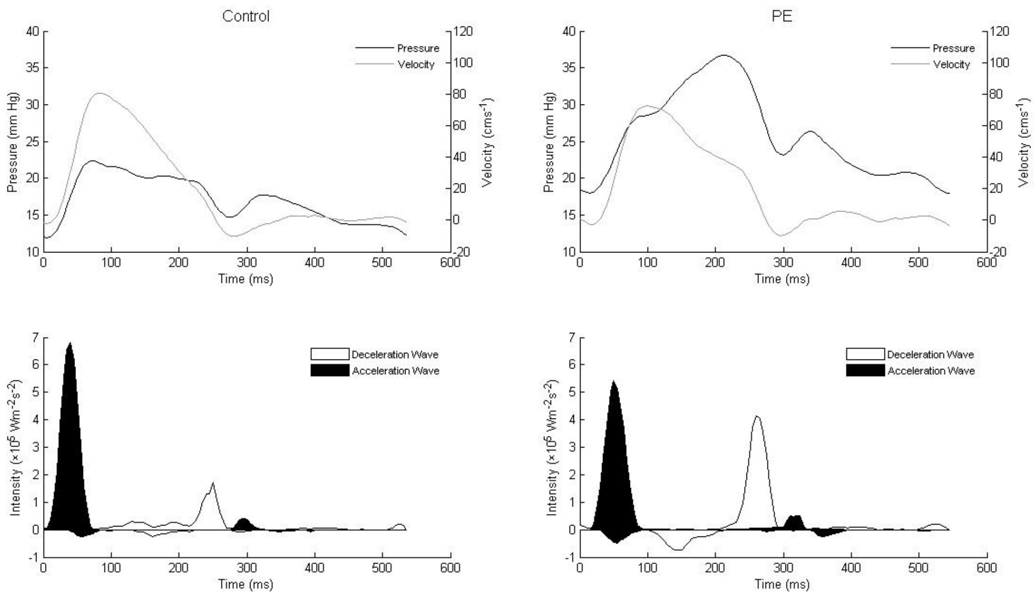

Figure 6-2. Wave Intensity at Rest and During Pulmonary Embolization.

6.3.3 Discussion

It was anticipated that the increased right ventricular afterload would manifest as an increase in each of the forward-travelling wave energies, reflecting the increased work of the right ventricle. Yet from Figure 6-2 it is apparent that the peak intensity of the initial forward compression wave falls. This should not be immediately interpreted as a reduction in the external work done by the heart as the mid-systolic backward-travelling compression wave also contributes greatly to the systolic workload. The peak blood velocities fell slightly but significantly from 0.85 ± 0.01 ms^{-1} to 0.82 ± ms^{-1} (p =0.03) during embolization. Furthermore, there was a reduction in the rate of velocity and pressure generation, therefore leading to a lower intensity (dP × dU). However, the slower rate of pressure and velocity rise during acute pulmonary hypertension, reflecting right ventricular strain, is maintained for longer resulting in a cumulative energy of the forward compression wave that is not statistically different at 221.10 ± 63.84 × 10^2 Wm^{-2}s^{-1} vs 229.82 ± 66.33 × 10^2 Wm^{-2}s^{-1} (p = 0.27). It is interesting that despite a similar increase in mean pulmonary artery pressure and less hypoxaemia as achieved during the hypoxia experiments, pulmonary embolization led to more severe myocardial impairment as indicated by the reduced forward compression wave intensity.

The increased energetic state of the right ventricle manifests in the increased energy of the forward-travelling expansion wave, which becomes a much greater proportion of total cumulative wave intensity at 42%. This finding was also seen during hypoxia, which is a situation that also increases right ventricular strain. An increased proportion of energy carried by the forward-travelling expansion wave may reflect a ventricle under strain, with greater energy cost, as there is a greater deceleration in the rate of myofibril shortening.

The dominant finding during pulmonary embolization was that a substantial backward-travelling compression wave arrived in the proximal pulmonary artery during mid-systole. The presence of obstructed small arteries led to enhanced closed-end reflection, such that 18% of the forward compression wave was reflected positively as a backward compression wave compared to only 2% at baseline. The backward compression wave arrived earlier in mid-systole, opposing flow out of the right ventricle and therefore increasing myocardial work.

Importantly the closed-end reflection site moved more proximally from 22.8 ± 8.7 cm to 15.9 ± 3.6 cm ($p < 0.001$). This was in keeping with examination of the explanted lung in several sheep, which demonstrated extensive 1-2 mm thrombi lodged in the small pulmonary arteries approximately 15-18 cm distal to the measurement location in the proximal pulmonary artery. These findings demonstrate that WIA has the capabilities to accurately define the site of vascular obstruction, at least during acute pulmonary hypertension.

It is likely that the enhanced closed-end reflection is simply a function of the vascular obstruction by emboli alone. There was unlikely to be a significant contribution from hypoxic vasoconstriction because the PaO_2 fell from 97 ± 9 to 73 ± 9 mmHg ($p = 0.01$), levels that do not appear to lead to backward compression waves. Nevertheless, the intrapulmonary vasomotor response to pulmonary emboli is poorly understood and a significant contribution from pulmonary vasoconstriction to the closed-end reflection cannot be excluded.

There was a substantial increase in wave speed from $2.2 \pm 0.3\ ms^{-1}$ to $3.1 \pm 0.7\ ms^{-1}$ ($p < 0.001$) during embolization. The increase in proximal pulmonary arterial wave speed occurred despite the site of vascular obstruction being downstream. This reinforces the notion that changes in the distal vasculature do influence the properties of the proximal pulmonary arteries. Mechanisms could be passive via effects of distension resulting from elevated pulmonary pressures or they could be active resulting from sympathetic vasoconstriction. As pulmonary blood volume has not been measured it is uncertain as to the dominant mechanism. However, the findings of reduced vascular compliance (increased wave speed) are in keeping with other reports of reduced pulmonary compliance and blood volume with macroembolism (Alpert *et al.*, 1974), suggesting active pulmonary vasoconstriction.

Pulmonary embolization did not abolish the early systolic backward expansion wave, indicating that the proximal open-end reflector remains. This was also observed with hypoxia suggesting acute increases in right ventricular afterload do not abolish the proximal open-end reflector site. The open-end reflection was in fact enhanced by pulmonary embolization, with 5% of the incident forward compression wave energy reflected as a backward expansion wave compared to just 2% at baseline. The distance to the proximal open-end reflector shifted from 2.7 ± 0.8 cm to a more proximal location at 1.5 ± 1.3 cm ($p < 0.001$). These results suggest that an increased area ratio of the daughter-to-parent vessels has occurred, probably resulting from marked distension of the pulmonary vasculature in response to the elevated pulmonary pressures. This distension was not transmitted to the most proximal part of the main pulmonary artery, perhaps related to its increased collagen content.

These results were observed with multiple small acute pulmonary emboli. No conclusions are able to be drawn regarding the pattern of wave reflection with a large pulmonary embolus, recurrent thromboembolism or the pathological entity chronic thromboembolic pulmonary hypertension. It would be expected that a large thrombus burden would enhance the positive reflection coefficient leading to increased energy of the backward-travelling compression wave.

6.4 Positive End-Expiratory Pressure

6.4.1 Anticipated Wave Intensity

Extrinsic positive end-expiratory pressure (PEEP) enhances lung volume (functional residual capacity) and is used in patients with hypoxaemic respiratory failure who are mechanically ventilated to improve arterial oxygenation (Acosta *et al.*, 2007). PEEP is known to have adverse haemodynamic effects in closed-chest preparations resulting from the increased intrathoracic pressure leading to increased central venous pressures and reduced cardiac filling due to decreased cardiac return (Huemer *et al.*, 1994). The increased intra-alveolar pressure compresses the small alveolar vessels and small pulmonary arteries to increase pulmonary vascular resistance and right ventricular afterload. It is anticipated that PEEP would act as a reversible method of vascular obstruction that would also lead to enhancement of the backward compression wave arising from the distal microcirculation.

6.4.2 Results

Administration of 20 cm H_2O (14.7 mmHg) extrinsic positive end-expiratory pressure (PEEP) resulted in the mean pulmonary artery pressure rising significantly from 15.6 ± 2.0 to 23.1 ± 2.5 mmHg ($p < 0.001$). Peak blood velocity fell from 0.94 ± 0.02 to 0.83 ± 0.02 ms^{-1} ($p < 0.001$) and cardiac output fell from 3.7 ± 0.8 to 3.1 ± 0.8 $Lmin^{-1}$ ($p < 0.001$). These haemodynamic changes resulted in an increase in the pulmonary vascular resistance from 3.9 ± 2.9 to 5.3 ± 3.3 Wood's Units ($p < 0.001$). Some of the increased intrathoracic pressure induced by PEEP was transmitted to the left ventricle, evidenced by a rise in left ventricular end-diastolic pressure (LVEDP) from 1.8 ± 9.2 to 5.6 ± 8.8 mmHg ($p = 0.01$). There was a small but significant increase in proximal pulmonary arterial wave speed from 2.0 ± 0.3 to 2.3 ± 0.4 ms^{-1} ($p < 0.001$).

The peak intensity of the early forward compression wave fell from 77.59 ± 28.64 to 52.18 ± 16.60 × 10^2 $Wm^{-2}s^{-2}$ ($p < 0.001$; Figure 6-3) and the cumulative intensity fell from 242.68 ± 64.92 to 171.31 ± 51.62 × 10^2 $Wm^{-2}s^{-1}$ ($p < 0.001$). The remaining waves had an increase in peak and cumulative energy with the exception of the late backward compression wave, which did not change significantly (Table 6-3).

The addition of PEEP increased the open-end reflection coefficient from -0.02 ± 0.02 to -0.04 ± 0.02 ($p < 0.001$). The distance to the open-end reflector did not alter significantly from 2.5 ± 0.9 to 1.8 ± 1.4 cm ($p = 0.43$). The reflection coefficient for the distal closed-end reflector increased, but not significantly so, from 0.02 ± 0.01 to 0.04 ± 0.03 ($p = 0.05$). The distance to the closed-end reflector increased modestly from 21.8 ± 5.1 to 25.5 ± 9.0 cm ($p = 0.03$).

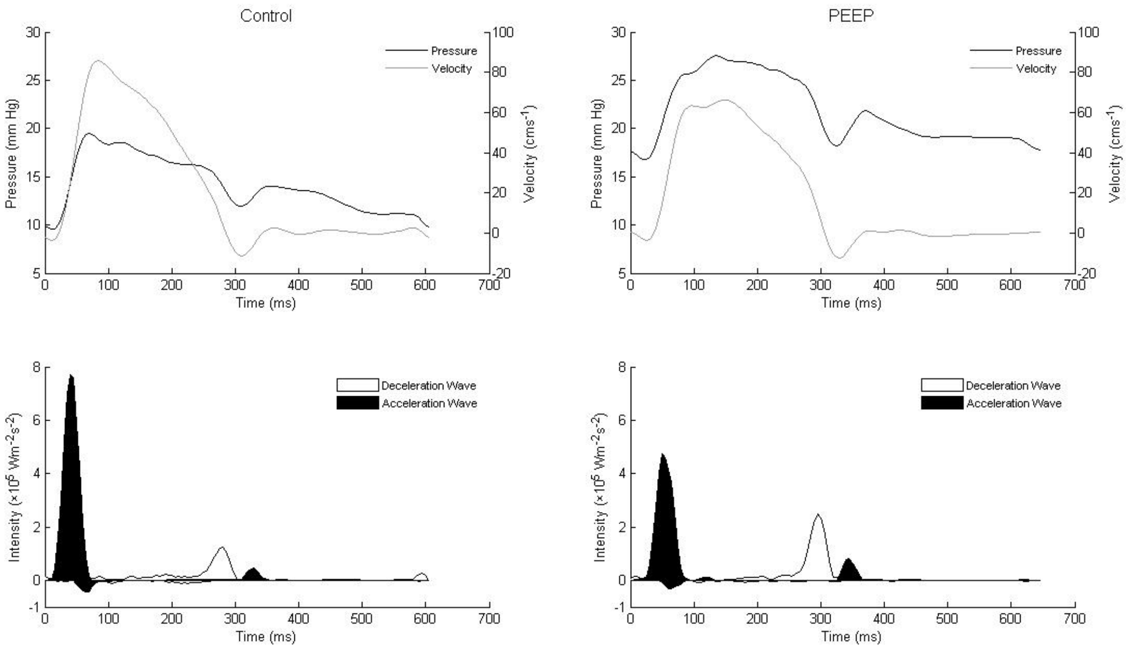

Figure 6-3. Wave Intensity at Rest and During Positive End Expiratory Pressure.

Table 6-3. Wave Intensity and Haemodynamic Parameters at Rest and During Positive End Expiratory Pressure

	Control (n = 9)	PEEP (n = 9)	P Value
Peak Wave Intensity ($\times 10^4$ Wm^{-2}s^{-2})			
Early Forward Compression	77.59 ± 28.64	52.18 ± 16.60	<0.001
Late Forward Expansion	28.47 ± 10.83	43.95 ± 16.09	<0.001
Late Forward Compression	4.20 ± 3.08	8.56 ± 5.24	<0.001
Early Backward Expansion	1.99 ± 2.07	2.55 ± 1.28	0.12
Backward Compression	1.79 ± 1.33	1.66 ± 1.44	0.78
Cumulative Wave Intensity ($\times 10^2$ Wm^{-2}s^{-1})			
Early Forward Compression	242.68 ± 64.92	171.31 ± 51.62	<0.001
Late Forward Expansion	137.57 ± 57.82	180.13 ± 77.17	<0.001
Late Forward Compression	10.56 ± 6.15	21.57 ± 12.15	<0.001
Early Backward Expansion	3.73 ± 4.41	6.93 ± 3.77	0.001
Backward Compression	5.60 ± 3.00	5.37 ± 4.22	0.83
Proportion of Cumulative Wave Intensity (%)			
Early Forward Compression	60.7 ± 10.9	45.2 ± 9.8	<0.001
Late Forward Expansion	34.1 ± 11.4	45.3 ± 9.5	<0.001
Late Forward Compression	2.8 ± 1.7	6.0 ± 3.1	<0.001
Early Backward Expansion	1.0 ± 1.2	1.9 ± 1.1	<0.001
Backward Compression	1.4 ± 0.6	1.6 ± 1.2	0.16
Reflection Coefficient			
BEW/FCW	-0.02 ± 0.02	-0.04 ± 0.02	<0.001
BCW/FCW	0.02 ± 0.01	0.04 ± 0.03	0.05
Wave Speed (ms^{-1})	2.0 ± 0.3	2.3 ± 0.4	<0.001
Distance to Reflection Site (cm)			
Early Backward Expansion	2.5 ± 0.9	1.8 ± 1.4	0.43
Late Backward Compression	21.8 ± 5.1	25.5 ± 9.0	0.03
Heart Rate (min^{-1})	109 ± 16	109 ± 16	0.78
Peak Blood Velocity (ms^{-1})	0.94 ± 0.02	0.83 ± 0.02	< 0.001
Cardiac Output (Lmin^{-1})	3.7 ± 0.8	3.1 ± 0.8	<0.001
LVEDP (mmHg)	1.8 ± 9.2	5.6 ± 8.8	0.01
Mean PA Pressure (mmHg)	15.6 ± 2.0	23.1 ± 2.5	<0.001
PVR (Wood's Units)	3.9 ± 2.9	5.3 ± 3.3	< 0.001

Values are means ± SD; BCW, backward compression wave; BEW, backward expansion wave; FCW, forward compression wave; LV, left ventricle; LVEDP, left ventricular end diastolic pressure; n, number of sheep; PA, pulmonary artery; PE, pulmonary embolus; PEEP, positive end-expiratory pressure; PVR, pulmonary vascular resistance.

6.4.3 Discussion

Despite using an open-chest animal model the administration of PEEP still led to marked and deleterious haemodynamic effects. The mean pulmonary pressure increased significantly by 7.5 mmHg (48%), whilst the cardiac output and peak blood velocity fell substantially. The haemodynamic changes of PEEP are complex. Some argue that the reduced cardiac output is simply a function of the reduced cardiac filling in response to reduced venous return rather than increased right ventricular afterload (Huemer *et al.*, 1994). However, these invasive results do demonstrate an increase in pulmonary vascular resistance and mean pulmonary artery pressure with PEEP indicating an increase in right ventricular afterload. The complex interaction of PEEP with cardiac haemodynamics is highlighted by the result that LVEDP increased with PEEP despite a fall in cardiac output, which suggests that in this animal model, the elevated intrapulmonary pressures may be transferred to the heart extrinsically. Strong conclusions cannot be drawn in this regard because the volume status of the left ventricle was not investigated. The reduced right ventricular preload is evidenced by the lower rates of pressure and velocity generation (manifest as lower peak and cumulative forward compression wave intensity) suggesting reduced contractility.

Despite the increased right ventricular afterload, wave speed only increased by 0.3 ms^{-1} (15%). This implies that the change in proximal pulmonary artery compliance was minimal with administration of PEEP. Indeed, it has been shown previously that PEEP does not alter the compliance of the proximal pulmonary artery greatly (Calvin Jr *et al.*, 1985; Fitzpatrick and Grant, 1990; Smith *et al.*, 1982). In comparison, hypoxia induced the same order of magnitude increase in mean pulmonary artery pressure (68%) whilst the wave speed increased more substantially by 38%. This implies that the increase in pulmonary artery pressure with PEEP is passive and suggests that with hypoxia there is an active increase in proximal pulmonary artery tone, leading to reduced compliance and increased wave speed.

Consequent to the slower rate of pressure and velocity generation with PEEP the peak and cumulative energies of the initial forward compression wave fell. This suggests PEEP reduces the rate at which right ventricular work is done in early systole. The peak and cumulative energy of the forward expansion wave in contrast rose significantly and this wave became a much greater proportion of total wave energy. This suggests that during PEEP, the rate of deceleration of myocardial shortening in late systole is much faster.

Despite a fall in the cumulative energy of the incident forward compression wave the cumulative energy of the reflected early backward expansion wave increased, representing enhanced negative reflection such that 4% of the incident wave energy was reflected compared to 2% at baseline. It is likely that the raised pulmonary pressures in response to PEEP caused distension of the daughter vessels to a greater degree than the main pulmonary artery leading to a raised area ratio resulting in an increased reflection coefficient. The distance to the open-end reflection site thought to be the bifurcation of the main pulmonary artery did not alter significantly.

Despite the increased right ventricular afterload a dominant backwards compression wave was not evident. In fact the cumulative wave intensity of the backward compression wave did not alter significantly. It is likely that the balance of distribution in closed-end reflection between the small pulmonary arteries and the alveolar vessels is altered by PEEP. Whilst PEEP compresses the alveolar vessels, the overriding action of PEEP and resultant alveolar distension is the splinting open of the alveolar corner vessels. This would serve to minimise closed-end reflection from the corner vessels. Indeed, the closed-end reflection site moved more distally from 21.8 ± 5.1 to 25.5 ± 9.0 cm ($p= 0.03$), suggesting that PEEP did have a tethering effect of opening the corner small pulmonary arteries and increasing the distance to the reflection source. The tethering and expansion effect of extra-alveolar vessels to the expanding lung, which occurs with PEEP, has been well described (Culver and Butler, 1980; Howell *et al.*, 1961).

6.5 Left Main Pulmonary Artery Clamping

6.5.1 Anticipated Wave Intensity

Clamping of the left main pulmonary artery was undertaken to simulate obstruction of the proximal pulmonary artery. It was anticipated that this proximal obstruction would lead to a backwards compression wave in very early systole that would oppose right ventricular emptying.

6.5.2 Results

Clamping of the left main pulmonary artery led to a reversible rise in the mean pulmonary artery pressure from 15.9 ± 3.0 to 22.1 ± 4.8 mmHg ($p < 0.001$) and an increase in the pulmonary vascular resistance from 4.2 ± 1.5 to 6.5 ± 1.9 Wood's Units ($p < 0.001$). The cardiac output did not alter significantly from 3.1 ± 0.7 to 3.0 ± 0.7 ($p = 0.05$). Clamping led to a very marked increase in the pulmonary arterial wave speed, rising from 2.2 ± 0.3 to 3.5 ± 0.9 ms^{-1}.

The late forward expansion and the backward compression waves were the only waves that significantly increased their peak and cumulative energies during clamping (Table 6-4). The backwards compression wave arrived earlier in mid-systole (Figure 6-4), yet, because of the increased wave speed, the distance to the closed-end reflector site remain unchanged at 21.6 ± 6.8 cm from 20.8 ± 5.7 cm ($p = 0.25$). The reflection coefficient for this closed-end reflector site increased from 0.03 ± 0.02 to 0.08 ± 0.07 ($p = 0.001$).

The presence of the early backward expansion wave remained during left main branch pulmonary clamping (Figure 6-4), though the cumulative wave intensity did not change significantly from 3.16 ± 3.90 to 4.25 ± 5.75 × 10^2 $Wm^{-2}s^{-1}$ ($p = 0.19$). In keeping with the unaltered energy, the reflection coefficient was unchanged from -0.02 ± 0.02 to -0.02 ± 0.02 ($p = 0.67$). The site of this open-end reflector did not change significantly at 2.4 ± 1.2 cm from 3.0 ± 0.9 cm ($p = 0.31$).

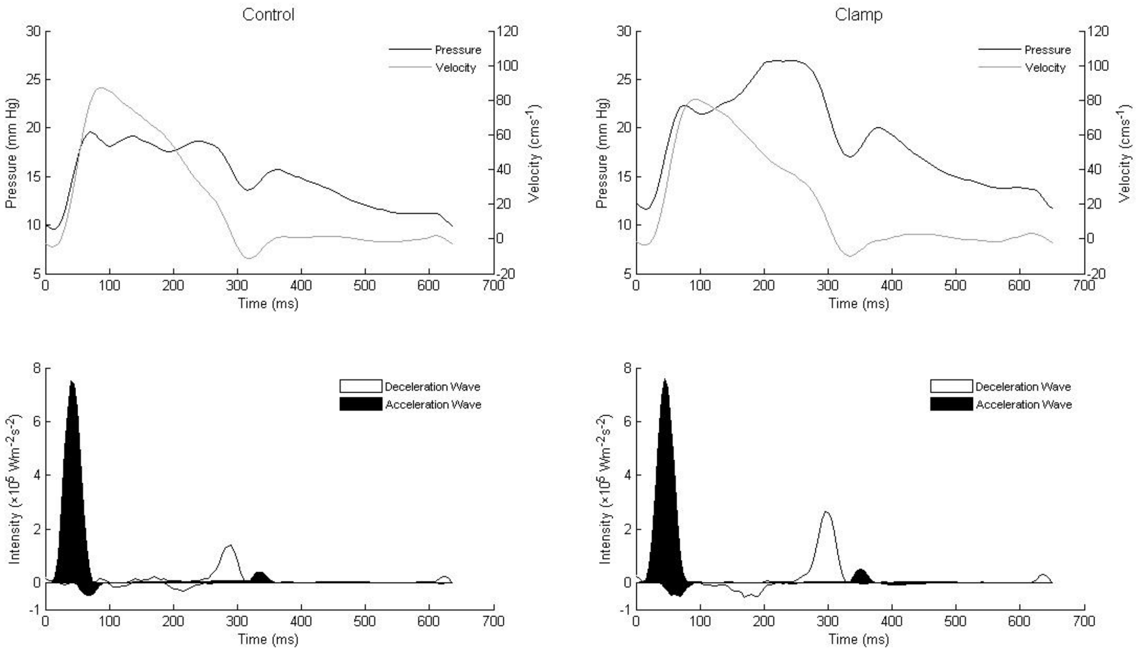

Figure 6-4. Wave Intensity at Rest and During Left Main Pulmonary Artery Clamping.

6.5.3 Discussion

Clamping of the left main pulmonary artery excluded 50% of the pulmonary vasculature from the blood circulation. Despite the entire unchanged cardiac output passing through the right lung, the rise in mean pulmonary artery pressure was minimal (levels that would not be considered pulmonary hypertension by current diagnostic criteria) and the pulmonary vascular resistance rose less than two-fold. This highlights the remarkable ability for this compliant circulation to distend and recruit blood vessels to minimise pressure changes and subsequent damage to the alveolar capillaries.

Nevertheless, clamping did lead to some important haemodynamic consequences. The distension of the pulmonary circulation and loss of compliance caused a marked 60% increase in pulmonary arterial wave speed. With pulmonary clamping the rate of myocardial work in early systole appears unchanged, as the intensity of the forward compression wave remains unchanged.

Table 6-4. Wave Intensity and Haemodynamic Parameters at Rest and During Left Main Pulmonary Artery Clamping

	Control (n = 8)	Clamp (n = 8)	P Value
Peak Wave Intensity ($\times 10^4$ $Wm^{-2}s^{-2}$)			
Early Forward Compression	60.18 ± 34.23	61.77 ± 27.88	0.64
Late Forward Expansion	26.18 ± 17.09	46.45 ± 30.03	<0.001
Late Forward Compression	5.55 ± 5.15	3.78 ± 2.49	0.16
Early Backward Expansion	1.36 ± 1.52	1.38 ± 1.91	0.92
Backward Compression	1.01 ± 0.72	3.63 ± 3.65	<0.001
Cumulative Wave Intensity ($\times 10^2$ $Wm^{-2}s^{-1}$)			
Early Forward Compression	188.49 ± 85.22	201.44 ± 75.81	0.17
Late Forward Expansion	100.58 ± 51.69	170.94 ± 91.02	<0.001
Late Forward Compression	12.90 ± 10.22	9.34 ± 7.07	0.23
Early Backward Expansion	3.16 ± 3.90	4.25 ± 5.75	0.19
Backward Compression	3.97 ± 2.86	17.92 ± 17.43	<0.001
Proportion of Cumulative Wave Intensity (%)			
Early Forward Compression	60.3 ± 11.8	51.5 ± 11.9	<0.001
Late Forward Expansion	32.3 ± 10.5	40.6 ± 10.6	<0.001
Late Forward Compression	4.8 ± 3.2	3.3 ± 3.8	0.053
Early Backward Expansion	1.1 ± 1.3	0.9 ± 1.2	0.38
Backward Compression	1.6 ± 1.2	3.8 ± 2.9	0.002
Reflection Coefficient			
BEW/FCW	-0.02 ± 0.02	-0.02 ± 0.02	0.67
BCW/FCW	0.03 ± 0.02	0.08 ± 0.07	0.001
Wave Speed (ms^{-1})	2.2 ± 0.3	3.5 ± 0.9	<0.001
Distance to Reflection Site (cm)			
Early Backward Expansion	3.0 ± 0.9	2.4 ± 1.2	0.31
Late Backward Compression	20.8 ± 5.7	21.6 ± 6.8	0.25
Heart Rate (min^{-1})	109 ± 18	106 ± 14	0.24
Peak Blood Velocity (ms^{-1})	0.77 ± 0.02	0.70 ± 0.02	< 0.001
Cardiac Output ($Lmin^{-1}$)	3.1 ± 0.7	3.0 ± 0.7	0.05
LVEDP (mmHg)	5.2 ± 2.9	6.0 ± 3.7	0.07
Mean PA Pressure (mmHg)	15.9 ± 3.0	22.1 ± 4.8	<0.001
PVR (Wood's Units)	4.2 ± 1.5	6.5 ± 1.9	<0.001

Values are means ± SD; BCW, backward compression wave; BEW, backward expansion wave; FCW, forward compression wave; LV, left ventricle; LVEDP, left ventricular end diastolic pressure; n, number of sheep; PA, pulmonary artery; PVR, pulmonary vascular resistance.

During clamping a large backward compression wave arrives in mid-systole, but is not reflected from a proximal obstructive source as anticipated. The backward compression wave is still reflected from the distal closed-end reflector approximately 21 cm downstream. Whilst the downstream closed-end reflector source remains unchanged, the large increase in wave speed means the wave arrives in mid-systole thus opposing flow out of the right ventricle. This may have energy cost implications to the right ventricle in patients who have a single lung explanted for example.

It is unclear why the closed-end reflection site did not move further distally with the distension of the pulmonary circulation, as occurred with fluid loading for example. Perhaps excessive distension of the pulmonary vasculature with clamping led to reduced compliance of the distal circulation and therefore increased wave speed as propagation occurred distally. Thus the calculation of proximal pulmonary arterial wave speed would underestimate the mean wave speed and consequently the true distance to the reflection site would be underestimated.

It would seem that clamping led to 8% of the incident forward compression wave being reflected as a backward compression wave compared to 3% at baseline. Distension of the distal circulation is likely to reduce rather than enhance the degree of closed-end reflection as observed. Therefore it is probable with the markedly increased wave speed that the incident wave travels distally much faster leading to less energy damping. Consequently there is more energy available than at baseline for reflection.

The increased distension and subsequent increase in cross sectional area seems to be equally distributed between the main pulmonary artery and its daughter vessels as the reflection coefficient of the proximal reflector site remained unchanged.

6.6 Left Main Pulmonary Artery Clamping in the Setting of Pulmonary Emboli

6.6.1 Anticipated Wave Intensity

It has been demonstrated that WIA was unable to identify a single proximal obstruction represented by left main pulmonary artery clamping whilst the remaining pulmonary vasculature remained healthy with the ability to distend and recruit blood vessels. Perhaps if the distal circulation was diseased, clamping of the left main pulmonary artery may lead to closed-end reflection from this proximal obstruction, manifest as an early backwards compression wave. In two animals that had undergone autologous blood clot pulmonary embolization to obstruct the distal circulation the left main pulmonary artery was clamped to investigate the changes in wave reflection.

6.6.2 Results

Clamping the left main pulmonary artery in the setting of pulmonary emboli led to an additional significant rise in mean pulmonary artery pressure from 28.2 ± 3.8 to 31.6 ± 2.0 mmHg ($p = 0.02$) and pulmonary vascular resistance from 7.3 ± 4.5 to 10.5 ± 6.2 Wood's Units ($p = 0.01$). In response to the further increase in afterload the cardiac output fell from 3.2 ± 0.9 to 2.6 ± 0.9 $Lmin^{-1}$. The wave speed increased substantially from 3.2 ± 0.6 to 4.2 ± 0.2 ms^{-1} ($p = 0.002$).

There were only two waves that had a significant change to their cumulative intensities (Table 6-5). The late forward compression wave fell from 14.42 ± 4.93 to 5.25 ± 1.53 × 10^2 $Wm^{-2}s^{-1}$ ($p = 0.002$) and the backward compression wave increased from 55.23 ± 32.95 × 10^2 $Wm^{-2}s^{-1}$ to 80.78 ± 23.04 × 10^2 $Wm^{-2}s^{-1}$ ($p = 0.005$). The appearance of the mid-systolic backward compression wave did not seem to alter (Figure 6-5).

The reflection coefficient of the proximal open-end reflector remained unchanged at -0.09 ± 0.03 from -0.08 ± 0.04 ($p = 0.76$). The distance to the open-end reflector changed from 1.8 ± 0.9 cm to 0.2 ± 0.4 cm ($p = 0.002$). In contrast, the reflection coefficient of the distal closed-end reflector increased further from 0.23 ± 0.15 to 0.35 ± 0.19 (p = 0.005) though the distance of origin was not significantly different at 19.7 ± 2.2 cm from 16.6 ± 2.2 cm (p = 0.13).

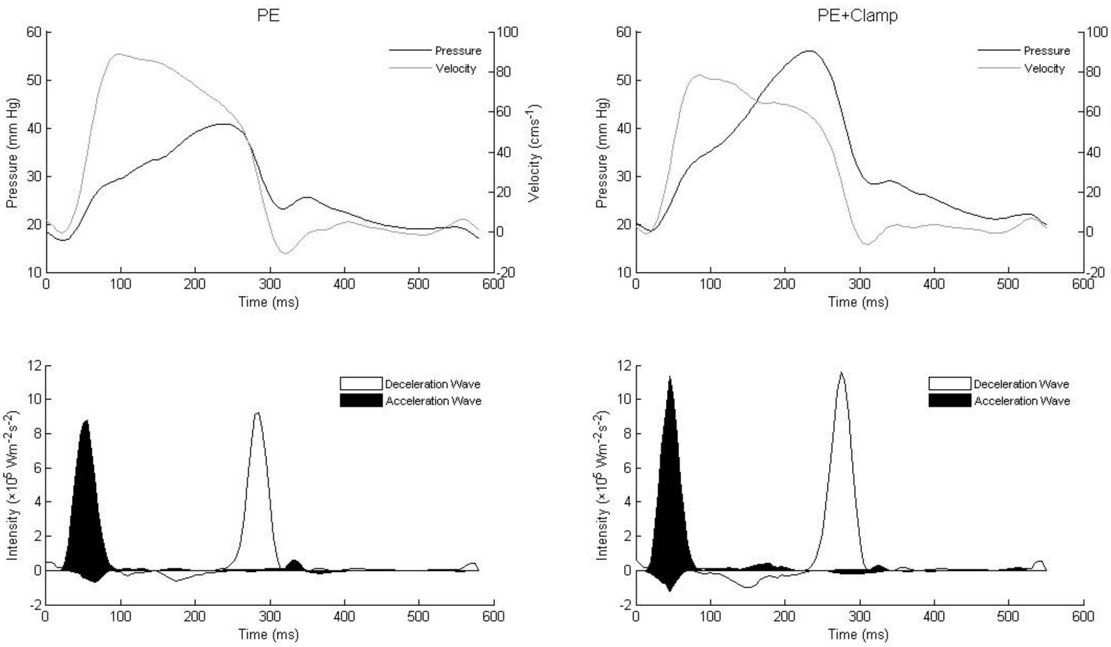

Figure 6-5. Wave Intensity During Pulmonary Embolization and with Additional Left Main Pulmonary Artery Clamping.

6.6.3 Discussion

WIA was again unable to clearly identify the presence of proximal pulmonary arterial obstruction. This may be because the anticipated early reflected compression wave from the proximal clamp is probably incorporated into the prominent mid-systolic backward compression wave arising approximately 19 cm downstream from the measurement site. The distal closed-end reflector appears to be enhanced with a further 12% of the incident forward compression wave reflected as a backward compression wave during additional clamping. The marked 31% increase in wave speed may contribute to the appearance of enhanced closed-end reflection by speeding up distal wave transmission. This results in less wave damping and therefore more incident wave energy is available for reflection. This more intense backward compression wave arises in mid-systole, which opposes flow out of the right ventricle likely increasing myocardial work.

Table 6-5. Wave Intensity and Haemodynamic Parameters During Pulmonary Embolization and with Additional Left Main Pulmonary Artery Clamping

	PE (n = 2)	PE + Clamp (n = 2)	P Value
Peak Wave Intensity ($\times 10^4$ Wm^{-2}s^{-2})			
Early Forward Compression	67.78 ± 15.28	83.61 ± 37.37	0.15
Late Forward Expansion	86.45 ± 6.16	87.64 ± 41.67	0.95
Late Forward Compression	8.25 ± 2.11	3.26 ± 0.68	<0.001
Early Backward Expansion	5.41 ± 1.23	8.80 ± 6.19	0.27
Backward Compression	11.27 ± 7.59	19.24 ± 11.34	0.01
Cumulative Wave Intensity ($\times 10^2$ Wm^{-2}s^{-1})			
Early Forward Compression	250.35 ± 23.81	268.83 ± 78.16	0.46
Late Forward Expansion	256.47 ± 18.98	282.44 ± 144.87	0.68
Late Forward Compression	14.42 ± 4.93	5.25 ± 1.53	0.002
Early Backward Expansion	19.03 ± 7.44	23.63 ± 11.04	0.55
Backward Compression	55.23 ± 32.95	80.78 ± 23.04	0.005
Proportion of Cumulative Wave Intensity (%)			
Early Forward Compression	42.2 ± 5.3	41.0 ± 1.8	0.67
Late Forward Expansion	43.1 ± 2.4	40.3 ± 9.6	0.45
Late Forward Compression	2.4 ± 0.8	0.9 ± 0.5	<0.001
Early Backward Expansion	3.2 ± 1.1	3.5 ± 1.1	0.67
Backward Compression	9.2 ± 5.3	14.3 ± 8.1	0.02
Reflection Coefficient			
BEW/FCW	-0.08 ± 0.04	-0.09 ± 0.03	0.76
BCW/FCW	0.23 ± 0.15	0.35 ± 0.19	0.005
Wave Speed (ms^{-1})	3.2 ± 0.6	4.2 ± 0.2	0.002
Distance to Reflection Site (cm)			
Early Backward Expansion	1.8 ± 0.9	0.2 ± 0.4	0.002
Late Backward Compression	16.6 ± 2.2	19.7 ± 2.2	0.13
Heart Rate (min^{-1})	105 ± 3	109 ± 4	0.013
Peak Blood Velocity (ms^{-1})	0.88 ± 0.02	0.76 ± 0.07	0.01
Cardiac Output (Lmin^{-1})	3.2 ± 0.9	2.6 ± 0.9	<0.001
LVEDP (mmHg)	7.8 ± 3.9	9.5 ± 4.6	0.01
Mean PA Pressure (mmHg)	28.2 ± 3.8	31.6 ± 2.0	0.02
PVR (Wood's Units)	7.3 ± 4.5	10.5 ± 6.2	0.01

Values are means ± SD; BCW, backward compression wave; BEW, backward expansion wave; FCW, forward compression wave; LV, left ventricle; LVEDP, left ventricular end diastolic pressure; n, number of sheep; PA, pulmonary artery; PE, pulmonary embolus; PVR, pulmonary vascular resistance.

It is not clear why the cumulative energy of the late forward compression wave falls during clamping in the setting of multiple pulmonary emboli. This wave is thought to be due to blood flow that has reversed direction in late systole having been positively reflected off the closed pulmonary valve. The brief flow reversal is still apparent on the velocity trace but the pressure rise is less prominent. It is possible this is a chance finding as only two sheep were investigated. The other anomalous finding is the shift in the open-end reflector location to a more proximal location. This sounds plausible in the setting of marked pulmonary distension caused by embolization and clamping, but the early backward expansion wave often preceded the incident forward compression wave, which has no physiological meaning. These observations remain unexplained but may reflect the study of only a limited number of animals and would require investigation in a larger number group.

6.7 Pulmonary Vein Clamping

6.7.1 Anticipated Wave Intensity

In order to simulate the effects of post pulmonary capillary vascular obstruction, it was attempted to temporarily clamp two of the four accessible pulmonary veins prior to their insertion into the left atrium. It is recognised that variations in left atrial pressure may be transmitted to the proximal pulmonary circulation and that flow within the pulmonary capillaries remains pulsatile. Therefore, it was anticipated that clamping the pulmonary veins would lead to a backward-travelling compression wave arriving late in systole as a result of the forward compression wave traversing the entire pulmonary circulation and meeting the closed-end reflection of the pulmonary venous clamp. Given that there are likely to be significant damping effects the size of the reflected wave would be small. It was anticipated that the backward-travelling compression wave from the distal pulmonary arteries would remain unchanged.

6.7.2 Results

Clamping the pulmonary veins led to significant haemodynamic changes that were fully reversible. The mean pulmonary artery pressure elevated substantially from 17.7 ± 5.1 to 37.6 ± 6.3 mmHg ($p < 0.001$). There was a small drop in the cardiac output from 3.2 ± 1.0 to 2.9 ± 0.8 $Lmin^{-1}$ though this was not significant ($p = 0.35$). The left ventricular end-diastolic pressure remained unchanged from 5.5 ± 6.7 to 6.4 ± 6.4 mmHg ($p = 0.50$). The calculated pulmonary vascular resistance increased from 3.8 ± 3.2 to 10.7 ± 4.7 Wood's Units ($p < 0.001$). The peak blood velocity fell substantially from 0.80 ± 0.01 to 0.66 ± 0.01 ms^{-1} ($p < 0.001$). The pulmonary arterial wave speed increased substantially from 1.8 ± 0.2 to 3.2 ± 0.5 ms^{-1} ($p < 0.001$).

The new finding with pulmonary vein clamping was the appearance of an additional late backward-travelling compression wave appearing 250-380 ms after the ECG R wave thus indicating a second site of positive or closed-end reflection (Figure 6-6). This distinct and consistent wave was of modest cumulative intensity at 4.4 ± 2.6 × 10^2 $Wm^{-2}s^{-1}$. The reflection coefficient for this new closed-end reflector was 0.04 ± 0.02 and arose from a site 47.4 ± 9.1 cm downstream.

The peak intensity of the early forward compression wave fell from 64.10 ± 28.39 × 10^2 $Wm^{-2}s^{-2}$ to 26.80 ± 11.25 × 10^2 $Wm^{-2}s^{-2}$ ($p < 0.001$). The cumulative intensity also fell from 185.26 ± 60.24 × 10^2 $Wm^{-2}s^{-2}$ to 116.52 ± 39.73 × 10^2 $Wm^{-2}s^{-1}$ ($p < 0.001$). The peak and cumulative intensity of both the forward expansion and late forward compression wave increased significantly (Table 6-6). The peak and cumulative intensity of both the backward expansion and backward compression wave increased significantly (Table 6-6).

The open-end reflection coefficient increased from -0.01 ± 0.00 to -0.05 ± 0.03 ($p = 0.003$), whilst the distance to the open-end reflector increased from 2.5 ± 0.6 cm to 3.9 ± 1.0 cm ($p = 0.002$). The closed-end reflection coefficient increased from 0.01 ± 0.01 to 0.08 ± 0.03 ($p = 0.001$) with the estimated distance to this closed-end reflection increasing from 17.7 ± 5.8 to 26.3 ± 6.7 cm ($p < 0.01$).

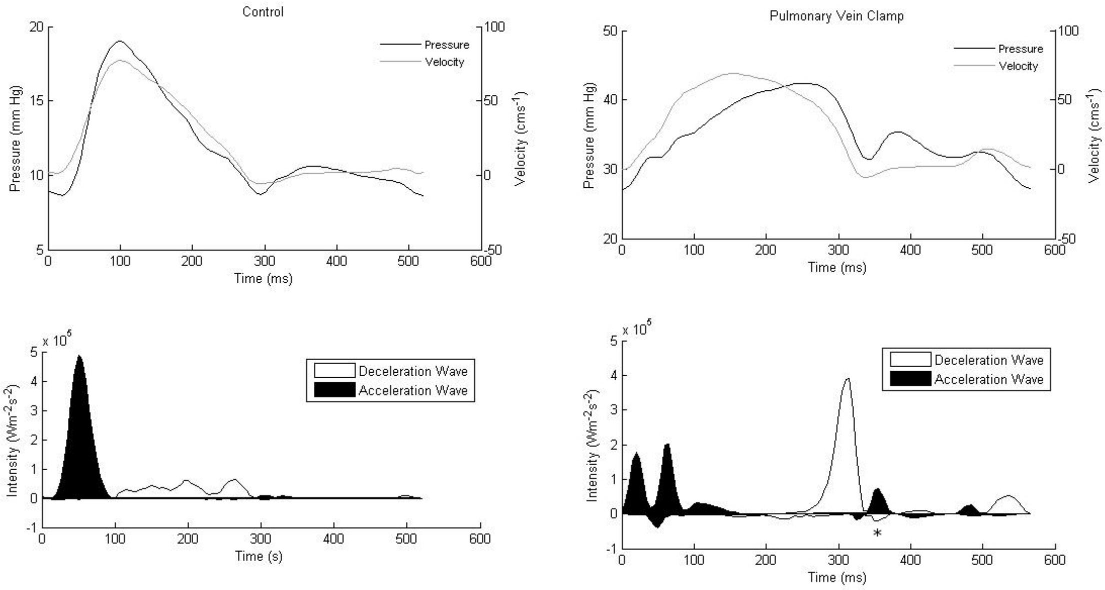

Figure 6-6. Wave Intensity at Rest and During Pulmonary Venous Clamping. The new late backward-travelling compression wave is marked with an asterisk.

6.7.3 Discussion

Clamping the pulmonary veins had significant haemodynamic consequences that are certainly complex. It remains unexplained why clamping two pulmonary veins would lead to haemodynamic changes that are so different from left main pulmonary artery clamping. Although the lungs are believed to be entirely in a zone 3 condition, it may be that the veins clamped were responsible for the majority of pulmonary venous drainage. More likely was that more than two pulmonary veins were inadvertently clamped due to limited visibility within the intrathoracic cavity. Regardless, with clamping the right ventricular afterload increased substantially as evidenced by the marked rise in mean pulmonary artery pressure. Left ventricular preload was expected to fall and via Starling's mechanism would lead to reduced contractility and reduced cardiac output. However, the left ventricular end-diastolic pressure (LVEDP) did not fall with the reduced pulmonary venous return (Table 6-6), thus indicating that the volume state of the ventricle and not the end-diastolic pressure adjusts with venous clamping.

Table 6-6. Wave intensity and haemodynamic parameters at rest and during pulmonary venous clamping

	Control (n = 5)	PV Clamp (n = 5)	P Value
Peak Wave Intensity ($\times 10^4$ $Wm^{-2}s^{-2}$)			
Early Forward Compression	64.10 ± 28.39	26.80 ± 11.25	< 0.001
Late Forward Expansion	12.11 ± 5.47	50.12 ± 13.51	< 0.001
Late Forward Compression	2.19 ± 2.19	22.32 ± 11.80	< 0.001
Early Backward Expansion	0.59 ± 0.75	3.07 ± 1.59	< 0.001
Backward Compression	0.89 ± 0.81	1.62 ± 0.85	0.03
Late Backward Compression	-	2.75 ± 1.60	
Cumulative Wave Intensity ($\times 10^2$ $Wm^{-2}s^{-1}$)			
Early Forward Compression	185.26 ± 60.24	116.52 ± 39.73	< 0.001
Late Forward Expansion	67.11 ± 19.55	198.61 ± 76.50	< 0.001
Late Forward Compression	5.79 ± 5.01	40.67 ± 24.22	< 0.001
Early Backward Expansion	0.82 ± 0.98	4.67 ± 2.41	< 0.001
Backward Compression	1.44 ± 1.46	9.29 ± 4.08	< 0.001
Late Backward Compression	-	4.41 ± 2.62	
Proportion of Cumulative Wave Intensity (%)			
Early Forward Compression	70.2 ± 6.2	31.8 ± 4.3	< 0.001
Late Forward Expansion	26.1 ± 2.9	52.7 ± 2.8	< 0.001
Late Forward Compression	2.7 ± 2.9	10.3 ± 2.9	< 0.001
Early Backward Expansion	0.3 ± 0.2	1.4 ± 0.8	< 0.001
Backward Compression	0.7 ± 0.6	2.7 ± 1.2	< 0.001
Late Backward Compression	-	1.1 ± 0.6	
Reflection Coefficient			
BEW/FCW	-0.01 ± 0.00	-0.05 ± 0.03	0.003
BCW/FCW	0.01 ± 0.01	0.08 ± 0.03	0.001
Late BCW/FCW	-	0.04 ± 0.02	
Wave Speed (ms^{-1})	1.8 ± 0.2	3.2 ± 0.5	< 0.001
Distance to Reflection Site (cm)			
Early Backward Expansion	2.5 ± 0.6	3.9 ± 1.0	0.002
Backward Compression	17.7 ± 5.8	26.3 ± 6.7	0.02
Late Backward Compression	-	47.4 ± 9.1	
Heart Rate (min^{-1})	111 ± 11	105 ± 7	0.001
Peak Blood Velocity (ms^{-1})	0.80 ± 0.01	0.66 ± 0.01	< 0.001
Cardiac Output ($Lmin^{-1}$)	3.2 ± 1.0	2.9 ± 0.8	0.35
LVSP (mmHg)	127.4 ± 8.7	109.8 ± 13.4	0.01
LVEDP (mmHg)	5.5 ± 6.7	6.4 ± 6.4	0.50
Mean PA Pressure (mmHg)	17.7 ± 5.1	37.6 ± 6.3	< 0.001
PVR (Wood's Units)	3.8 ± 3.2	10.7 ± 4.7	< 0.001

Values are means ± SD; BCW, backward compression wave; BEW, backward expansion wave; FCW, forward compression wave; LV, left ventricle; LVEDP, left ventricular end diastolic pressure; LVSP, left ventricular systolic pressure; n, number of sheep; PA, pulmonary artery; PV, pulmonary vein; PVR, pulmonary vascular resistance.

The calculated pulmonary vascular resistance increased substantially but this was an artefact of using LVEDP instead of pulmonary capillary wedge pressure in the calculation of transpulmonary gradient. With elevations in pulmonary artery pressures in response to post-capillary pulmonary vascular obstruction the pulmonary vascular resistance should be normal or low.

The marked increase in mean pulmonary arterial pressure led to pulmonary vascular distension and reduced proximal compliance leading to a 78% increase in wave speed. The reduced right ventricular preload and contractility was manifest as slow rates of pressure and velocity generation and subsequently reduced peak and cumulative intensities of the forward compression wave (Table 6-6). The right ventricular strain was manifest in the prolonged systole and an observed jerky motion to contraction leading to several distinct peaks of the initial forward compression wave (Figure 6-6). While the cumulative intensity of the forward compression wave fell it is important to stress that wave intensity reflects the working state of the heart but by no means represents the total work done by the heart. It is best to think of wave intensity as a measure of the energy flux density, that is the rate at which work is done normalised for arterial cross-sectional area.

Of interest is that only the first peak of the forward compression wave was reflected in an open-end manner as a backward expansion wave. This again supports the notion that the open-end reflector is not fixed throughout the cardiac cycle. The open-end reflector is likely to be present only in early systole after which geometrical changes occur in the daughter vessels of the main pulmonary artery. This may be in response to cardiac motion or the blood that is ejected into the daughter vessels leading to a reduction in the area ratio of daughter-to-parent vessels.

As previously demonstrated whenever the right ventricle is under strain, the rate of myofibril shortening falls in late systole resulting in a late forward expansion wave of substantial intensity. This also leads to substantial deceleration of the column of blood within the pulmonary artery, which briefly reverses its flow and reflects as a secondary forward compression wave with increased intensity off the closed pulmonary valve.

The detection of a new late backward compression with pulmonary venous clamping suggests that wave intensity analysis is capable of detecting waves that arise from the post-capillary side of the pulmonary circulation. The late backward compression wave was neither broad nor indistinct suggesting that the closed-end reflection site was not spatially diverse. This supports the notion that this wave is reflected from a well-localised fixed obstruction. Indeed the late backward compression wave arises 47.4 ± 9.1 cm downstream from our measurement location, placing the reflector site on the pulmonary venous side of the circulation. Yet, given the pulmonary circulation is approximately 34 cm long in sheep, this places the reflection site distal to the pulmonary venous clamp. It is possible that proximal pulmonary artery wave speed overestimates pulmonary venous wave speed, thus overestimating the true distance covered.

It is not clear why each of the forward compression peaks do not lead to a late backward compression wave. It is possible that only the highest energy wave has sufficient energy to traverse the pulmonary circulation without critical damping allowing it to arrive with enough energy to be reflected backwards in a positive manner. This leads to another source of error in the distance calculation and arises from the fact that the time to first peak of the forward compression wave was always used as the onset time to determine the pulmonary circulation traverse time. Often the second or third peak was larger, which may be the only wave with sufficient energy to traverse the pulmonary circulation. Hence, the transit time may be systematically overestimated and therefore so may the distance covered.

The backward compression wave from the distal pulmonary arteries remained but was broader, suggesting that the post-capillary obstruction and resultant pulmonary artery distension has extended the spatial dispersion of the reflection site. The estimated distance to the original closed-end reflector increased significantly to 26 cm with pulmonary venous clamping. It is possible that pulmonary distension led to the closed-end reflector site moving much further distally. Errors in calculating the distance travelled are more likely however. The broad mid-to-late systolic backward compression wave resulted in difficulty determining the peak intensity from which the distances are calculated. The incident forward compression wave with multiple late peaks further compounds the issues of accurately determining the distance.

6.8 Limitations

Although changes in wave intensity parameters with various interventions were interpreted to signify changes in vascular distension or vasomotor activity, it is only possible to truly know what the vasoactive state of the pulmonary circulation is by measuring pulmonary blood volume simultaneously with pulmonary pressure.

6.9 Conclusions

WIA is able to detect changes in the distal pulmonary circulation by looking at changes in the timing and energy of reflected waves. WIA is able to accurately determine the distance to an open-end or closed-end reflection site. Changes that affect the distal microcirculation lead to alterations in proximal pulmonary compliance manifest as changes in wave speed. This may be a result of passive distension or active constriction via sympathetic activity. Increased wave speed and enhanced distal reflection with acute increases in right ventricular afterload lead to a substantial backward-travelling compression wave arriving in the proximal pulmonary artery in mid-systole. This wave serves to oppose flow out of the right ventricle, thus increasing right ventricular myocardial energy requirements. The open-end reflector remains and is even enhanced by increased right ventricular afterload, which may help the right ventricle to maintain efficiency by enhancing forward flow in early systole.

Whilst wave intensity does not allow the calculation of the total work done by the heart (only hydraulic power is able to be calculated), it does give insights into the working state of the ventricle by providing information on the rate at which work is done. For example if contractility is increased the forward compression wave is of greater intensity. If preload is reduced substantially the forward compression wave is of lesser intensity. Under periods of increased afterload and increased right ventricular strain, the rate of myofibril deceleration in late systole is increased such that forward expansion wave has increased intensity and becomes a much greater proportion of total cumulative wave intensity.

WIA provides useful insights into the changes in wave travel associated with acute increases in right ventricular afterload but these results do not provide understanding of the adaptive response to chronic elevations in right ventricular afterload. Further study is required to understand the adaptive responses that influence wave travel with chronic elevations in pulmonary pressures.

Chapter 7 Pulmonary Arterial Wave Intensity Analysis with Progressive Microsphere Administration

7.1 Anticipated Wave Intensity

It was shown in Chapter 6 that in the resting pulmonary artery wave reflection from the distal circulation is minimal and with increased downstream obstruction enhanced closed-end reflection leads to increases in backward compression wave energy. WIA was able to accurately determine the location of the obstruction. Downstream changes to the small pulmonary vessels also led to reduction in proximal pulmonary artery compliance manifest as increases in wave speed. Therefore it is hypothesised that increased pulmonary arterial wave speed and increases in backward compression wave energy may be early markers of pulmonary vascular disease before gross elevations in pulmonary artery pressure are evident. To investigate this 70-110 μm microspheres were progressively delivered to the pulmonary microcirculation (Table 7-1) and anticipated that there would be a dose responsive increase in pulmonary wave speed and backward-travelling compression wave energy.

Table 7-1. Microsphere Dosing Schedule

70-110 μm Microsphere Dose	Mass (gm)	No. Beads ($\times 10^4$)	Cumulative No. Beads ($\times 10^4$)
M1	0.10	0.2	0.2
M2	0.25	0.5	0.7
M3	0.50	1.0	1.7
M4	0.75	1.5	3.2
M5	1.00	2.0	5.2
M6	1.00	2.0	7.2
M7	1.00	2.0	9.2
M8	1.00	2.0	11.2
M9	1.00	2.0	13.2
M10	1.00	2.0	15.2

No., number.

7.2 Results

The progressive administration of microspheres did lead to a dose responsive increase in the proximal pulmonary arterial wave speed ($p < 0.001$; Figure 7-1 & Table 7-2). Yet using multiple comparison techniques only the final three doses had a wave speed that differed significantly from baseline. The mean pulmonary artery pressure rose in a dose responsive manner ($p < 0.001$), with only the highest three doses differing significantly from baseline (Table 7-2). There was a dose responsive fall in the cardiac output but this did not reach statistical significance ($p = 0.31$). Pulmonary vascular resistance was not significantly altered with microsphere administration ($p = 0.06$). The embolization of distal pulmonary arteries did not lead to a dramatic fall in the partial pressure of systemic arterial oxygen, though the pre- and post-levels at the highest two doses of microspheres did reach statistical significance (Table 7-3).

The cumulative energy of the incident forward compression wave progressively fell ($p = 0.05$), whilst the cumulative energy of the forward expansion wave increased ($p = 0.01$) and became the greatest proportion of total cumulative wave energy (Table 7-4 to Table 7-6). With progressive microsphere administration a backward compression wave appeared and the peak and cumulative intensities progressively increased significantly and became a greater proportion of total wave energy (Table 7-4 to Table 7-6 & Figure 7-2 to Figure 7-4). The reflection coefficient for the distal closed-end reflector increased with progressive microsphere administration ($p < 0.001$), as did the estimated distance to this reflection site ($p = 0.01$; Table 7-7).

The peak intensity of the backward expansion wave increased but not significantly so ($p = 0.22$). However, the cumulative intensity of the backward expansion wave did increase significantly ($p = 0.004$) as did the proximal open-end reflection coefficient ($p = 0.01$). The estimated distance to this proximal open-end reflector remained unchanged ($p = 0.17$; Table 7-7).

Table 7-2. Haemodynamic Changes with Microsphere Administration

Micro-sphere Dose	Mean PA Pressure (mmHg)	Cardiac Output ($Lmin^{-1}$)	LVSP (mmHg)	LVEDP (mmHg)	PVR (Wood's Units)	Wave Speed (ms^{-1})
Control	14.8 ± 1.2	2.27 ± 0.34	128.2 ± 24.9	3.7 ± 1.7	4.8 ± 0.9	1.68 ± 0.12
M1	14.9 ± 1.4	2.26 ± 0.23	114.4 ± 35.9	1.4 ± 0.6	5.8 ± 1.4	1.66 ± 0.09
M2	14.5 ± 0.4	2.16 ± 0.41	114.8 ± 19.0	3.1 ± 2.7	5.2 ± 1.4	1.61 ± 0.12
M3	15.1 ± 0.3	2.14 ± 0.27	110.1 ± 21.9	3.7 ± 2.6	5.2 ± 1.4	1.84 ± 0.35
M4	15.6 ± 0.6	2.22 ± 0.24	94.8 ± 18.9	1.3 ± 1.9	6.3 ± 1.1	1.78 ± 0.25
M5	16.8 ± 0.7	2.02 ± 0.32	103.3 ± 22.3	5.7 ± 3.1	5.5 ± 1.7	1.85 ± 0.21
M6	18.1 ± 0.6	2.01 ± 0.35	97.9 ± 23.4	6.6 ± 3.3	5.6 ± 1.8	1.91 ± 0.29
M7	20.4 ± 1.1	2.11 ± 0.35	95.2 ± 24.7	7.5 ± 3.2	6.0 ± 1.5	1.95 ± 0.27
M8	23.6 ± 3.2	2.06 ± 0.42	85.5 ± 17.8	7.4 ± 5.2	7.7 ± 1.9	2.42 ± 0.29
M9	26.3 ± 5.7	1.88 ± 0.15	74.0 ± 30.7	12.7 ± 9.5	6.8 ± 1.5	2.72 ± 0.79
M10	28.3 ± 4.7	1.75 ± 0.23	72.0 ± 22.2	16.7 ± 9.0	6.0 ± 1.9	3.12 ± 0.76
P Value	< 0.001	0.31	0.002	< 0.001	0.06	<0.001

Values are means ± SD; LVEDP, left ventricular end diastolic pressure; LVSP, left ventricular systolic pressure; PA, pulmonary artery; PVR, pulmonary vascular resistance.

Table 7-3. Systemic Oxygenation Changes with Microsphere Administration

70-110 µm Microsphere Dose	Cumulative # Beads (× 10^4)	Pre PaO_2 (mmHg)	Post PaO_2 (mmHg)	P Value
M1	0.2	106 ± 9	110 ± 11	0.21
M2	0.7	108 ± 9	105 ± 10	0.08
M3	1.7	108 ± 8	103 ± 7	0.21
M4	3.2	107 ± 10	104 ± 10	0.34
M5	5.2	104 ± 8	97 ± 13	0.24
M6	7.2	99 ± 5	86 ± 13	0.16
M7	9.2	97 ± 11	96 ± 10	0.87
M8	11.2	98 ± 6	94 ± 13	0.43
M9	13.2	98 ± 7	84 ± 6	0.01
M10	15.2	90 ± 4	82 ± 2	0.04

PaO_2, systemic arterial partial pressure of oxygen; #, number

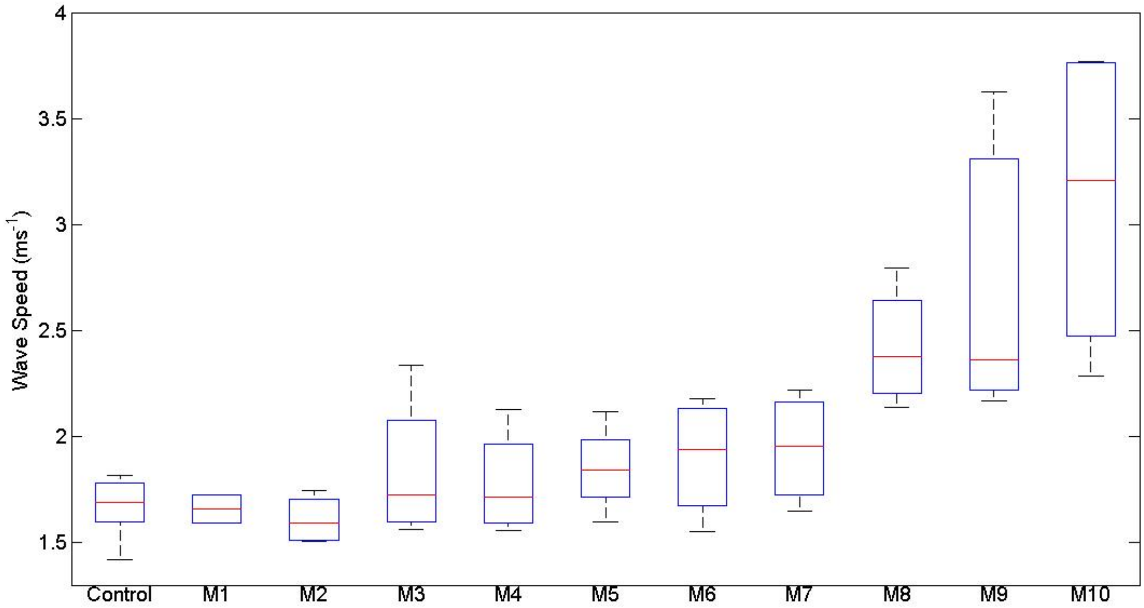

Figure 7-1. Box Plot of Pulmonary Arterial Wave Speed at Each Microsphere Dose.

Table 7-4. Peak wave intensities (× 10^4 $Wm^{-2}s^{-2}$) at each microsphere dose

Microsphere Dose	FCW	FEW	Late FCW	BEW	BCW
Control	31.40 ± 16.67	10.97 ± 4.37	2.00 ± 1.41	0.50 ± 0.45	0.00 ± 0.00
M1	31.07 ± 16.42	15.06 ± 4.43	2.29 ± 1.43	0.59 ± 0.59	0.00 ± 0.00
M2	28.24 ± 14.75	13.79 ± 6.68	2.31 ± 1.64	0.39 ± 0.35	0.04 ± 0.08
M3	24.41 ± 13.80	14.00 ± 6.39	2.69 ± 1.78	0.24 ± 0.22	0.52 ± 0.23
M4	20.20 ± 10.02	16.22 ± 7.67	3.75 ± 2.61	1.08 ± 1.09	0.63 ± 0.53
M5	16.09 ± 10.27	19.48 ± 11.72	6.72 ± 6.39	0.69 ± 0.35	0.61 ± 0.25
M6	15.79 ± 8.17	22.10 ± 12.12	9.35 ± 8.72	0.62 ± 0.36	0.52 ± 0.16
M7	16.12 ± 6.64	24.03 ± 10.81	11.93 ± 9.67	0.62 ± 0.63	1.46 ± 0.53
M8	14.63 ± 6.80	26.53 ± 7.36	12.52 ± 9.86	1.22 ± 0.97	2.74 ± 1.16
M9	17.30 ± 2.45	25.36 ± 3.81	12.12 ± 6.61	0.81 ± 0.03	2.06 ± 0.74
M10	16.90 ± 2.49	24.13 ± 4.06	11.73 ± 2.57	1.01 ± 0.28	2.60 ± 1.11
P Value	0.02	0.001	0.001	0.22	< 0.001

Values are means ± SD; BCW, backwards compression wave; BEW, backwards expansion wave; FCW, forwards compression wave; FEW, forwards expansion wave.

Table 7-5. Cumulative Wave Intensities (× 10^2 $Wm^{-2}s^{-1}$) at each microsphere dose

Microsphere Dose	FCW	FEW	Late FCW	BEW	BCW
Control	109.35 ± 31.56	50.56 ± 8.53	5.28 ± 4.15	0.78 ± 0.54	0.00 ± 0.00
M1	101.66 ± 33.17	58.77 ± 17.95	6.35 ± 5.43	0.75 ± 0.52	0.00 ± 0.00
M2	102.01 ± 42.08	54.55 ± 16.46	6.78 ± 5.09	0.63 ± 0.35	0.11 ± 0.21
M3	88.46 ± 45.55	56.91 ± 12.57	7.26 ± 5.64	0.58 ± 0.56	1.53 ± 0.79
M4	79.25 ± 33.10	62.91 ± 21.94	10.06 ± 7.74	1.90 ± 1.36	2.57 ± 2.33
M5	71.11 ± 33.98	73.37 ± 37.15	16.72 ± 13.76	1.42 ± 0.72	3.09 ± 0.96
M6	70.19 ± 29.56	76.43 ± 36.47	22.54 ± 18.74	1.53 ± 0.86	3.38 ± 1.07
M7	71.27 ± 20.89	84.14 ± 38.13	25.68 ± 19.51	1.48 ± 1.56	7.11 ± 1.54
M8	67.19 ± 16.48	88.98 ± 22.61	22.51 ± 14.72	2.94 ± 1.91	14.14 ± 5.47
M9	69.65 ± 12.53	85.15 ± 10.63	21.30 ± 10.97	1.74 ± 0.56	14.16 ± 4.85
M10	60.02 ± 19.07	81.87 ± 11.16	19.93 ± 8.35	2.36 ± 0.98	18.31 ± 8.53
P Value	0.05	0.01	0.004	0.004	< 0.001

Values are means ± SD; BCW, backwards compression wave; BEW, backwards expansion wave; FCW, forwards compression wave; FEW, forwards expansion wave.

Table 7-6. Proportion of total cumulative wave intensity (%) at each microsphere dose

Microsphere Dose	FCW	FEW	Late FCW	BEW	BCW
Control	65.9 ± 8.2	30.5 ± 5.4	3.1 ± 3.4	0.5 ± 0.3	0.0 ± 0.0
M1	60.7 ± 8.3	35.1 ± 5.6	3.7 ± 3.4	0.5 ± 0.2	0.0 ± 0.0
M2	62.2 ± 10.1	33.3 ± 6.9	4.1 ± 3.6	0.4 ± 0.2	0.1 ± 0.1
M3	57.2 ± 11.6	36.8 ± 8.3	4.7 ± 3.7	0.4 ± 0.2	0.9 ± 0.5
M4	50.6 ± 12.7	40.2 ± 8.8	6.4 ± 3.9	1.2 ± 0.5	1.6 ± 0.9
M5	42.9 ± 14.9	44.3 ± 10.2	10.1 ± 4.7	0.9 ± 0.4	1.8 ± 0.9
M6	40.3 ± 15.5	43.9 ± 9.7	13.0 ± 5.8	0.9 ± 0.4	1.9 ± 0.9
M7	37.6 ± 15.4	44.4 ± 9.2	13.4 ± 5.9	0.8 ± 0.5	3.8 ± 1.8
M8	34.3 ± 15.6	45.5 ± 8.6	11.5 ± 5.5	1.5 ± 0.6	7.2 ± 3.1
M9	36.3 ± 14.5	44.4 ± 8.2	11.0 ± 4.3	0.9 ± 0.5	7.4 ± 3.6
M10	32.9 ± 16.2	44.9 ± 8.7	10.9 ± 4.7	1.3 ± 0.5	10.0 ± 4.6
P Value	< 0.001	0.06	0.03	0.02	< 0.001

Values are means ± SD; BCW, backwards compression wave; BEW, backwards expansion wave; FCW, forwards compression wave; FEW, forwards expansion wave.

Table 7-7. Reflection coefficients and estimated distances to reflection sites at each microsphere dose

Microsphere Dose	Reflection Coefficient BEW/FCW	Reflection Coefficient BCW/FCW	Distance to Reflection Site BEW (cm)	Distance to Reflection Site BCW (cm)
Control	-0.01 ± 0.01	0.00 ± 0.00	1.92 ± 0.35	0.00 ± 0.00
M1	-0.01 ± 0.00	0.00 ± 0.00	2.46 ± 1.04	0.00 ± 0.00
M2	-0.01 ± 0.00	0.00 ± 0.00	3.12 ± 1.09	0.00 ± 0.00
M3	-0.01 ± 0.01	0.02 ± 0.02	3.17 ± 1.49	12.30 ± 3.80
M4	-0.03 ± 0.02	0.04 ± 0.03	2.61 ± 0.61	11.05 ± 2.77
M5	-0.02 ± 0.01	0.05 ± 0.02	3.62 ± 2.05	14.98 ± 1.60
M6	-0.02 ± 0.01	0.05 ± 0.03	3.27 ± 1.89	16.77 ± 1.86
M7	-0.02 ± 0.01	0.10 ± 0.02	2.71 ± 2.12	15.38 ± 3.50
M8	-0.03 ± 0.04	0.22 ± 0.07	3.69 ± 0.97	18.87 ± 3.18
M9	-0.03 ± 0.02	0.21 ± 0.09	2.54 ± 1.73	16.26 ± 2.66
M10	-0.04 ± 0.04	0.32 ± 0.18	3.34 ± 0.39	20.42 ± 3.82
P Value	0.01	< 0.001	0.17	0.01

Values are means ± SD; BCW, backwards compression wave; BEW, backwards expansion wave; FCW, forwards compression wave; FEW, forwards expansion wave.

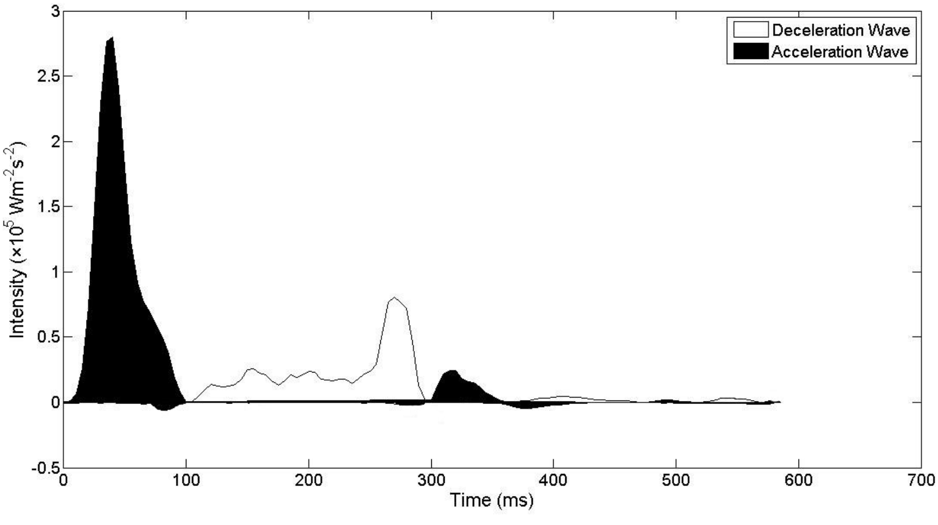

Figure 7-2. Wave intensity at rest prior to microsphere administration.

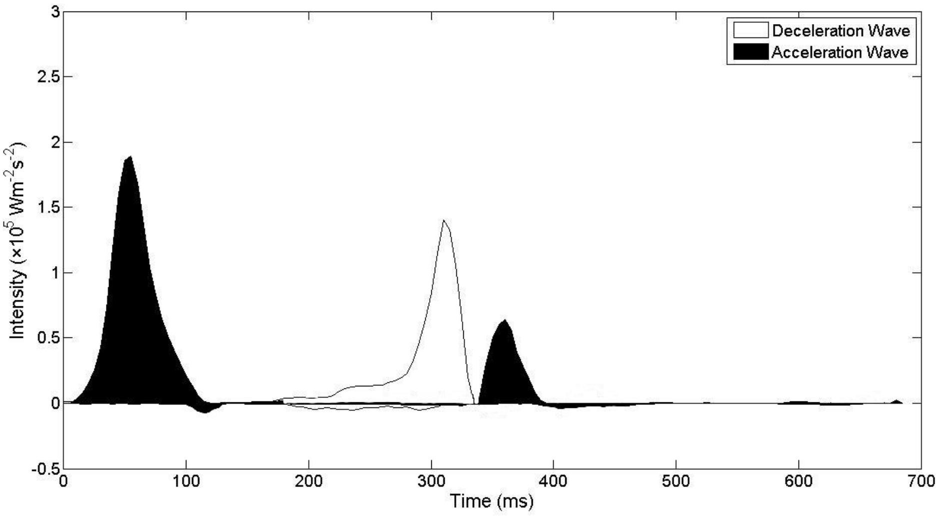

Figure 7-3. Wave intensity after cumulative administration of 5.2 × 10^4 microspheres.

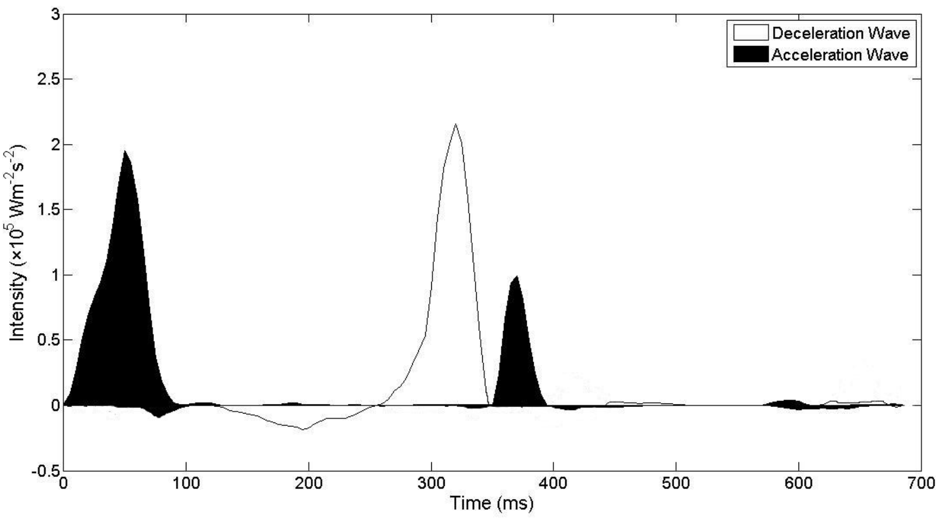

Figure 7-4. Wave intensity after cumulative administration of 15.2 × 10^4 microspheres.

7.3 Discussion

The important novel finding in this experiment was the strong relationship between the energy carried by the backward compression wave reflected from the distal vasculature and the dose of microspheres. It was evident the closed-end nature of this obstruction increased as, at the highest doses, 32% of the incident energy was reflected compared to 0% at baseline. The presence of the increasing backward compression wave with progressive microsphere administration cannot be attributed to hypoxic pulmonary vasoconstriction. Whilst the PaO_2 following microsphere delivery was significantly different at the two highest doses, experience has shown the resulting PaO_2 levels of around 80 mmHg is insufficient to lead to backward compression waves. In previous canine experiments gas exchange was only significantly altered by large clots of 10 mm diameter (Delcroix *et al.*, 1993).

It appears that the estimated distance to the closed-end reflection site increases progressively with microsphere administration. It was noted that at low microsphere doses the backward compression wave was of minimal intensity and broad indicating a spatially diverse reflection site. The flat and broad nature of this wave may have led to underestimation of the distances involved, as it was difficult for the automated analysis scripts to pick a distinct peak. Certainly as the microsphere dose increased, the backward compression wave became more organised with a prominent peak, suggesting a more fixed distal, less spatially diverse obstruction and calculation of the estimated distance could be considered more reliable. Indeed at the highest microsphere doses the closed-end reflection site at around 18 cm would correspond to the region of small arterioles obstructed by the microspheres.

There was a small but significant increase in the proximal open-end reflection coefficient such that 4% of the incident forward compression wave was reflected as a backward expansion wave compared to 1% at baseline ($p = 0.01$). Despite a fall in the incident forward compression wave energy the increased reflection coefficient led to increased energy of the early backward expansion wave. The nature and timing of this wave would enhance right ventricular emptying during early systole, thus potentially minimising the myocardial energy cost.

There was a strong relationship between pulmonary arterial wave speed and the microsphere dose ($p < 0.001$). But the mean pulmonary pressures needed to rise above 20 mmHg for individual doses to become significantly different from control values. Thus it may be argued that pulmonary arterial wave speed would not contribute anything further to the diagnosis of pulmonary hypertension than mean pulmonary pressure alone, but it is important to recognise that even at the highest two microsphere doses mean pulmonary pressure was only minimally raised above thresholds that are traditionally considered hypertensive. Knowledge of the relationship between loss of the pulmonary microcirculation and the pulmonary artery wave speed is important, as this wave speed modifies the arrival time of reflected waves in the proximal pulmonary artery and therefore the final afterload that the right ventricle faces. It is very clear that downstream vascular changes affect proximal pulmonary compliance, wave speed and therefore the timing and intensity of waves that arrive in the proximal pulmonary circulation.

Delivery of microspheres would be expected to increase pulmonary vascular resistance. Yet, despite an increase in mean pulmonary artery pressure and fall in cardiac output, pulmonary vascular resistance was not significantly altered with microsphere administration. This may be attributed to a paradoxical and significant ($p < 0.001$) progressive rise in the left ventricular end diastolic pressure (LVEDP), which lowers the transpulmonary gradient. Microvascular obstruction would be expected to reduce pulmonary venous return and therefore reduce left ventricular preload leading to a fall in LVEDP and thus the calculated pulmonary vascular resistance would rise.

The rising LVEDP suggests that the left ventricle was affected by microsphere administration over and above simple changes in preload. The left ventricular systolic pressure fell progressively from 128 ± 25 mmHg at baseline to 72 ± 22 mmHg at the peak microsphere dose ($p = 0.002$; Table 7-2). The stroke volume falls from 22.5 ± 2.7 mL/beat to 18.4 ± 2.6 mL/beat ($p = 0.01$). It is possible that there was a loss of left ventricular contractility that may result from myocardial ischaemia. In a variety of species the mean pulmonary capillary diameter is 7.5 ± 2.3 μm (Doerschuk *et al.*, 1993; Redenbach *et al.*, 1997), thus the microspheres used are sufficiently large as to prevent transmission across the pulmonary vascular bed and ultimately into the coronary circulation. Embolization, however, may lead to the development of intrapulmonary shunts that may allow the microspheres to be delivered to the coronary circulation leading to myocardial ischaemia and stiffening. The alternative explanation that elevated right ventricular pressures were transmitted via the interventricular septum to the left ventricle does not seem plausible as: right ventricular end diastolic pressures were not significantly raised; such a relationship was not observed with much greater elevations in pulmonary pressures in previous experiments; and the open pericardium was not constraining the heart to allow such interventricular dependence. Interestingly, in dose ranging experiments for this protocol, the delivery of smaller microspheres (10-50 and 40-70 μm) led to a more marked reduction in systemic blood pressure with simultaneous elevation in LVEDP, further strengthening the idea that the microspheres could lead to left ventricular ischaemia.

As has been demonstrated in Chapter 6, the increased right ventricular strain as a result of increased right ventricular afterload achieved with microsphere administration is manifest as an increase in the forward expansion wave energy and thus becomes the dominant wave of the cardiac cycle. It is likely the increased strain leads to a much faster rate of deceleration of myofibril shortening in late systole consequently leading to a dominant forward expansion wave. Thus the proportion of forward expansion energy to total wave energy may be a marker of myocardial strain.

The findings discussed above are observed with acute haemodynamic changes. They may not mirror changes that occur with chronic progressive pulmonary vascular remodelling. It is expected, however, that progressive pulmonary vascular disease will similarly lead to loss of pulmonary compliance, increased pulmonary wave speed and earlier arrival of the backward compression wave to oppose flow out of the right ventricle. It is not clear from these experiments what minimum pulmonary vessel loss is required to be able to detect an important rise in pulmonary wave speed or cumulative energy of the backward compression wave. These experiments need to be repeated in a larger number of sheep with smaller multiple incremental doses of microspheres.

7.4 Conclusions

Progressive microsphere administration leads to a dose responsive increase in pulmonary arterial wave speed, which manifests before a gross elevation in pulmonary pressures occurs. This relationship is modest at low doses, however, and does not become significant until the mean pulmonary pressure is greater than 20 mmHg. The administration of microspheres also leads to a dose responsive increase in cumulative backward compression wave energy as a result of increased closed-end reflection from obstructed blood vessels. This prominent wave arrives in mid-systole and opposes blood flow out of the right ventricle, increasing the energy cost of the right ventricle. Yet, the right ventricular afterload may not appear significantly great if judged by mean pulmonary pressure alone. The pulmonary arterial wave speed may become a useful discriminator for those patients with mild elevations in pulmonary pressure, as significant pulmonary vascular disease will likely affect the proximal pulmonary compliance to increase wave speed. Additionally, the late forward expansion wave energy proportion of total cumulative wave energy may be a marker of right ventricular strain.

Chapter 8 Pulmonary Arterial Wave Intensity Analysis Following Windkessel Modelling

8.1 Anticipated Wave Intensity

The compliant pulmonary circulation acts as a reservoir for blood, which continuously empties via the distal vessels during diastole. This reservoir function is termed the Windkessel. It is clear that not all changes in pressure are due to wave travel. Pressure also fluctuates in response to volume changes inside the compliant pulmonary vessels. These observations led to the development of the Reservoir-Wave Hypothesis (Wang *et al.*, 2003), the theoretical benefits of which are more completely outlined in Section 1.3.7. Here the measured pressure (P) is separated into a Windkessel (reservoir) pressure (P_{res}) and an excess pressure (P_{ex}), which is thought of as the pressure that drives waves:

$$P = P_{res} + P_{ex}$$

How the reservoir pressure is calculated is outlined in Sections 1.3.7 & 2.3.5. The reservoir pressure accounts for the majority of the measured pressure during diastole and so the wave pressure is effectively zero during diastole. WIA may then be performed on the excess pressure (which determines wave travel) using a wave speed value determined on the measured pressure and velocity.

There may be value in considering reservoir effects prior to analysing wave motion, but the incremental benefits of this more complex approach to the study of wave travel and reflection is not known. Therefore the influence that performing wave intensity analysis on the excess pressure has on wave travel in the resting pulmonary artery, during hypoxia, and during the highest dose of microspheres delivered was systematically explored. It was anticipated that the qualitative pattern of wave travel and reflection would remain unchanged. Although the excess pressure is an order of magnitude less than measured pressure, the rate of pressure change should be the same and therefore the intensities of the forward travelling waves would be similar. The effects on backward (reflected) wave intensity are unknown and cannot be predicted.

8.2 Resting Pulmonary Artery Results

An example of a fitted Windkessel pressure is shown in Figure 8-1 and an example of calculated excess pressure is shown in Figure 8-2. The curve fitting parameters used for analysis is shown in Table 8-1. Where the excess pressure does not rise and fall at the same rate as flow, superimposed wave travel is likely. After the reservoir pressure was accounted for the pattern of wave travel was qualitatively unchanged in the resting pulmonary artery (Figure 8-3 & Figure 8-4). The peak intensities of the forward compression and forward expansion fell slightly yet significantly ($p < 0.001$ and $p = 0.001$ respectively). Despite a fall in peak intensity of the forward expansion wave the cumulative intensity was not significantly different ($p = 0.62$), implying this wave was broader. The peak and cumulative intensities of the late forward compression, early backward expansion and backward compression wave increased significantly (Table 8-2). The backward-travelling waves became a much greater proportion of total wave intensity after the reservoir had been accounted for (Table 8-2). As a result, the reflection coefficient for the proximal open-end reflector increases from -0.01 ± 0.01 to -0.08 ± 0.06 ($p < 0.001$) and for the distal closed-end reflector from 0.01 ± 0.01 to 0.06 ± 0.06 ($p = 0.001$). The distance to the open-end reflector increased trivially from 2.4 ± 0.6 cm to 2.6 ± 0.6 cm ($p = 0.04$). The distance to the closed-end reflector remained unchanged from 21.3 ± 3.0 cm to 21.8 ± 3.1 cm ($p = 0.12$).

Table 8-1. Windkessel curve-fitting parameters used to analyse the three groups

Windkessel Parameters	Resting	Hypoxia	Microsphere
P_∞ (mmHg)	9.4 ± 6.7	15.8 ± 4.5	-19.4 ± 8.1
R ($mmHg.mL^{-1}.sec^{-1}$)	0.10 ± 0.08	0.14 ± 0.06	1.5 ± 0.17
C ($mL.mmHg^{-1}$)	2.0 ± 0.8	1.3 ± 0.7	1.6 ± 0.5
τ (seconds)	0.22 ± 0.25	0.15 ± 0.05	2.2 ± 0.5

C, compliance; P_∞, asymptotic pressure; R, Windkessel related resistance; τ, diastolic exponential time constant.

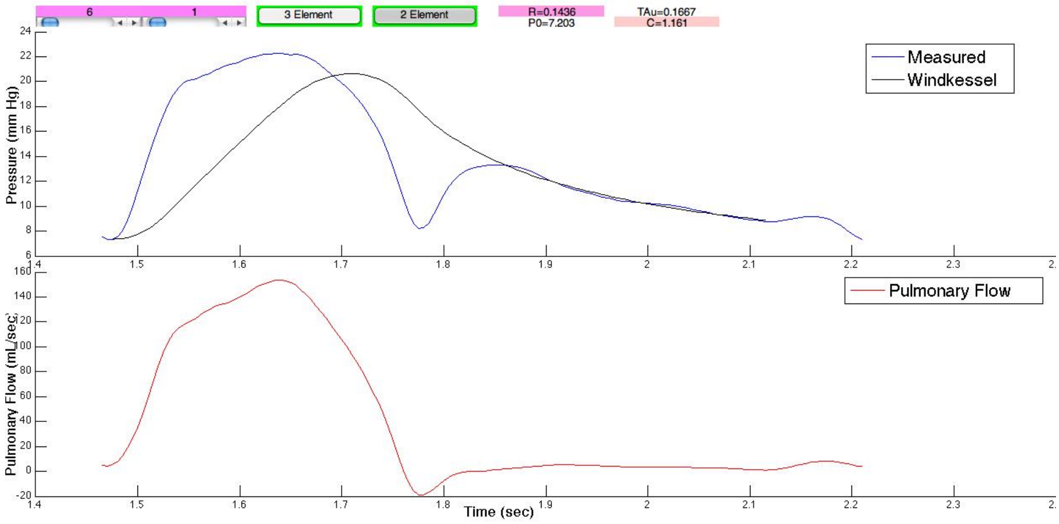

Figure 8-1. Resting pulmonary artery pressure as measured (blue) with calculated Windkessel pressure (black) with simultaneous pulmonary blood flow (red) over a single cardiac cycle.

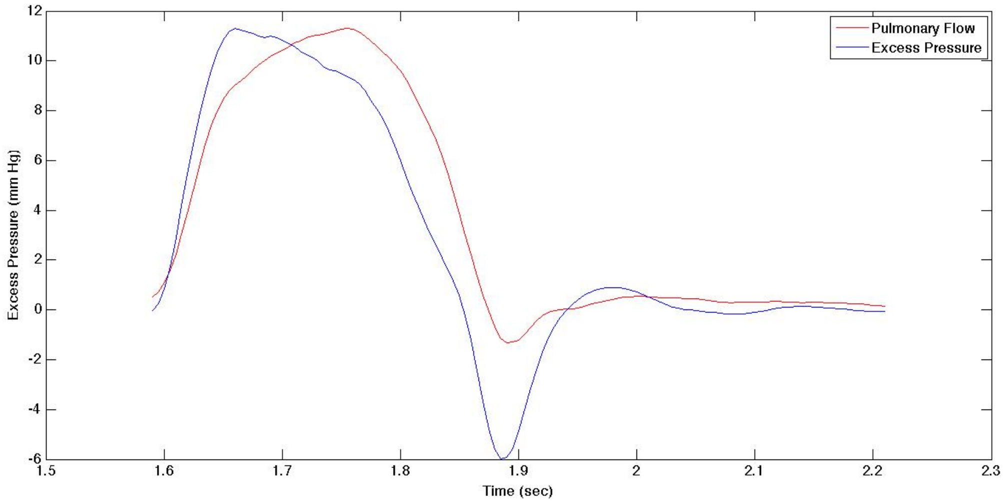

Figure 8-2. Excess pressure (blue), calculated by subtracting Windkessel pressure from measured pulmonary pressure in a normal resting artery, and aortic flow plotted against time with the scales adjusted so that the peak values coincide.

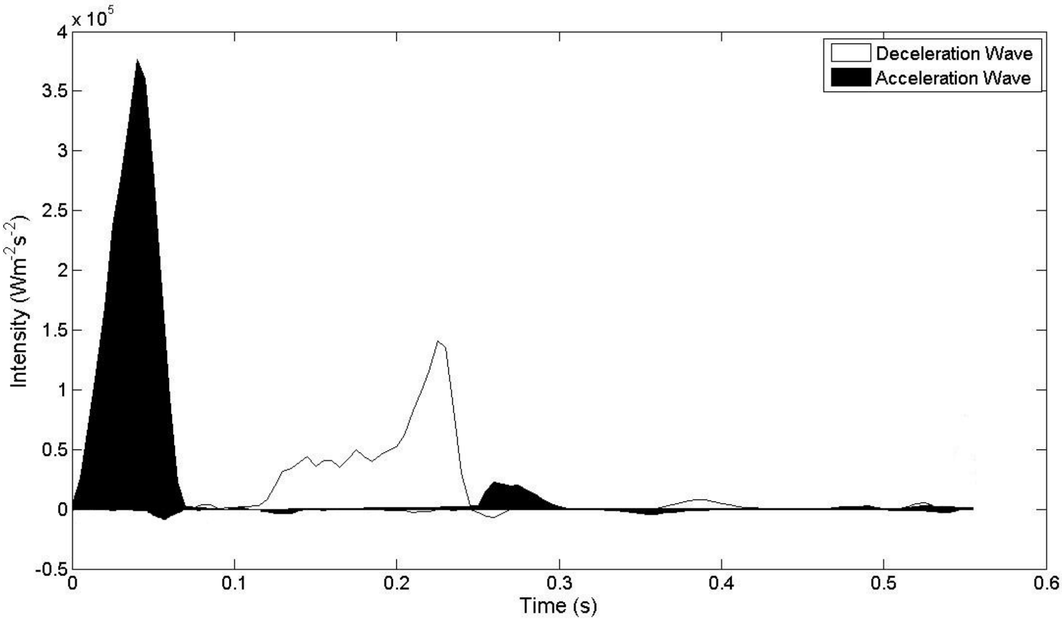

Figure 8-3. Wave intensity in the resting pulmonary artery.

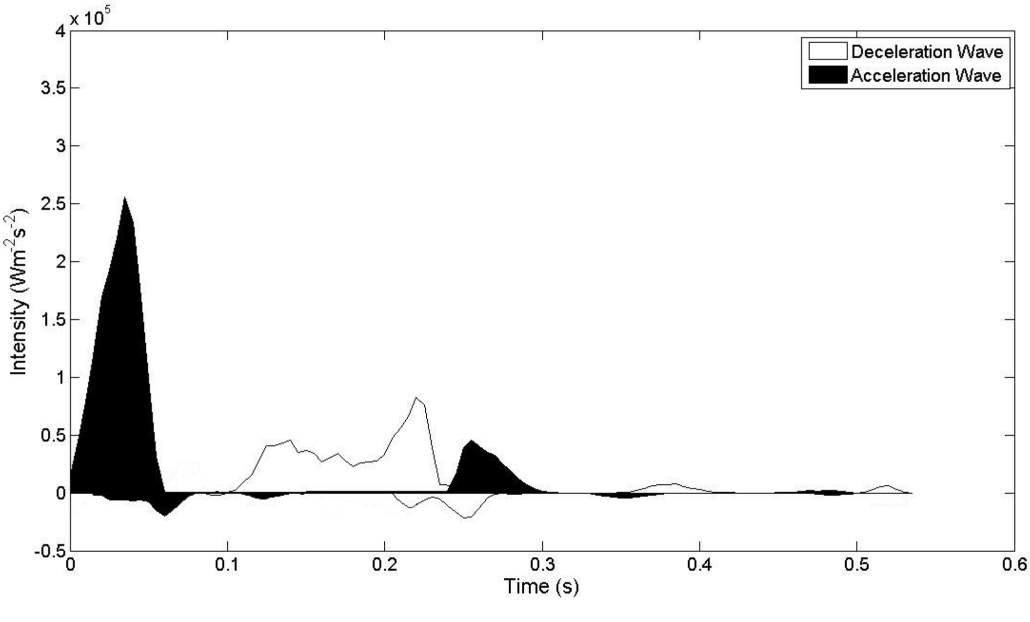

Figure 8-4. Wave intensity in the resting pulmonary artery performed on excess pressure after the reservoir pressure has been accounted for.

Table 8-2. Wave intensity parameters in the resting pulmonary artery before and after Windkessel analysis

	Control (n = 8)	Windkessel (n = 8)	P Value
Peak Wave Intensity ($\times 10^4$ $Wm^{-2}s^{-2}$)			
Early Forward Compression	59.43 ± 22.27	50.63 ± 20.38	< 0.001
Late Forward Expansion	13.00 ± 5.44	11.17 ± 4.42	0.001
Late Forward Compression	1.76 ± 1.41	3.01 ± 1.89	< 0.001
Early Backward Expansion	0.98 ± 0.57	3.83 ± 2.55	< 0.001
Backward Compression	0.91 ± 0.70	2.24 ± 1.48	< 0.001
Cumulative Wave Intensity ($\times 10^2$ $Wm^{-2}s^{-1}$)			
Early Forward Compression	178.06 ± 48.78	141.66 ± 44.26	< 0.001
Late Forward Expansion	71.75 ± 21.71	70.47 ± 21.13	0.62
Late Forward Compression	5.42 ± 4.11	11.08 ± 7.77	< 0.001
Early Backward Expansion	1.64 ± 0.99	9.24 ± 6.85	< 0.001
Backward Compression	1.90 ± 1.54	7.44 ± 6.63	< 0.001
Proportion of Cumulative Wave Intensity (%)			
Early Forward Compression	68.5 ± 5.5	58.8 ± 8.9	< 0.001
Late Forward Expansion	27.8 ± 3.9	29.5 ± 4.2	0.001
Late Forward Compression	2.2 ± 2.0	4.6 ± 3.0	< 0.001
Early Backward Expansion	0.7 ± 0.5	4.1 ± 2.8	< 0.001
Backward Compression	0.8 ± 0.6	3.0 ± 2.2	< 0.001
Reflection Coefficient			
BEW/FCW	0.01 ± 0.01	0.08 ± 0.06	< 0.001
BCW/FCW	0.01 ± 0.01	0.06 ± 0.06	0.001
Wave Speed (ms^{-1})	1.78 ± 0.21	1.78 ± 0.21	-
Distance to Reflection Site (cm)			
Early Backward Expansion	2.38 ± 0.62	2.62 ± 0.63	0.04
Late Backward Compression	21.30 ± 3.00	21.77 ± 3.11	0.12

Values are means ± SD; BCW, backward compression wave; BEW, backward expansion wave; FCW, forward compression wave; n, number of sheep.

8.3 Hypoxia Results

After the reservoir pressure was accounted for, the pattern of wave travel was qualitatively unchanged during hypoxia (Figure 8-5 & Figure 8-6) but the peak and cumulative intensities of the forward compression, forward expansion and backward compression wave fell significantly (Table 8-3). The peak and cumulative intensities of the late forward compression and early backward expansion increased significantly (Table 8-3). The reflection coefficient of the proximal open-end reflector increases from -0.07 ± 0.05 to -0.25 ± 0.15 ($p < 0.001$) and for the distal closed-end reflector from 0.14 ± 0.06 to 0.08 ± 0.04 ($p < 0.001$). The distance to the open-end reflector remained unchanged from 2.9 ± 0.5 cm to 3.0 ± 0.9 cm ($p = 0.22$). The distance to the closed-end reflector increased slightly from 13.1 ± 3.3 cm to 15.3 ± 4.8 cm ($p = 0.04$).

8.4 High Microsphere Dose Results

After the reservoir pressure was accounted for, the pattern of wave travel was qualitatively unchanged with microsphere administration (Figure 8-7 & Figure 8-8) but the peak and cumulative intensities of the forward compression, forward expansion and backward compression wave fell significantly (Table 8-4). The peak and cumulative intensities of the late forward compression and early backward expansion increased significantly (Table 8-4). The reflection coefficient of the proximal open-end reflector increased from -0.03 ± 0.01 to -0.11 ± 0.04 ($p = 0.02$) and for the distal closed-end reflector from 0.24 ± 0.13 to 0.14 ± 0.09 ($p = 0.02$). The distance to the open-end reflector fell from 3.3 ± 1.4 cm to 2.6 ± 1.4 cm but not significantly so ($p = 0.10$). The distance to the closed-end reflector increased slightly from 18.6 ± 3.8 cm to 20.8 ± 2.5 cm but was also not significant ($p = 0.45$).

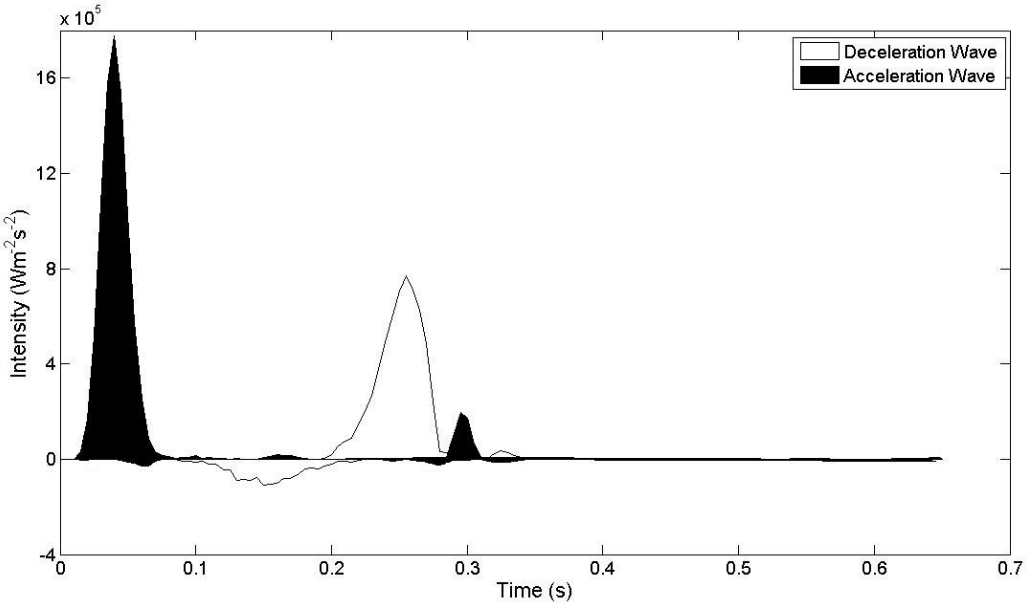

Figure 8-5. Wave intensity during hypoxia performed on the measured pressure.

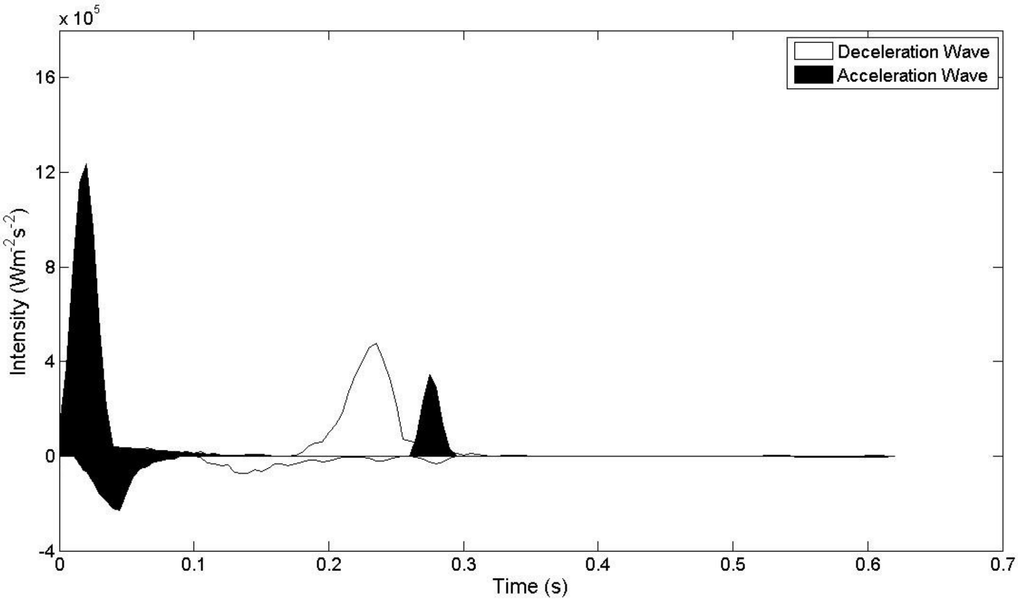

Figure 8-6. Wave intensity during hypoxia performed on the excess pressure after the reservoir pressure has been accounted for.

Table 8-3. Wave intensity parameters during hypoxia with and without Windkessel analysis

	Hypoxia (n = 8)	Windkessel (n = 8)	P Value
Peak Wave Intensity ($\times 10^4$ $Wm^{-2}s^{-2}$)			
Early Forward Compression	117.08 ± 39.64	99.13 ± 30.04	0.001
Late Forward Expansion	68.51 ± 34.75	54.34 ± 28.15	< 0.001
Late Forward Compression	11.64 ± 13.24	17.93 ± 15.04	< 0.001
Early Backward Expansion	8.80 ± 6.11	21.04 ± 11.19	< 0.001
Backward Compression	9.16 ± 3.67	5.24 ± 2.69	< 0.001
Cumulative Wave Intensity ($\times 10^2$ $Wm^{-2}s^{-1}$)			
Early Forward Compression	314.05 ± 67.11	232.24 ± 45.03	< 0.001
Late Forward Expansion	266.59 ± 87.74	213.27 ± 66.66	0.001
Late Forward Compression	19.99 ± 31.06	33.84 ± 32.90	< 0.001
Early Backward Expansion	19.58 ± 13.46	56.17 ± 32.66	0.002
Backward Compression	43.28 ± 17.76	19.27 ± 9.51	< 0.001
Proportion of Cumulative Wave Intensity (%)			
Early Forward Compression	48.1 ± 9.5	41.9 ± 8.4	< 0.001
Late Forward Expansion	39.5 ± 7.4	38.4 ± 7.8	0.10
Late Forward Compression	3.0 ± 4.9	6.1 ± 5.4	0.001
Early Backward Expansion	2.9 ± 2.2	10.1 ± 5.1	< 0.001
Backward Compression	6.5 ± 2.5	3.5 ± 1.5	0.001
Reflection Coefficient			
BEW/FCW	-0.07 ± 0.05	-0.25 ± 0.15	< 0.001
BCW/FCW	0.14 ± 0.06	0.08 ± 0.04	< 0.001
Wave Speed (ms^{-1})	2.68 ± 0.5	2.68 ± 0.5	-
Distance to Reflection Site (cm)			
Early Backward Expansion	2.91 ± 0.5	3.04 ± 0.9	0.22
Late Backward Compression	13.11 ± 3.26	15.32 ± 4.84	0.04

Values are means ± SD; BCW, backward compression wave; BEW, backward expansion wave; FCW, forward compression wave; n, number of sheep.

Table 8-4. Wave intensity parameters after high dose microsphere administration with and without Windkessel analysis

	15.2×10^4 70-110 µm Microspheres (n = 4)	Windkessel (n = 4)	P Value
Peak Wave Intensity ($\times 10^4$ $Wm^{-2}s^{-2}$)			
Early Forward Compression	400.38 ± 95.04	361.18 ± 93.34	0.03
Late Forward Expansion	680.42 ± 104.10	630.70 ± 100.63	< 0.001
Late Forward Compression	226.68 ± 79.47	272.74 ± 86.22	0.001
Early Backward Expansion	16.08 ± 4.75	41.36 ± 12.19	0.007
Backward Compression	55.31 ± 15.10	30.65 ± 7.46	0.01
Cumulative Wave Intensity ($\times 10^2$ $Wm^{-2}s^{-1}$)			
Early Forward Compression	362.16 ± 98.33	303.00 ± 113.75	0.01
Late Forward Expansion	420.66 ± 33.67	400.02 ± 35.43	0.04
Late Forward Compression	97.46 ± 38.06	124.61 ± 45.64	0.01
Early Backward Expansion	11.99 ± 5.96	34.11 ± 15.14	0.02
Backward Compression	80.33 ± 33.07	35.82 ± 14.96	0.02
Proportion of Cumulative Wave Intensity (%)			
Early Forward Compression	37.2 ± 6.6	33.8 ± 8.2	0.02
Late Forward Expansion	43.3 ± 6.0	44.6 ± 9.3	0.43
Late Forward Compression	10.0 ± 4.3	13.8 ± 5.1	0.003
Early Backward Expansion	1.2 ± 0.5	3.8 ± 1.4	0.02
Backward Compression	8.3 ± 3.5	4.0 ± 1.9	0.01
Reflection Coefficient			
BEW/FCW	-0.03 ± 0.01	-0.11 ± 0.04	0.02
BCW/FCW	0.24 ± 0.13	0.14 ± 0.09	0.02
Wave Speed (ms^{-1})	2.66 ± 0.69	2.66 ± 0.69	-
Distance to Reflection Site (cm)			
Early Backward Expansion	3.26 ± 1.37	2.64 ± 1.40	0.10
Late Backward Compression	18.62 ± 3.81	20.83 ± 2.54	0.45

Values are means ± SD; BCW, backward compression wave; BEW, backward expansion wave; FCW, forward compression wave; n, number of sheep.

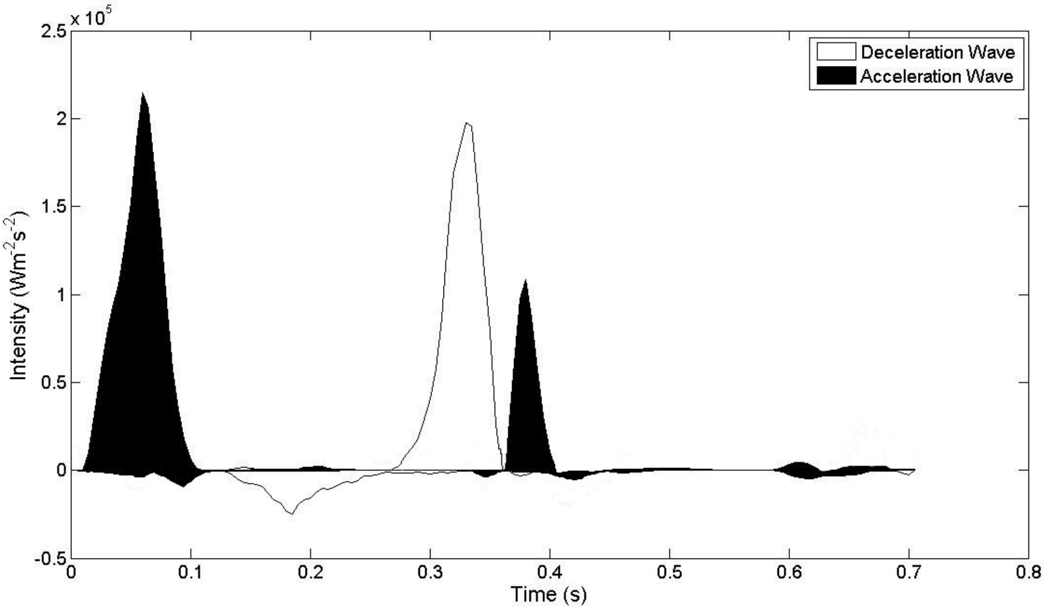

Figure 8-7. Wave intensity during high dose microsphere administration performed on the measured pressure.

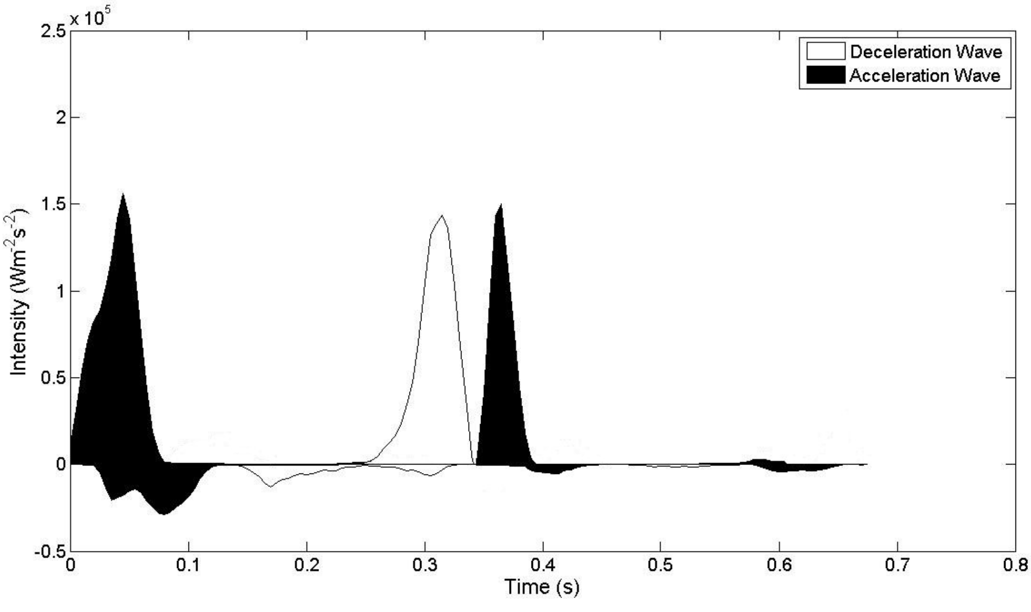

Figure 8-8. Wave intensity during high dose microsphere administration performed on the excess pressure after the reservoir pressure has been accounted for.

8.5 Discussion

Other authors have shown that reservoir pressure has a larger contribution to the total pressure waveform than does the wave pressure in the aorta (Aguado-Sierra *et al.*, 2008; Tyberg *et al.*, 2009). The present results support that this is also true in the pulmonary artery (Figure 8-1 & Figure 8-2), implying that the reservoir pressure is responsible for most of the perfusion of the microcirculation. The waves are necessary to generate the reservoir pressure, yet, they have little effect on the net perfusion. It is an attractive proposition to be able to separate ventricular work into the work done to "fill" the reservoir and the work done to generate the arterial waves to better understand physiological processes. Indeed others have shown that the energy associated with wave-induced acceleration and deceleration was 1% of the total hydraulic work, which the authors interpret is work done to overcome proximal resistance (Tyberg *et al.*, 2009; Wang *et al.*, 2008). However, in terms of using wave intensity analysis to understand wave reflection as a marker of a healthy or diseased pulmonary vasculature, the reservoir-wave hypothesis does not contribute significantly.

Performing wave intensity analysis on the excess rather than the measured pressure does not alter the qualitative interpretation of wave travel and reflection in the pulmonary artery. However, there are some quantitative effects. After accounting for the reservoir, the effects on wave intensity for the largest waves in the cardiac cycle were minimal. This is because the reservoir pressure is the result of a capacitive-like process and responds less quickly to the initial compression phase of the right ventricle. It was observed that the cumulative energy of the initial forward compression and late forward expansion wave fall minimally, whilst the energy carried by the late forward compression wave increases slightly. For small backwards-travelling waves, the effect of subtracting the reservoir pressure from the measured pressure had a much larger effect. The cumulative energy of the early backward expansion wave increased for the control, hypoxia, and microsphere group. This suggests that in early systole the rate of change in backward excess pressure was greater than the change in backward measured pressure. Whilst these changes were observed it is difficult to provide these findings with physiological meaning. Furthermore, the backward compression wave becomes much less prominent after the reservoir effects are accounted for with hypoxia or microsphere administration. This suggests that in late systole the rate of change in backward excess pressure is less than the change in backward measured pressure.

There are potential sources of error in this work. The model to fit the reservoir pressure works best when there is a long diastolic run off period. It appears to be more difficult to determine the Windkessel parameters if the heart rate is faster than 70 beats/min (Tyberg *et al.*, 2009; Wang *et al.*, 2006). No attempts were made to pace the heart at slower rates to enable a longer period of diastolic outflow. The analysis was performed on the data as collected, which may not have a smooth diastolic run-off, thus potentially influencing the calculated excess pressure. The Windkessel curve-fitting parameters shown in Table 8-1 are all plausible values with the exception of the asymptotic pressure and RC time for the microsphere study. The asymptotic pressure is the pressure to which the diastolic pressure would ultimately fall to when flow across the pulmonary circulation ceases. A negative asymptotic pressure for the microsphere group has no physiological meaning or plausibility and leads to a very long RC time of > 2 seconds, implying that there may have been curve-fitting errors.

The impact of pressure separation on the sum-of-squares method for calculation of the wave speed has not been studied before. It was unclear whether the wave speed should be calculated on the measured pressure and velocity or the excess pressure and velocity. It was decided that as wave speed is a function of the arterial properties, it should be calculated on the pressure and velocity that the artery "experiences", that is the measured pressure and velocity. However, when the sum-of-squares (single-point) technique was used to calculate wave speed on the measured and excess pressure in five randomly selected animals at baseline, there was no significant difference between them, 2.05 ± 0.43 and 2.16 ± 0.33 respectively ($p = 0.30$). The physiological implications of wave speeds that are not different on measured and excess pressure need further exploring and confirmation in other studies.

The reservoir-wave hypothesis is criticised for its assumption of infinite wave travel; that is the reservoir pressure varies only over time not space. Therefore some may argue that wave travel on a time-only varying reservoir cannot exist. However, Wang (2003) clearly demonstrated that in the aorta during late diastole, pressure is dependent on time only and is independent of distance, supporting the notion that the reservoir pressure varies only with time. Preliminary data here supports the idea that this may also be true in the pulmonary circulation. The pressure transducer was pulled back from the distal circulation to the proximal pulmonary artery by 1 cm increments in a single animal (Figure 8-9 & Figure 8-10). This would need to be repeated in a larger number of animals to confirm that pressure in late diastole is only dependent on time. These findings and those of Wang (2003) imply that compliance falls in the more distal vessels so that emptying from the distal reservoir occurs at the same rate as the more compliant proximal segments. Data from Caro and Saffman (1965) support this notion, as they showed progressive stiffening of pulmonary vascular walls between the major vessels and periphery in rabbits. However, there is disagreement about how compliance of the pulmonary vascular bed varies along its length (Gan and Yen, 1994; Shoukas, 1975; West *et al.*, 1975).

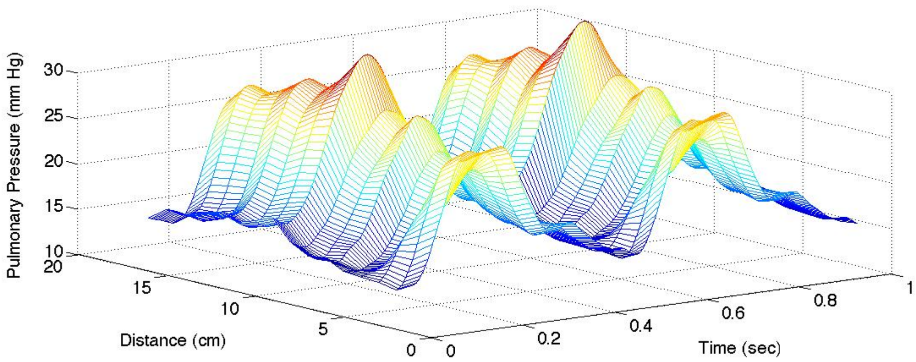

Figure 8-9. Pressure was recorded in the pulmonary artery of a single animal at centimetre increments from distal (16 cm) to proximal (0 cm). Despite variations in peak systolic pressure the pulse pressure was approximately the same throughout the length.

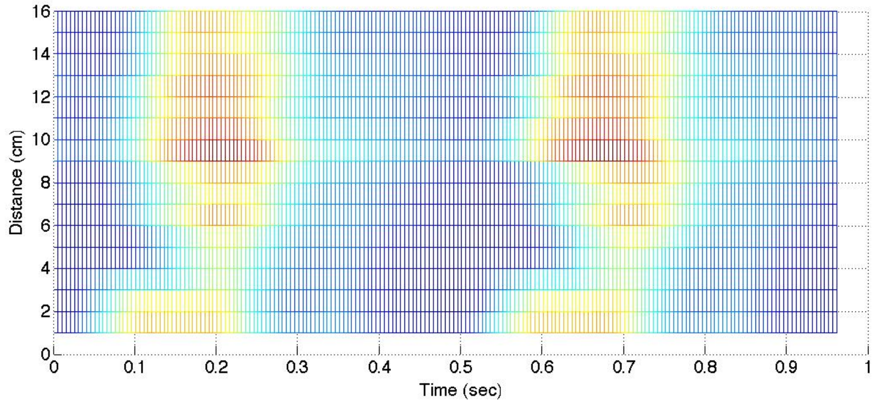

Figure 8-10. An aerial view of the data in Figure 8-9 where the highest pressures are indicated in red and the lowest in dark blue. Despite systole occurring earlier proximally the diastolic pressure falls approximately independently of distance and is related to time.

The Windkessel parameters have been used to assess right ventricular afterload in many animal species (Lucas, 1984). It has also been used to successfully assess resistance and compliance relationships in different forms of human pulmonary arterial hypertension (Lankhaar *et al.*, 2006). The three-element (resistance, compliance, and characteristic impedance) Windkessel model used could differentiate between different forms of pulmonary hypertension but was too simple a model to be able to classify individual patients. Other authors have reported different values of τ (RC) to the present results; 0.75 seconds (Lankhaar *et al.*, 2006) and 0.33 (Reuben, 1971). The discrepancies are explained by the different estimation methods used. Reuben used PVR instead of R and Lankhaar *et al.* used the energy balance method and R instead of PVR. It has previously been demonstrated that the pulmonary circulation keeps the RC time constant during pulmonary hypertension (Lankhaar *et al.*, 2006). This appears plausible as increased resistance leads to increased pressure, which in turn leads to a decrease in compliance by a shift in the position on the pressure-volume relationship of the large pulmonary arteries. The present results did not demonstrate a constant RC time from the resting to the acutely hypertensive state. This may reflect the acute and not chronic nature of the pulmonary hypertension induced here, which may have a different relationship between R and C. Whilst the three-element Windkessel is known to overestimate compliance (Segers *et al.*, 1999), the values for C compare favourably to the range of 0.5-4 $mLmmHg^{-1}$ reported in healthy and diseased humans by Lankhaar *et al.* (2006) estimated by a number of independent techniques. Similarly the values for R compare to Lankhaar *et al.*'s results of 0.2-1.1 $mmHg.s.mL^{-1}$, with R increasing with progressive pulmonary vasoconstriction.

As the Windkessel is a lumped parameter model, it does not contain spatial information and on its own is unable to describe wave travel and reflection. The three-element Windkessel model has the advantage that it is easy to interpret with parameters that have physiological meaning and further the understanding of right ventricular afterload. Studies of wave reflection add to the understanding of right ventricular afterload and the state of the pulmonary circulation. Therefore the hybrid reservoir-wave model may have future clinical merit to completely describe right ventricular afterload, but on its own does not contribute greatly to the understanding of wave travel and reflection.

8.6 Conclusion

The reservoir-wave hypothesis may be a more complete model of blood flow in a distensible system, allowing more detailed interpretation of the mechanics that generate the typical pulse waveforms. It does not, however, contribute any further to the qualitative interpretation of wave travel and reflection in the pulmonary artery. It seems that the extra mathematical complexity required to determine excess pressure is unnecessary for the study of wave reflection alone and has the potential to introduce errors. The effect of separation into reservoir and excess (wave) pressure on wave intensity analysis needs to be explored in detail in other systems and species. The hybrid reservoir-wave model has potential future clinical merit by allowing determination of vascular compliance as well as wave reflection that may provide additional diagnostic and prognostic information.

Chapter 9 Human Pulmonary Arterial Wave Intensity Analysis in Health and Disease

It has been demonstrated in animals that wave intensity analysis provides useful insights into right ventricular-pulmonary arterial interactions, that is, the upstream (ventricular) and downstream (vascular) properties, including wave reflection, which influence net pulmonary blood flow. Wave intensity provides information on the rate at which right ventricular work is done, thus giving insight into the working state of the ventricle. This is information that can only otherwise be provided by pressure-volume loop analysis, which is challenging in the right ventricle. Studying wave reflection in humans allows this additional component of right ventricular afterload to be investigated, thus helping understanding of the mechanisms that lead to right ventricular failure. Here the first reported studies in human pulmonary arterial wave intensity analysis were undertaken.

9.1 Anticipated Wave Intensity Analysis

The healthy pulmonary vasculature is likely to be characterised by minimal wave reflection at rest. With progressive pulmonary vasculature remodelling and the development of pulmonary hypertension, it is anticipated that a backward-travelling compression wave would arrive in the proximal pulmonary artery in mid-systole, which would serve to oppose flow out of the right ventricle. Furthermore, it was expected that pulmonary arterial wave speed would rise with increasing severity of pulmonary arterial hypertension as a result of pulmonary distension and reduced proximal compliance, resulting in increased and earlier wave reflection.

9.2 Results

Twenty-five patients who were undergoing right heart catheterisation for the investigation of dyspnoea agreed to participate in the study. Seven patients had normal resting pulmonary haemodynamics and were considered to have a normal pulmonary vasculature. Ten patients had mild resting pulmonary arterial hypertension (mean pulmonary artery pressure, mean PAP, ≥ 25-34 mmHg); four had moderate PAH (mean PAP ≥ 35-44 mmHg); and 4 had severe PAH (mean PAP ≥ 45 mmHg). Patients in the moderate and severe PAH categories were combined into a group of 8 for the purposes of analysis.

As expected the mean pulmonary artery pressure and pulmonary vascular resistance index increased significantly ($p < 0.001$ and $p = 0.002$ respectively) across the three categories of pulmonary vascular disease (normal, mild, and moderate-severe; Table 9-1). Cardiac index was well maintained across the groups, averaging 3.2 $Lmin^{-1}m^{-2}$ ($p = 0.65$). The mean right atrial pressure and mean pulmonary capillary wedge pressure increased with disease severity but did not reach statistical significance ($p = 0.10$ and $p = 0.05$ respectively). The peak and mean pulmonary artery blood velocity remained unchanged across the three groups ($p = 0.93$ and $p = 0.81$ respectively).

Pulmonary arterial wave speed increased significantly with worsening pulmonary vascular disease ($p = 0.003$). Those patients with normal haemodynamics had a wave speed of 1.9 ± 0.7 ms^{-1}, whilst those with moderate-to-severe pulmonary vascular disease had a wave speed of 4.8 ± 2.4 ms^{-1}. Pulmonary wave speed is linearly related to mean pulmonary artery pressure (Figure 9-1) with a modest correlation coefficient, $r = 0.65$ (95% CI 0.35 to 0.83; $p < 0.001$). A linear relationship also exists between wave speed and pulmonary vascular resistance index (Figure 9-2), $r = 0.67$ (95% CI 0.36 to 0.85; $p < 0.001$).

Four dominant waves were identified with wave intensity analysis in the human proximal pulmonary artery in all three pulmonary vascular groups (Figure 9-4, Figure 9-6 & Figure 9-8). The corresponding measured pressure and velocity waveforms are shown in Figure 9-3, Figure 9-5 & Figure 9-7. An initial early systolic forward compression wave was followed by a broad systolic forward expansion wave. Two backward-travelling waves were identified: a very early systolic backward expansion wave and a mid-systolic backward compression wave.

Across the severities of pulmonary vascular disease the peak wave intensities increased for each of the four waves but did not reach statistical significance (Table 9-1). The cumulative wave intensities also increased with worsening pulmonary vascular disease severity but only reached statistical significance for the forward compression wave ($p = 0.01$) and the backward compression wave ($p = 0.03$). Across the severity range of pulmonary vascular disease the proportions of individual waves relative to the total wave energies remained unchanged (Table 9-1).

The reflection coefficient of the backward compression wave to forward compression wave increases across the group severities but not significantly ($p = 0.08$). The estimated distance to this closed-end reflector also increased from an unusually close distance of 5.4 ± 3.5 cm in the normal haemodynamic group to 27.3 ± 24.1 cm in the moderate-severe group ($p = 0.08$). The early backward expansion wave precedes the incident forward compression wave, raising the strong likelihood that the backward travelling waves are artefacts and therefore further analysis of them is not justified. These issues are expanded in the discussion section.

Table 9-1. Wave intensity and haemodynamic parameters across the spectrum of pulmonary vascular disease severity

	Normal (n = 7)	**Mild PH (n = 10)**	**Mod-Severe PH (n = 8)**	**P Value**
Peak Wave Intensity ($\times 10^4$ $Wm^{-2}s^{-2}$)				
Early Forward Compression	17.93 ± 8.94	23.19 ± 9.75	33.62 ± 17.62	0.07
Late Forward Expansion	3.81 ± 1.26	5.49 ± 2.25	7.55 ± 6.84	0.24
Early Backward Expansion	16.90 ± 9.75	22.29 ± 11.47	31.66 ± 19.76	0.15
Backward Compression	1.40 ± 0.75	3.41 ± 3.30	6.45 ± 6.31	0.08
Cumulative Wave Intensity ($\times 10^2$ $Wm^{-2}s^{-1}$)				
Early Forward Compression	99.99 ± 31.93	150.02 ± 47.03	190.05 ± 73.14	0.01
Late Forward Expansion	34.86 ± 11.43	48.56 ± 9.67	69.80 ± 50.65	0.09
Early Backward Expansion	51.78 ± 29.07	73.11 ± 41.14	110.36 ± 56.82	0.05
Backward Compression	6.22 ± 3.30	19.80 ± 16.19	42.93 ± 39.42	0.03
Proportion of Cumulative Wave Intensity (%)				
Early Forward Compression	52.1 ± 3.9	52.9 ± 6.0	47.3 ± 6.8	0.12
Late Forward Expansion	18.7 ± 5.5	18.3 ± 5.8	17.3 ± 7.8	0.91
Early Backward Expansion	25.9 ± 7.7	22.9 ± 8.7	25.6 ± 7.3	0.69
Backward Compression	3.3 ± 1.4	5.9 ± 3.4	9.8 ± 8.0	0.07
Reflection Coefficient				
BCW/FCW	0.07 ± 0.03	0.12 ± 0.08	0.23 ± 0.22	0.08
Distance to Reflection Site (cm)				
Late Backward Compression	5.4 ± 3.5	18.9 ± 17.9	27.3 ± 24.1	0.08
Wave Speed (ms^{-1})	1.93 ± 0.69	2.98 ± 0.63	4.76 ± 2.36	0.003
Peak Blood Velocity (cms^{-1})	75.9 ± 6.3	79.03 ± 17.5	76.5 ± 23.9	0.93
Mean Blood Velocity (cms^{-1})	31.5 ± 5.4	29.7 ± 6.5	29.1 ± 8.9	0.81
Mean PA Pressure (mmHg)	14.7 ± 2.6	28.3 ± 3.0	45.0 ± 5.6	< 0.001
Mean PCWP (mmHg)	9.1 ± 4.0	12.7 ± 4.0	14.4 ± 3.5	0.05
Mean RA Pressure (mmHg)	6.5 ± 3.4	7.6 ± 5.3	11.6 ± 3.5	0.10
Cardiac Output ($Lmin^{-1}$)	5.8 ± 1.0	5.2 ± 1.6	5.8 ± 1.6	0.65
Cardiac Index ($Lmin^{-1}m^{-2}$)	3.4 ± 0.8	3.0 ± 0.9	3.2 ± 0.9	0.65
PVR (Wood's Units)	1.0 ± 0.5	2.9 ± 1.1	6.0 ± 3.5	0.001
PVRI (Wood's Units/m^2)	1.6 ± 0.8	4.7 ± 1.6	9.8 ± 6.5	0.002
Mean Age (Years)	46.6 ± 12.2	65.7 ± 9.1	60.5 ± 14.4	0.01

Values are means ± SD; BCW, backward compression wave; BEW, backward expansion wave; FCW, forward compression wave; n, number of human subjects; PA, pulmonary artery; PCWP, pulmonary capillary wedge pressure; PVR, pulmonary vascular resistance; PVRI, pulmonary vascular resistance index; RA, right atrial.

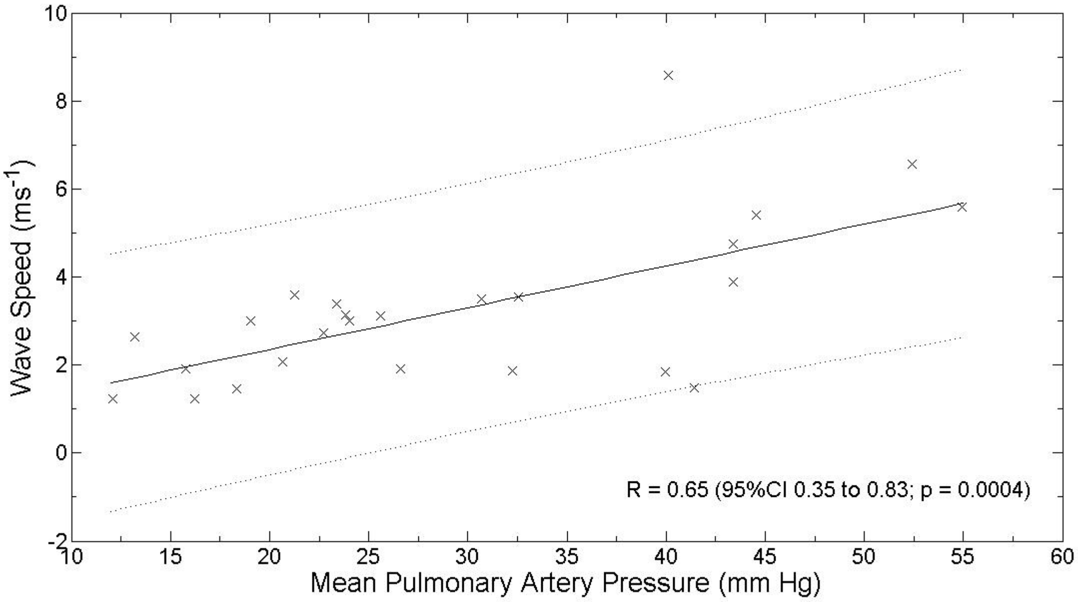

Figure 9-1. Plot of pulmonary arterial wave speed against mean pulmonary artery pressure demonstrating a modestly strong linear relationship.

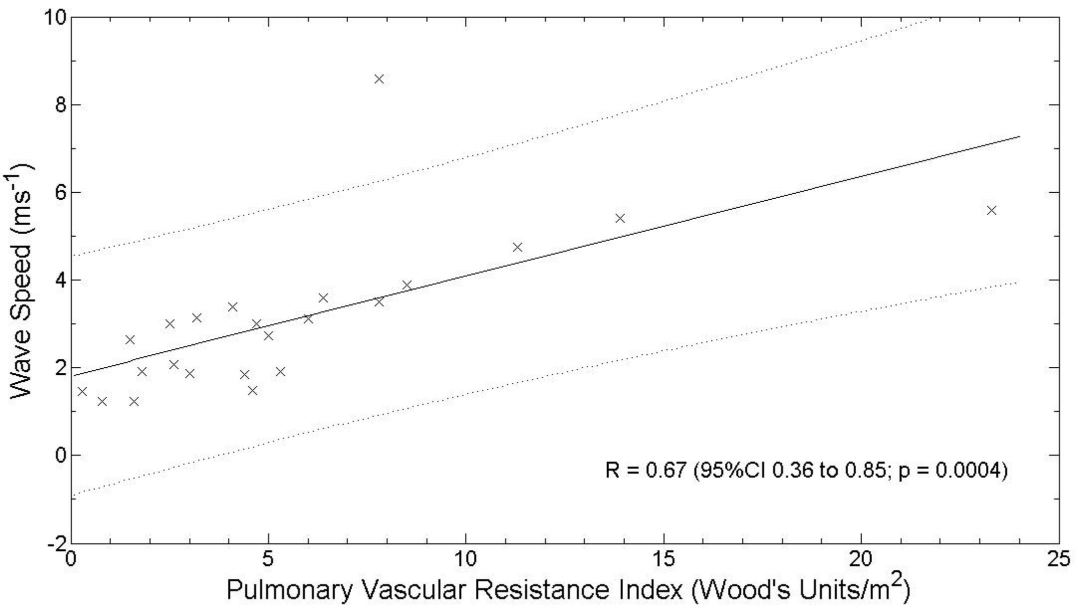

Figure 9-2. Plot of pulmonary arterial wave speed against pulmonary vascular resistance index demonstrating a modestly strong linear relationship.

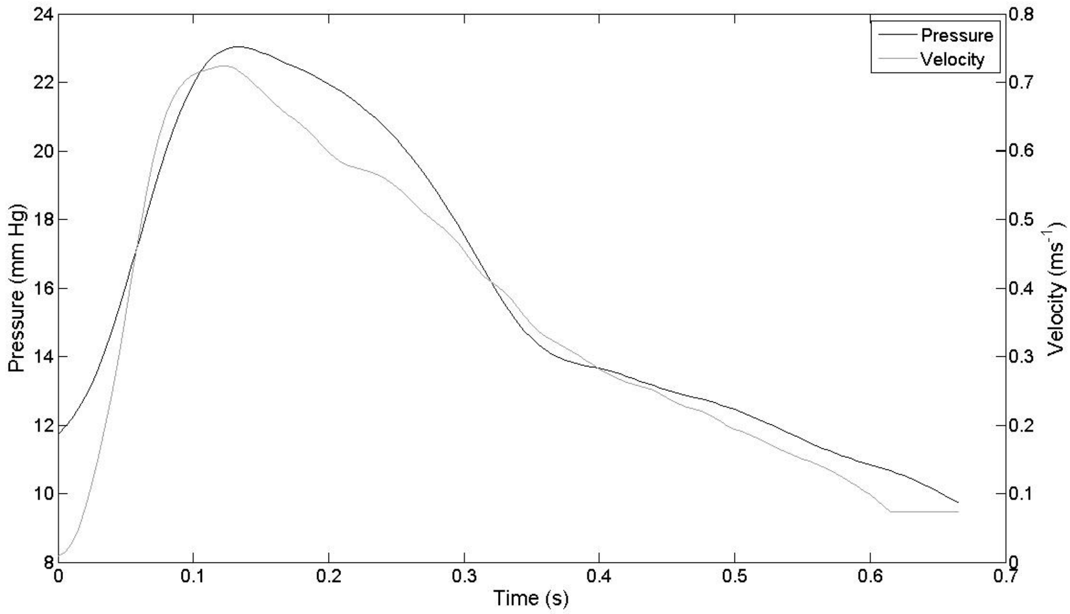

Figure 9-3. Human pulmonary arterial pressure and velocity traces in a patient with normal pulmonary vasculature.

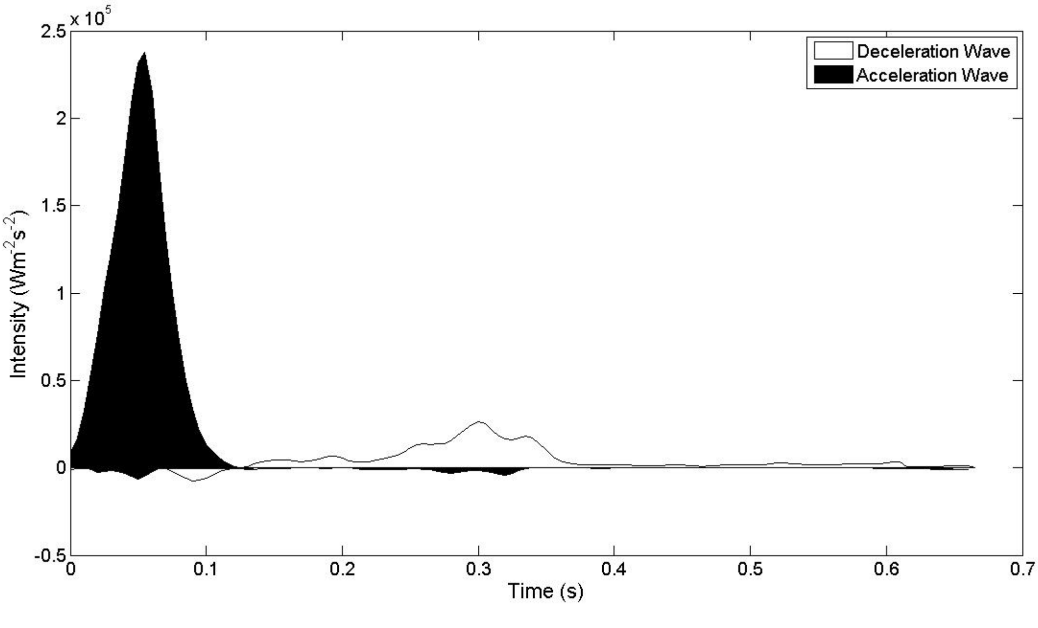

Figure 9-4. Corresponding wave intensity in a patient with normal pulmonary vasculature.

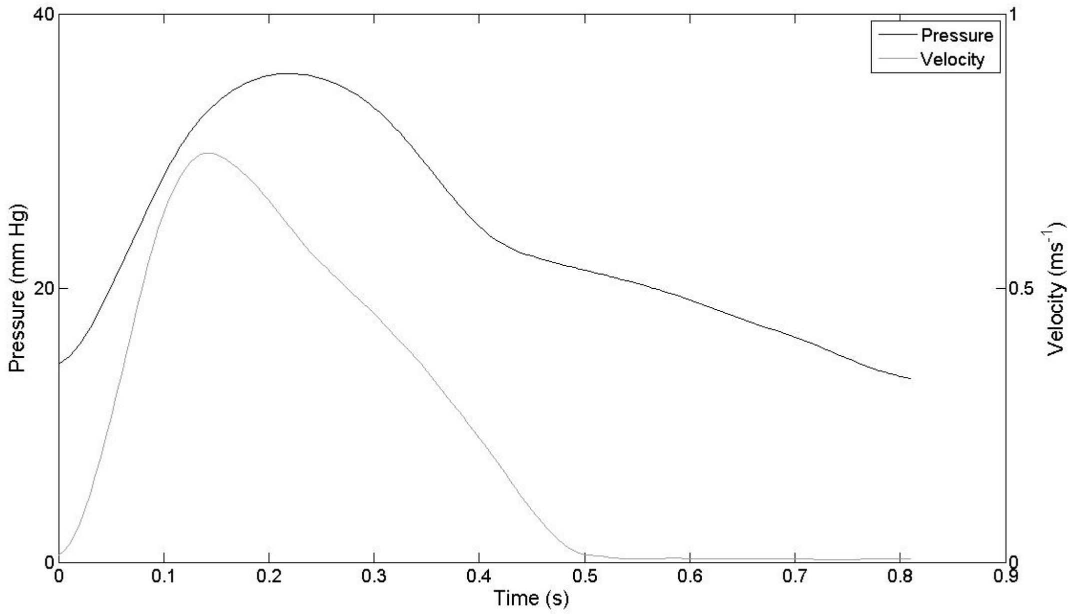

Figure 9-5. Human pulmonary arterial pressure and velocity trace in a patient with mild pulmonary vascular disease.

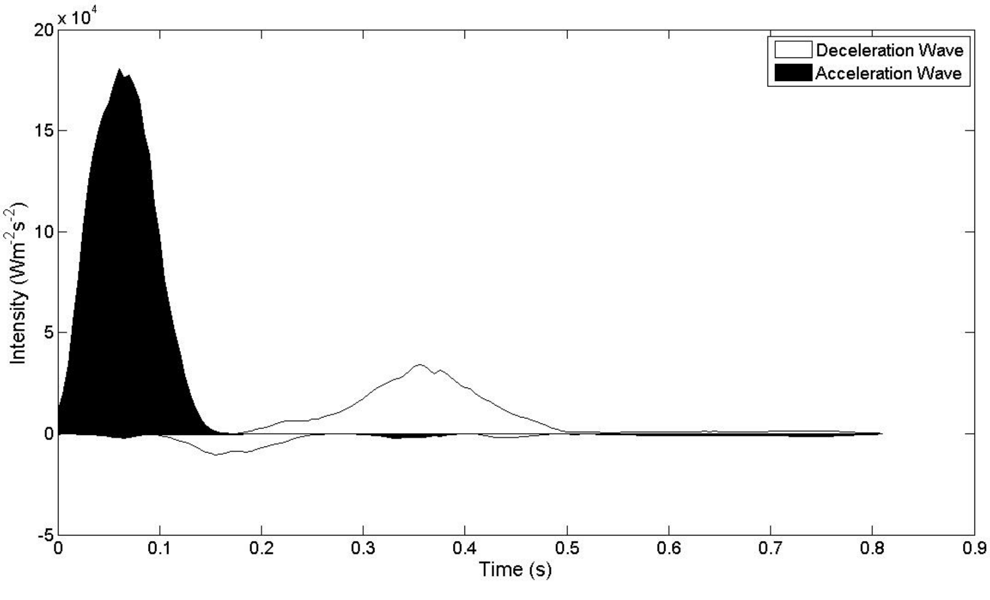

Figure 9-6. Wave intensity in a patient with mild pulmonary vascular disease.

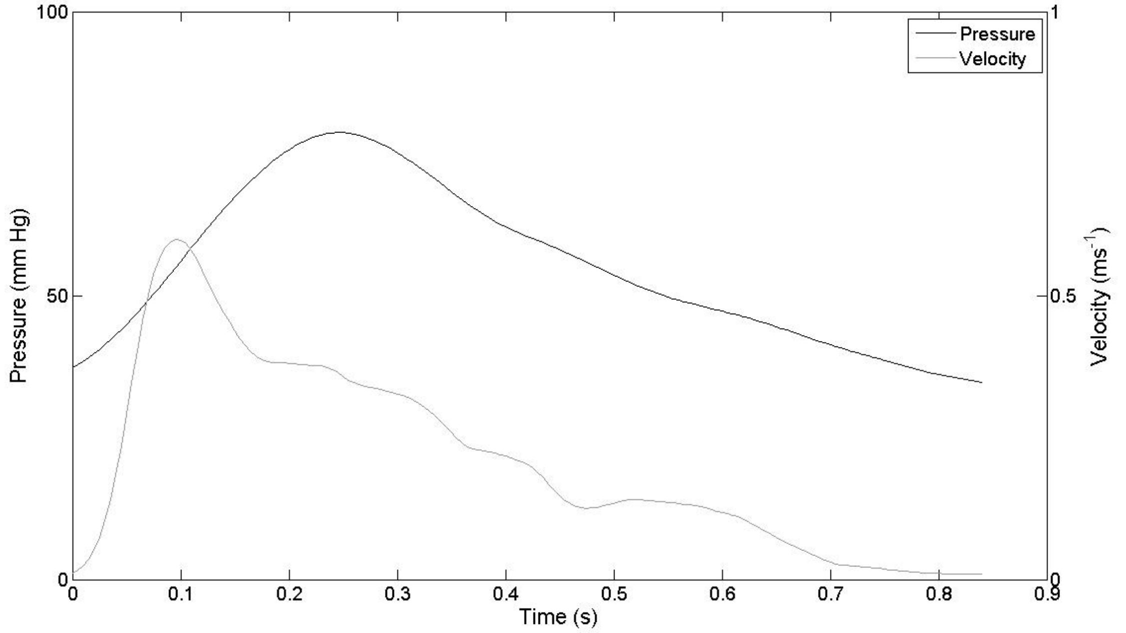

Figure 9-7. Human pulmonary arterial pressure and velocity trace in a patient with severe pulmonary vascular disease.

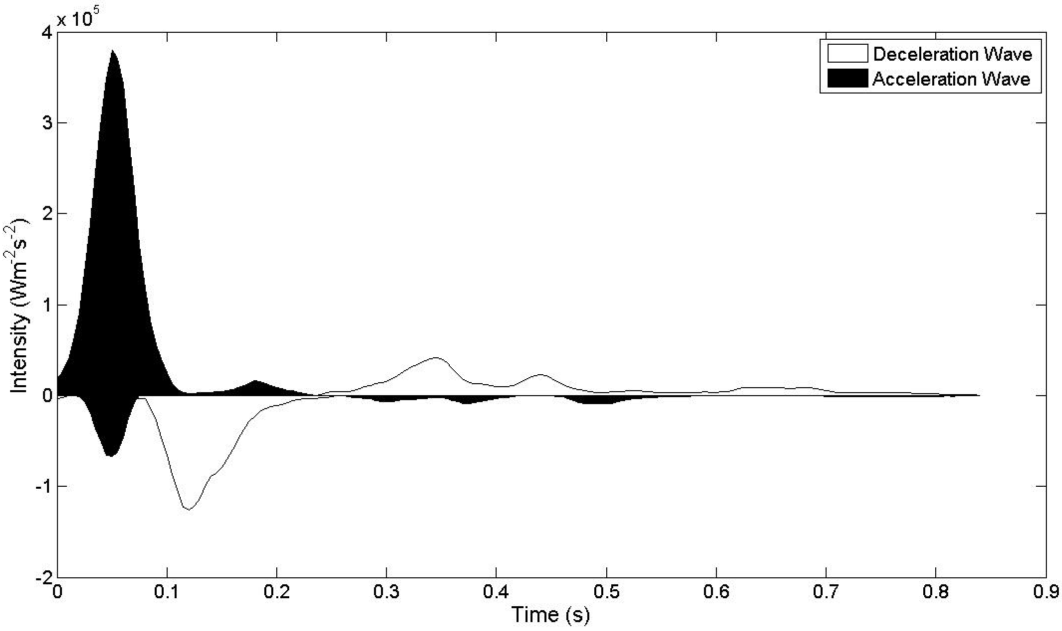

Figure 9-8. Wave intensity in a patient with severe pulmonary vascular disease.

9.3 Discussion

Despite the difficulties resolving the backward-travelling waves in the human pulmonary artery, the pressure and velocity data are of sufficient quality to determine pulmonary arterial wave speed and forward-travelling waves within reasonable limits. With increasing severity of pulmonary vascular disease the total energy carried by the forward waves increased, though not significantly. This reflects the increased work done by the right ventricle against increased afterload.

Importantly, wave speed determined in the proximal pulmonary artery was shown to increase linearly with mean pulmonary artery pressure and pulmonary vascular resistance (Figure 9-1 & Figure 9-2). Elevated wave speeds have been previously demonstrated in patients with pulmonary hypertension compared to controls (Caro, 1978; Chen *et al.*, 1990; Kussmaul *et al.*, 1992; Milnor *et al.*, 1969; Reuben, 1970). The present results are, however, the first demonstration of a linear relationship of wave speed with pulmonary vascular pressure and resistance. Reuben (1970) showed that in pulmonary hypertensive humans the shortest flow conduction times across the pulmonary circulation (a surrogate of wave speed as path lengths were not known) were in patients with the highest mean pulmonary pressures as an inverse curvilinear relationship. These findings show that increases in resistance across the pulmonary microcirculation lead to reductions in proximal pulmonary artery compliance, thus increasing wave speed and the transmission of incident and reflected waves that may impair right ventricular emptying.

It is known from human studies that aortic wave speed increases with age and is a marker of aortic wall stiffness (Avolio *et al.*, 1983). The mean age of the patients did increase significantly with worsening disease severity ($p = 0.01$). However, only the mild pulmonary vascular disease group had a mean age significantly different from those with a normal pulmonary circulation. Also, in humans the wave speed does not increase as dramatically with age as occurs in the systemic circulation (Gozna *et al.*, 1974). Therefore, the increasing pulmonary wave speed with disease severity is unlikely to be a confounder related to age.

There is insufficient data in enough healthy individuals to draw a firm conclusion on a normal pulmonary artery wave speed range. It is likely to be well below 2.5 ms^{-1} based upon the available data. Furthermore, it is difficult to know whether pulmonary wave speed will be a sufficient marker of pulmonary vascular disease before the onset of elevated pulmonary pressures. Such a conclusion would require correlation of increased wave speed with histopathological evidence of pulmonary vascular remodelling in patients without pulmonary hypertension. This would be an extremely rare and difficult group to study. Yet, with further study in enough individuals, elevations in wave speed may become a useful discriminator for the detection of pulmonary vascular disease in patients who have borderline elevations in pulmonary pressures.

The patients classed with normal pulmonary haemodynamics consisted of patients with unexplained complaints such as breathlessness that led to the suspicion of pulmonary vascular disease. These patients, therefore, may not be completely normal subjects. The patients studied, even with severe pulmonary vascular disease, were well compensated with preserved right ventricular systolic function. The cardiac index was well maintained across the groups, although the mean pulmonary arterial and right atrial pressures increased across the groups signifying worse pulmonary vascular disease. In the future, therefore, patients with decompensated right heart failure will need to be studied to understand the ventricular-arterial interactions and wave reflection in such a group.

Several major limitations of the analysis make it impossible to draw any conclusions about the nature of backward-travelling waves in the human pulmonary artery either in health or disease. It is very likely that the two observed backward-travelling waves were artefacts for several reasons. Firstly, the initial backward expansion wave peak preceded the incident forward compression wave peak. This does not appear to have physiological plausibility as it is known that all reflected waves dissipate in diastole (Dujardin *et al.*, 1982; Nichols *et al.*, 2005). Secondly, in healthy individuals the distance to the closed-end reflection site was 5 cm. There is no known plausible closed-end reflection site that arises so proximally in the pulmonary vascular bed. Thirdly, the backward-travelling waves were observed even in the healthy pulmonary vasculature where minimal wave reflection is expected, as observed in the animal model. It was previously shown in Chapter 4 that such unexplained waves are very likely to be related to signal-timing errors.

A significant limitation was related to the ability to adequately track the spectral Doppler envelope used to determine peak velocities over time. The Matlab algorithm created to track the edge of the spectral Doppler envelope worked exceptionally well in early systole, but when the edges of the envelope became less distinct in late systole, the tracking performed less well and introduced random noise into the signal (Figure 9-9). The edge-tracking algorithm could not be successfully optimised to improve the tracking, which reflected the difficulties in obtaining proximal pulmonary arterial Doppler signals in supine patients who frequently had difficulty holding their breath in end-expiration through narrow acoustic windows. It was felt that manually tracing the velocity envelope would lead to bias so was not pursued. Therefore it is likely that the processed velocity signal in late systole is not an accurate reflection of the in-vivo profile, making it extremely difficult to accurately resolve backward-travelling waves and draw conclusions about human pulmonary arterial wave reflection.

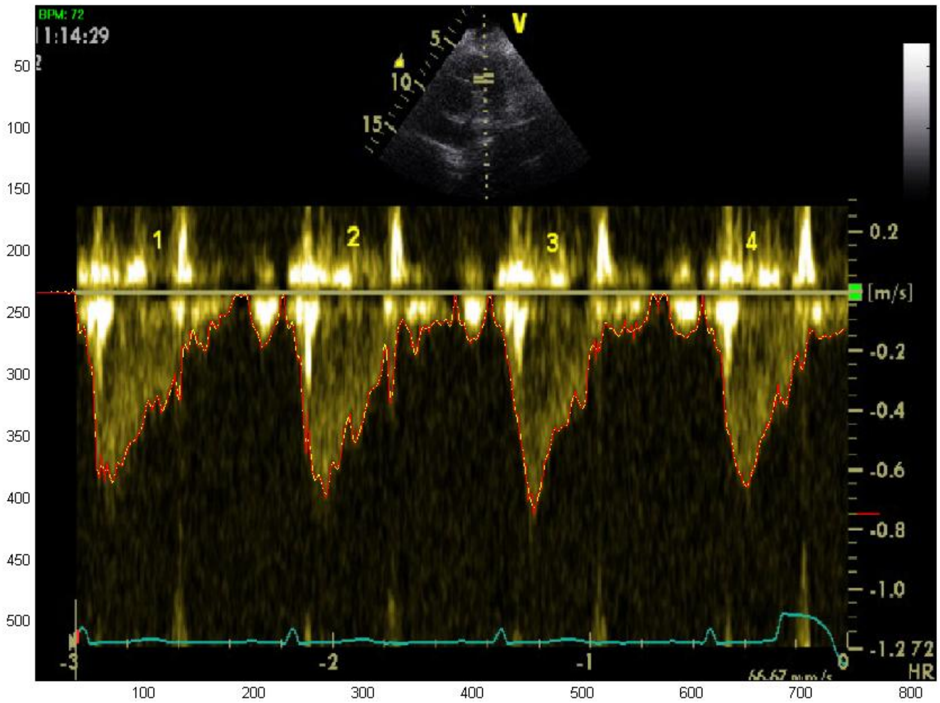

Figure 9-9. The automated algorithm for Matlab tracks the peak velocity signals well, but the indistinct profile in late systole leads to the introduction of random noise.

The 7-Fr 110 cm length Swan-Ganz catheters used have a natural (resonant) frequency of 10.1 Hz and a damping coefficient of 0.32. The maximal frequency these catheters may therefore reproduce within acceptable tolerances is 2.4 Hz with a propagation time delay of 12 ms (Kinefuchi *et al.*, 1994; Lankhaar *et al.*, 2006). It is possible to attenuate the pressure pulse amplification for the frequency components reaching the resonant frequency of the catheter by in-line mechanical damping devices or electronic filters. This, however, comes at the expense of increasing the propagation times to 19 ms (Kinefuchi *et al.*, 1994; Promonet *et al.*, 2000). It is also recognised that over time the natural frequency of these catheter-manometer systems falls as a result of microscopic air bubbles that come out of solution with warming of the fluid to body temperature (Kinefuchi *et al.*, 1994; Promonet *et al.*, 2000). The change in resonant frequency of fluid-filled catheters over time was minimised by frequent flushing of the lines and keeping the procedure time to less than one hour. The frequency response of the fluid-filled catheters initially appeared acceptable for our research needs (Gardner, 1981), but differences in phase reproduction between the pressure and velocity transducers is critical in wave intensity studies as outlined in Chapter 4 and may have introduced significant errors.

The frequency response of most commercially available echocardiographic systems is extremely high. The Fourier spectrogram from which velocity information is obtained has a time resolution of 2 to 6 ms and a velocity resolution of 0.04 ms^{-1} (Padmanabhan *et al.*, 1998). This allows accurate reproduction of blood velocity signals, generally overestimating the true value by less than 5% (Walker, 2009). When a velocity phantom triggered to an electrocardiographic signal was sent to a variety of echocardiographic machines, the displayed velocity signal lagged behind the electrocardiograph signal by 10 to 90 ms (Walker, 2009). The delays depended upon the system, velocity scale, velocity baseline, sweep speed, and whether the Doppler mode was in a live or frozen display as a response to post-signal acquisition and data processing times. There are no published data for these parameters discussed for the General-Electric echocardiographic machine used in this research.

Although the independently acquired velocity and pressure signals were gated to the electrocardiogram, it was impossible to determine the individual delays in signal processing that take place in the haemodynamic and echocardiographic equipment. Great care was taken to account for pressure-velocity signal delays by use of the pressure-velocity loop. This was to ensure that the best linear relationship between pressure and velocity existed in early systole as mandated by the water hammer equation. It proved difficult, however, as the rate of pressure rise in the fluid-filled catheter did not match the rate of velocity generation as detected by Doppler, reflecting the poor frequency response of fluid filled catheters. The relative delays in rates of pressure and velocity change are readily appreciated in Figure 9-5 & Figure 9-7. As is outlined in Chapter 4 pressure-velocity signal delays can enhance or even generate artefactual backward-travelling waves.

It is suspected that the backward compression wave is an artefact of poor algorithm tracking of the late systolic portion of the velocity profile. This serves to lower velocity whilst pressure is still rising from the lower fidelity fluid-filled catheter (Figure 9-5 & Figure 9-7), thus artificially detecting a backward compression wave (Figure 9-6 & Figure 9-8). Similarly, the backward expansion that appears in early systole, even before the incident forward compression wave has peaked (Figure 9-6 & Figure 9-8), results from velocity rising before pressure rises (Figure 9-5 & Figure 9-7). This again attests to the notion that the Swan-Ganz catheter lacks sufficient fidelity for accurate wave intensity analysis.

When these issues became apparent other high-fidelity techniques for recording pressure and velocity were sought. Simultaneous measurement of pressure and flow in the human pulmonary artery is difficult due to the anatomic position of the artery. Furthermore, accurately measuring blood velocity in-vivo is extremely difficult and no perfect technique exists (see Mills, 1972; Nichols *et al.*, 2005 for an excellent overview). Catheter based electromagnetic flow meters used in previous experiments (Murgo and Westerhof, 1984) are no longer available and the only commercial technology for use in humans are Doppler based. Velocity-encoded phase-contrast magnetic resonance has been used to successfully determine pulmonary blood flow in humans (Muthurangu *et al.*, 2005). It is unlikely, however, that this technique has adequate temporal resolution for wave intensity analysis and is not widely accessible at this institution. Ultimately, a system that measures high fidelity pressure and velocity via a 0.36 mm diameter guide wire was purchased (ComboMap, Volcano Corporation, Rancho Cordova, CA, USA). This ComboWire was passed via a Swan-Ganz catheter into the proximal pulmonary artery in six patients and provided excellent pressure and velocity reproduction (Figure 9-10). Despite obtaining satisfactory velocity profiles, the inbuilt tracking algorithm was unable to sufficiently track the peak velocities due to background noise that could not be eliminated. This equipment was ultimately found to be faulty, which the company has replaced but in insufficient time to collect data to include in this thesis. Despite these disappointments the equipment now provides an exciting avenue of future research with the promising wave intensity technique.

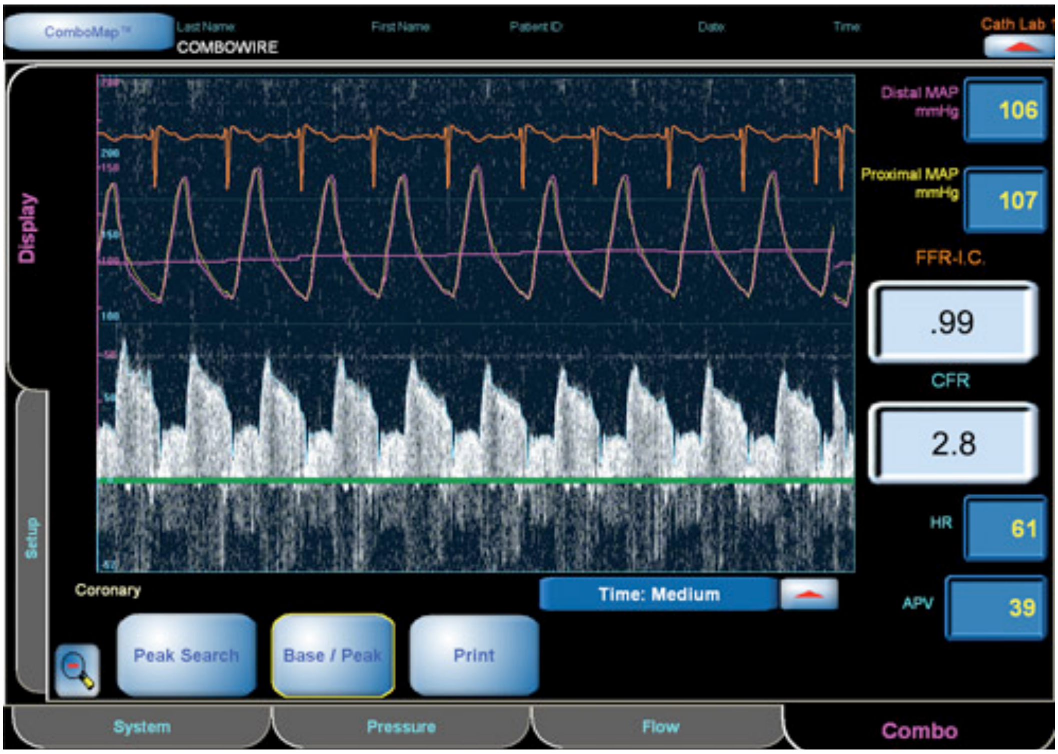

Figure 9-10. A screenshot of the quality recordings that may be obtained with the pressure-flow wire from a coronary artery with careful wire manipulation.

9.4 Conclusion

The technical difficulties in determining pulmonary flow in vivo with enough accuracy has prevented the ability to sufficiently resolve the presence and type of backward-travelling (reflected) waves in the human pulmonary circulation. Regardless, forward-travelling wave energy increased with worsening disease severity, which is a useful surrogate of the increased right ventricular myocardial work. The proximal pulmonary arterial wave speed increased linearly with mean pulmonary artery pressure and pulmonary vascular resistance. This further highlights that downstream remodelling in small pulmonary arteries does affect proximal pulmonary artery compliance. Further detailed work is required in humans to understand wave reflection in healthy and diseased pulmonary vasculature. Such studies are now achievable with the pressure-flow wire technology and are likely to provide useful insights into mismatching of the right ventricle to its afterload. This may better explain clinical worsening than steady state quantities such as pulmonary vascular resistance and mean pulmonary artery pressure.

Chapter 10 Conclusion

10.1 Conclusions

Wave intensity analysis is a useful research tool allowing the separation of intravascular pressure and velocity waveforms into forward- and backward-travelling waves. These allow for the accurate determination of wave reflection sites in the pulmonary vascular bed as well as providing insights into right ventricular-pulmonary arterial interactions. As analysis remains in the time-domain the resultant information is more easily understood by clinician-scientists than are the results of the prevailing frequency domain approach. It is important however to carefully consider and account for even small delays in the pressure-velocity signals (arising from signal processing times or non-simultaneous location of transducers) so that exaggeration or creation of backward-travelling waves does not occur.

In the healthy pulmonary vasculature of sheep the normal pulmonary arterial wave speed in sheep is 2.1 ± 0.3 ms^{-1}. Wave reflection is minimal and not invariably present, suggesting that the right ventricle and pulmonary vascular bed are well matched in terms of impedance. The healthy pulmonary circulation is characterised by two sources of wave reflection. The proximal main pulmonary artery bifurcation behaves as an open-end (negative) reflector, such that the incident forward compression wave is reflected as an early systolic backward-travelling expansion wave, enhancing right ventricular emptying. This open-end reflector is not fixed and disappears in mid-to-late systole, perhaps due to changes in the geometric relationship of daughter-to-parent vessels during the cardiac cycle. The distal microcirculation behaves as a closed-end (positive) reflector, such that the incident forward compression wave is reflected as a late systolic backward-travelling compression wave that opposes right ventricular emptying. The reflection coefficients of both reflection sites are low resulting in the two backward-travelling waves carrying only 2-3% of the incident wave energy. It is likely that enhancement of these waves will serve as important physiological markers of pulmonary vascular disease.

Conditions that increase cardiac output or cause distension of the distal pulmonary circulation lead to enhancement of the open-end reflection and thus increases in the backward expansion wave energy aiding flow out of the right-ventricle at a lower energy cost. Enhancement of the backward expansion wave occurs with increased cardiac output and is maintained during high afterload conditions, suggesting that open-end reflection is a fundamental geometrical property of the proximal pulmonary circulation that allows the heart to maintain efficiency during these conditions.

Conditions that lead to vasoconstriction or intravascular obstruction lead to enhanced closed-end reflection and increased pulmonary arterial wave speed that result in backward-travelling compression waves arriving in the proximal pulmonary artery in mid-systole. These oppose flow out of the right ventricle and increase myocardial work. However, the open-end reflector in early systole remains thus allowing the backward expansion wave to enhance right ventricular emptying in early systole.

Increasing pulmonary artery pressure leads to reductions in proximal pulmonary artery compliance, even if changes are limited to the distal pulmonary circulation, such as occurs with microsphere administration. Reductions in pulmonary arterial compliance manifest as significant changes in the proximal pulmonary arterial wave speed. This may be either by passive distension or active constriction secondary to sympathetic stimulation. Whilst progressive administration of microspheres leads to a dose-responsive increase in pulmonary arterial wave speed, these increases do not become significant until the mean pulmonary pressure reaches 20 mmHg. Thus more investigations are required before wave speed alone may be used as an early marker of pulmonary vascular disease.

Although accounting for the Windkessel is a more accurate model of wave travel (accounting for the ever increasing waves during diastole), it does not appear to contribute greatly to the qualitative interpretation of wave travel and reflection in the pulmonary circulation. Thus, the extra complexity required for the mathematical modelling does not make accounting for the Windkessel essential.

The difficulties in measuring human pulmonary arterial blood velocity in vivo limited the ability to resolve the presence and timing of backward-travelling waves. Nevertheless, the pressure and velocity relationships were determined with sufficient accuracy as to demonstrate a linear relationship between proximal pulmonary arterial wave speed and pulmonary vascular resistance.

10.2 Future Directions

The recent acquisition of equipment with pressure- and Doppler-sensing tipped guide wires in this laboratory leads to immediate application in the human pulmonary artery by allowing the accurate acquisition of pressure and velocity signals to undertake wave intensity analysis and hopefully allow better resolution of reflected waves. It is planned to immediately reinvestigate this work in healthy humans as well as those with pulmonary vascular disease to establish the pattern of wave reflection and range of wave speeds.

To better understand the relationship between total ventricular work and wave intensity dedicated animal experiments need to be conducted with simultaneous ventricular pressure-volume loops analysis and wave intensity analysis whilst preload, afterload and contractility are individually manipulated.

It would be interesting to repeat the microsphere experiments in a larger number of animals with smaller incremental doses to better establish if changes in wave speed precede the development of pressure rises. This information is important to the understanding of how distal vascular changes influence proximal pulmonary arterial compliance.

References

Abdel Kafi, S., Melot, C., Vachiery, J.-L., Brimioulle, S. & Naeije, R. (1998) Partitioning of Pulmonary Vascular Resistance in Primary Pulmonary Hypertension. *Journal of the American College of Cardiology.* 31 (6): 1372-1376.

Acosta, P., Santisbon, E. & Varon, J. (2007) The Use of Positive End-Expiratory Pressure in Mechanical Ventilation. *Critical Care Clinics.* 23 (2): 251-261.

Aguado-Sierra, J., Parker, K.H., Davies, J.E., Francis, D., Hughes, A.D. & Mayet, J. (2006) Arterial pulse wave velocity in coronary arteries. Annual International Conference of the IEEE Engineering in Medicine and Biology - Proceedings. New York City. 867-870

Alpert, J.S., Haynes, F.W., Dalen, J.E. & Dexter, L. (1974) Experimental Pulmonary Embolism: Effect on Pulmonary Blood Volume and Vascular Compliance. *Circulation.* 49 (1): 152-157.

Anthonisen, N.R. & Milic-Emili, J. (1966) Distribution of pulmonary perfusion in erect man. *Journal of Applied Physiology.* 21 (3): 760-766.

Attinger, E.O. (1963) Pressure Transmission in Pulmonary Arteries Related to Frequency and Geometry. *Circulation Research.* 12 (6): 623-641.

Attinger, E.O., Anne, A. & Mcdonald, D.A. (1966) Use of Fourier series for the analysis of biological systems. *Biophysical Journal.* 6 (3): 291-304.

Avolio, A.P., Chen, S.G., Wang, R.P., Zhang, C.L., Li, M.F. & O' Rourke, M.F. (1983) Effects of aging on changing arterial compliance and left ventricular load in a northern Chinese urban community. *Circulation.* 68 (1): 50-58.

Badesch, D.B., Champion, H.C., Gomez Sanchez, M.A., Hoeper, M.M., Loyd, J.E., Manes, A., Mcgoon, M., Naeije, R., Olschewski, H., Oudiz, R.J. & Torbicki, A. (2009) Diagnosis and Assessment of Pulmonary Arterial Hypertension. *Journal of the American College of Cardiology.* 54 (Supplement 1): S55-S66.

Baim, D.S. & Grossman, W. (2006) *Grossman's Cardiac Catheterization, Angiography, and Intervention.,* Philadelphia, Lippincott Williams & Wilkins.

Bargainer, J.D. (1967) Pulse Wave Velocity in the Main Pulmonary Artery of the Dog. *Circulation Research.* 20 (6): 630-637.

Barnes, P.J. & Liu, S.F. (1995) Regulation of pulmonary vascular tone. *Pharmacological Reviews.* 47 (1): 87-131.

Beck, K.C. & Hildebrandt, J. (1983) Adaptation of vascular pressure-flow-volume hysteresis in isolated rabbit lungs. *Journal of Applied Physiology Respiratory Environmental and Exercise Physiology.* 54 (3): 671-679.

Bergel, D.H. & Milnor, W.R. (1965) Pulmonary Vascular Impedance in the Dog. *Circulation Research.* 16: 401-15.

Bevegard, S., Holmgren, A. & Jonsson, B. (1963) Circulatory studies in well trained athletes at rest and during heavy exercise: with special reference to stroke volume and the influence of body position. *Acta Physiologica Scandinavica.* 57: 26-50.

Bossone, E., Duong-Wagner, T.H., Paciocco, G., Oral, H., Ricciardi, M., Bach, D.S., Rubenfire, M. & Armstrong, W.F. (1999a) Echocardiographic features of primary pulmonary hypertension. *Journal of the American Society of Echocardiography.* 12 (8): 655-662.

Bossone, E., Rubenfire, M., Bach, D.S., Ricciardi, M. & Armstrong, W.F. (1999b) Range of tricuspid regurgitation velocity at rest and during exercise in normal adult men: Implications for the diagnosis of pulmonary hypertension. *Journal of the American College of Cardiology.* 33 (6): 1662-1666.

Braunwald, E., Fishman, A.P. & Cournand, A. (1956) Time relationship of dynamic events in the cardiac chambers, pulmonary artery and aorta in man. *Circulation Research.* 4 (1): 100-7.

Bryan, A.C., Bentivoglio, L.G., Beerel, F., Macleish, H., Zidulka, A. & Bates, D.V. (1964) Factors Affecting Regional Distribution of Ventilation and Perfusion in the Lung. *Journal of Applied Physiology.* 19: 395-402.

Calvin Jr, J.E., Baer, R.W. & Glantz, S.A. (1985) Pulmonary artery constriction produces a greater right ventricular dynamic afterload than lung microvascular injury in the open chest dog. *Circulation Research.* 56 (1): 40-56.

Cappello, A., Gnudi, G. & Lamberti, C. (1995) Identification of the three-element windkessel model incorporating a pressure-dependent compliance. *Annals of Biomedical Engineering.* 23 (2): 164-177.

Caro, C.G. (1978) *The Mechanics of the Circulation,* Oxford, Oxford University Press.

Caro, C.G. & Harrison, G.K. (1962) Observations on pulse wave velocity and pulsatile blood pressure in the human pulmonary circulation. *Clinical Science.* 23: 317-329.

Caro, C.G. & Saffman, P.G. (1965) Extensibility of blood vessels in isolated rabbit lungs. *The Journal of Physiology.* 178 (2): 193-193.

Castelain, V., Herve, P., Lecarpentier, Y., Duroux, P., Simonneau, G. & Chemla, D. (2001) Pulmonary artery pulse pressure and wave reflection in chronic pulmonary thromboembolism and primary pulmonary hypertension. *Journal of the American College of Cardiology.* 37 (4): 1085-1092.

Chen, Y.T., Chen, K.S., Chen, J.S., Lin, W.W., Hu, W.H., Chang, M.K., Lee, D.Y., Lee, Y.S., Lin, J.R. & Chiang, B.N. (1990) Aortic and pulmonary input impedance in patients with cor pulmonale. *Japanese Heart Journal.* 31 (5): 619-629.

Collins, R. & Maccario, J.A. (1979) Blood flow in the lung. *Journal of Biomechanics.* 12 (5): 373-395.

Conradson, T.B., Clarke, B., Dixon, C.M., Dalton, R.N. & Barnes, P.J. (1987) Effects of adenosine on autonomic control of heart rate in man. *Acta Physiologica Scandinavica.* 131 (4): 525-531.

Culver, B.H. & Butler, J. (1980) Mechanical influences on the pulmonary microcirculation. *Annual Review of Physiology.* 42: 187-198.

Dabestani, A., Mahan, G. & Gardin, J.M. (1987) Evaluation of pulmonary artery pressure and resistance by pulsed Doppler echocardiography. *The American Journal of Cardiology.* 59 (6): 662-668.

Dalen, J.E., Haynes, F.W., Hoppin Jr, F.G., Evans, G.L., Bhardwaj, P. & Dexter, L. (1967) Cardiovascular responses to experimental pulmonary embolism. *The American Journal of Cardiology.* 20 (1): 3-9.

Dalen, J.E., Mathur, V.S., Evans, H., Haynes, F.W., Pur-Shahriari, A.A., Stein, P.D. & Dexter, L. (1966) Pulmonary angiography in experimental pulmonary embolism. *American Heart Journal.* 72 (4): 509-520.

Davies, J.E., Whinnett, Z.I., Francis, D.P., Manisty, C.H., Aguado-Sierra, J., Willson, K., Foale, R.A., Malik, I.S., Hughes, A.D., Parker, K.H. & Mayet, J. (2006a) Evidence of a dominant backward-propagating "suction" wave responsible for diastolic coronary filling in humans, attenuated in left ventricular hypertrophy. *Circulation.* 113 (14): 1768-1778.

Davies, J.E., Whinnett, Z.I., Francis, D.P., Willson, K., Foale, R.A., Malik, I.S., Hughes, A.D., Parker, K.H. & Mayet, J. (2006b) Use of simultaneous pressure and velocity measurements to estimate arterial wave speed at a single site in humans. *American Journal of Physiology - Heart and Circulatory Physiology.* 290 (2): H878-85.

Dawson, C.A., Grimm, D.J. & Linehan, J.H. (1979) Lung inflation and longitudinal distribution of pulmonary vascular resistance during hypoxia. *Journal of Applied Physiology - Respiratory Environmental and Exercise Physiology.* 47 (3): 532-536.

Delcroix, M., Melot, C., Vanderhoeft, P. & Naeije, R. (1993) Embolus size affects gas exchange in canine autologous blood clot pulmonary embolism. *Journal of Applied Physiology.* 74 (3): 1140-1148.

Doerschuk, C.M., Beyers, N., Coxson, H.O., Wiggs, B. & Hogg, J.C. (1993) Comparison of neutrophil and capillary diameters and their relation to neutrophil sequestration in the lung. *Journal of Applied Physiology.* 74 (6): 3040-3045.

Downing, S.E. & Lee, J.C. (1980) Nervous control of the pulmonary circulation. *Annual Review of Physiology.* 42: 199-210.

Dujardin, J.P., Stone, D.N., Forcino, C.D., Paul, L.T. & Pieper, H.P. (1982) Effects of blood volume changes on characteristic impedance of the pulmonary artery. *The American Journal of Physiology.* 242 (2): H197-202.

Dujardin, J.P.L. & Stone, D.N. (1981) Characteristic impedance of the proximal aorta determined in the time and frequency domain: a comparison. *Medical and Biological Engineering and Computing.* 19 (5): 565-568.

Ekelund, L.G. & Holmgren, A. (1967) Central hemodynamics during exercise. *Circulation Research.* XX and XXI (Supplement 1): 33-43.

Elkins, R.C. & Milnor, W.R. (1971) Pulmonary vascular response to exercise in the dog. *Circulation Research.* 29 (6): 591-599.

Elzinga, G., Piene, H. & De Jong, J.P. (1980) Left and right ventricular pump function and consequences of having two pumps in one heart. A study on the isolated cat heart. *Circulation Research.* 46 (4): 564-574.

Fishman, A.P. & Fisher, A.B. (1985) *The Respiratory System,* Bethesda, Baltimore, American Physiological Society; Distributed by Williams & Wilkins.

Fitzpatrick, J.M. & Grant, B.J.B. (1990) Effects of pulmonary vascular obstruction on right ventricular afterload. *American Review of Respiratory Disease.* 141 (4): 944-952.

Flewitt, J.A., Hobson, T.N., Wang Jr, J., Johnston, C.R., Shrive, N.G., Belenkie, I., Parker, K.H. & Tyberg, J.V. (2007) Wave intensity analysis of left ventricular filling: Application of windkessel theory. *American Journal of Physiology - Heart and Circulatory Physiology.* 292 (6): H2817-H2823.

Fry, D.L., Patel, D.J. & De Freitas, F.M. (1962) Relation of geometry to certain aspects of hydrodynamics in larger pulmonary arteries. *Journal of Applied Physiology.* 17 (3): 492-496.

Furuno, Y., Nagamoto, Y., Fujita, M., Kaku, T., Sakurai, S. & Kuroiwa, A. (1991) Reflection as a cause of mid-systolic deceleration of pulmonary flow wave in dogs with acute pulmonary hypertension: Comparison of pulmonary artery constriction with pulmonary embolisation. *Cardiovascular Research.* 25 (2): 118-124.

Gan, R.Z. & Yen, R.T. (1994) Vascular impedance analysis in dog lung with detailed morphometric and elasticity data. *Journal of Applied Physiology.* 77 (2): 706-717.

Gardner, R.M. (1981) Direct blood pressure measurement - dynamic response requirements. *Anesthesiology.* 54 (3): 227-236.

Ghidaoui, M.S., Zhao, M., Mcinnis, D.A. & Axworthy, D.H. (2005) A Review of Water Hammer Theory and Practice. *Applied Mechanics Reviews.* 58 (1): 49-49.

Glazier, J.B., Hughes, J.M., Maloney, J.E. & West, J.B. (1969) Measurements of capillary dimensions and blood volume in rapidly frozen lungs. *Journal of Applied Physiology.* 26 (1): 65-76.

Gozna, E.R., Marble, A.E., Shaw, A. & Holland, J.G. (1974) Age-related changes in the mechanics of the aorta and pulmonary artery of man. *Journal of Applied Physiology.* 36 (4): 407-411.

Granath, A., Jonsson, B. & Strandell, T. (1964) Circulation in Healthy Old Men, Studied by Right Heart Catheterization at Rest and During Exercise in Supine and Sitting Position. *Acta Medica Scandinavica.* 176: 425-46.

Granath, A. & Strandell, T. (1964) Relationships between Cardiac Output, Stroke Volume and Intracardiac Pressures at Rest and During Exercise in Supine Position and Some Anthropometric Data in Healthy Old Men. *Acta Medica Scandinavica.* 176: 447-66.

Grant, B.J.B. & Canty Jr, J.M. (1989) Effect of cardiac output on pulmonary hemodynamics. *Respiration Physiology.* 76 (3): 303-317.

Groves, B.M., Reeves, J.T., Sutton, J.R., Wagner, P.D., Cymerman, A., Malconian, M.K., Rock, P.B., Young, P.M. & Houston, C.S. (1987) Operation Everest II: Elevated high-altitude pulmonary resistance unresponsive to oxygen. *Journal of Applied Physiology.* 63 (2): 521-530.

Gurtner, H.P., Walser, P. & Faessler, B. (1975) Normal values for pulmonary hemodynamics at rest and during exercise in man. *Progress in Respiratory Research.* 9: 295-315.

Harada, A., Okada, T., Niki, K., Chang, D. & Sugawara, M. (2002) On-line noninvasive one-point measurements of pulse wave velocity. *Heart and Vessels.* 17 (2): 61-68.

Harris, P. & Heath, D. (1962) *The Human Pulmonary Circulation: Its Form and Function in Health and Disease.,* Baltimore, Williams and Wilkins.

Hedqvist, P. & Fredholm, B.B. (1979) Inhibitory effect of adenosine on adrenergic neuroeffector transmission in the rabbit heart. *Acta Physiologica Scandinavica.* 105 (1): 120-122.

Hillier, S.C., Graham, J.A., Hanger, C.C., Godbey, P.S., Glenny, R.W. & Wagner, W.W., Jr. (1997) Hypoxic vasoconstriction in pulmonary arterioles and venules. *Journal of Applied Physiology.* 82 (4): 1084-1090.

Hisland, M.B. & Anliker, M.A.X. (1973) Influence of Flow and Pressure on Wave Propagation in the Canine Aorta. *Circulation Research.* 32 (4): 524-529.

Hobson, T.N., Flewitt, J.A., Belenkie, I. & Tyberg, J.V. (2007) Wave intensity analysis of left atrial mechanics and energetics in anesthetized dogs. *American Journal of Physiology - Heart and Circulatory Physiology.* 292 (3).

Hollander, E.H. (1998) Wave-Intensity Analysis of Pulmonary Arterial Blood Flow In Anesthetized Dogs (PhD Thesis). *Department of Cardiovascular Sciences.* Calgary, Alberta, Canada, University of Calgary.

Hollander, E.H., Dobson, G.M., Wang, J.J., Parker, K.H. & Tyberg, J.V. (2004) Direct and series transmission of left atrial pressure perturbations to the pulmonary artery: A study using wave-intensity analysis. *American Journal of Physiology - Heart and Circulatory Physiology.* 286 (55-1): H267-H275.

Hollander, E.H., Wang, J.J., Dobson, G.M., Parker, K.H. & Tyberg, J.V. (2001) Negative wave reflections in pulmonary arteries. *American Journal of Physiology - Heart and Circulatory Physiology.* 281 (50-2): H895-H902.

Holmgren, A., Jonsson, B. & Sjostrand, T. (1960) Circulatory data in normal subjects at rest and during exercise in recumbent position, with special reference to the stroke volume at different work intensities. *Acta Physiologica Scandinavica.* 49: 343-63.

Horgan, M.J., Pinheiro, J.M. & Malik, A.B. (1991) Mechanism of endothelin-1-induced pulmonary vasoconstriction. *Circulation Research.* 69 (1): 157-164.

Horsfield, K. (1978) Morphometry of the small pulmonary arteries in man. *Circulation Research.* 42 (5): 593-597.

Horsfield, K. & Gordon, W. (1981) Morphometry of pulmonary veins in man. *Lung.* 159 (1): 211-218.

Howell, J.B., Permutt, S., Proctor, D.F. & Riley, R.L. (1961) Effect of inflation of the lung on different parts of pulmonary vascular bed. *Journal of Applied Physiology.* 16: 71-76.

Huemer, G., Kolev, N., Kurz, A. & Zimpfer, M. (1994) Influence of positive end-expiratory pressure on right and left ventricular performance assessed by Doppler two-dimensional echocardiography. *Chest.* 106 (1): 67-73.

Hughes, A., Parker, K. & Davies, J. (2008) Waves in arteries: A review of wave intensity analysis in the systemic and coronary circulations. *Artery Research.* 2 (2): 51-59.

Hughes, J.M., Glazier, J.B., Maloney, J.E. & West, J.B. (1968) Effect of lung volume on the distribution of pulmonary blood flow in man. *Respiration Physiology.* 4 (1): 58-72.

Jabr, R.I., Toland, H., Gelband, C.H., Wang, X.X. & Hume, J.R. (1997) Prominent role of intracellular Ca2+ release in hypoxic vasoconstriction of canine pulmonary artery. *British Journal of Pharmacology.* 122 (1): 21-30.

Jager, G.N., Westerhof, N. & Noordergraaf, A. (1965) Oscillatory Flow Impedance in Electrical Analog of Arterial System: Representation of Sleeve Effect and Non-Newtonian Properties of Blood. *Circulation Research.* 16 (2): 121-133.

Janicki, J.S., Weber, K.T., Likoff, M.J. & Fishman, A.P. (1985) The pressure-flow response of the pulmonary circulation in patients with heart failure and pulmonary vascular disease. *Circulation.* 72 (6): 1270-1278.

Jones, C.J., Parker, K.H., Hughes, R. & Sheridan, D.J. (1992) Nonlinearity of human arterial pulse wave transmission. *Journal of Biomechanical Engineering.* 114 (1): 10-4.

Jones, C.J. & Sugawara, M. (1993) "Wavefronts" in the aorta--implications for the mechanisms of left ventricular ejection and aortic valve closure. *Cardiovascular Research.* 27 (11): 1902-5.

Jones, C.J.H., Sugawara, M., Kondoh, Y., Uchida, K. & Parker, K.H. (2002) Compression and expansion wavefront travel in canine ascending aortic flow: Wave intensity analysis. *Heart and Vessels.* 16 (3): 91-98.

Joukowski, N.E. (1898) Memoirs of the Imperial Academy Society of St. Petersburg. 9 (5). (Russian translated by O' Simon 1904). *Proceedings American Water Works Association.* 24: 341-424.

Karakash, J.J. (1950) *Transmission Lines and Filter Networks,* New York, Macmillan.

Khir, A.W., Henein, M.Y., Koh, T., Das, S.K., Parker, K.H. & Gibson, D.G. (2001a) Arterial waves in humans during peripheral vascular surgery. *Clinical Science.* 101 (6): 749-757.

Khir, A.W., O' Brien, A., Gibbs, J.S. & Parker, K.H. (2001b) Determination of wave speed and wave separation in the arteries. *Journal of Biomechanics.* 34 (9): 1145-55.

Khir, A.W. & Parker, K.H. (2002) Measurements of wave speed and reflected waves in elastic tubes and bifurcations. *Journal of Biomechanics.* 35 (6): 775-783.

Khir, A.W. & Parker, K.H. (2005) Wave intensity in the ascending aorta: Effects of arterial occlusion. *Journal of Biomechanics.* 38 (4): 647-655.

Khir, A.W., Price, S., Henein, M.Y., Parker, K.H. & Pepper, J.R. (2003) Intra-aortic balloon pumping: Effects on left ventricular diastolic function. *European Journal of Cardiothoracic Surgery.* 24 (2): 277-282.

Khir, A.W., Swalen, M.J.P., Feng, J. & Parker, K.H. (2007) Simultaneous determination of wave speed and arrival time of reflected waves using the pressure-velocity loop. *Medical and Biological Engineering and Computing.* 45 (12): 1201-1210.

Khir, A.W., Zambanini, A. & Parker, K.H. (2004) Local and regional wave speed in the aorta: Effects of arterial occlusion. *Medical Engineering and Physics.* 26 (1): 23-29.

Kinefuchi, Y., Suzuki, T., Takiguchi, M., Yamasaki, Y. & Yamamoto, M. (1994) Evaluation of dynamic response of catheter-manometer systems for pulmonary arterial pressure. *Journal of Applied Physiology.* 77 (4): 2023-2028.

Kitabatake, A., Inoue, M. & Asao, M. (1983) Noninvasive evaluation of pulmonary hypertension by a pulsed Doppler technique. *Circulation.* 68 (2): 302-309.

Klabunde, R.E. (1983) Dipyridamole inhibition of adenosine metabolism in human blood. *European Journal of Pharmacology.* 93 (1-2): 21-26.

Koh, T.W., Pepper, J.R., Desouza, A.C. & Parker, K.H. (1998) Analysis of wave reflections in the arterial system using wave intensity: A novel method for predicting the timing and amplitude of reflected waves. *Heart and Vessels.* 13 (3): 103-113.

Kolyva, C., Spaan, J.A.E., Piek, J.J. & Siebes, M. (2008) Windkesselness of coronary arteries hampers assessment of human coronary wave speed by single-point technique. *American Journal of Physiology - Heart and Circulatory Physiology.* 295 (2): H482-H490.

Konduri, G.G. & Mital, S. (2000) Adenosine and ATP cause nitric oxide-dependent pulmonary vasodilation in fetal lambs. *Biology of the Neonate.* 78 (3): 220-229.

Kornet, L., Jansen, J.R.C., Te Nijenhuis, F.C.A.M., Langewouters, G.J. & Versprille, A. (1998) The compliance of the porcine pulmonary artery depends on pressure and heart rate. *The Journal of Physiology.* 512 (3): 917-926.

Kovacs, G., Berghold, A., Scheidl, S. & Olschewski, H. (2009) Pulmonary arterial pressure during rest and exercise in healthy subjects: a systematic review. *European Respiratory Journal.* 34 (4): 888-894.

Kussmaul, W.G., Altschuler, J.A., Herrmann, H.C. & Laskey, W.K. (1992) Effects of pacing tachycardia and balloon valvuloplasty on pulmonary artery impedance and hydraulic power in mitral stenosis. *Circulation.* 86 (6): 1770-1779.

Kussmaul, W.G., Wieland, J.M. & Laskey, W.K. (1988) Pressure-flow relations in the pulmonary artery during myocardial ischaemia: implications for right ventricular function in coronary disease. *Cardiovascular Research.* 22 (9): 627-638.

Lai-Fook, S.J. (1993) Mechanical factors in lung liquid distribution. *Annual Review of Physiology.* 55: 155-179.

Lamm, W.J.E., Kirk, K.R., Hanson, W.L., Wagner Jr, W.W. & Albert, R.K. (1991) Flow through zone 1 lungs utilizes alveolar corner vessels. *Journal of Applied Physiology.* 70 (4): 1518-1523.

Lankhaar, J.-W., Westerhof, N., Faes, T.J.C., Marques, K.M.J., Marcus, J.T., Postmus, P.E. & Vonk-Noordegraaf, A. (2006) Quantification of right ventricular afterload in patients with and without pulmonary hypertension. *American Journal of Physiology - Heart and Circulatory Physiology.* 291 (4): H1731-1737.

Lanoye, L.L., Vierendeels, J.A., Segers, P. & Verdonck, P.R. (2005) Wave intensity analysis of left ventricular filling. *Journal of Biomechanical Engineering.* 127 (5): 862-867.

Liepmann, H.W. & Roshko, A. (1957) *Elements of Gas Dynamics,* New York, Wiley.

Lighthill, M.J. (1978) *Waves in Fluids,* Cambridge, Cambridge University Press.

Lucas, C.L. (1984) Fluid mechanics of the pulmonary circulation. *Critical Reviews in Biomedical Engineering.* 10 (4): 317-393.

Macrae, J.M., Sun, Y.H., Isaac, D.L., Dobson, G.M., Cheng, C.P., Little, W.C., Parker, K.H. & Tyberg, J.V. (1997) Wave-intensity analysis: A new approach to left ventricular filling dynamics. *Heart and Vessels.* 12 (2): 53-59.

Maggiorini, M., Melot, C., Pierre, S., Pfeiffer, F., Greve, I., Sartori, C., Lepori, M., Hauser, M., Scherrer, U. & Naeije, R. (2001) High-altitude pulmonary edema is initially caused by an increase in capillary pressure. *Circulation.* 103 (16): 2078-2083.

Mahjoub, H., Levy, F., Cassol, M., Meimoun, P., Peltier, M., Rusinaru, D. & Tribouilloy, C. (2009) Effects of age on pulmonary artery systolic pressure at rest and during exercise in normal adults. *European Journal of Echocardiography.* 10 (5): 635-640.

Maloney, J.E., Bergel, D.H., Glazier, J.B., Hughes, J.M. & West, J.B. (1968) Transmission of pulsatile blood pressure and flow through the isolated lung. *Circulation Research.* 23 (1): 11-24.

Maloney, J.E., Rooholamini, S.A. & Wexler, L. (1970) Pressure-diameter relations of small blood vessels in isolated dog lung. *Microvascular Research.* 2 (1): 1-12.

Marshall, C. & Marshall, B. (1983) Site and sensitivity for stimulation of hypoxic pulmonary vasoconstriction. *Journal of Applied Physiology - Respiratory, Environmental and Exercise Physiology.* 55 (3): 711-716.

Mazzeo, R.S., Bender, P.R., Brooks, G.A., Butterfield, G.E., Groves, B.M., Sutton, J.R., Wolfel, E.E. & Reeves, J.T. (1991) Arterial catecholamine responses during exercise with acute and chronic high-altitude exposure. *American Journal of Physiology - Endocrinology and Metabolism.* 261 (24-4): E419-E424.

Mcdonald, D.A. (1968) Regional pulse-wave velocity in the arterial tree. *Journal of Applied Physiology.* 24 (1): 73-78.

Melot, C., Delcroix, M., Closset, J., Vanderhoeft, P., Lejeune, P., Leeman, M. & Naeije, R. (1995) Starling resistor vs. distensible vessel models for embolic pulmonary hypertension. *American Journal of Physiology - Heart and Circulatory Physiology.* 268 (37-2): H817-827.

Melot, C., Naeije, R. & Hallemans, R. (1987) Hypoxic pulmonary vasoconstriction and pulmonary gas exchange in normal man. *Respiration Physiology.* 68 (1): 11-27.

Mills, C. (1972) Measurement of Pulsatile Flow and Flow Velocity. In Bergel, D (Ed.) *Cardiovascular Fluid Dynamics.* London, Academic Press.

Milnor, W.R., Bergel, D.H. & Bargainer, J.D. (1966) Hydraulic power associated with pulmonary blood flow and its relation to heart rate. *Circulation Research.* 19 (3): 467-480.

Milnor, W.R., Conti, C.R., Lewis, K.B. & O' Rourke, M.F. (1969) Pulmonary arterial pulse wave velocity and impedance in man. *Circulation Research.* 25 (6): 637-649.

Murgo, J.P. & Westerhof, N. (1984) Input impedance of the pulmonary arterial system in normal man. Effects of respiration and comparison to systemic impedance. *Circulation Research.* 54 (6): 666-673.

Murgo, J.P., Westerhof, N., Giolma, J.P. & Altobelli, S.A. (1980) Aortic input impedance in normal man: Relationship to pressure wave forms. *Circulation.* 62 (1): 105-116.

Murgo, J.P., Westerhof, N., Giolma, J.P. & Altobelli, S.A. (1981) Manipulation of ascending aortic pressure and flow wave reflections with the Valsalva maneuver: Relationship to input impedance. *Circulation.* 63 (1): 122-132.

Muthurangu, V., Atkinson, D., Sermesant, M., Miquel, M.E., Hegde, S., Johnson, R., Andriantsimiavona, R., Taylor, A.M., Baker, E., Tulloh, R. & Others (2005) Measurement of total pulmonary arterial compliance using invasive pressure monitoring and MR flow quantification during MR-guided cardiac catheterization. *American Journal of Physiology- Heart and Circulatory Physiology.* 289 (3): H1301-H1306.

Naeije, R. (2004) Pulmonary Vascular Function. In Peacock, A & Rubin, L (Eds.) *Pulmonary Circulation: Diseases and Their Treatment.* Second ed. London, Arnold.

Naeije, R., Melot, C., Mols, P. & Hallemans, R. (1982) Effects of vasodilators on hypoxic pulmonary vasoconstriction in normal man. *Chest.* 82 (4): 404-410.

Nakayama, Y., Nakanishi, N., Hayashi, T., Nagaya, N., Sakamaki, F., Satoh, N., Ohya, H. & Kyotani, S. (2001) Pulmonary artery reflection for differentially diagnosing primary pulmonary hypertension and chronic pulmonary thromboembolism. *Journal of the American College of Cardiology.* 38 (1): 214-218.

Nakayama, Y., Nakanishi, N., Sugimachi, M., Takaki, H., Kyotani, S., Satoh, T., Okano, Y., Kunieda, T. & Sunagawa, K. (1997) Characteristics of pulmonary artery pressure waveform for differential diagnosis of chronic pulmonary thromboembolism and primary pulmonary hypertension. *Journal of the American College of Cardiology.* 29 (6): 1311-1316.

Nichols, W.W. (2005) Clinical measurement of arterial stiffness obtained from noninvasive pressure waveforms. *American Journal of Hypertension.* 18 (Supplement 1): 3S-10S.

Nichols, W.W., O' Rourke, M.F. & Mcdonald, D.A. (2005) *McDonald's Blood Flow in Arteries: Theoretic, Experimental, and Clinical Principles,* London, Hodder Arnold.

Niki, K., Sugawara, M., Chang, D., Harada, A., Okada, T., Sakai, R., Uchida, K., Tanaka, R. & Mumford, C.E. (2002) A new noninvasive measurement system for wave intensity: Evaluation of carotid arterial wave intensity and reproducibility. *Heart and Vessels.* 17 (1): 12-21.

Niki, K., Sugawara, M., Uchida, K., Tanaka, R., Tanimoto, K., Imamura, H., Sakomura, Y., Ishizuka, N., Koyanagi, H. & Kasanuki, H. (1999) A noninvasive method of measuring wave intensity, a new hemodynamic index: Application to the carotid artery in patients with mitral regurgitation before and after surgery. *Heart and Vessels.* 14 (6): 263-271.

O' Rourke, M.F. & Milnor, W.R. (1971) Relation between differential pressure and flow in the pulmonary artery of the dog. *Cardiovascular Research.* 5 (4): 558-565.

Ohte, N., Narita, H., Sugawara, M., Niki, K., Okada, T., Harada, A., Hayano, J. & Kimura, G. (2003) Clinical usefulness of carotid arterial wave intensity in assessing left ventricular systolic and early diastolic performance. *Heart and Vessels.* 18 (3): 107-111.

Padmanabhan, K., Nedumaran, D. & Ananthi, S. (1998) Gabor spectra for Doppler echocardiography. *Medical & Biological Engineering & Computing.* 36 (3): 270-275.

Pagnamenta, A., Bouckaert, Y., Wauthy, P., Brimioulle, S. & Naeije, R. (2000) Continuous versus pulsatile pulmonary hemodynamics in canine oleic acid lung injury. *American Journal of Respiratory and Critical Care Medicine.* 162 (3 I): 936-940.

Parker & Jones, C.J. (1990) Forward and backward running waves in the arteries: analysis using the method of characteristics. *Journal of Biomechanical Engineering.* 112 (3): 322-6.

Parker, K.H., Jones, C.J., Dawson, J.R. & Gibson, D.G. (1988) What stops the flow of blood from the heart? *Heart Vessels.* 4 (4): 241-5.

Patel, D.J., Defreitas, F.M. & Fry, D.L. (1963) Hydraulic input impedance to aorta and pulmonary artery in dogs. *Journal of Applied Physiology.* 18 (1): 134-140.

Patel, D.J., Mason, D.T., Ross, J., Jr. & Braunwald, E. (1965) Harmonic Analysis of Pressure Pulses Obtained from the Heart and Great Vessels of Man. *American Heart Journal.* 69: 785-94.

Patel, D.J., Schilder, D.P. & Mallos, A.J. (1960) Mechanical properties and dimensions of the major pulmonary arteries. *Journal of Applied Physiology.* 15 (1): 92-96.

Peacock, A.J. & Rubin, L.J. (2004) *Pulmonary Circulation: Diseases and their Treatment,* London, Arnold.

Penny, D.J., Mynard, J.P. & Smolich, J.J. (2008) Aortic wave intensity analysis of ventricular-vascular interaction during incremental dobutamine infusion in adult sheep. *American Journal of Physiology - Heart and Circulatory Physiology.* 294 (1): H481-489.

Permutt, S., Bromberger-Barnea, B. & Bane, H.N. (1962) Alveolar pressure, pulmonary venous pressure, and the vascular waterfall. *Medicina Thoracalis.* 19: 239-60.

Piene, H. (1976) Influence of vessel distension and myogenic tone on pulmonary arterial input impedance. A study using a computer model of rabbit lung. *Acta Physiologica Scandinavica.* 98 (1): 54-66.

Piene, H. & Sund, T. (1982) Does normal pulmonary impedance constitute the optimum load for the right ventricle? *American Journal of Physiology - Heart and Circulatory Physiology.* 242 (2): H154-160.

Pinkerson, A.L. (1967) Pulse-wave propagation through the pulmonary vascular bed of dogs. *American Journal of Physiology.* 213 (2): 450-454.

Prioreschi, P. (1996) Galenicae Quaestiones Disputatae Duae: rete mirabile and pulmonary circulation. *Vesalius: Acta Internationales Historiae Medicinae.* 2 (2): 67-78.

Promonet, C., Anglade, D., Menaouar, A., Bayat, S., Durand, M., Eberhard, A. & Grimbert, F.A. (2000) Time-dependent pressure distortion in a catheter-transducer system: correction by fast flush. *Anesthesiology.* 92 (1): 208-218.

Pythoud, F., Stergiopulos, N. & Meister, J.J. (1996a) Separation of arterial pressure waves into their forward and backward running components. *Journal of Biomechanical Engineering.* 118 (3): 295-301.

Pythoud, F., Stergiopulos, N., Westerhof, N. & Meister, J.J. (1996b) Method for determining distribution of reflection sites in the arterial system. *American Journal of Physiology - Heart and Circulatory Physiology.* 271 (40-5): H1807-H1813.

Ramsey, M.W. & Sugawara, M. (1997) Arterial wave intensity and ventriculoarterial interaction. *Heart and Vessels.* 12 (Supplement 12): 128-134.

Redenbach, D.M., English, D. & Hogg, J.C. (1997) The nature of leukocyte shape changes in the pulmonary capillaries. *American Journal of Physiology - Lung Cellular and Molecular Physiology.* 273 (4): L733-740.

Reid, P.G., Fraser, A.G., Watt, A.H., Henderson, A.H. & Routledge, P.A. (1990) Acute haemodynamic effects of intravenous infusion of adenosine in conscious man. *European Heart Journal.* 11 (11): 1018-1028.

Reuben, S.R. (1970) Wave Transmission in the Pulmonary Arterial System in Disease in Man. *Circulation Research.* 27 (4): 523-529.

Reuben, S.R. (1971) Compliance of the human pulmonary arterial system in disease. *Circulation Research.* 29 (1): 40-50.

Reuben, S.R., Gersh, B.J., Swadling, J.P. & Lee, G.J. (1970a) Measurement of pulmonary arterial distensibility in the dog. *Cardiovascular Research.* 4 (4): 473-481.

Reuben, S.R., Swadling, J.P., Gersh, B.J. & Lee, G.D.J. (1971) Impedance and transmission properties of the pulmonary arterial system. *Cardiovascular Research.* 5 (1): 1-9.

Reuben, S.R., Swadling, J.P. & Lee, G.D.J. (1970b) Velocity Profiles in the Main Pulmonary Artery of Dogs and Man, Measured with a Thin-Film Resistance Anemometer. *Circulation Research.* 27 (6): 995-1001.

Rosenzweig, D.Y., Hughes, J.M. & Glazier, J.B. (1970) Effects of transpulmonary and vascular pressures on pulmonary blood volume in isolated lung. *Journal of Applied Physiology.* 28 (5): 553-560.

Sagawa, K., Lie, R.K. & Schaefer, J. (1990) Translation of Otto Frank's Paper 'Die Grundform des Arteriellen Pulses' Zeitschrift fur Biologie 37: 483-526 (1899). *Journal of Molecular and Cellular Cardiology.* 22 (3): 253-277.

Savitzky, A. & Golay, M.J.E. (1964) Smoothing and differentiation of data by simplified least squares procedures. *Analytical Chemistry.* 36 (8): 1627-1639.

Segers, P., Brimioulle, S., Stergiopulos, N., Westerhof, N., Naeije, R., Maggiorini, M. & Verdonck, P. (1999) Pulmonary arterial compliance in dogs and pigs: the three-element windkessel model revisited. *American Journal of Physiology - Heart and Circulatory Physiology.* 277 (2): H725-731.

Segers, P., Rietzschel, E.R., De Buyzere, M.L., De Bacquer, D., Van Bortel, L.M., De Backer, G., Gillebert, T.C. & Verdonck, P.R. (2007) Assessment of pressure wave reflection: Getting the timing right! *Physiological Measurement.* 28 (9): 1045-1056.

Segers, P., Rietzschel, E.R., De Buyzere, M.L., Stergiopulos, N., Westerhof, N., Van Bortel, L.M., Gillebert, T. & Verdonck, P.R. (2008) Three-and-four-element Windkessel models: Assessment of their fitting performance in a large cohort of healthy middle-aged individuals. *Proceedings of the Institution of Mechanical Engineers, Part H: Journal of Engineering in Medicine.* 222 (4): 417-428.

Shoukas, A.A. (1975) Pressure-flow and pressure-volume relations in the entire pulmonary vascular bed of the dog determined by two-port analysis. *Circulation Research.* 37 (6): 809-818.

Singhal, S., Henderson, R., Horsfield, K., Harding, K. & Cumming, G. (1973) Morphometry of the Human Pulmonary Arterial Tree. *Circulation Research.* 33 (2): 190-197.

Skalak, R. (1972) The Synthesis of a Complete Circulation. In Bergel, D (Ed.) *Cardiovascular Fluid Dynamics.* London, Academic Press.

Smith, P.K., Tyson Jr, G.S. & Hammon Jr, J.W. (1982) Cardiovascular effects of ventilation with positive expiratory airway pressure. *Annals of Surgery.* 195 (2): 121-130.

Smolich, J.J., Mynard, J.P. & Penny, D.J. (2008) Simultaneous pulmonary trunk and pulmonary arterial wave intensity analysis in fetal lambs: evidence for cyclical, midsystolic pulmonary vasoconstriction. *American Journal of Physiology - Regulatory, Integrative and Comparative Physiology.* 294 (5): R1554-1562.

Sniderman, A.D. & Fitchett, D.H. (1988) Vasodilators and pulmonary arterial hypertension: the paradox of therapeutic success and clinical failure. *International Journal of Cardiology.* 20 (2): 173-181.

Sugawara, M., Niki, K., Furuhata, H., Ohnishi, S. & Suzuki, S. (2000) Relationship between the pressure and diameter of the carotid artery in humans. *Heart and Vessels.* 15 (1): 49-51.

Sugawara, M., Niki, K., Ohte, N., Okada, T. & Harada, A. (2009) Clinical usefulness of wave intensity analysis. *Medical and Biological Engineering and Computing.* 47 (2): 197-206.

Sun, Y., Belenkie, I., Wang Jr, J. & Tyberg, J.V. (2006) Assessment of right ventricular diastolic suction in dogs with the use of wave intensity analysis. *American Journal of Physiology - Heart and Circulatory Physiology.* 291 (6): H3114-3121.

Sun, Y.H., Anderson, T.J., Parker, K.H. & Tyberg, J.V. (2000) Wave-intensity analysis: A new approach to coronary hemodynamics. *Journal of Applied Physiology.* 89 (4): 1636-1644.

Sun, Y.H., Anderson, T.J., Parker, K.H. & Tyberg, J.V. (2004) Effects of left ventricular contractility and coronary vascular resistance on coronary dynamics. *American Journal of Physiology - Heart and Circulatory Physiology.* 286 (4): 55-4.

Swalen, M.J.P. & Khir, A.W. (2009) Resolving the time lag between pressure and flow for the determination of local wave speed in elastic tubes and arteries. *Journal of Biomechanics.* 42 (10): 1574-1577.

Swan, H.J.C., Ganz, W., Forreste.J, Marcus, H., Diamond, G. & Chonette, D. (1970) Catheterization of Heart in Man with Use of Flow-Directed Balloon-Tipped Catheter. *New England Journal of Medicine.* 283 (9): 447-451.

Van Den Bos, G.C., Westerhof, N., Elzinga, G. & Sipkema, P. (1976) Reflection in the systemic arterial system: effects of aortic and carotid occlusion. *Cardiovascular Research.* 10 (5): 565-573.

Van Den Bos, G.C., Westerhof, N. & Randall, O.S. (1982) Pulse wave reflection: can it explain the differences between systemic and pulmonary pressure and flow waves? A study in dogs. *Circulation Research.* 51 (4): 479-485.

Van Den Wijngaard, J., Siebes, M. & Westerhof, B. (2008) Comparison of arterial waves derived by classical wave separation and wave intensity analysis in a model of aortic coarctation. *Medical and Biological Engineering and Computing.* 47 (2): 211-220.

Vogel, W.M., Apstein, C.S., Briggs, L.L., Gaasch, W.H. & Ahn, J. (1982) Acute alterations in left ventricular diastolic chamber stiffness. Role of the "erectile" effect of coronary arterial pressure and flow in normal and damaged hearts. *Circulation Research.* 51 (4): 465-478.

Von Euler, U.S. & Liljestrand, G. (1946) Observations on the pulmonary arterial blood pressure in the cat. *Acta Physiologica Scandinavica.* 12 (1): 301-20.

Vreim, C.E. & Staub, N.C. (1973) Indirect and direct capillary blood volume in anesthetized open-thorax cats. *Journal of Applied Physiology.* 34 (4): 452-459.

Wagner, P.D., Gale, G.E. & Moon, R.E. (1986) Pulmonary gas exchange in humans exercising at sea level and simulated altitude. *Journal of Applied Physiology.* 61 (1): 260-270.

Walker, A. (2009) Testing of Doppler Ultrasound Systems (PhD Thesis). *Department of Biomedical Engineering.* Linkoping, Linkoping University.

Wang, J.J. (1997) Wave Propagation in a Model of the Human Arterial System (PhD Thesis). London, University of London.

Wang, J.J., Flewitt, J.A., Shrive, N.G., Parker, K.H. & Tyberg, J.V. (2006) Systemic venous circulation. Waves propagating on a windkessel: Relation of arterial and venous windkessels to systemic vascular resistance. *American Journal of Physiology - Heart and Circulatory Physiology.* 290 (1): H154-162.

Wang, J.J., O' Brien, A.B., Shrive, N.G., Parker, K.H. & Tyberg, J.V. (2003) Time-domain representation of ventricular-arterial coupling as a windkessel and wave system. *American Journal of Physiology - Heart and Circulatory Physiology.* 284 (4): H1358-1368.

Wang, Z., Jalali, F., Sun, Y.H., Wang, J.J., Parker, K.H. & Tyberg, J.V. (2005) Assessment of left ventricular diastolic suction in dogs using wave-intensity analysis. *American Journal of Physiology - Heart and Circulatory Physiology.* 288 (57-4): H1641-H1651.

Weibel, E.R. (1963) *Morphometry of the Human Lung,* Berlin, Springer.

Weibel, E.R. & Gil, J. (1977) *Structure-function relationships at the alveolar level,* New York, M. Dekker.

Weir, E.K. & Archer, S.L. (1995) The mechanism of acute hypoxic pulmonary vasoconstriction: the tale of two channels. *The Journal of the Federation of American Societies for Experimental Biology* 9(2): 183-189.

West, J.B., Dollery, C.T. & Naimark, A. (1964) Distribution of blood flow in isolated lung; relation to vascular and alveolar pressures. *Journal of Applied Physiology.* 19 (4): 713-724.

West, J.B., Schneider, A.M. & Mitchell, M.M. (1975) Recruitment in networks of pulmonary capillaries. *Journal of Applied Physiology.* 39 (6): 976-984.

Westerhof, B.E., Guelen, I., Westerhof, N., Karemaker, J.M. & Avolio, A. (2006) Quantification of wave reflection in the human aorta from pressure alone: A proof of principle. *Hypertension.* 48 (4): 595-601.

Westerhof, N., Elzinga, G. & Van Den Bos, G.C. (1973) Influence of central and peripheral changes on the hydraulic input impedance of the systemic arterial tree. *Medical and Biological Engineering.* 11 (6): 710-723.

Westerhof, N., Lankhaar, J.-W. & Westerhof, B.E. (2009) The arterial Windkessel. *Medical & Biological Engineering & Computing.* 47 (2): 131-141.

Westerhof, N. & Noordergraaf, A. (1970) Errors in the measurement of hydraulic input impedance. *Journal of Biomechanics.* 3 (3): 351-356.

Westerhof, N., Sipkema, P., Van Den Bos, G.C. & Elzinga, G. (1972) Forward and backward waves in the arterial system. *Cardiovascular Research.* 6 (6): 648-656.

Wetterer, E. (1956) [Effect of heart activity on dynamics of arterial system]. *Verh Dtsch Ges Kreislaufforsch.* 22: 26-60.

Wiener, F., Morkin, E., Skalak, R. & Fishman, A.P. (1966) Wave Propagation in the Pulmonary Circulation. *Circulation Research.* 19 (4): 834-850.

Womersley, J.R. (1958) Oscillatory Flow in Arteries. II: The Reflection of the Pulse Wave at Junctions and Rigid Inserts in the Arterial System. *Physics in Medicine and Biology.* 2 (4): 313-323.

Yin, F.C., Guzman, P.A., Brin, K.P., Maughan, W.L., Brinker, J.A., Traill, T.A., Weiss, J.L. & Weisfeldt, M.L. (1983) Effect of nitroprusside on hydraulic vascular loads on the right and left ventricle of patients with heart failure. *Circulation.* 67 (6): 1330-1339.

Young, T. (1809) The Croonian Lecture: On the Functions of the Heart and Arteries. *Philosophical Transactions of the Royal Society of London (1776-1886).* 99 (1): 1-31.

Yu, P.N. (1969) *Pulmonary Blood Volume in Health and Disease,* Philadelphia, Lea & Febiger.

Zambanini, A., Cunningham, S.L., Parker, K.H., Khir, A.W., Thom, S.A.M. & Hughes, A.D. (2005) Wave-energy patterns in carotid, brachial, and radial arteries: A noninvasive approach using wave-intensity analysis. *American Journal of Physiology - Heart and Circulatory Physiology.* 289 (58-1): H270-H276.

Zuckerman, B.D., Orton, E.C., Latham, L.P., Barbiere, C.C., Stenmark, K.R. & Reeves, J.T. (1992) Pulmonary vascular impedance and wave reflections in the hypoxic calf. *Journal of Applied Physiology.* 72 (6): 2118-2127.